

INTEGRATED MODELING OF THE TAMPA BAY ESTUARINE SYSTEM

By

EDUARDO AYRES YASSUDA

A DISSERTATION PRESENTED TO THE GRADUATE SCHOOL
OF THE UNIVERSITY OF FLORIDA IN PARTIAL FULFILLMENT
OF THE REQUIREMENTS FOR THE DEGREE OF
DOCTOR OF PHILOSOPHY

UNIVERSITY OF FLORIDA

1996

ACKNOWLEDGMENTS

First, I would like to express my gratitude to the CNPq - Conselho Nacional de Desenvolvimento Científico e Tecnológico (Brazilian Research Council) for the financial support during my graduate program at the University of Florida. Several University of Florida research projects provided the opportunities for me to gain experience in hydrodynamics and water quality modeling and field work. These projects include the Lake Okeechobee Phosphorus Dynamics Study funded by the South Florida Water Management District, the Sarasota Bay Field and Modeling Study funded by the Sarasota Bay National Estuary Program and United States Geological Survey, the Tampa Bay Circulation Modeling Study funded by the Tampa Bay National Estuary Program, the Roberts Bay Water Quality Modeling Study funded by the Sarasota Bay National Estuary Program, and the Indian River Hydrodynamics and Water Quality Modeling Study funded by the St. Johns River Water Management District.

My appreciation is extended to my advisor and chairman of the supervisory committee, Prof. Peter Sheng, for his guidance, financial support, and patience throughout this study; to Prof. A. Mehta, and Prof. R. Thieke from the Coastal Engineering Department for their comments and advice; to Prof. K.R. Reddy from the Soil and Water Science Department for helping us bridge the gap between experimentalists and modelers; and to Prof. C. Montague from the Environmental Engineering and Science Department, for his

unconditional support and high motivation. Two former students deserve special acknowledgment: Steve Peene and Xinjian Chen.

I also want to thank my professors at the Oceanographic Institute of the University of São Paulo, specially Prof. Joseph Harari, Prof. Luiz B. de Miranda, and Prof. Moyses Tessler for their invaluable contributions to my career.

It would not be possible to complete this work if not for the technical guidance and help of the following scientists and researchers: Mr. Richard Boler, Dr. Kate Bosley, Mr. Michael DelCharco, Dr. Kent Fanning, Dr. Peggy Fong, Ms. Holly Greening, Dr. Kurt Hess, Mr. Ronald Miller, Dr. Gerold Morrison, and Dr. David Tomasko.

Grateful thanks goes to my buddies in room 429, H.K. Lee, Yang, Justin, Liu, and Kevin, in our quest for "bugs," and for reviewing the manuscript. I would like to express my gratitude to Sidney Schofield, "Professor" Mark Gosselin, and "Wally" Yigong Li for bailing me out in a great number of opportunities throughout this program. Life would not be the same without the Coastal Lab and its staff. Acknowledgment goes to all of them. Deserving special honors also are Subarna Malakar, Becky Hudson, Sandra Bivins, Lucy Hamm, Helen Twedell, and John Davis.

My most sincere appreciation is extended to the DelCharco family, for adopting and taking us as one of their own during all family occasions.

I would like to dedicate this dissertation to my parents, because only now, as Daniel's father, do I realize how much effort they had to spend educating me.

Finally, I want to thank Monica for being there for me all the time, sharing the ups and downs of this never-ending challenge.

TABLE OF CONTENTS

ACKNOWLEDGMENTS	ii
ABSTRACT	xix
CHAPTERS	
1 INTRODUCTION	1
Background	1
Water Quality Modeling	2
Integrated Modeling Approach for Estuarine Systems	4
Objectives	6
2 TAMPA BAY CHARACTERIZATION	8
Climate	10
Tides	11
Salinity Distribution	11
Rainfall	12
Wind	12
Bathymetry	15
Freshwater Inflow	15
Hillsborough River	17
Alafia River	18
Little Manatee River	19
Manatee River	20
Rocky Creek	20
Lake Tarpon Canal	21
Sweetwater Creek	21
Non-Point Sources	21
Nutrients Distribution and Loading	22
Sediment Type and Distribution	25
3 THE CIRCULATION AND TRANSPORT MODEL	29
Previous Work	29
Circulation Model	31
Continuity Equation	31

X-component of Momentum Equation	32
Y-component of Momentum Equation	32
Hydrostatic Pressure Relation	32
Salinity Equation	33
Equation of State	34
Conservative Species Equation	34
Sediment Transport Model	35
Curvilinear Boundary-Fitted and Sigma Grid	36
Boundary and Initial Conditions	38
Vertical Boundary Conditions	38
Lateral Boundary Conditions	40
 4 THE WATER QUALITY MODEL	 42
Previous Work	42
Development of the Numerical Model	47
Mathematical Formulation	49
Nutrient Dynamics in Estuarine Systems	50
Ammonia Nitrogen	52
Dissolved Ammonium Nitrogen	53
Nitrite+Nitrate Nitrogen	55
Soluble Organic Nitrogen	57
Particulate Organic Nitrogen	58
Particulate Inorganic Nitrogen	58
Algal Nitrogen	59
Zooplankton Nitrogen	59
Sorption and Desorption Reactions	60
Phytoplankton Dynamics in Estuarine Systems	61
Oxygen Balance in Estuarine Systems	63
Light Attenuation in Estuarine Systems	66
Model Coefficients	70
 5 THE SEAGRASS MODEL	 75
Using Seagrass as a Bioindicator of the Estuarine System	75
Seagrass Ecosystems	76
Previous Work	79
Development of the Numerical Model	81
Mathematical Formulation	84
Light	84
Temperature	85
Density-dependent Growth Rate	85
Growth Rate Dependence on Light	87

Growth Rate Dependence on Salinity	89
Growth Rate Dependence on Temperature	92
Growth Rate Dependence on Sediment Nutrients	94
6 APPLICATION OF THE CIRCULATION AND TRANSPORT MODEL	95
Design of Tampa Bay Grid	95
Forcing Mechanisms and Boundary Conditions	101
Modeling Strategy	111
Results of the Barotropic Simulation	111
Results of the Baroclinic Simulation	115
Tides	117
Currents	124
Salinity	144
Validation of the Model	153
Residual Circulation	164
Results of the Suspended Sediment Simulation	173
7 CALIBRATION OF THE WATER QUALITY MODEL	181
Initial and Boundary Conditions of the Water Quality Model	184
Water Column	184
Sediment Column	197
Modeling Strategy	208
Sensitivity Analysis	208
Simulation of the Summer 1991 Condition	220
Dissolved Oxygen	221
Phytoplankton	234
Nitrogen Species	246
Tidal Exchange	257
Nutrient Budget	261
Load Reduction Simulations	265
Comparison with ASCl (1996) study	267
Comparison with Coastal Inc. (1995) study	270
Advantages and Limitations of this Integrated Modeling Approach	271
8 CALIBRATION OF THE SEAGRASS MODEL	273
Initial Conditions	276
Sensitivity Analysis	278
Simulation of the Summer 1991 Condition	290
Load Reduction Simulation	292

9 CONCLUSION AND RECOMMENDATIONS	299
APPENDICES	
A NUMERICAL SOLUTION OF THE EQUATIONS	304
B MODELING SEDIMENT DYNAMICS	324
C DISSOLVED OXYGEN SATURATION AND REAERATION EQUATIONS	334
D LIGHT MODEL EQUATIONS	335
E RESULTS OF THE SUMMER 1991 SIMULATION	337
F SENSITIVITY TESTS OF THE SEAGRASS MODEL	357
REFERENCES	370
BIOGRAPHICAL SKETCH	388

LIST OF FIGURES

<u>Figure</u>	<u>page</u>
2.1 - Tampa Bay Estuarine System subdivisions as defined by Lewis and Whitman (1985) (from Wolfe and Drew, 1990).	9
2.2 - Monthly rainfall in Tampa Bay (Wooten, 1985).	13
2.3 - Seasonal wind pattern in Florida (Echternacht, 1975).	14
2.4 - Tampa Bay watershed (Wolfe and Drew, 1990).	16
2.5 - Surface Sediments in Tampa Bay (Goodell and Gorsline, 1961).	27
2.6 - Mud zone in Hillsborough Bay (Johansson and Squires, 1989).	28
5.1 - Seagrass species commonly found in west Florida (from Phillips and Meñez, 1987).	78
5.2 - Structure and components of the numerical seagrass model used for this study.	82
5.3 - Epiphytic algae model flow chart.	83
5.4 - Seagrass model flow chart.	83
5.5 - Seagrass density-dependent maximum growth rate: <i>Thalassia</i> (dotted line), <i>Halodule</i> (solid line), and <i>Syringodium</i> (dash-dotted line).	86
5.6 - Seagrass growth rate dependence on light: <i>Thalassia</i> (dotted line), <i>Halodule</i> (solid line), and <i>Syringodium</i> (dash-dotted line).	87
5.7 - Seagrass growth rate dependence on salinity: <i>Thalassia</i> (dotted line), <i>Halodule</i> (solid line), and <i>Syringodium</i> (dash-dotted line).	91
5.8 - Seagrass growth rate dependence on temperature: <i>Thalassia</i> (dotted line), <i>Halodule</i> (solid line), and <i>Syringodium</i> (dash-dotted line).	93

6.1 - NOAA's TOP station locations in Tampa Bay.	97
6.2 - A boundary-fitted grid for the Tampa Bay Estuarine System.	98
6.3 - Tampa Bay bathymetric contours.	99
6.4 - Bay segments (Sheng and Yassuda, 1995).	100
6.5 - Tidal forcing for the 1990 simulation.	102
6.6 - Tidal forcing for the 1991 simulation.	103
6.7 - Initial salinity distribution (surface) for the 1990 simulation.	104
6.8 - Initial salinity distribution (surface) for the 1991 simulation.	105
6.9 - Rainfall data for the 1990 and 1991 simulations.	107
6.10 - River discharges for the 1990 and 1991 simulations.	108
6.11 - Wind velocity for the 1990 simulation.	109
6.12 - Wind velocity for the 1991 simulation.	110
6.13 - Surface elevation at Egmont Key and St.Petersburg (September 1990).	113
6.14 - Surface elevation at Davis Island and Old Tampa Bay (September 1990).	114
6.15 - Spectra of water surface elevation for the 1990 simulation.	119
6.16 - Simulated and measured bottom velocity at Egmont Channel - September/1990.	126
6.17 - Simulated and measured surface velocity at Egmont Channel - September/1990.	127
6.18 - Simulated and measured bottom velocity at Skyway Bridge - September/1990.	129
6.19 - Simulated and measured mid-depth velocity at Skyway Bridge - September/1990.	130

6.20 - Simulated and measured surface velocity at Skyway Bridge - September/1990.	131
6.21 - Simulated and measured bottom velocity at Port of Manatee Channel - September/1990.	133
6.22 - Simulated and measured surface velocity at Port of Manatee Channel - September/1990.	134
6.23 - Simulated and measured bottom velocity at Port of Tampa Channel - September/1990.	135
6.24 - Simulated and measured bottom velocity at Port of Tampa Channel - September/1990.	137
6.25 - Energy density spectra of bottom currents at Skyway Bridge - September/1990.	140
6.26 - Energy density spectra of surface currents at Skyway Bridge - September/1990.	141
6.27 - Tidal current ellipses for the semi-diurnal components - September/1990. .	145
6.28 - Tidal current ellipses for the diurnal components - September/1990.	146
6.29 - Near-bottom salinity (solid line) and temperature (dashed line) at NOAA station S-4 starting at Julian Day 150 in 1990.	147
6.30 - Simulated and measured near-bottom salinity at NOAA station C-21 - September/1990.	149
6.31 - Simulated and measured near-bottom salinity at C-23 - September/1990.	150
6.32 - Simulated and measured near-bottom salinity at C-4 - September/1990.	151
6.33 - Surface elevation at St.Petersburg and Davis Island - "Marco" Storm - October/1990.	152
6.34 - Surface elevation at St.Petersburg and Davis Island - July/1991.	154

6.35 - Simulated and measured bottom current at Skyway Bridge - "Marco" Storm (October/1990).	157
6.36 - Simulated and measured surface current at Skyway Bridge - "Marco" Storm (October/1990).	158
6.37 - Simulated and measured near-bottom salinity at station S-4 - (July/1991).	159
6.38 - Simulated and measured near-surface salinity at station S-4 - (July/1991).	160
6.39 - Relative flushing for several bay segments - September/1990.	163
6.40 - Residual circulation after 30 days - September/1990.	165
6.41 - Simulated velocity field representing maximum ebb currents - September/29/1990 - 18:00.	167
6.42 - Simulated velocity field representing maximum flood currents - September/29/1990 - 10:00.	168
6.43 - Velocity cross-section at Skyway Bridge looking up the Bay. Vertical scale in meters, and horizontal scale in computational grid j-index.	170
6.44 - Salinity cross-section at Skyway Bridge looking up the Bay. Vertical scale in meters, and horizontal scale in computational grid j-index.	171
6.45 - Longitudinal distribution of salinity along the navigation channel. Vertical scale in meters, and horizontal scale in computational grid i-index.	172
6.46 - Location of the USGS station in Old Tampa Bay (Schoellhammer, 1993).	176
6.47 - Wind speed and direction, and suspended sediment concentration at USGS station during tropical storm "Marco" (Schoellhammer, 1993).	177
6.48 - Simulated significant wave height and period during tropical storm "Marco" (October/1990).	178
6.49 - Simulated wave-induced bottom shear stress and suspended sediment concentration at the USGS station for October 10 and 11, 1990.	179

6.50 - Simulated suspended sediment concentration at 6:00am - October 11, 1990.	180
7.1 - Water quality monitoring stations of the Hillsborough County Environmental Protection Commission (EPC) (Boler, 1992).	185
7.2 - Measured near-bottom dissolved oxygen concentration (mg/L) in Tampa Bay (June 1991).	186
7.3 - Measured near-surface dissolved oxygen concentration (mg/L) in Tampa Bay (June 1991).	187
7.4 - Measured organic nitrogen concentration (mg/L) in Tampa Bay (June 1991).	188
7.5 - Measured dissolved ammonium-nitrogen concentration (mg/L) in Tampa Bay (June 1991).	189
7.6 - Measured nitrite+nitrate concentration (mg/L) in Tampa Bay (June 1991).	190
7.7 - Measured chlorophyll-a concentration ($\mu\text{g/L}$) in Tampa Bay (June 1991).	191
7.8 - Measured color (Pt-Co) in Tampa Bay (June 1991).	192
7.9 - Measured turbidity (NTU) in Tampa Bay (June 1991).	193
7.10 - Water quality zones in Tampa Bay used in the model simulations of the summer of 1991 conditions.	196
7.11 - Total organic nitrogen (dry weight %) in the surface sediments of Tampa Bay during 1963 (Taylor and Saloman, 1969).	200
7.12 - Total Kjeldahl nitrogen (dry weight %) in Tampa Bay sediments, 1982-86 (Brooks and Doyle, 1992).	201
7.13 - Sedimentary nitrogen (dry weight %) in Hillsborough Bay in 1986 (COT, 1988).	202
7.14 - Location of the NOAA sediment sampling stations in 1991 (phase 1) and 1992 (phase 2) (NOAA, 1994).	203

7.15 - Total sediment nitrogen (dry weight %) obtained from NOAA (1994) data.	204
7.16 - Dry density profile for water quality zone 1 in Tampa Bay (Sheng <i>et al.</i> , 1993).	205
7.17 - Water quality parameters after 30 days for a simulation using the lower limit of the mineralization constant rate.	217
7.18 - Water quality parameters after 30 days for a simulation using the higher limit of the mineralization constant rate.	220
7.19 - Near-bottom dissolved oxygen levels after 30 days for the mineralization constant rate tests.	221
7.20 - Near-bottom dissolved oxygen concentration in Tampa Bay for June 26, after 30 days of simulation.	222
7.21 - Near-bottom dissolved oxygen concentration in Tampa Bay for July 26, after 60 days of simulation.	223
7.22 - Near-bottom dissolved oxygen concentration in Tampa Bay for August 25, after 90 days of simulation.	224
7.23 - Near-bottom dissolved oxygen concentration in Tampa Bay for September 24, after 120 days of simulation.	225
7.24 - Model results for segment-averaged near-bottom DO (solid line), segment maximum and minimum (dashed line), and the EPC data inside Hillsborough Bay.	227
7.25 - Model results for segment-averaged near-bottom DO (solid line), segment maximum and minimum (dashed line), and the EPC data inside Old Tampa Bay.	228
7.26 - Model results and measured data for near-bottom DO at EPC stations 70 and 8.	229
7.27 - Model results and measured data for near-bottom DO at EPC stations 73 and 80.	230

7.28 - Model results for segment-averaged near-bottom DO (solid line), segment maximum and minimum (dashed line), and the EPC data inside Middle Tampa Bay.	232
7.29 - Model results for segment-averaged near-bottom DO (solid line), segment maximum and minimum (dashed line), and the EPC data inside Lower Tampa Bay.	233
7.30 - Near-surface chlorophyll-a concentration in Tampa Bay for June 26, after 30 days	236
7.31 - Near-surface chlorophyll-a concentration in Tampa Bay for July 26, after 60 days	237
7.32 - Near-surface chlorophyll-a concentration in Tampa Bay for August 25, after 90 day	238
7.33 - Near-surface chlorophyll-a concentration in Tampa Bay for September 24, after 120	239
7.34 - Model results for segment-averaged near-surface chlorophyll-a (solid line) and the EPC data inside Hillsborough Bay.	241
7.35 - Model results for segment-averaged near-surface chlorophyll-a (solid line) and the EPC data inside Old Tampa Bay.	242
7.36 - Model results for segment-averaged near-surface chlorophyll-a (solid line) and the EPC data inside Middle Tampa Bay.	244
7.37 - Model results for segment-averaged near-surface chlorophyll-a (solid line) and the EPC data inside Lower Tampa Bay.	245
7.38 - Near-surface Kjeldahl nitrogen concentration in Tampa Bay for June 26, after 30 days of simulation	247
7.39 - Near-surface Kjeldahl nitrogen concentration in Tampa Bay for July 26, after 60 days of simulation	248
7.40 - Near-surface Kjeldahl nitrogen concentration in Tampa Bay for August 25, after 90 days of simulation	249
7.41 - Near-surface Kjeldahl nitrogen concentration in Tampa Bay for September 24, after 120 days of simulation	250

7.42 - Model results for near-bottom segment-averaged Kjeldahl nitrogen (solid line) and the EPC data inside Hillsborough Bay.	252
7.43 - Model results for near-bottom segment-averaged Kjeldahl nitrogen (solid line) and the EPC data inside Old Tampa Bay.	253
7.44 - Model results for near-bottom segment-averaged Kjeldahl nitrogen (solid line) and the EPC data inside Middle Tampa Bay.	254
7.45 - Model results for near-bottom segment-averaged Kjeldahl nitrogen (solid line) and the EPC data inside Lower Tampa Bay.	256
7.46 - Measured and simulated transport across the mouth of Hillsborough Bay, along with the Kjeldahl nitrogen concentration (mean and standard deviation) presented by Rines (1991).	259
7.47 - Measured and simulated transport across the entrance of Tampa Bay, along with the Kjeldahl nitrogen concentration (mean and standard deviation) presented by Rines (1991).	260
7.48 - Simulated nitrogen cycle for the summer of 1991 conditions: (a) Loading, (b) biogeochemical processes in the water column, (c) biogeochemical processes in the sediment column.	264
7.49 - Near-bottom dissolved oxygen concentration in Tampa Bay, after 60 days of the load reduction simulation.	268
7.50 - Near-surface chlorophyll-a concentration in Tampa Bay, after 60 days of the load reduction simulation.	269
8.1 - Extent of seagrass meadows in Tampa Bay. (a) corresponding to 1943, and (b) to 1983 (Lewis <i>et al.</i> , 1985).	274
8.2 - Initial seagrass distribution in the computational grid. Dark areas indicate seagrass meadows (100 gdw/m ²).	277
8.3 - Simulated seagrass biomass in Tampa Bay.	279
8.4 - Growth rate dependence on temperature.	281
8.5 - Growth rate dependence on light.	282

8.6 - Growth rate dependence on salinity.	283
8.7 - Growth rate dependence on sediment nutrient concentration.	284
8.8 - Simulated seasonal distribution of <i>Thalassia</i>	286
8.9 - Simulated <i>Thalassia</i> biomass in Tampa Bay for July 26, after 60 days of simulation.	293
8.10 - Simulated <i>Halodule</i> biomass in Tampa Bay for July 26, after 60 days of simulation.	294
8.11 - Simulated <i>Syringodium</i> biomass in Tampa Bay for July 26, after 60 days of simulation.	295
8.12 - Near-bottom light levels in Tampa Bay for July 26, after 60 days of simulation.	296
8.13 - Comparison between simulated light levels for the Present Condition simulation (solid line) and the 100% Load Reduction (dashed line).	297

LIST OF TABLES

<u>Table</u>	<u>page</u>
2.1 - Area of the subdivisions in Tampa Bay (Lewis and Whitman, 1985).	10
2.2 - Surface water discharges to Tampa Bay (Lewis and Estevez, 1985).	17
2.3 - 1991 annual average water quality of eight point sources discharging into Tampa Bay (Boler, 1992) and (USGS, 1991) (mg/L).	22
2.4 - Mean annual total nitrogen loading into each segment of Tampa Bay (Coastal, 1994)	25
4.1 - Description of the coefficients used in the water quality model.	70
4.2 - Literature ranges and values of the coefficients used in the water quality model.	72
6.1 - The rms error (Erms) between measured and simulated water surface elevation - September/90.	117
6.2 - The distribution of tidal energy for water surface elevation - September 1990.	120
6.3 - Major tidal constituents in Tampa Bay - September/1990.	123
6.4 - The rms error between measured and simulated bottom (b) and surface (s) currents - September/1990.	138
6.5 - The distribution of tidal energy for bottom (b) and surface (s) currents - September 1990.	142
6.6 - The rms error between measured and simulated salinity - September 1990.	153
6.7 - The rms error between measured and simulated water surface elevation October/1990 and July/91.	155

6.8 - The rms error between measured and simulated bottom (b) and surface (s) currents - "Marco" Storm.	156
6.9 - The rms error between measured and simulated salinity - July/1991.	161
7.1 - Estimated total suspended solids concentration (TSS), and calculated water column partition coefficients for particulate organic nitrogen (pcon) and adsorbed ammonium (pcan).	197
7.2 - Estimated dry density for the sandy zones of Tampa Bay.	206
7.3 - Initial nitrogen concentration in the sediment (Ae) aerobic layer, and (An) anaerobic layer for each water quality zone. (SON) soluble organic nitrogen, (NH4) dissolved ammonium nitrogen, (NO3) nitrite+nitrate.	207
7.4 - Model coefficients in the (W) water column, (Ae) aerobic layer, and (An) anaerobic layer for each water quality zone.	207
7.5 - Parameters, baseline values, and range used in the sensitivity analysis.	210
7.6 - Sensitivity tests description.	211
7.7 - Sensitivity analysis results.	213
7.8 - Nitrogen budget between July 1 and August 31, 1991.	263
8.1 - Sensitivity tests description.	287
8.2 - Simulated and reported seagrass biomass in the Tampa Bay area.	290

Abstract of Dissertation Presented to the Graduate School
of the University of Florida in Partial Fulfillment of the
Requirements for the Degree of Doctor of Philosophy

INTEGRATED MODELING OF THE TAMPA BAY ESTUARINE SYSTEM

By

Eduardo Ayres Yassuda

December 1996

Chairperson: Dr. Y. Peter Sheng

Major Department: Coastal and Oceanographic Engineering

Integrated modeling of the Tampa Bay Estuarine System is conducted in an attempt to further the understanding of estuaries as integrated systems, and to provide quantitative assessment of various management practices. The primary objective is to use models and field data to produce a detailed characterization of the hydrodynamics and water quality dynamics within the system. To test the hypothesis that seagrass is a bioindicator of the overall health state of the estuarine system, a conceptual seagrass model is coupled to the hydrodynamics and water quality models. The integrated model is then used to study the effect of anthropogenic inputs to the estuarine system.

This study combines the enhanced versions of a 3-D hydrodynamics model (Sheng, 1989), a 3-D water quality model (Chen and Sheng, 1994), and a seagrass model (Fong and Harwell, 1994) to simulate the circulation, transport, water quality, and seagrass dynamics in Tampa Bay. The hydrodynamics component of this integrated model has been successfully calibrated and verified using Tampa Bay data provided by the National Oceanic

and Atmospheric Administration (NOAA) and the United States Geological Survey (USGS). The effects of hydrodynamics have been incorporated into the water quality model by using the same grid spacing and time step, hence eliminating the need for ad-hoc tuning of advective fluxes and dispersion coefficients. The water quality component has been tested using monthly water quality data provided by the Hillsborough County Environmental Protection Commission (EPC), although a more comprehensive data set is needed to fully validate the water quality model. Results of previous statistical and mass-balance models were used to determine the relevant biogeochemical processes, and to test causal relationships among state variables. These simple models also proved to be useful tools for calibration of the water quality model coefficients in the absence of process-specific data (e.g., remineralization, nitrification, denitrification). Incident-light data provided by USGS allowed the calibration of a light model of the MacPherson and Miller (1994) type. The seagrass model has been used to investigate the ecological relationships between nutrient loading, water quality dynamics, and the response of seagrass.

Once validated, this integrated model can be used to determine nutrient loading reduction targets required to maintain and expand seagrass meadows in Tampa Bay. Simulated load reduction scenarios indicate that water quality can respond quickly (within 2 months), while seagrass responds more slowly (more than 6 months) to load reduction. Nevertheless, the results indicate that integrated modeling is a viable approach to provide quantitative assessment of various management practices for restoring estuarine systems.

CHAPTER 1 INTRODUCTION

Background

Historically, an estuary has been defined as "a semi-enclosed coastal body of water which has a free connection with the open sea and within which the sea water is measurably diluted with fresh water derived from continental drainage" (Cameron and Pritchard, 1963 - p. 306). In order to assess environmental problems along the entire coastal zone, the classical definition of estuary was revised by the National Research Council (1977) to include not only the estuary from the classical definition, but also all coastal environments characterized as transitional zones. Following this new definition, an estuarine system comprises bays, coastal lagoons, inlets, deltas, and salt marshes; all affected by different tidal regimes and freshwater discharges.

In an estuarine system, the region characterized by accentuated gradients of some specific properties is defined as the mixing zone (Harleman, 1971). It is usually located between two stable zones, the freshwater and the oceanic ecosystems, wherein these properties are treated as "reservoirs," with relative slower temporal variations.

Salinity is the primary physical property that presents a markedly longitudinal gradient. Upstream from the tidal portion of the river, salinity is usually constant and nearly equal to

zero. In the coastal zone beyond the region of freshwater influence, salinity is equal to the "oceanic reservoir" condition.

In a cross-section, the mixing zone reveals important vertical gradients. The most evident is the intertidal zone, which is periodically flooded and exposed. In the intertidal zone, there may be salt marshes, mangroves, beaches, and oyster banks. To overcome the stresses originated by flood and dry conditions, organisms living in this zone have developed special adaptations. Human presence is visible through structures like seawalls, piers, and harbors.

According to Day *et al.* (1989), a second important vertical gradient is light attenuation, going from a lighted, euphotic zone to a light depleted, aphotic zone. Where the euphotic zone reaches the bottom, submerged aquatic vegetation like seagrasses is able to thrive. Usually, water clarity also increases towards the ocean side. Another extremely important gradient for biogeochemical processes is the redox potential in the sediment layer, ranging from oxidized to reduced conditions. In a healthy estuarine system, the water column is usually aerobic, but the bottom sediments become anaerobic in a very short distance (order of few centimeters) from the water-sediment interface.

Water Quality Modeling

The primary requirement in any estuarine water quality modeling is a thorough understanding of the circulation and transport processes. Differently from freshwater systems, where uni-directional flow and steady-state conditions may be applied in a variety of cases,

estuaries are complex systems where the circulation dynamics are driven by tides, wind, river discharges, waves, Coriolis force, and density gradients, which give the estuarine circulation an unsteady, multi-dimensional character. The baroclinic effect in estuarine circulation has been studied by various investigators, including the classical works of Pritchard (1956), Cameron and Pritchard (1963), and Hansen and Rattray (1965).

Weisberg and Williams (1991) demonstrated that horizontal salinity gradients in Tampa Bay are capable of creating a density-driven circulation, through the generation of a baroclinic forcing. Galperin *et al.* (1991) refuted the barotropic residual circulation pattern obtained by Goodwin (1987) and Ross *et al.* (1984) in Tampa Bay, showing that when baroclinic effects are included, the residual circulation changed substantially.

Models with a limited resolution (spatial and time scales) are useful tools to depict a general trend in the overall circulation pattern or to study the response of the system to a specific forcing mechanism. However, estuarine processes are not in steady state, and they often present a three-dimensional distribution. Biogeochemical and ecological processes occurring inside an estuarine system are primarily driven by physical factors with an unsteady, multi-dimensional character. To implement an integrated hydrodynamics, water quality and ecological model, it is essential to fully understand the coupling among the hydrodynamics, water quality and ecological processes.

Integrated Modeling Approach for Estuarine Systems

Competitive demands for natural resources in estuarine systems can lead to a serious deterioration of the environment. Solutions to environmental problems have been attempted by resources management agencies to support a holistic approach to environmental management. For example, the Florida Department of Environmental Protection has been emphasizing that ecosystem management is an integrated, flexible approach to manage Florida's biological and physical environment.

An efficient strategy to prevent or reverse the degradation of important estuarine systems makes use of numerical models in conjunction with monitoring programs. Through monitoring, not only the present state of the system can be obtained, but it is also possible to evaluate the effectiveness of past management efforts.

Numerical models can be used to study management options and the corresponding response of the system. In estuarine systems, numerical models can be applied to study the hydrodynamics, sediment dynamics, water quality dynamics and system ecology.

Hydrodynamics and sediment dynamics models have been significantly advanced during the past decade (e.g., Sheng, 1994). The developments in numerical techniques and computer technology have been fully capitalized. Also, advancement in instrumentation and basic understanding has led to the development of process-based models rather than empirical lumped-process models.

On the other hand, applications of traditional water quality models (e.g., Ambrose *et al.*, 1994) are often based on coupling the hydrodynamics and water quality dynamics on an

intertidal basis (i.e., tidally averaged). This simplification was supported by high computational cost of robust multi-dimensional models and the large time scale of the kinetics in water quality models. But, by doing so, several hydrodynamic processes (e.g., wave actions) and sediment dynamics (e.g., resuspension, deposition) which can significantly affect the water quality dynamics are not accurately represented. Chen and Sheng (1994) developed an integrated hydrodynamics-sediment-water quality model applied it to Lake Okeechobee. A coupled hydrodynamics-water quality model has been used to study the response of Chesapeake Bay to various loading scenarios (Chesapeake Bay Program, 1994).

A useful application of a reliable water quality model is the development of a budget for the specific pollutant of interest. In the case of Tampa Bay, where eutrophication is one of the issues of greatest concern, nutrient loading levels have to be defined. To develop a nutrient budget it is essential to quantify the sources of (Sheng *et al.*, 1993): (i) external nutrient loading from tributaries and non-point sources, (ii) nutrient fluxes into and from the connecting ocean, and (iii) benthic nutrient fluxes. The most difficult source to quantify is the benthic flux, due to measurement techniques, and the competing influences of molecular diffusion, resuspension, and groundwater seepage. Consequently, it is common to find nutrient budgets that consider the net benthic flux to be simply the difference between the external loading and flux to the ocean. However, the oceanic flux, induced primarily by tidal forcing is also difficult to estimate; hence, subtracting tidally-averaged oceanic flux from the external loading may not give the correct benthic flux. Results of McClelland (1984) nutrient box model of Tampa Bay shows that nitrogen benthic flux can be as much as twice the external loading of point and non-point sources. The author suggested that the supply of

nitrogen through sediment resuspension and biogeochemical reactions in the water column are likely important. Results of Johansson and Squires (1989) nutrient budget for Tampa Bay suggest that the internal loading of nitrogen associated with sediment resuspension events can be quite significant.

Ecological models are the primary tool in developing an overall picture of the system. Using energy flow and Emergy concept (Odum, 1994), it is possible to identify the main forcing functions that drive the system, and the causal relationships between state variables. The conflicts between the "apparently" adversarial uses of an estuarine system can be better mediated when they are evaluated on a common measure. System ecology models can be used to connect environmental products with human use. The Emergy of the system measures both the work of nature and that of humans in generating products and services. By selecting choices that maximize Emergy production and use, policies and judgments can favor those environmental alternatives that maximize real wealth, the whole economy, and the public benefit (Odum, 1971).

In estuarine systems where seagrass has declined due to anthropogenic effects, restoration of seagrass beds can be linked exclusively to environmental quality. In this sense, seagrass provides a more direct assessment of the restoration processes (Dennison *et al.*, 1993). Seagrasses serve as habitat for fish and benthic invertebrates. Seagrass leaves provide substrate for many epiphytic organisms. Herbivores such as manatees, fishes, sea turtles, and sea urchins graze directly on seagrass blades. Dead leaves can constitute the majority of the detritus pool. Seagrass also interacts with the physical components of the estuary by slowing down the currents and enhancing the deposition of organic and inorganic material from the water column. Their presence also inhibit the resuspension of sediments, which also affects the nutrient cycles. Therefore, seagrass is a crucial indicator of the state of the estuary.

Objectives

Recognizing the important relationships among the various ecological components (including hydrodynamics, sediment dynamics, water quality, aquatic vegetation, etc.), it is now appropriate to take advantage of the advancement in computer resources and scientific understanding to integrate models with multiple dimensions, more robust and coupled processes. The purpose of this effort would be to further the understanding of estuaries as an integrated system, and to provide a quantitative evaluation of various management practices.

The goals of this study are to conduct an integrated modeling of the Tampa Bay Estuarine System, and to produce a detailed characterization of the hydrodynamics and water quality dynamics within the system. In order to test the hypothesis that seagrass is a bioindicator of the overall health state of the Tampa Bay Estuarine System, a conceptual seagrass model is coupled to the hydrodynamics and water quality models. This integrated model will then be used to provide mechanisms for relating anthropogenic inputs to the overall health of the estuary. The following questions have to be addressed in order to accomplish these goals:

- 1) How important are the three-dimensional characteristics of the estuarine circulation in the overall dynamics of the system?
- 2) What are the most important environmental parameters and biogeochemical processes in the water quality dynamics of the estuarine system?
- 3) Can the integrated modeling provide a quantitative assessment of various management practices for restoring the estuarine system?

CHAPTER 2

TAMPA BAY CHARACTERIZATION

Tampa Bay, classified as a subtropical estuarine system (Lewis and Estevez, 1988), is the largest coastal plain estuary in the state of Florida. It is located on the west central part of the Florida peninsula, between coordinates 27° 30' and 28° 02' N, and 82° 20' and 82° 50' W. The Y-shaped bay is approximately 60 km long, 15 km wide, covering approximately 1,000 km², and having a shoreline 1450 km long (Lewis and Whitman, 1985). It is a highly complex system composed of numerous basins and subdivisions (Figure 2.1). Some of them (e.g. Hillsborough Bay) are bordered by highly industrialized and urbanized areas and others are bordered by mangroves, bayous, and seagrasses (e.g. Boca Ciega Bay). Table 2.1 shows the morphometric features of each subdivision (Lewis and Whitman, 1985). Major anthropogenic modifications that have altered the natural evolution of the system are the four causeways (Sunshine Skyway Bridge, Courtney-Campbell Parkway, W. Howard Frankland Bridge, and Gandy Bridge), an extensive network of dredged channels, turning basins, and spoil islands.

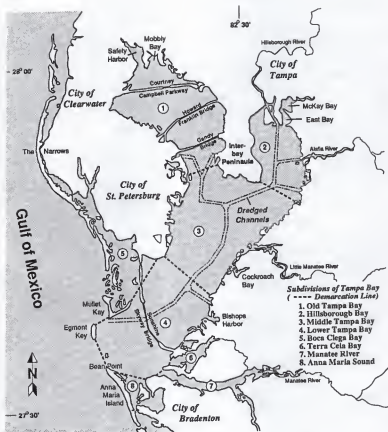


Figure 2.1 - Tampa Bay Estuarine System subdivisions as defined by Lewis and Whitman (1985) (from Wolfe and Drew, 1990).

Table 2.1 - Area of the subdivisions in Tampa Bay (Lewis and Whitman, 1985).

Subdivision	Area (km ²)
Old Tampa Bay	201
Hillsborough Bay	105
Middle Tampa Bay	310
Lower Tampa Bay	247
Boca Ciega Bay	93
Terra Ceia Bay	21
Manatee River	55
Total	1032

Climate

The Tampa Bay Estuarine System is located in a zone of transition between a temperate continental climate and a tropical Caribbean one (Lewis and Estevez, 1988). The climate of the Tampa Bay area generally consists of a warm humid summer and a relatively dry cool winter. Lewis and Estevez (1988) suggested three weather regimes for the Bay: the warm, dry period between late April to mid-June, the warm, wet period during summer and early fall, and the dry cold period between November to April. Based on four decades of records, the mean annually averaged temperature in Tampa Bay is 22.3 °C, with a low mean of 16.0 °C in January and a high mean of 27.8 °C in August (Lewis and Estevez, 1988). Annual variation in water temperature ranges from 16 to 30 °C, with a vertical stratification of no more than 2 °C (Boler, 1992).

Tides

Tides and currents in the Gulf of Mexico are classified as mixed type, with K_1 , O_1 , and P_1 the major diurnal and M_2 and S_2 the major semi-diurnal components. The strong diurnal components are attributed to the interaction between co-oscillating tides propagating from the Florida Straits and Yucatan Channel and the natural frequency of the Gulf of Mexico basin. The average tidal range is 0.67 m, while typical current speeds range from 1.2 to 1.8 m/s at the entrance (Egmont Channel), to much smaller values in the upper reaches of the Bay (NOAA, 1993). The tidal wave takes approximately three hours to travel from the mouth to the upper reaches of Hillsborough Bay, and approximately 4 hours to upper Old Tampa Bay. Harmonic analysis of year-long tidal records at St. Petersburg (NOAA, 1993) yielded amplitudes of 37 constituents, which indicated that the shallow water components are relatively small, and overtides are not significant in the overall circulation pattern of the Bay.

Salinity Distribution

As in any other typical estuarine system, Tampa Bay generally exhibits significant horizontal gradients in salinity. The higher salinity values in the adjacent Gulf of Mexico fluctuate around 36 ppt, whereas the lowest salinity levels occur near the mouth of creeks and rivers. Generally, the salinity distribution follows the annual precipitation pattern (Boler, 1992). Higher salinity tends to extend further up into the Bay during the dry winter and spring, and the entire Bay becomes less saline, specially in the upper parts, during the wet

summer and fall. Vertically, salinity generally shows a homogeneous profile, with vertical difference rarely exceeding 2 ppt.

Rainfall

Mean annual precipitation is approximately 140 cm (Heath and Connover, 1981), which on an annual basis balances with evapotranspiration (Palmer, 1978). Dry season rains vary from 5 to 6.5 cm per month. Wet season rainfall is much more variable, both temporally and spatially, ranging from 13 to over 20 cm (Palmer, 1978). Figure 2.2 illustrates the monthly rainfall pattern for Tampa Bay.

Wind

The annual average wind speed is 3.9 m/s from the east. The four seasonal wind-field patterns are shown in Figure 2.3. In the winter months, the easterly trade winds dominate the region south of latitude 27° N, while the westerlies dominate the area north of latitude 29° N. Spring and Summer generally exhibit more southerly winds, and Fall is characterized by easterly or northeasterly winds. Wind speed can exceed 10 m/s during the passage of winter storms or during summer squalls, hurricanes and tornadoes (Wolfe and Drew, 1990).

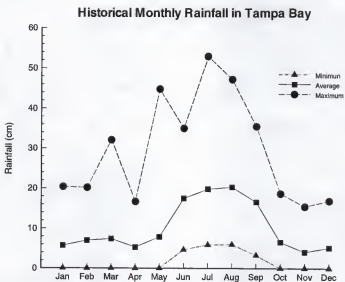


Figure 2.2 - Monthly rainfall in Tampa Bay (Wooten, 1985).

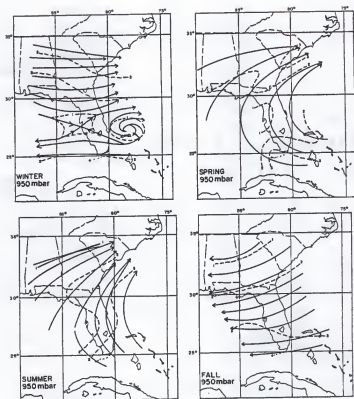


Figure 2.3 - Seasonal wind pattern in Florida (Echternacht, 1975).

Bathymetry

Tampa Bay is a relatively wide and shallow estuarine system, with an average depth of 3.7 m (Goodwin, 1987). Depth generally does not exceed 10 m, except along the 96-km-long navigational channel, which has been dredged to about 15 m. The navigational channel extends parallel to the shorelines from the mouth to the upper reaches of Middle Tampa Bay, where it splits into two branches, one connecting to the Port of Tampa in Old Tampa Bay, and the other one entering Hillsborough Bay.

Freshwater Inflow

Unlike other well-studied estuarine systems in the U.S. (e.g. Chesapeake Bay, Delaware Bay, etc.), Tampa Bay is not associated with any large river. All tributaries flowing into Tampa Bay originate in the Florida peninsula, and therefore are relatively small (Figure 2.4). The Bay receives drainage from a watershed that covers approximately 5700 km², which delivers an average annual discharge of about 63 m³/s (Lewis and Estevez, 1988). The analysis of existing and historical freshwater inflows to Tampa Bay (Coastal, 1994) demonstrated that inflows have not changed significantly in the past fifty years.

Table 2.2 shows the historical average discharge values for seven rivers or streams flowing into Tampa Bay. The primary source of freshwater are the four major tributaries (Hillsborough River, Alafia River, Little Manatee River, and Manatee River) which supply about 70% of the total discharge. It has been estimated that Hillsborough Bay receives 63 to 77% of the total freshwater inflow to Tampa Bay (Lewis and Estevez, 1988).

Table 2.2 - Surface water discharges to Tampa Bay (Lewis and Estevez, 1985).

River	Period of Record (years)	Average annual discharge (m ³ /s)
Hillsborough River	39	17.0
Alafia River	45	14.0
Little Manatee River	38	6.0
Manatee River	11	11.0
Rocky Creek	24	1.3
Lake Tarpon Canal	3	0.8
Sweetwater Creek	26	0.6
Others	-	12.3
Total		63.0

Hillsborough River

Draining a highly urbanized area, the Hillsborough River watershed collects the discharge from most of Tampa, Temple Terrace, the eastern Interbay Peninsula, and Davis Island. A dam constructed in 1945 (approximately 16 km from the mouth of the river in Hillsborough Bay) separates two distinct water quality and hydrological environments: upstream of the dam, the river is a freshwater reservoir, which provides freshwater to the City of Tampa; and downstream of the river proper, which is tidal and brackish. Freshwater discharges are controlled by the dam and range from 3.5 m³/s in the dry season to 48 m³/s during the wet season, averaging 17 m³/s (Dooris and Dooris, 1985). Tidal action can be found at 16 km upstream the mouth (Wolfe and Drew, 1990). The salt wedge can penetrate

as far as 13 km into the river during low-flow conditions ($< 3 \text{ m}^3/\text{s}$), or it can be flushed downstream to near 4 km from the mouth when the flow exceeds $25 \text{ m}^3/\text{s}$ (Wolfe and Drew, 1990). Low flow rates and upstream salt wedge location seem to be well correlated with low dissolved oxygen (DO) value and high nutrient concentrations inside the Hillsborough River. A report from the Hillsborough County Environmental Protection Commission (EPC) (Boler, 1992) shows DO levels in the bottom saltier layer inside Hillsborough River below 4.0 mg/L , with lowest values ($< 2.0 \text{ mg/L}$) in May and June when flow is minimal. Surface values of DO are generally above saturation (7.9 mg/L). BOD is reported to be less than 2.0 mg/L throughout the year.

Ammonia and nitrate concentrations generally show a well mixed vertical distribution upstream the salt wedge location, where the saltier water contains higher concentrations, specially ammonia. Combined ammonia and nitrate values in the river range from 0 to 0.7 mg/L . In the dry season ammonia concentrations vary from 0.05 mg/L close to the dam to $0.2\text{-}0.3 \text{ mg/L}$ towards the Bay. Nitrate concentrations vary from zero to 0.4 mg/L , and organic nitrogen ranges from 0.38 to 5.60 mg/L (Wolfe and Drew, 1990).

Alafia River

The Alafia River watershed drains about 105 km^2 , south of the Hillsborough River watershed. Flow in the Alafia River averages $14 \text{ m}^3/\text{s}$ and ranges from $5.4 \text{ m}^3/\text{s}$ in the dry season to $28.3 \text{ m}^3/\text{s}$ during the wet season (Dooris and Dooris, 1985). Tidal action is present up to 18 km upstream from the mouth. Johansson and Squires (1989) found that the Alafia River, a major source of dissolved material to the Bay, can supply 51% of the Bay's

phosphate uptake for phytoplankton growth, and sediment flux rates are sufficient to meet 140% of the uptake. The authors attributed the high phosphate concentrations to leaching of Florida's phosphate beds, fertilizer drainage from agricultural lands, and industrial and sewage inputs. Phosphate concentration ranges from 4.8 mg/L in the upper reaches of the river, decreasing to 1.2 mg/L near the Bay (Wolfe and Drew, 1990).

The salt wedge penetration depends on the river discharge and tidal regime, ranging from 16 km during high tide and low flow condition to 4 km during low tide high flow situation (Giovannelli, 1981).

Dissolved oxygen exhibits a vertical stratification near the mouth, ranging from below 4.0 mg/L at middle and bottom layers to saturation levels (7.9 mg/L) at the surface (Boyer, 1992), where chlorophyll-*a* averages 24.1 $\mu\text{g/L}$.

The Alafia River tributaries exhibit high levels of nutrients. The poor water quality in the North Prong is due to mining activities, and a greater number of phosphate and chemical dischargers (Wolf and Drew, 1990). High levels of ammonia can reach as much as 85-120 mg/L, and nitrate values as high as 3.0 mg/L. Dissolved oxygen remains below 5 mg/L 50% of the time.

Little Manatee River

The Little Manatee watershed is the least urbanized of the four major rivers, and it generally exhibits the best water quality conditions (Flannery, 1989). Flow averages 6 m^3/s and ranges from 1.7 m^3/s in the dry season to 17 m^3/s during the wet season (Dooris and Dooris, 1985). Tidal action is found up to 25 km upstream the mouth (Wolfe and Drew,

1990). Salinity close to the mouth averages 9.0 to 12.0 ppt (EPC, 1984). Flannery (1989) presented some water quality data for a station 25 km upstream from the mouth, which showed the following average concentrations: 0.63 mg/L of nitrate+nitrite, 0.09 mg/L of ammonia, 1.3 mg/L of BOD, 0.60 mg/L of organic nitrogen, and 7.0 mg/L of DO.

Manatee River

The Manatee River is impounded 38 km upstream from the Bay. Downstream of the dam, the Manatee River and its major tributary, the Braden River, collect drainage from the cities of Palmetto and Bradenton before discharge into the Bay. Flow averages $11 \text{ m}^3/\text{s}$ and ranges from $1 \text{ m}^3/\text{s}$ in the dry season to $25 \text{ m}^3/\text{s}$ during the wet season (Dooris and Dooris, 1985). Tidal action is present up to 31 km upstream from the mouth. Nutrient levels are high and generally decrease from the dam to the river mouth (Wolfe and Drew, 1990). Salinity ranges from 14 to 26 ppt in the dry season to 2 to 19 ppt during the wet season (Heyl, 1982). Close to the mouth, dissolved oxygen levels are low during summer months, ranging from 2.0 to 4.0 mg/L. Concentrations of total nitrogen, mostly in the organic nitrogen form, varies between 0.1 to 4.4 mg/L (Heyl, 1982).

Rocky Creek

The Rocky Creek drainage area is approximately 115 km^2 . The discharge 9.5 km upstream from the river mouth averages $1.3 \text{ m}^3/\text{s}$, ranging from 6.9 (wet season) to $0.05 \text{ m}^3/\text{s}$ (dry season) (USGS, 1991). In its upper reaches, water quality is generally good with pockets of high concentrations of ammonia and total phosphorus (Wolfe and Drew, 1990). Dissolved oxygen is usually below saturation.

Lake Tarpon Canal

The Lake Tarpon Canal is a man-made canal which was completed in 1971 to control flooding. A saltwater-barrier/flood-control structure is located midway between Lake Tarpon and Old Tampa Bay. Discharges from the canal average $0.8 \text{ m}^3/\text{s}$, ranging from $22 \text{ m}^3/\text{s}$ in wet season to no flow in dry season (USGS, 1991). DO levels are usually high (7.0 to 8.0 mg/L) in the canal, pH is neutral (7.0), and nutrient concentrations are low (Dooris and Dooris, 1985).

Sweetwater Creek

Sweetwater Creek is 17 km long and drains about 65 km^2 of a primarily urban region. The discharge at 6 km upstream from the river mouth averages $0.6 \text{ m}^3/\text{s}$, with a range between 4.4 (wet season) to $0.03 \text{ m}^3/\text{s}$ (dry season) (USGS, 1991). In the tidal portion of the creek, DO (3.7 mg/L), BOD (6.0 mg/L), and nutrient concentrations (Ammonia concentration ranging from 0.1 to 0.4 mg/L) indicate poor water quality (Wolfe and Drew, 1990).

Non-Point Sources

Coastal, Inc. (1994) developed a statistical model for the Tampa Bay National Estuary Program (TBNEP) to support the preparation of the "Pollutant Load Reduction Goals" (PLRG) for total nitrogen, total phosphorus, and total suspended solids for Tampa Bay. They used measured data to develop regression relationships to describe the response of the watershed to flow and loadings from non-point surface water sources, given a set of rainfall

and land use conditions. Results of that study indicate that non-point sources can have a significant contribution to the total nutrient loading. Moreover, the study showed that groundwater and nutrient inflow to Tampa Bay represent a smaller fraction of the total loading. Table 2.3 summarizes the water quality of the seven point sources discharging into Tampa Bay.

Table 2.3 - 1991 annual average water quality of seven point sources discharging into Tampa Bay (Boler, 1992) and (USGS, 1991) (mg/L).

River	Near-Bottom Dissolved Oxygen	Soluble Organic Nitrogen	Ammonium Nitrogen	Nitrate + Nitrite
Hillsborough River	5.0	0.66	0.07	0.04
Alafia River	4.3	0.68	0.06	0.36
Little Manatee River	5.3	0.75	0.05	0.11
Manatee River	7.1	0.52	0.01	0.08
Rocky Creek	3.0	0.93	0.07	0.02
Lake Tarpon Canal	4.4	0.89	0.10	0.04
Sweetwater Creek	4.7	0.85	0.14	0.35

Nutrients Distribution and Loading

Tampa Bay has high phosphate levels in both water column and sediment layer, especially in Hillsborough Bay. Tiffany and Wilkinson (1989) reported that 20% of world's phosphate production and 80% of all United States phosphate output take place in the area. Approximately 50% of all tonnage leaving Tampa Bay is composed of phosphate related

products. The mean annual water column phosphate concentration in Hillsborough Bay can be as high as 1.28 mg/L (Fanning and Bell, 1985).

Nitrogen, however, is probably the single most important macro nutrient that limits primary production in Tampa Bay. Assuming that phytoplankton assimilates N and P in proportion to the Redfield C:N:P atomic ratios of 106:16:1, if N:P is higher than 16, the system is primarily phosphorus limited. Otherwise, the system is considered to be nitrogen limited. Fanning and Bell (1985) reported that the N:P ratio in Tampa Bay ranged from 0.3 to 1.3 in 1981, and concluded that phytoplankton have been historically nitrogen limited.

According to Simon (1974), municipal sewage treatment plants are the primary source of nitrogen to Tampa Bay. The Alafia River provides the highest annual loading of nitrate to Tampa Bay (about 3.9×10^5 kg/yr), followed by the Manatee and Hillsborough Rivers (each about 9.0×10^4 kg/yr). In terms of organic nitrogen, the Manatee and Alafia Rivers have the highest loadings (2.5×10^5 kg/yr), followed by the Hillsborough River with 2.0×10^5 kg/yr (Dooris and Dooris, 1985). High levels of organic nitrogen in the Manatee River have been related to the Bradenton sewage treatment plant and pulp effluent from citrus processing plant (DeGrove, 1984). McClelland (1984) reported municipal sewage treatment plants elsewhere around the Bay as significant nitrogen sources. Goetz and Goodwin (1980), summarizing data collected between 1972 to 1976, obtained a mean organic nitrogen concentration ranging from 0.5-1.0 mg/L in Old Tampa Bay, around 0.5 mg/L in upper Tampa Bay, and the same level or below in the Lower Bay. In all three areas, seasonal and year-to-year variation was low. On the other hand, mean organic nitrogen concentration in Hillsborough Bay ranged from 0.75 to 1.25 mg/L, and temporal variation was greater. Nitrite

and nitrate concentrations were similarly low and steady everywhere in the Bay, except in Hillsborough Bay. Ammonia levels were variable in all zones. Seasonal minima were less than 0.1 mg/L in most places but more than 0.1 mg/L in Hillsborough Bay. Fanning and Bell (1985) reported a mean ratio of ammonia to inorganic nitrogen of 0.84 (ranging from 0.54 to 0.99) in Hillsborough Bay. Seasonality was evident for total inorganic nitrogen, which decreases substantially after rainy seasons, without an apparent reason (Lewis and Estevez, 1988).

In a preliminary nitrogen budget for Tampa Bay, Ross *et al.* (1984) suggested a nitrogen storage of 3.87×10^7 kg, an input from rainfall and anthropogenic sources of 21,470 kg/day, and a benthic release of 55,750 kg/day. Exports would occur in tidal exchange (16,100 kg/day), biological losses (8,140 kg/day), and benthic uptake (53,000 kg/day). Fanning and Bell (1985) estimated a turnover rate for nitrate and nitrite of 42 days, due to runoff, and that benthic releases of ammonia could replace the overlying ammonia in 14 days.

Coastal, Inc. (1994) developed estimates of total nitrogen, total phosphorus, and total suspended solids loading, as well as total freshwater inflow, to Tampa Bay. Two scenarios (existing and "benchmark" conditions) were presented for the major seven segments of the Bay. In order to account for ungaged areas, the Coastal, Inc. study used a statistical model that related watershed characteristics to streamflow. Table 2.4 summarizes the mean annual total nitrogen loading into each segment of Tampa Bay.

Table 2.4 - Mean annual total nitrogen loading into each segment of Tampa Bay (Coastal, 1994).

Bay Segment	Loading (tons/year)
Old Tampa Bay	600
Hillsborough Bay	2100
Middle Tampa Bay	1100
Lower Tampa Bay	500
Boca Ciega Bay	300
Terra Ceia Bay	80
Manatee River	600

Sediment Type and Distribution

Goodell and Gorsline (1961) studied the surface sediments composition and distribution from all major areas of the Bay. They reported that Tampa Bay sediments are a mixture of eroded quartz sands from Pleistocene terrace deposits and carbonates from shell fragments produced within the system. The present sediment distribution is related to tide generated currents, while sedimentary types correspond with bathymetric features. In sand and grass flats less than 2 m deep, mean grain size was determined as 0.132 mm and sediment was 2.7% carbonate. In deeper natural channels (> 6 m), mean grain size was 0.241 mm and sediment was 25.2% carbonate, whereas mangrove areas contained no carbonate. Mean grain size decreased from 0.218 mm at the mouth to 0.109 mm at the upper reaches of the Bay. Mean carbonate content decreased from 16% to 2% over the same distance. Figure 2.5

shows the surface sediment distribution for Tampa Bay. According to Johansson and Squires (1989), the descriptive work of Goodell and Gorsline (1961), conducted thirty five years ago, did not intend to map fine grained sediments specifically, so the areal coverage of these sediments was not well defined as the mud zone delineated in later studies. Figure 2.6 shows the mud zones in Hillsborough Bay delineated by the Bay Study Group of the City of Tampa Sanitary Sewer Department in 1986.

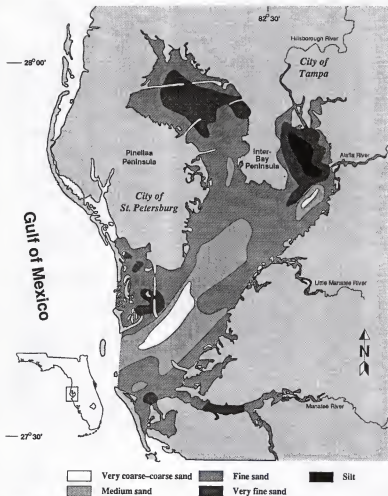


Figure 2.5 - Surface Sediments in Tampa Bay (Goodell and Gorsline, 1961).



Figure 2.6 - Mud zone in Hillsborough Bay (Johansson and Squires, 1989).

CHAPTER 3 THE CIRCULATION AND TRANSPORT MODEL

Previous Work

Circulation and sediment transport models for estuaries have been significantly advanced during the past 30 years. Sheng (1994) provided a comprehensive review on circulation models for shallow waters. Sheng (1986) and Sheng *et al.* (1991) presented comprehensive reviews of sediment transport models for estuaries and lakes.

Circulation in Tampa Bay has previously been modeled by Ross *et al.* (1984), Goodwin (1987), Galperin *et al.* (1991), Sheng and Peene (1992), Peene *et al.* (1992), and Hess (1994). The Ross *et al.* (1984) modeling system consisted of an integrated set of a 2-D vertically-averaged circulation model, and box models for water quality and particulate transport. Goodwin (1987) used a 2-D vertically-averaged model to study the effects of the dredged navigation channel and dredged disposal sites on the circulation of Tampa Bay. The residual circulation obtained from both studies (Ross *et al.*, 1984 and Goodwin, 1987) showed a complex pattern of numerous gyres, that were assumed to be responsible for poor flushing conditions. Galperin *et al.* (1991) demonstrated that the barotropic residual circulation pattern, obtained by Ross *et al.* (1984) and Goodwin (1987) in Tampa Bay, can be completely overwhelmed by baroclinic effects. The baroclinic residual circulation obtained

by Galperin *et al.* (1991) exhibited a classical two-layer flow, with the surface layer flowing out of the Bay and the saltier bottom layer flowing into the Bay. Sheng and Peene (1992), studying the circulation and transport in Sarasota Bay, used a coarse grid (grid spacing on the order of 1 to 2 km) to describe the circulation in Tampa Bay. Tampa Bay was added to the Sarasota Bay grid of that study to evaluate the importance of Manatee River discharge on the residual circulation of Anna Maria Sound. Peene *et al.* (1992) simulated the tide- and wind-driven circulation in the Sarasota and Tampa Bay system during the passage of Tropical Storm Marco in October 1990 using an earlier version of the three-dimensional boundary-fitted grid model used in this study. Hess (1994) developed a three-dimensional orthogonal curvilinear model with seven sigma grid layers for Tampa Bay, based on the Princeton University ocean model (Blumberg and Mellor, 1987). The main goals of Hess (1994) were to update the NOAA tidal current atlas for Tampa Bay, and to synthesize the extensive observational data set obtained during the survey performed by NOAA in 1990-91.

The three-dimensional hydrodynamics model CH3D (Sheng, 1989) forms the basis of the numerical simulations in this study. The model framework has been improved and modified from earlier versions (e.g., Sheng, 1989; Sheng *et al.*, 1991; Sheng and Peene, 1992) in order to develop an integrated model that couples hydrodynamics, sediment and water quality dynamics. The application (model setup, calibration, and validation) of the circulation and transport model to produce a detailed characterization of the hydrodynamics within system constituted the most important step in the development of the integrated model of the Tampa Bay Estuarine System. Within the scope of this dissertation, the complete details of

model equations in the curvilinear boundary-fitted and sigma coordinates are of secondary interest, and are therefore presented in Appendix A.

Circulation Model

The governing equations that describe the velocity and surface elevation fields in shallow water are derived from the Navier-Stokes equations. In general, four simplifying approximations are applied. First, it is assumed that the water is incompressible, which results in a simplified continuity equation. Second, based on the fact that the characteristic vertical length scale is much smaller than the horizontal counterpart, i.e., $H/L \ll 1$, the vertical velocity is small and the vertical acceleration may be neglected. Hence, the vertical momentum equation is reduced to the hydrostatic pressure relation. Third, with the Boussinesq approximation, an average density can be used in the equations except in the buoyancy term. Finally, the eddy-viscosity concept, which assumes that the turbulent Reynolds stresses are the product of mean velocity gradients and "eddy viscosities", is employed. In the transport equation, this concept means that the turbulent mass fluxes are the product of mean concentration gradients and "eddy diffusivities".

With the above assumptions, the basic equations of motion in a right-handed Cartesian coordinate system (x, y, z) are as follows:

Continuity Equation

$$\frac{\partial u}{\partial x} + \frac{\partial v}{\partial y} + \frac{\partial w}{\partial z} = 0 \quad (3.1)$$

X-component of Momentum Equation

$$\begin{aligned} \frac{\partial u}{\partial t} + \frac{\partial uu}{\partial x} + \frac{\partial uv}{\partial y} + \frac{\partial uw}{\partial z} = f_v - \frac{1}{\rho_o} \frac{\partial p}{\partial x} + \frac{\partial}{\partial x} \left(A_H \frac{\partial u}{\partial x} \right) \\ + \frac{\partial}{\partial y} \left(A_H \frac{\partial u}{\partial y} \right) + \frac{\partial}{\partial z} \left(A_V \frac{\partial u}{\partial z} \right) \end{aligned} \quad (3.2)$$

Y-component of Momentum Equation

$$\begin{aligned} \frac{\partial v}{\partial t} + \frac{\partial uv}{\partial x} + \frac{\partial vv}{\partial y} + \frac{\partial vw}{\partial z} = -f_u - \frac{1}{\rho_o} \frac{\partial p}{\partial y} + \frac{\partial}{\partial x} \left(A_H \frac{\partial v}{\partial x} \right) \\ + \frac{\partial}{\partial y} \left(A_H \frac{\partial v}{\partial y} \right) + \frac{\partial}{\partial z} \left(A_V \frac{\partial v}{\partial z} \right) \end{aligned} \quad (3.3)$$

Hydrostatic Pressure Relation

$$\frac{\partial p}{\partial z} = -\rho g \quad (3.4)$$

where (u, v, w) are mean fluid velocities in the (x, y, z) directions, p is pressure, g is the Earth's gravitational acceleration, ρ_o is a reference fluid density, $\rho(x,y,z)$ is the fluid density, and f is the Coriolis parameter. A_H and A_V are the horizontal and vertical turbulent eddy viscosity coefficients, respectively.

Salinity Equation

In Cartesian coordinates, the conservation of salt can be written as:

$$\frac{\partial S}{\partial t} + \frac{\partial(uS)}{\partial x} + \frac{\partial(vS)}{\partial y} + \frac{\partial(wS)}{\partial z} = \frac{\partial}{\partial x} \left(D_H \frac{\partial S}{\partial x} \right) + \frac{\partial}{\partial y} \left(D_H \frac{\partial S}{\partial y} \right) + \frac{\partial}{\partial z} \left(D_V \frac{\partial S}{\partial z} \right) \quad (3.5)$$

where S is the salinity, D_H and D_V are the horizontal and vertical turbulent eddy diffusivity coefficients, respectively.

Since the length scales of horizontal motion in estuarine systems are much greater than those of vertical motion, it is common to treat the vertical turbulence and horizontal turbulence separately. It has been shown (e.g. Sheng *et al.*, 1995) that in shallow estuaries, the effect of the horizontal eddy viscosities on circulation is much smaller than the effect of the vertical one. In the model, the horizontal turbulent mixing, which describes the effect of sub-grid scale motion, is represented by a constant diffusion coefficient.

Vertical turbulent mixing is an important process which can significantly affect the circulation and transport in an estuary. Since turbulence is a property of the flow instead of the fluid, it is essential to use a robust turbulence model to parameterize the vertical turbulent mixing. In this study, the vertical eddy coefficients (A_V and D_V) are computed from a simplified second-order closure model developed by Sheng and Chiu (1986) and Sheng and Villaret (1989).

Equation of State

$$\rho = \rho(T, S) \quad (3.6)$$

where ρ is density, T is temperature.

Various forms of the equation of state can be used. In the present model, the equation given by Eckert (1958) is used:

$$\begin{aligned} \rho &= P/(\alpha + 0.698P) \\ P &= 5890 + 38T - 0.375T^2 + 3S \\ \alpha &= 1779.5 + 11.25T - 0.0745T^2 - (3.8 + 0.10T)S \end{aligned} \quad (3.7)$$

where T is in $^{\circ}\text{C}$, S is in ppt and ρ is in g/cm^3 .

Conservative Species Equation

Flushing and residence time studies in an estuarine system can be carried out by solving the conservation equation for a conservative species, c_s :

$$\begin{aligned} \frac{\partial c_s}{\partial t} + \frac{\partial(u c_s)}{\partial x} + \frac{\partial(v c_s)}{\partial y} + \frac{\partial(w c_s)}{\partial z} = \\ + \frac{\partial}{\partial x} \left(D_H \frac{\partial c_s}{\partial x} \right) + \frac{\partial}{\partial y} \left(D_H \frac{\partial c_s}{\partial y} \right) + \frac{\partial}{\partial z} \left(D_V \frac{\partial c_s}{\partial z} \right) \end{aligned} \quad (3.8)$$

First, the estuarine system needs to be divided into segments with similar circulation characteristics. To study the tidal flushing, a uniform concentration is released into all the cells of a specific segment, while the concentration in the other ones are given zero values. As the simulation proceeds, the remaining mass of the conservative species in each segment

is calculated as a fraction of the original mass. The flushing capacity of each segment is then defined in terms of the reduction in the relative mass (Sheng *et al.*, 1996).

Sediment Transport Model

An integrated model of the Tampa Bay Estuarine System must contain a sediment transport model that can be used to address environmental problems related to dredging operations in the navigation channels, and especially, the ecological problems related to the adsorptive capacity of fine sediments to carry particulate forms of nutrients, heavy metals, PCB's, and other organic pollutants.

The suspended sediment model includes the advection-diffusion processes, which are computed by the hydrodynamics model, as well as such processes as erosion, deposition, flocculation, settling, consolidation, and entrainment (Sheng, 1986; Mehta, 1986).

The governing equation that represents the transport of suspended sediments is given by:

$$\begin{aligned} \frac{\partial c}{\partial t} + \frac{\partial u c}{\partial x} + \frac{\partial v c}{\partial y} + \frac{\partial (w - w_s) c}{\partial z} = \\ + \frac{\partial}{\partial x} \left(D_H \frac{\partial c}{\partial x} \right) + \frac{\partial}{\partial y} \left(D_H \frac{\partial c}{\partial y} \right) + \frac{\partial}{\partial z} \left(D_V \frac{\partial c}{\partial z} \right) \end{aligned} \quad (3.9)$$

where c is the suspended sediment concentration, w_s is the settling velocity of suspended sediment particles (positive downward), D_H is the horizontal turbulent eddy diffusivity, and D_V is the vertical turbulent eddy diffusivity.

Three simplifying approximations are implied in Equation (3.9). First, the concept of eddy diffusivity is valid for the turbulent mixing of suspended sediments. Second, the suspended sediment dynamics are represented by the concentration of a single particle size group, assuming a homogeneous distribution of sediment particles size. Third, the suspended sediment concentration is sufficiently low (≤ 1000 mg/L) such that non-Newtonian behavior can be neglected.

In this study, the determination of settling, flocculation, deposition, erosion, fluidization, and consolidation processes is based on the previous work of Sheng and Lick (1979), Sheng(1986), Hwang and Mehta (1989), Sheng *et al.* (1991), and Chen and Sheng(1994), and is described in Appendix B.

Model Equations in Curvilinear Boundary-Fitted and Sigma Grid

In three-dimensional modeling, complex bottom topographies can be better represented with the application of σ -stretching (Sheng, 1983), since it is possible to obtain the same vertical resolution for the shallow coastal areas and the deeper navigation channels. The vertical coordinate z is transformed into a new coordinate σ by (Phillips, 1957):

$$\sigma = \frac{z - \zeta(x,y,t)}{h(x,y) + \zeta(x,y,t)} \quad (3.10)$$

where ζ is the surface elevation, and h is the mean water depth.

With this transformation, the numerical grid in the computational plane becomes constant in space and time. However, in the physical plane, since the water surface is constantly changing in time due to dynamic forcing conditions, the sigma grid is time

dependent. A σ -grid formulation is suitable for simulating flow and salinity transport in regions of gradual bathymetric variations and gives a more accurate estimation of bottom stress than a z -grid model, which resolves the depth with "stair-step" grids. Nevertheless, recent studies (Sheng *et al.*, 1989a; Haney, 1991) showed that a σ -grid model is accurate only when there are sufficient grid points across regions of sharp bathymetric gradients. In the case of insufficient grid points, Sheng *et al.* (1989a) suggested a direct evaluation of the horizontal density gradient terms along constant z -plane, and avoiding higher-order advective schemes along the sharp bathymetric variation, to reduce numerical error.

Using non-orthogonal boundary-fitted horizontal grid, it is possible to better represent the circulation and transport processes in estuarine systems with complex geometries. Thompson (1983) developed a method to generate 2-D boundary-fitted grids in complex domain by solving a set of elliptic equations. These equations relate the generally non-orthogonal curvilinear coordinates in the physical plane x and y with the uniformly-spaced coordinates in the transformed plane, ξ and η .

The spatial coordinates in the physical plane, (x, y, z) , have dimensions of length, while the coordinate system in the computational plane, (ξ, η, σ) , is dimensionless. In this new coordinate system (ξ, η, σ) , the velocity vector are expressed in terms of contravariant components, with dimension of $[t^{-1}]$ (Sheng, 1989). The equations of motion in the (ξ, η, σ) coordinates are shown in Appendix A.

Boundary and Initial Conditions

In order to numerically solve the set of equations presented, boundary conditions are required for the dependent variables.

Vertical Boundary Conditions

The boundary conditions for Equations (3.1), (3.2), (3.3), (3.5), and (3.9) at the free surface ($\sigma = 0$) are:

$$\begin{aligned} \rho_a A_V \left(\frac{\partial u}{\partial z}, \frac{\partial v}{\partial z} \right) &= (\tau_{xx}, \tau_{yy}) \\ \frac{\partial S}{\partial \sigma} &= 0 \\ -(w + w_s)c + D_V \frac{\partial c}{\partial z} &= 0 \end{aligned} \quad (3.11)$$

At the free surface, wind velocity is converted to stress by:

$$(\tau_{xx}, \tau_{yy}) = \rho_a C_{ds} (u_w^2 + v_w^2)^{1/2} (u_w, v_w) \quad (3.12)$$

where τ_{xx} , and τ_{yy} are the components of the wind stress, ρ_a is the air density (0.0012 g/cm^3), u_w and v_w are the components of wind speed measured at some height above the sea level. C_{ds} , the drag coefficient, is given as a function of the wind speed measured at 10 meters above the water surface by (Garra, 1977):

$$C_{ds} = (0.075 + 0.067 W_s) 0.001 \quad (3.13)$$

where W_s is the wind speed magnitude in m/s.

The vertical velocity is obtained from the kinematic boundary condition imposed at the surface:

$$w = \frac{\partial \zeta}{\partial t} + u \frac{\partial \zeta}{\partial x} + v \frac{\partial \zeta}{\partial y} \quad (3.14)$$

The boundary conditions for Equations (3.1), (3.2), (3.3), (3.5), and (3.9) at the bottom
($\sigma = -1$) are:

$$\begin{aligned} \rho_o A_V \left(\frac{\partial u}{\partial z}, \frac{\partial v}{\partial z} \right) &= (\tau_{bx}, \tau_{by}) \\ &= C_{db} (u_1^2 + v_1^2)^{1/2} (u_1, v_1) \\ \frac{\partial S}{\partial \sigma} &= 0 \end{aligned} \quad (3.15)$$

$$-(w + w_z)c + D_V \frac{\partial c}{\partial z} = v_d c - E$$

where v_d is the deposition velocity, E is the rate of erosion, A_V , and D_V are vertical turbulent eddy coefficients, C_{db} is the bottom friction coefficient, and u_1, v_1 represent the velocity components at the first grid point above the bottom. Taking z_1 as half of the bottom layer thickness (which starts at the bottom roughness height, z_o), C_{db} , for a hydraulic rough flow, is given by (Sheng, 1983):

$$C_{db} = \kappa^2 \left[\ln \left(\frac{z_1}{z_o} \right) \right]^{-2} \quad (3.16)$$

where κ is the von Karman constant.

Lateral Boundary Conditions

Along the shoreline where river inflow or outflow may occur, the conditions are generally:

$$\begin{aligned} u &= u(x, y, z, t) \\ v &= v(x, y, z, t) \\ w &= 0 \end{aligned} \quad (3.17)$$

Along a solid boundary, the normal velocity component is zero. In addition, the normal derivatives of salinity and suspended sediment concentration are assumed to be zero.

Along an open boundary, the surface elevation, ζ , is given by either a time series of measured data or specified through harmonic constituents using the following equation:

$$\zeta = \zeta(x, y, t) = \sum_{n=1}^{n_{\max}} A_n \cos \left(\frac{2\pi t}{T_n} + \phi_n \right) \quad (3.18)$$

where A_n , T_n , and ϕ_n are the amplitude, period, and phase angle of the astronomical tidal constituents.

When open boundary conditions are given in terms of ζ , the normal velocity component is assumed to be of zero slope while the tangential velocity component may be either zero, of zero slope, or computed from the momentum equations.

The salinity and suspended sediment concentration along an open boundary or river entrance is computed from a 1-D advection equation during the outflow. During the inflow, the concentration takes on a prescribed value.

Contravariant velocity components provide lateral boundary conditions similar to those in the (x, y) system. Along solid boundaries, the normal velocity is zero. When flow is specified at the open boundary, the normal velocity component is prescribed.

To initiate a simulation, the initial spatial distributions of ζ , u , v , S and c need to be specified. When initial data are unknown, the simulation starts with zero initial fields. When initial data are known at a limited number of locations, an initial field can be interpolated. For salinity simulations, the "spin-up" time is longer and sufficient time should be allowed in model simulations.

CHAPTER 4 THE WATER QUALITY MODEL

Previous Work

Considerable effort has been expended in the past 20 years to develop water quality models for freshwater and marine systems. In freshwater systems, Streeter and Phelps (1925) were the first researchers to introduce a set of equations for predicting the biochemical oxygen demand (BOD) and dissolved oxygen (DO) concentrations. Since then, simple zero- and first-order exponential decay, dilution and sedimentation terms have been added to predict other conservative and non-conservative species. Sheng (1994) provided a comprehensive review on water quality models for shallow waters. Jørgensen *et al.* (1996) provided the most recent review of environmental models developed in the last two decades.

Water quality models can be classified in terms of the approach undertaken for solution and analysis. Steady-state models are usually simpler and require less computational effort than dynamic models. On the other hand, multi-dimension, robust models can provide more detailed and comprehensive information on the water quality. Stochastic models require more data for calibration and validation than deterministic models. Water quality parameters simulated by deterministic models are expressed in terms of expected values, while simulations performed by stochastic models explicitly take into account the uncertainty of

physical and biogeochemical processes. Validation of stochastic models is particularly difficult due to the quantity of observational data required to compare probability distributions of variables rather than just their expected or mean values (Loucks, 1981). Moreover, it is more meaningful, in terms of interpretation, to estimate biogeochemical parameters like growth and nitrification rates than empirical parameters like autoregressive and moving average coefficients (Solow, 1995).

Until recently, water quality models, originally developed for rivers and stream flows, were indiscriminately used in estuarine systems. The assumption of steady or quasi-steady state of the hydrodynamics processes justified the use of coarse grids, and models were either uncoupled or loosely coupled with hydrodynamics models. However, even in freshwater systems, there is increasing evidence that hydrodynamics processes have very significant effects on water quality and ecological processes. Chen and Sheng (1994) found that the internal loading of nutrients from bottom sediments in Lake Okeechobee could not be accurately calculated by a water quality model using a large time step of 6 hours. During one time step, the internal loading of nutrients from bottom sediments calculated by a conventional water quality model may be zero, because of the zero average net flux from the bottom sediments in this 6-hour period. In reality, the resuspension and deposition processes can significantly affect internal loading through sorption/desorption processes. Model simulations which include such effects produced results that agree well with field data (Sheng *et al.*, 1993). The water quality model developed by Chen and Sheng (1994) forms the basis of the water quality model of the present study, although their model did not include the dissolved oxygen balance and was limited to rectangular grid system.

In estuarine systems, the necessity to accurately represent hydrodynamics and biogeochemical processes is even more relevant. Estuarine systems are physically dominated ecosystems, where the action of the sun, tides, wind, atmospheric disturbances, river discharges, and complex geomorphometric features interact. It is the balance of these physical forces acting as subsidies and stresses that will dictate the water quality dynamics of each estuarine system.

In traditional water quality box models like WASP (Ambrose *et al.*, 1994), salinity data is used to obtain the so-called "dispersive coefficients" during model calibration. This salinity calibration consists of first averaging the flows over the calibration period and then estimating tidal dispersion coefficients, assuming steady-state conditions (AScI, 1996). In an estuarine environment, this approach is questionable since salinity is an active species. Its concentration and gradients affect the temporal and spatial distribution of the density field, driving baroclinic forces that completely change the hydrodynamic characteristics of the flow.

AScI (1996) has applied WASP4 in Tampa Bay aiming at the development of a "broad-based, management-oriented model". The primary objective of the AScI study is to provide the Southwest Florida Water Management District (SWFWMD) with a modeling tool to define eutrophication management strategies. The rationale of this approach was that the hydrodynamic and water quality data gathered in Tampa Bay, from 1985 to 1991, was sufficient for the determination of the dispersive and the other "ad-hoc" coefficients of the model. In addition to the 28 model coefficients, sediment oxygen demand and benthic fluxes were also determined for specific Bay segments during the calibration process. Another

model from capturing episodic events. Schoellhammer (1993) showed that resuspension in Old Tampa Bay is closely related to storm systems and local wind-generated waves. Sheng *et al.* (1993) showed that the contribution of resuspension flux to the internal loading during episodic events can be orders of magnitude greater than the normal diffusive benthic flux.

Coastal, Inc. (1995) developed a statistical model to investigate the relationships among nutrient loading, water quality parameters (chlorophyll-*a*), and light attenuation coefficients. Like the ASCI (1996) study, the rationale supporting this simple approach was the large amount of data gathered between 1985 and 1991. It was thought that if the available water quality data were sufficient to calibrate and validate this empirically-based model, it would serve as a management tool to determine external nitrogen loadings consistent with seagrass light requirements. Using regression analysis, Coastal, Inc. determined the relationships between total nitrogen loading, chlorophyll-*a*, turbidity and light attenuation coefficients in the four major Bay segments (Old Tampa Bay, Hillsborough Bay, Middle Tampa Bay, and Lower Tampa Bay). The conclusions of the Coastal, Inc. study was that no reduction in annual average nitrogen loading and chlorophyll *a* concentration would be required for the 20% near-bottom light level target for the four major Bay segments. However, a substantial reduction in nitrogen loads would be required in order to achieve the 25% light level target.

The limitations of the Coastal, Inc. study are related to the fact that the simplifying assumptions applied (linear correlation between cause and effect) proved deficient to explain any correlation between external loading and nitrogen and chlorophyll-*a* concentrations inside the Bay (Coastal, 1995). This limitation suggests that the internal loading has a

significant role in the nutrient budget, and consequently should be considered in the strategies to control the eutrophication process. Furthermore, another uncertainty of the Coastal analysis was originated from their conclusion that a three month cumulative lag period for nitrogen loads could explain the variation in the chlorophyll-*a* data. Johansson (1991), using a similar statistical approach presented evidences for a three-year lag between external nitrogen loading and chlorophyll-*a* response. Again, different rates of internal nitrogen loading may explained the lag difference between Coastal, Inc. (1995) and Johansson (1991) studies.

These previous modeling efforts on Tampa Bay provided useful foundation for this more comprehensive modeling study. Despite their simplified approach, these studies were able to isolate relevant processes and determine some specific model coefficients. At the end of this chapter, Table 4.2 presents the model coefficients used in this study, the range of each coefficient found in the literature, and the values used by ASCL (1996). In order to account for both point and non-point sources of nitrogen loading into the Bay, the water quality species concentration along model boundaries were determined from the nutrient loadings presented by Coastal, Inc. (1994). Total nitrogen loadings were converted to concentrations and used along with river discharges.

The water quality component of this integrated model for Tampa Bay focuses on the interactions between oxygen balance, nutrient dynamics, light attenuation, phytoplankton and zooplankton dynamics. To develop the water quality model, the mass conservation principle can be applied to each water quality parameter related to the phytoplankton and zooplankton dynamics, phosphorus cycle, nitrogen cycle, and oxygen balance. With regard to nutrients,

the nitrogen cycle is more important than the phosphorus cycle since nitrogen has been the macro-nutrient limiting phytoplankton growth in Tampa Bay (FWCA, 1969; Lewis and Estevez, 1988; Johansson, 1991; Coastal, 1995; ASCL, 1996). Hence phosphorus cycle is not included as part of the water quality model for Tampa Bay.

Development of the Numerical Model

The nitrogen cycle in Tampa Bay is modeled through a series of first-order kinetics, which start with the biogeochemical process controlling nitrogen fixation. Phytoplankton growth controls ammonia and nitrate uptake. The uptake rate for each species is proportional to its concentration relative to the total inorganic nitrogen content, and a preferential factor for ammonia uptake. Nitrogen returns from the planktonic biomass pool as dissolved and particulate organic nitrogen and as dissolved inorganic nitrogen through endogenous respiration and non-predatory mortality. Organic nitrogen is converted to ammonia (mineralization) at a temperature-dependent rate, and ammonia is then converted to nitrate (nitrification) in a temperature and oxygen-dependent rate. The stability of the dissolved form of ammonium in water is pH dependent. It can exist in its ionic form, ammonium (NH_4^+) or as ammonia (NH_3), with the latter being lost from the system through volatilization. Low levels of dissolved oxygen may induce a bacterial-mediated transformation of nitrate into nitrogen gas (denitrification) at a temperature-dependent rate.

The oxygen balance couples dissolved oxygen to the other state variables. Reaeration through the atmosphere-water interface, and phytoplankton production during photosynthesis

are the main sources for oxygen. Oxidation of organic matter and carbonaceous material, respiration by zoo and phytoplankton, and oxygen consumption during the nitrification process are collectively grouped into the CBOD (carbonaceous-biochemical oxygen demand) variable, which is a sink for dissolved oxygen (Ambrose *et al.*, 1994).

The light penetration inside water can be determined through measurements of turbidity, color, and light penetration (Kirk, 1994). In the integrated model for Tampa Bay, the primary concern is the availability of photosynthetically active radiation (PAR), which is influenced by the intensity of incident solar radiation, solar elevation angle, weather conditions, water depth, tidal range, concentrations of sediments, detritus and phytoplankton (Miller and McPherson, 1995).

Phytoplankton kinetics is the central part of this water quality model, since the primary water quality issue in the Tampa Bay Estuarine System is eutrophication (Boler *et al.*, 1991). Phytoplankton population is a complex variable to obtain in the field. For single species, a direct measurement of the population size is the number of cells per unit of volume. However, in natural multi-species environment, it is difficult to distinguish viable and non-viable cells and, for species that tend to colonize, counting requires an extra effort to separate individual cells because the size of the colonies are quite variable (Ambrose *et al.*, 1994). An alternate solution is to measure phytoplankton population through chlorophyll analysis, although this is not an absolute indicator of planktonic biomass. Some species do not contain chlorophyll and when chloroplasts (chlorophyll-containing structures found in algal and green plant cells) are present, they vary in number, size and pigment content per cell (Boler *et al.*,

1991). The conversion to phytoplankton dry weight or carbon involves further species-dependent constants that depend on nutrient and light levels.

The rationale behind this water quality modeling effort is that planktonic organisms have a fast response to environmental conditions. In other words, by combining chlorophyll with nutrient levels, dissolved oxygen balance, and light attenuation, it is possible to evaluate and quantify short and long term water quality processes such as hypoxia and eutrophication.

Mathematical Formulation

In this study, the water quality equations are derived from an Eulerian approach, using a control volume formulation. In this method, the time rate of change of the concentration of any substance within this control volume is the net result of (i) concentration fluxes through the sides of the control volume, and (ii) production and sink inside the control volume. The conservation equation for each of the water quality parameters is given by:

$$\underbrace{\frac{\partial \phi}{\partial t}}_{(i)} + \underbrace{\nabla \cdot (\phi \vec{u})}_{(ii)} = \underbrace{\nabla \cdot [D \nabla (\phi \vec{u})]}_{(iii)} + \underbrace{Q}_{(iv)} \quad (4.1)$$

where (i) is the evolution term (rate of change of concentration in the control volume), (ii) is the advection term (fluxes into/out of the control volume due to advection of the flow field), (iii) is the dispersion term (fluxes into/out of the control volume due to turbulent diffusion of the flow field), and (iv) is the sink/source term, representing the kinetics and transformations due to sorption/desorption, oxidation, excretion, decay, growth,

biodegradation, etc. The water quality equations in the curvilinear non-orthogonal boundary-fitted system (ξ, η, σ) are given by:

$$\begin{aligned} \frac{1}{H} \frac{\partial H \phi}{\partial t} = & \frac{1}{H^2} \frac{\partial}{\partial \sigma} \left(D_v \frac{\partial \phi}{\partial \sigma} \right) \\ & - \frac{1}{H \sqrt{g_{\sigma\sigma}}} \left[\frac{\partial}{\partial \xi} \left(\sqrt{g_{\sigma\sigma}} H u \phi \right) + \frac{\partial}{\partial \eta} \left(\sqrt{g_{\sigma\sigma}} H v \phi \right) \right] - \frac{1}{H} \frac{\partial H \omega \phi}{\partial \sigma} \\ & + D_H \left[g^{11} \frac{\partial^2 \phi}{\partial \xi^2} + 2 g^{12} \frac{\partial^2 \phi}{\partial \xi \partial \eta} + g^{22} \frac{\partial^2 \phi}{\partial \eta^2} \right] + Q \end{aligned} \quad (4.2)$$

where ϕ represents any water quality parameter, $\sqrt{g_{\sigma\sigma}}$ is the Jacobian of horizontal transformation, (g^{11}, g^{12}, g^{22}) are the metric coefficients of coordinate transformation, and Q represents the biogeochemical processes.

In the following sections, the biogeochemical processes controlling the sink/source term of Equation (4.2) will be discussed in detail for the nutrient dynamics, zooplankton and phytoplankton dynamics, and oxygen balance in estuarine systems.

Nutrient Dynamics in Estuarine Systems

As explained earlier, the nutrient dynamics will be centered in the nitrogen cycle, assuming it is the macro-nutrient that limits phytoplankton growth. For the present study, the basic transformation processes for the nitrogen cycle are similar to those described in Chen and Sheng (1994).

Nitrogen comprises 78% of the atmosphere, mostly molecular N_2 . This form is biologically unavailable except for fixation by procaryotic organisms containing the enzyme

nitrogenase. Considering the kinetic pathway *organic nitrogen* \rightarrow *ammonia* \rightarrow *nitrate* $\rightarrow N_2$, fixed forms of nitrogen such as nitrate, ammonium, and organic nitrogen would gradually be depleted from the biosphere if not for nitrogen fixation.

Nitrogen inputs to estuarine systems are related to point and non-point sources from land, atmospheric deposition, and fixation. Additionally, internal loadings such as from resuspended sediments containing inorganic and organic forms are also important. The specification and quantification of each of these contributions is the first step towards the determination of nitrogen budget in an estuarine system.

As shown in Equation (4.2), the nitrogen cycle is highly dependent on the hydrodynamics and sediment dynamics of the estuarine system. Resuspension events, combined with desorption processes can significantly change the input and budget of nitrogen in the system. On the other hand, deposition and sorption may contribute to major losses of nitrogen from the water column. The hydrodynamics not only drive the sediment processes, but also affect the sorption/desorption reactions, through turbulent mixing.

The processes simulated in this study include:

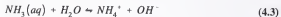
- a) Mineralization of organic nitrogen
- b) Nitrification of ammonium
- c) Volatilization of ammonia
- d) Denitrification of nitrate
- e) Uptake of ammonia and nitrate by phytoplankton
- f) Conversion of algal-nitrogen into zooplankton-nitrogen through grazing
- g) Excretion by algae and zooplankton

For the purpose of studying its cycle, the nitrogen species are first divided into dissolved and particulate groups. This division is usually established in the laboratory using filtering techniques. In the dissolved group, this study will consider nitrogen as ammonia nitrogen, represented by the state variable NH_3 ; dissolved ammonium nitrogen, represented by the state variable NH_4 ; nitrate+nitrite nitrogen, represented by the state variable NO_3 ; and dissolved or soluble organic nitrogen (SON). Particulate nitrogen includes: particulate inorganic nitrogen (PIN), and particulate organic nitrogen (PON). Zooplankton nitrogen (ZOON), and algal nitrogen (ALGN) relate biomass to nitrogen concentration through fixed stoichiometric ratios: zooplankton nitrogen to carbon ratio (z_{NC}), and algal nitrogen to carbon ratio (a_{NC}).

In order to couple the water quality model with hydrodynamics and sediment dynamics, Equation (4.2) needs to be modified for the particulate forms of nitrogen, so that it includes a settling velocity. For the inorganic species, it is reasonable to assume the same settling velocity of the suspended sediment particles. For phytoplankton, literature values of algae settling velocity, which accounts for the limited vertical motion of these organisms will be used.

Ammonia Nitrogen

Ammonia volatilization is a physico-chemical process where ammonium N is in equilibrium between its gaseous and hydroxyl form:



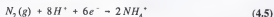
As stated, the process is pH dependent, with an alkaline environment driving the reaction to the left, i.e. favoring the aqueous form. Since the concentration of ammonia in the atmosphere is very low, the partial pressure difference may produce a sink for nitrogen in the system, according to Henry's law. The kinetic pathway for ammonia nitrogen (state variable NH_3) is represented in the sink term of Equation (4.2) as:

$$Q = K_{Af} \cdot \frac{pH}{H_{ai} + pH} \cdot NH_4 - K_{vol} \cdot [h_v \cdot NH_3 - (NH_3)_{atm}] \quad (4.4)$$

where K_{Af} is the ammonia conversion rate constant, and H_{ai} is the half-saturation constant for ammonia conversion. K_{vol} is the volatilization rate constant, h_v is Henry's constant, and $(NH_3)_{atm}$ is the ammonia concentration in the air.

Dissolved Ammonium Nitrogen

Nitrogen fixation is a biogeochemical process mediated by a variety of autotrophic and heterotrophic bacteria, by which nitrogen gas is reduced to ammonium:



In aquatic systems, this reaction is only possible in very reduced environments (Snoeyink and Jenkins, 1980). Such an environment exists inside photosynthetic cells of blue-green algae, and in the symbiotic association in root nodules between bacteria of the genus *Rhizobium* and certain plants. It has been reported that cyanobacteria are responsible for most planktonic fixation in aquatic environments, with a high correlation between fixation rates and cyanobacteria biomass (Howarth *et al.*, 1988). In most estuaries, the biomass of

these nitrogen-fixing species of cyanobacteria usually makes up a very small percentage of the phytoplanktonic biomass (< 1%), suggesting insignificant amount of nitrogen fixation (Howarth *et al.*, 1988). Johansson *et al.* (1985) showed that, prior to 1984, planktonic filamentous blue-green algae (*Schizothrix calcicola sensu* Drouet) dominated the phytoplankton population in Tampa Bay from early summer to early winter. However, Johansson (1991) stated that there was no information to support that this blue-green algae is responsible for nitrogen fixation in Tampa Bay. Actually, it has been estimated that nitrogen fixation should account for no more than 5% of the total nitrogen budget in the Bay (Johansson, personal communication). These evidences support the hypothesis generally accepted that many estuaries are nitrogen limited in part due to the low rates of nitrogen fixation. Hence, nitrogen fixation was not considered in this study.

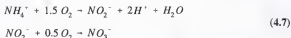
The biogeochemical transformation of organic nitrogen to ammonium is defined as ammonification. Another source for dissolved ammonium is the release of NH_4 during mortality and excretion of algae and zooplankton, and the sorption/desorption reaction with sediment particles. The kinetic pathway of ammonium nitrogen (state variable NH_4) is represented in the source term of Equation (4.2) by a first-order reaction (Rao *et al.*, 1984), and a partitioning between particulate and dissolved form regulated by the sorption/desorption kinetics (Chen and Sheng, 1994):

$$\begin{aligned}
Q = & K_{ONM} \cdot SON - K_{NN} \cdot \frac{DO}{H_{nr} + DO} \cdot NH4 \\
& + d_{on} (PIN - p_{on} \cdot c \cdot NH4) \\
& - P_n \mu_a \cdot ALGN + K_{ax} \cdot ALGN + K_{zx} \cdot ZOON \\
& - K_{AJ} \cdot \frac{pH}{H_m + pH} \cdot NH4
\end{aligned} \tag{4.6}$$

where K_{ONM} , the rate of organic nitrogen mineralization is a function of water temperature, pH, and the C/N ratio of the residue (Reddy and Patrick, 1984). K_{NN} is the nitrification rate constant, DO is the dissolved oxygen concentration, H_{nr} is the half saturation constant for oxygen limitation. d_{on} is the desorption rate of $NH4$ from sediment particles, p_{on} is the partition coefficient between $NH4$ and PIN , and c is the suspend sediment concentration. P_n is the ammonium preference factor for algae uptake, μ_a is the algae growth rate, K_{ax} and K_{zx} are the algae and zooplankton excretion rate constants, respectively. All coefficients related to zoo and phytoplankton dynamics will be discussed later in this Chapter.

Nitrite+Nitrate Nitrogen

In an aerobic environment, the mineralization of organic nitrogen proceeds with a bacterial-mediated transformation of ammonium into nitrate. The nitrification process is a two step process, in which the chemoautotrophic bacteria of the genera *Nitrosomonas* mediate the formation of nitrite, and bacteria of the genera *Nitrobacter* the formation of nitrate:



Nitrification is a strictly aerobic process, occurring only in the water column and in the aerobic layer of the sediment column. Equation (4.7) shows that the nitrification process is a sink for dissolved oxygen in the system.

Denitrification is defined as the biogeochemical transformation of nitrate N to gaseous end products such as molecular nitrogen or nitrous oxide (Reddy and Patrick, 1984). Like volatilization, denitrification represents a sink for nitrogen in the system. Under anaerobic conditions and in the presence of available organic substrate, denitrifying bacteria (e.g. *Pseudomonas denitrificans*) can use nitrate as an electron acceptor during anaerobic respiration. As an example, the oxidation of a carbohydrate substrate to CO_2 and H_2O using nitrate instead of oxygen can be given as:



This irreversible reaction is actually a two-step process in which nitrate is reduced to nitrous oxide before being converted into molecular nitrogen. Nitrous oxide has been related to the Earth's "greenhouse" effect because N_2O reacts and breaks down atmospheric ozone (McElroy *et al.*, 1978). Reddy *et al.* (1978) showed that under carbon-limiting conditions,

the denitrification process described in Equation (4.8) can be represented by a first-order reaction.

In this study, the kinetic pathway of nitrite+nitrate (state variable NO_3) is represented in the source term of Equation (4.2) as a sequence of first-order reactions, limited by the dissolved oxygen concentration:

$$Q = K_{DN} \cdot \frac{DO}{H_{nit} + DO} \cdot NH_4 - K_{DN} \cdot \frac{H_{NO_3}}{H_{NO_3} + DO} \cdot NO_3 - (1 - P_n) \cdot \mu_a \cdot ALGN \quad (4.9)$$

where K_{DN} is the denitrification rate constant, and H_{NO_3} is the half saturation constant for denitrification, which can be calibrated to only allow the denitrification process to occur under low dissolved oxygen conditions (Ambrose *et al.*, 1994).

Soluble Organic Nitrogen

Besides N_2 , the largest pool of nitrogen in estuarine systems are dissolved and particulate organic nitrogen. The kinetic pathway of dissolved or soluble organic nitrogen is the conversion of SON to NH_4 during ammonification, and the sorption/desorption reaction with sediment particles. For soluble organic nitrogen (state variable SON), the source term of Equation (4.2) can be represented by:

$$Q = -K_{DNM} \cdot SON + d_{on} \cdot (PON - p_{on} \cdot c \cdot SON) \quad (4.10)$$

where d_{on} is the desorption rate of SON from the sediment particles, and p_{on} is the partition coefficient between SON and PON .

Particulate Organic Nitrogen

The kinetic pathway of particulate organic nitrogen is the release of *PON* during mortality and excretion of algae and zooplankton, and the sorption/desorption reaction with sediment particles. In estuarine systems with organic-rich sediments, benthic mineralization of detritus can be a major recycling pathway, and account for a significant fraction of the nutrient requirements of primary producers in overlying water column (Klump and Martens, 1981). For particulate organic nitrogen (state variable *PON*), the source term of Equation (4.2) can be represented as:

$$Q = K_{ax} \cdot ALGN + K_{zx} \cdot ZOON - d_{on} \cdot (PON - p_{on} \cdot c \cdot SON) \quad (4.11)$$

where K_{zx} is the mortality rate of zooplankton.

Particulate Inorganic Nitrogen

Sources of *PIN* are related to nitrogen contained in the suspended particulate matter derived from landward and seaward origin (Keefe, 1994). There have been several studies, at various spatial and temporal scales, of particulate nitrogen distribution in estuarine systems (Sharp *et al.*, 1982; Edmond *et al.*, 1985; Wafar *et al.*, 1989). Nevertheless, little insight is available concerning the partitioning between the inorganic and organic fraction of these materials (Froelich, 1988). The kinetic pathway of particulate inorganic nitrogen (state variable *PIN*) is related to the sorption/desorption reaction with sediment particles, and the source term of Equation (4.2) can be written as:

$$Q = -d_{an} \cdot (PIN - p_{an} \cdot c \cdot NH4) \quad (4.12)$$

Algal Nitrogen

Through uptake of inorganic nitrogen, algae assimilates nitrogen in proportion to its growth rate. The particulate nitrogen recycles to the inorganic pool by means of excretion and non-predatory mortality. Inasmuch as there is no data on excretion of zoo and phytoplankton under field conditions, most of water quality models consider constant excretion and mortality rates proportional to the biomass (Jørgensen, 1983; Najarian *et al.*, 1984; Ambrose *et al.*, 1994; Chen and Sheng, 1994). Another sink for *ALGN* is due to grazing by zooplankton, at a rate proportional to the zooplankton growth rate. Growth rates for phytoplankton and zooplankton in estuarine systems are complex functions of the species present, and they will be discussed later in this Chapter.

The algal nitrogen (state variable *ALGN*) is represented in this model by a fixed stoichiometric ratio relating algal biomass and nitrogen concentration as:

$$ALGN = a_{NC} \cdot (\text{Algal Biomass}) \quad (4.13)$$

where a_{NC} is the algal nitrogen to carbon constant ratio.

Zooplankton Nitrogen

Similar to *ALGN*, the kinetic pathway of particulate zooplankton nitrogen depends on growth, excretion, and mortality rates. In this case, the zooplankton nitrogen (state variable *ZOON*) is given by:

$$ZOON = z_{NC} \cdot (\text{Zooplankton Biomass})$$

where z_{NC} is the zooplankton nitrogen to carbon constant ratio.

Sorption and Desorption Reactions

In the nitrogen cycle, sorption processes refer to the conversion from soluble to solid phase of inorganic and organic species, while desorption reactions describe the inverse process. Sorption/desorption processes, combined with resuspension events can significantly alter the nitrogen cycle in the system.

The kinetics of sorption/desorption reactions are dependent on each nitrogen species characteristics, sediment properties, pH, temperature, and dissolved oxygen concentration (Simon, 1989). Some studies have shown that sorption/desorption processes can be more important in marine environment than in freshwater. The primary reason has been attributed to a six times higher adsorptive capacity of clays for organic matter in seawater than in freshwater, due to salinity effects (Pocklington, 1977; Martinova, 1993).

The most commonly used mathematical representation of sorption/desorption processes is the linear, reversible, isotherm (Berkheiser *et al.*, 1980; Reddy *et al.*, 1988):

$$\frac{\partial N_{ad}}{\partial t} = -D_r N_{ad} + S_r N_s \quad (4.15)$$

where D_r is the desorption rate constant, S_r is the sorption rate constant, N_{ad} is the adsorbed nitrogen concentration, and N_s is the dissolved nitrogen concentration.

Equation (4.15) can be reformulated, considering that at equilibrium, the ratio between the desorption and sorption rates gives the partition coefficient between dissolved and particulate forms:

$$\frac{\partial N_{ad}}{\partial t} = -D_r(N_{ad} - p_c N_s) \quad (4.16)$$

where p_c is the partition coefficient.

Phytoplankton Dynamics in Estuarine Systems

The overall water quality in the Tampa Bay Estuarine System is markedly influenced by the dynamics of the zoo and phytoplankton communities (Lewis and Estevez, 1988; Boler *et al.*, 1991; ASCL, 1996). In a review of the phytoplankton in Tampa Bay, Steidinger and Gardiner (1985) reported the dominance of nanoplankton (less than 20 μm), with a head to mouth gradient, following the salinity distribution. The authors also reported that Tampa Bay presents more than 250 species of phytoplankton, with diatoms making up the bulk of the distribution. However, the lack of data on each specific species prevented a more detailed characterization, and the entire phytoplanktonic community is represented in this study by a single state variable.

In this study, a quantitative model of phytoplankton population dynamics also uses the conservation of mass principle, in which hydrodynamics transport plays a major role. Phytoplankton growth is represented by a temperature-dependent maximum growth rate that is limited by nutrient availability and light. Light limitation is formulated according to the equation first proposed by Steele (1965). The nutrient limitation is represented by a modified version of the Michaelis-Menton formulation. Some researchers (e.g. Jørgensen, 1976) suggest that the nutrient-limited growth rate of phytoplankton is a function of the internal

nutrient content. According to this approach, external nutrients are taken up by phytoplankton and stored. Ensuing growth would then be related to this internal nutrient content. Assuming a dynamic state of equilibrium between the external concentration and internal content (Di Toro, 1980), it is possible to represent the nutrient limitation according to the formulation suggested by Riley and Stefan (1988).

In this study, the phytoplankton growth rate is represented by:

$$\mu_a = (\mu_a)_{\max} \cdot \theta_a^{T-20} \cdot \frac{I}{I_s} \exp\left(1 - \frac{I}{I_s}\right) \cdot \frac{NH_4 + NO_3}{H_n + NH_4 + NO_3} \quad (4.17)$$

where $(\mu_a)_{\max}$ is the algae maximum growth rate, θ is the temperature correction factor, I is the light intensity, I_s is the optimum light intensity for algal growth, H_n is the half saturation constant for algal growth.

The phytoplankton kinetics are represented by growth, respiration, non-predatory mortality, grazing by zooplankton, and a settling term which accounts for the limited vertical motion. The source term of Equation (4.2) can be written as:

$$Q = \frac{\partial}{\partial z} (ws_{algae} \cdot PHY) + (\mu_a - K_{ax} - K_{ar}) \cdot PHY - \mu_z \cdot ZOO \quad (4.18)$$

where ws_{algae} is the phytoplankton settling velocity. Chen and Sheng (1994) reviewed algal settling rate measured in eutrophic water bodies, and showed that it is not only species dependent, but it also a function of flocculation and senescence.

Zooplankton are the lower-trophic level consumers that constitute the primary herbivorous component of an estuarine ecosystem (Kennish, 1990). In this study,

phytoplankton are the object of concern, therefore, no attempt is made to investigate the details of the zooplankton dynamics. Zooplankton is only considered as the predators of phytoplankton, utilizing their available biomass as food supply.

Zooplankton growth is represented by a temperature-dependent maximum growth rate, that is limited by phytoplankton availability:

$$\mu_z = (\mu_z)_{\max} \cdot \theta_z^{T-20} \cdot \frac{PHY}{H_{phy} + PHY} \quad (4.19)$$

where $(\mu_z)_{\max}$ is the maximum growth rate for zooplankton, θ_z is the temperature limiting function for zooplankton, and H_{phy} is the half saturation constant for phytoplankton uptake.

The zooplankton kinetics, influenced by growth, respiration, and mortality, is represented in the source term of Equation (4.2) by:

$$Q = (\mu_z - K_{rz} - K_{mz}) \cdot ZOO \quad (4.20)$$

Oxygen Balance in Estuarine Systems

Dissolved oxygen dynamics in aquatic systems have been extensively studied (Streeter and Phelps, 1925; O'Connor and Thomann, 1972; Orlob, 1983; Ambrose *et al.*, 1994). Dissolved oxygen evolution depends on the balance between photosynthetic production, total respiration, and exchanges with the atmosphere. Oxygen, as a byproduct of photosynthesis, increases as a result of autotrophs' growth. Dissolved oxygen saturation in seawater is determined as function of temperature and salinity (APHA, 1985). For dissolved oxygen

levels below saturation, DO diffuses into surface waters. When the water is super-saturated, mainly as a result of primary production, oxygen will be diffused out to the atmosphere. As any other water quality parameter, dissolved oxygen is also subject to advective transport in the estuarine system.

In this study, the formulation of the oxygen balance is based on the WASP5 model, with some modifications. The rate of dissolved oxygen production is assumed to be proportional to the growth rate of the phytoplankton in a fixed stoichiometry reaction. For each milligram of phytoplankton carbon produced by growth using nitrate, a fixed amount of phytoplankton nitrogen ($ALGN$) is reduced, and $(48/14) a_{nc}$ (phytoplankton nitrogen/carbon ratio) mg of O_2 is produced. The dissolved oxygen fluxes on the air-water interface are determined as a product of a reaeration coefficient multiplied by the difference between dissolved oxygen saturation and the dissolved oxygen concentration at the surface layer. The reaeration coefficient is assumed to be proportional to the water velocity, depth, and wind speed (Thomann and Fitzpatrick, 1982). Details of the dissolved oxygen saturation and reaeration coefficient calculations are presented in Appendix C.

In this model, there are two options for the kinetic pathway of DO . The first one, describing the oxygen balance through a full non-linear equation is represented in the source term of Equation (4.2) as:

$$\begin{aligned}
Q = & K_{AE} \cdot (DO_s - DO) + \mu_a \left[\frac{32}{12} + \frac{48}{14} \frac{14}{12} (1 - P_n) \right] \cdot ALGN \\
& - \frac{32}{12} K_{ax} \cdot a_{oc} \cdot PHY - K_D \cdot \frac{DO}{H_{bod} + DO} \cdot CBOD \\
& - \frac{64}{14} K_{NV} \cdot \frac{DO}{H_{NH} + DO} \cdot NH4
\end{aligned} \tag{4.21}$$

where DO_s is the saturation value for dissolved oxygen concentration, K_{AE} is the reaeration coefficient, and a_{oc} is the constant oxygen to carbon ratio for phytoplankton respiration (gO_2 / gC).

In order to minimize "spin-up" time due to the non-linear character of Equation (4.21), a second option describes the oxygen balance through a linear equation where the source term of Equation (4.2) is given as (Ambrose *et al.* 1994):

$$\begin{aligned}
Q = & K_{AE} \cdot (DO_s - DO) + \frac{32}{12} [\mu_a - (K_{ax} + K_{ax})] \cdot PHY \\
& - K_D \cdot CBOD - \frac{64}{14} K_{NV} \cdot NH4
\end{aligned} \tag{4.22}$$

The use of carbonaceous oxygen demand (CBOD) as a measure of the oxygen-demanding processes simplifies modeling efforts by aggregating their potential effects (Ambrose *et al.* 1994). Oxidation organic matter, nitrification, non-predatory mortality and respiration by zoo and phytoplankton are nitrogenous-carbonaceous-oxygen-demand, collectively combined into the state variable *CBOD*.

The kinetic pathway of *CBOD* is represented in the source term of Equation (4.2) as:

$$\begin{aligned}
 Q = & - \frac{\partial}{\partial z} \left[ws_{CBOD} \cdot (1 - fd_{CBOD}) \cdot CBOD \right] \\
 & - K_D \cdot \frac{DO}{H_{bod} + DO} \cdot CBOD \\
 & - \frac{5}{4} \frac{32}{14} \cdot K_{DN} \cdot \frac{K_{no3}}{H_{no3} + DO} \cdot NO3 \\
 & + K_{as} \cdot ALGN + K_{bz} \cdot ZOON
 \end{aligned} \tag{4.23}$$

where fd_{CBOD} corresponds to the fraction of the dissolved CBOD, and ws_{CBOD} is the settling velocity for the particulate fraction of CBOD. fd_{CBOD} and ws_{CBOD} are empirically-based coefficients that represent the fact that under quiescent flow conditions, the particulate fraction of CBOD can settle through the water column, and eventually deposit on the bottom (Ambrose *et al.* 1994). The determination of both coefficients should proceed in terms of the best fit between measured and modeled data (Jørgensen and Gromiec, 1989).

Light Attenuation in Estuarine Systems

The solar radiation that reaches the ocean's surface includes the ultraviolet range (290-380 nm), the visible range (380-760 nm), and the infra-red (760-3000 nm). As to primary production in estuarine systems, ecologists are normally concerned with light in the range of wavelengths from 400-700 nm. Defined as "Photosynthetically Active Radiation" (PAR), this range of irradiance provides the predominant source of energy for autotrophic organisms (Day *et al.*, 1989). Moreover, instead of measuring *PAR* in terms of energy,

commercially available quantum meters record the number of quanta (or photons, in the visible range) received per unit area per unit time. The unit of this photon flux density is micro Einstein per squared meter per second ($\mu E m^{-2} s^{-1}$).

The incident light can be reflected, absorbed, and refracted by dissolved and suspended substances in the water and by the water itself. The Beer-Lambert law can be used to describe the light distribution with depth (Day *et al.*, 1989):

$$I_z = I_0 e^{-K_v z} \quad (4.24)$$

where I_0 is light intensity at the water surface, I_z is light intensity at depth z , z is the depth in meters, and K_v is the vertical light attenuation coefficient in m^{-1} .

For long term simulations, the seasonal variation of surface irradiance in Tampa Bay can be represented by a sine curve:

$$I_0 = 1800 + \left(400 \cdot \sin \left(\frac{3\pi}{2} + 2\pi \cdot \left(\frac{day}{365} \right) \right) \right) \quad (4.25)$$

corresponding to an average solar radiation of $1800 \mu E/m^2 s$. Monthly variations range from 1600 in January to $2200 \mu E m^{-2} s^{-1}$ in mid July.

Some studies reported higher values in middle to late spring rather than summer because of increased precipitation and cloud cover associated with the rainy season (Wolfe and Drew, 1990). For this study, real data of surface irradiance, obtained by USGS (Tampa Bay) between June 1990 and September 1991, was used.

McPherson and Miller (1994) and Miller and McPherson (1995) developed a model by partially adjusting the attenuation coefficient in Tampa Bay for changing solar elevation,

and used multiple regression analysis to partition the coefficient into the relative contribution of seawater, water color, chlorophyll and non-chlorophyll suspended matter.

A simplified geometric description of the incident direct solar beam and diffuse skylight is used to describe the effects of solar elevation angle and cloudiness on the amount of *PAR* that passes through the air-sea interface. Since so far there is no process-based model that relates optical characteristics of the water to mass (or concentration) of constituents inside the water column, a large data set which covers a wide range of conditions is required to determine statistical correlations. In their work, Miller and McPherson (1995) used 16083 observations (255 days between 6/02/90 and 9/29/91) of scalar *PAR*, measured in air and at two depths in the water column, to evaluate irradiance that entered the water and subsequent attenuation.

The attenuation coefficient is obtained as the product of the partitioned coefficient and a correction term that accounts for the geometry of the incident irradiance:

$$K_o = \mu_{wd} \cdot K_{adj} \quad (4.26)$$

where μ_{wd} is the correction factor (weighted average cosine), and K_{adj} is the partitioned attenuation coefficient. The formulation for the correction factor, μ_{wd} , developed in Miller and McPherson (1995) is presented in Appendix D.

Lorenzen (1970) showed that the vertical attenuation of *PAR* can be linearly partitioned into a set of partial attenuation coefficients:

$$K_{adj} = K_w + K_c + K_d + K_p \quad (4.27)$$

where K_w is the attenuation coefficient due to water, K_c is due to the presence of chlorophyll a , K_d is due to dissolved substances, and K_p is due to non-algal particulate matter. Nevertheless, other researchers have shown that the partitioning of the components of light attenuation into an empirical model using standard water quality parameters is not precise (e.g. Mote Marine Lab, 1995).

According to Kirk (1994), the inherent properties of the water can be determined by linear superposition of the partial contributions (e.g. color, chlorophyll, etc.). However, the vertical attenuation coefficient is an "apparent" optical property of the water (Kirk, 1994), and it is not only a function of the inherent properties of absorption and scatter, but also the angular and spectral distribution of the incident light.

Originally, McPherson and Miller (1994) partitioned the attenuation coefficient into a set of partial attenuation coefficients:

$$K_{adj} = k_w + E_2 \cdot C_2 + E_3 \cdot C_3 + E_4 \cdot C_4 \quad (4.28)$$

where k_w is the PAR-waveband average attenuation coefficient of seawater, 0.0384 m^{-1} (Lorenzen, 1972); E_2 is the attenuation coefficient of dissolved matter, in $(\text{m Pt-Co units})^{-1}$; C_2 is the water color, in Pt-Co units; E_3 is the attenuation coefficient of chlorophyll and other matter associated with chlorophyll a , in $\text{m}^2 \text{mg}^{-1}$; C_3 is the concentration of chlorophyll a , in mg m^{-3} ; E_4 is the attenuation coefficient of nonchlorophyll suspended matter (NSM), which includes inorganic and organic particulate not directly associated with color or chlorophyll a , in $\text{m}^2 \text{mg}^{-1}$; and C_4 is the concentration of NSM, in mg m^{-3} .

The lack of good measurements of NSM (in terms of total suspended solids and turbidity) constrained the determination of the " $E_4 \cdot C_4$ " term, and the equation was modified to (McPherson and Miller, 1994):

$$K_{adj} = 0.014 \cdot C_2 + 0.062 \cdot (\text{turbidity}) + 0.049 \cdot C_3 + 0.30 \quad (4.29)$$

with the coefficients E_2 and E_3 determined from Tampa Bay and Charlotte Harbor data. In this study, the adjusted attenuation coefficient is determined from Equation (4.29), with C_2 representing the average water color, in Pt-Co units; C_3 is the chlorophyll *a* concentration in mg/m^3 ; and turbidity is given in NTU. Data of water color and turbidity for each segment of the Bay was obtained from the EPC reports (Boler, 1992). Chlorophyll-*a* concentration is determined from the water quality portion of the model.

After determining the correction factor (μ_{nd}), and the partitioned attenuation coefficient (K_{adj}), the attenuation coefficient (K_o) is obtained from Equation (4.26).

Model Coefficients

The model parameters required to simulate the water quality dynamics in the Tampa Bay Estuarine System, are described in Table 4.1. During the implementation phase, model coefficients were determined by isolating specific processes in a test grid with a similar spatial scale as Tampa Bay, and initial values were obtained from literature and previous modeling studies (e.g. AS&I, 1996). The value of the coefficients used in this study are presented in Table 4.2.

Table 4.1 - Description of the coefficients used in the water quality model.

Coefficient	Description	Units
$(\theta_{AD})^{T-20}$	temperature coefficient for NH ₄ desorption	-
$(\theta_a)^{T-20}$	temperature coefficient for algae growth	-
$(\theta_{AI})^{T-20}$	temperature coefficient for ammonium instability	-
$(\theta_{BOD})^{T-20}$	temperature coefficient for CBOD oxidation	-
$(\theta_{DN})^{T-20}$	temperature coefficient for denitrification	-
$(\theta_{NN})^{T-20}$	temperature coefficient for nitrification	-
$(\theta_{OD})^{T-20}$	temperature coefficient for SON desorption	-
$(\theta_{ONM})^{T-20}$	temperature coefficient for mineralization	-
$(\theta_{RESP})^{T-20}$	temperature coefficient for algae respiration	-
$(\theta_z)^{T-20}$	temperature coefficient for zooplankton growth	-
$(\mu_a)_{max}$	algae maximum growth rate	1/day
$(\mu_z)_{max}$	zooplankton maximum growth rate	1/day
$(NH_3)_{air}$	ammonia concentration in the air	µg/L
$a_{chl a}$	algal carbon-chlorophyll-a ratio	mg C / mg Chl-a
a_{nc}	algal nitrogen-carbon ratio	mg N / mg C
a_{oc}	algal oxygen-carbon ratio	mg O ₂ / mg C
d_{aa}	desorption rate of adsorbed ammonium nitrogen	1/day
d_{on}	desorption rate of adsorbed organic nitrogen	1/day
d_{mol}	molecular diffusion coefficient for dissolved species	cm ² /s
E_2	light attenuation coefficient due to dissolved matter	1/(m Pt-Co)
E_3	light attenuation coefficient due to chlorophyll <i>a</i>	1/(m µg/L)
E_4	light attenuation coefficient due to NSM	1/(m mg/L)
fd_{CBOD}	fraction of dissolved CBOD	-
H_m	half-saturation constant for ammonia conversion	(pH unit)
H_{hod}	half-saturation constant for CBOD oxidation	mg O ₂

Table 4.1 - continued.

Coefficient	Description	Units
H_n	half-saturation constant for algae uptake	mg/L
H_{ni}	half-saturation constant for nitrification	mg O_2
H_{no3}	half-saturation constant for denitrification	mg O_2
h_v	Henry's constant	mg/L-atm
I_s	optimum light intensity for algal growth	$\mu E / m^2 / s$
K_{ex}	excretion rate by algae	1/day
K_{mz}	mortality rate of algae	1/day
K_{AE}	reaeration rate constant	1/day
K_{AI}	ammonia conversion rate constant	1/day
K_{DN}	denitrification rate constant	1/day
K_D	organic carbon (as CBOD) decomposition rate	1/day
K_{NN}	nitrification rate constant	1/day
K_{ONM}	organic nitrogen mineralization rate constant	1/day
K_{VOL}	volatilization rate constant	1/day
K_{exz}	excretion rate by zooplankton	1/day
K_{mz}	mortality rate of zooplankton	1/day
P_{aa}	partition coefficient for ammonia nitrogen	1/mg
P_{on}	partition coefficient for organic nitrogen	1/mg
ws_{CBOD}	settling velocity for the particulate fraction of CBOD	m/day
ws_{algae}	algal settling velocity	m/day

Table 4.2 - Literature ranges and values of the coefficients used in the water quality model.

Coefficient	Literature Range	Tampa Bay	Source
$(\theta_{AO})^{T-20}$	1.08	1.08	Assumption
$(\theta_s)^{T-20}$	1.01-1.2	1.08	Di Toro & Connolly(1980);AScI(1996)
$(\theta_M)^{T-20}$	1.08	1.08	Assumption
$(\theta_{BOO})^{T-20}$	1.02-1.15	1.08	Bowie <i>et al.</i> (1980); AScI (1996)
$(\theta_{ON})^{T-20}$	1.02-1.09	1.08	Baca & Arnett (1976); AScI (1996)
$(\theta_{NN})^{T-20}$	1.02-1.08	1.08	Bowie <i>et al.</i> (1980); AScI (1996)
$(\theta_{OD})^{T-20}$	1.08	1.08	Assumption
$(\theta_{ONM})^{T-20}$	1.02-1.09	1.08	Baca & Arnett (1976); AScI (1996)
$(\theta_{RESP})^{T-20}$	1.045	1.05	Ambrose <i>et al.</i> (1994); AScI (1996)
$(\theta_z)^{T-20}$	1.01-1.2	1.08	Di Toro & Connolly (1980)
$(\mu_n)_{\max}$	0.2-8.	1.47	Baca & Arnett (1976); AScI (1996)
$(\mu_z)_{\max}$	0.15-0.5	0.5	Jørgensen (1976)
$(NH_3)_{\max}$	0.1	0.1	Freney <i>et al.</i> (1981)
a_{cha}	10 ~ 112	112	Jørgensen (1976);AScI (1996)
a_{nc}	0.05-0.43	0.15	Jørgensen (1976); AScI (1996)
a_{oc}	2.67	2.67	Ambrose <i>et al.</i> (1994); AScI (1996)
d_{sn}	-	4.0	Simon (1989)
d_{on}	-	4.0	Assumption
d_{nol}	4.E-6-1.E-5	1.E-5	Rao <i>et al.</i> (1984);Krom & Berner (1980)
E_2	-	0.014	Miller & McPherson (1995)
E_3	-	0.062	Miller & McPherson (1995)
E_4	-	0.30	Miller & McPherson (1995)
fd_{CBOD}	-	0.7	Assumption
H_{n1}	9.0	9.0	Freney <i>et al.</i> (1981)
H_{bod}	0.02-5.6	0.18	AScI (1996)
H_n	0.0015-0.4	0.05	AScI (1996)

Table 4.2 - continued.

Coefficient	Literature Range	Tampa Bay	Source
H_{ss}	0.1~2.0	2.0	Ambrose <i>et al.</i> (1994); AScl (1996)
$H_{\text{ss},0.3}$	0.1	0.1	Ambrose <i>et al.</i> (1994); AScl (1996)
h_v	43.8	43.8	Sawyer & McCarty (1978)
I_s	300-350	200.	Di Toro & Connolly(1980);AScl(1996)
K_{ss}	0.05~0.2	0.15	Jørgensen (1976); AScl (1996)
K_{ss}	0.01-0.1	0.08	Jørgensen (1976); AScl (1996)
K_{AI}	-	-	see Appendix C
K_{AI}	0.003~0.008	0.003	Reddy <i>et al.</i> (1990)
K_{D}	0.02~0.6	0.15	Bowie <i>et al.</i> (1980); AScl (1996)
$K_{\text{D}N}$	0.02~1.0	0.90	Baca & Arnett (1976); Assumption
K_{NN}	0.001~0.6	0.08	AScl (1996); Reddy <i>et al.</i> (1990)
$K_{\text{D}NM}$	0.01~0.4	0.1	Di Toro & Connolly(1980);AScl(1996)
K_{VOL}	3.5~9.0	7.0	Fillery and DeDatta (1986)
K_{ss}	0.05~0.3	0.05	Baca & Arnett (1976)
K_{ss}	0.03~0.075	0.05	Jørgensen (1976)
P_{ss}	0.5E-7~1.0E-5	1.0E-5	Simon (1989)
P_{ss}	1.0E-5	1.0E-5	Simon (1989)
ws_{CBOD}	-	5.0	Assumption
ws_{algae}	0.0~30.	5.0	Jørgensen (1976)

CHAPTER 5 THE SEAGRASS MODEL

Using Seagrass as a Bioindicator of the Estuarine System

Seagrasses have an important role in the ecology of estuarine systems where they are present (e.g. Culter, 1992; Tomasko *et al.*, 1996; Phillips and Meñez, 1988; Short, 1980). They serve as habitat for fish and benthic invertebrates. Seagrass leaves provide substrate for many epiphytic organisms. Herbivores such as manatees, fishes, sea turtles, and sea urchins graze directly on seagrass blades. Dead leaves constitute the majority of the detritus pool in seagrass beds. Seagrass also interacts with the physical components of the estuary by slowing down the currents (Fonseca *et al.*, 1982). Their presence also inhibits the resuspension of sediments, which also affects nutrient cycles by reinforcing the deposition of organic and inorganic material from the water column (Bartleson, 1988).

Since each species of seagrass has its own particular response to physical and oceanographical factors, one species is usually dominant in any given area (Dawes *et al.*, 1985; Williams, 1990; Short *et al.*, 1989). Some studies even suggest that succession or replacement can be attributed to the water quality and trophic state of the system (Tomasko *et al.*, 1996). According to the authors, *Thalassia* can be characterized as a truly oligotrophic species, which cannot prevail in areas of elevated nutrient loading.

Therefore, in estuarine systems where seagrass has declined due to anthropogenic effects, restoration of seagrass beds can be linked exclusively to environmental quality. In this sense, seagrass provides a direct assessment of the success of the restoration processes (Dennison *et al.*, 1993).

Seagrass Ecosystems

Seagrasses are unique for the marine environment as they are the only flowering plants that have totally returned to the sea (Zieman, 1982). Florida enjoys one the largest seagrass resources on Earth. Of the 10,000 km² of seagrass bed in the Gulf of Mexico, over 8,500 km² are in Florida waters, primarily in the southern end of the peninsula. Physical and oceanographical factors drastically reduce the amount of seagrass bed north of Florida Bay, on both coasts. Along the Atlantic coast, a wave dominated environment with a relatively unstable substrate, seagrass beds are confined to inlets and lagoons. On the Gulf of Mexico coast, seagrass beds diminish due to the high-turbidity waters and reduced salinity coming from land drainage. North of this area, several bays, including Tampa Bay and Boca Ciega Bay, formerly possessed extensive seagrass coverage, but anthropogenic perturbations have greatly reduced the extent of these beds (Zieman, 1982).

According to den Hartog (1970), marine aquatic angiosperms referred to as seagrasses include approximately 49 species in 12 genera. The three dominant species of the west coast of Florida are *Thalassia testudinum*, *Halodule wrightii*, and *Syringodium filiforme* (Zieman and Zieman, 1989). A detailed description of physiology and production ecology of seagrasses can be found in McRoy and Helfferich (1977), Phillips and McRoy (1980),

Zieman (1982), and Phillips and Meñez (1987). The following is a brief description of each species reproduced from Zieman (1982). Figure 5.1 shows a schematic picture of the three species.

Thalassia testudinum (turtle grass) is the largest and most vigorous of the southwest Florida seagrasses. Leaves are ribbon-like, typically 4 to 12 mm wide with rounded tips and are 10 to 35 cm in length. There are commonly two to five leaves per turion. Rhizomes are typically 3 to 5 mm wide and may be found as deep as 25 cm in the sediment. Turtle grass forms extensive meadows throughout most of its range.

Halodule wrightii (shoal grass) is an early colonizer of disturbed areas. It is found primarily in disturbed areas where *Thalassia* or *Syringodium* are excluded because of prevailing conditions such as repeated exposure to air. Leaves are flat, typically 1 to 3 mm wide and 10 to 20 cm long, and arise from erect shoots. The tips of the leaves are not rounded, but have two or three points, an important recognition character. Shoal grass has been reported to be the most tolerant of all seagrasses to variations in salinity, and exposure to air (e.g., McMillan, 1974). However, recent low salinity and seagrass distributions in Florida Bay may suggest that *Thalassia* could be more tolerant to prolonged lower salinity levels (Montague, person. comm.).

Syringodium filiforme (manatee grass) is distinctive in having cylindrical leaves. There are commonly two to four leaves per turion, and these are 1.0 to 1.5 mm in diameter. Length is highly variable, but can exceed 50 cm. The rhizome is less robust than that of *Thalassia* and more superficially rooted. Manatee grass is commonly mixed with the other seagrasses, or in small, dense, monospecific patches.

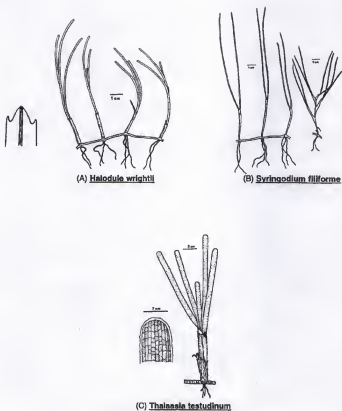


Figure 5.1 - Seagrass species commonly found in west Florida (from Phillips and Meñez, 1987).

Previous Work

The development of a numerical model of the seagrass community may provide a mechanism for synthesizing all the dynamic functions (hydrodynamics, water quality, primary production, etc.) of an estuarine ecosystem. Short (1980), using energy flow diagrams (Odum, 1971), developed a seagrass community model to investigate the mechanisms of temperate seagrass (eelgrass) production. Results of that study predicted an average production rate for Charlestown Pond (Rhode Island) that was comparable to observed rates.

Bach (1993) extended a general eutrophication model for the Denmark coastal area to include the seasonal variations in growth of seagrass. Coupling between the eutrophication and seagrass models was performed by seagrass nutrient uptake and detritus. Hydrodynamics effects were coupled to the model simulation through a hydrodynamics box model.

Fears (1993) used a numerical model developed by Dr. C. Montague (unpublished manuscript) to study the salinity fluctuations effects on seagrass distribution, abundance, and species composition. The salinity fluctuations were represented in the model by step functions, single short-lived pulses, or sinusoidal functions. For each seagrass species, literature and experimental values were assigned for maximum growth rate, optimal salinity, range of salinity tolerance, and death rate. Model sensitivity analysis showed maximum growth rate and minimum death rate as the crucial parameters of the model. Optimal salinity coefficient and tolerance range were key parameters in determining the cause/effect relationship between salinity fluctuations and seagrass response.

Fong and Harwell (1994) developed a STELLA model to predict changes in the biomass of five components (three species of tropical seagrass, epiphytic algae, and macroalgae) of the seagrass community of Florida Bay. Environmental parameters (light, temperature, salinity, sediment nutrients, water column nutrients) were represented by literature values or sinusoidal functions, with no coupling with hydrodynamics. The most important model parameters were productivity/biomass relationships, differential tolerances to extreme salinity, and P/I curves. An important characteristic of Fong and Harwell's model is the feedback loop between the abundance of epiphytes and the amount of light reaching the seagrass blades, leading to a competition type of relationship.

Erftemeijer and Middelburg (1995) studied the nutrient cycling in tropical seagrass using a simple mass balance model. Model simulations used measured data on nutrient availability, seagrass primary production, community oxygen metabolism, seagrass tissue nutrient contents, and sediment-water nutrient exchange rates from South Sulawesi (Indonesia). Results of that study, showed that the ratio between leaf vs. root nutrient uptake depend on internal nutrient recycling (translocation from old plant parts to new growing parts), with higher internal recycling increasing the importance of leaf uptake. Throughout the internal recycling range (from 0 to 50%), the model showed that nutrient is predominantly uptaken by the root-system.

Sheng *et al.* (1995) developed a coupled 2-D hydrodynamics-water quality-light-seagrass model to quantify the impact of reduced nutrient loading on the water quality and light/seagrass dynamics in Roberts Bay, Florida. The results of that study showed that reduced nutrient loading led to increased DO and light, and reduced phytoplankton, CBOD,

dissolved organic nitrogen and ammonium nitrogen. However, there was no noticeable increase in seagrass biomass, since sediment nutrient concentration, which controlled the seagrass growth in the model, was still saturated. With a 100% load reduction, the study showed a more pronounced impact for such parameters as nitrogen and phytoplankton, but not significantly different for light and seagrass, again due to saturated nutrient concentration in the sediment column.

Development of the Numerical Model

The conceptual model used in this study was originally developed by Fong and Harwell (1994), and was shown to be able to describe some dynamic interactions of the seagrass community structure in the Florida Keys. In this study, the conceptual model is improved to: (a) adapt the model to the Tampa Bay conditions; (b) give the model a spatial dimension; (c) add a more realistic mathematical description of the available light to the seagrass bed; and (d) incorporate the three-dimensional structure of the hydrodynamics, sediment and water quality dynamics model into the simulations.

This seagrass model consists of four biotic variables, including three species of seagrass found in Tampa Bay, *Thalassia testudinum*, *Halodule wrightii*, and *Syringodium filiforme*, and a functional form of epiphytic algae on seagrass (Figure 5.2). In the model the epiphytic algae is controlled by light, temperature, water-column nutrient concentration, and available substrate (seagrass density) (Figure 5.3). The abundance of each species of seagrass

is controlled by available light, temperature, salinity, sediment nutrient concentration, and physical disturbance through bottom shear stress (Figure 5.4).

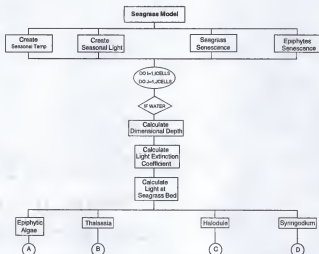


Figure 5.2 - Structure and components of the numerical seagrass model used for this study.

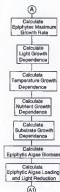


Figure 5.3 - Epiphytic algae model flow chart.

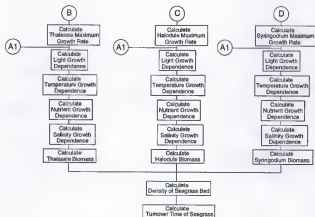


Figure 5.4 - Seagrass model flow chart.

Mathematical Formulation

For each species of seagrass, literature values of maximum growth rates and biomass are obtained, and incorporated to a density-dependent growth function. Subsequently, environmental variability in light, temperature, salinity, and sediment nutrient concentration would result in stresses to the growth rate, reducing the maximum growth rate according to species-specific sensitivity. Death rates are accelerated when extreme values of salinity and temperature are endured for an extended period of time. Next, the mathematical formulation describing environmental factors that affect the seagrass community will be presented, followed by the relationships controlling seagrass productivity.

Light

Light regime is the primary environmental factor influencing photosynthesis, growth and depth distribution of seagrasses (Dennison, 1987). Light availability is often the primary limiting factor for seagrass growth (e.g. Wetzel and Penhale, 1983; Dennison and Alberte, 1985). Studies showing the decline of seagrass due to increases in water turbidity demonstrate the crucial role of light in determining seagrass distribution (Orth and Moore, 1983; Cambridge and McComb, 1984). Therefore, the determination of the relationship between available light and seagrass growth and distribution is of extreme importance in a modeling effort. The amount of photosynthetically active radiance (PAR) reaching the seagrass bed is obtained from the water quality component of this integrated model.

Temperature

The seasonal variation of water temperature is represented in the model by a sine curve:

$$Temp = 23 + \left(7 \cdot \sin \left(\frac{3\pi}{2} + 2\pi \cdot \left(\frac{day}{365} \right) \right) \right) \quad (5.1)$$

corresponding to an annual average of 23 °C, higher temperature levels during summer (maximum of 30 °C) and the lowest levels during winter (minimum of 16° C) (Zieman and Zieman, 1989).

Salinity

Montague and Ley (1993) reviewed previous studies on salinity tolerance of major species of seagrass, and discussed possible effects of salinity fluctuation on seagrass abundance in Northeastern Florida Bay. Their study showed that salinity changes could cause changes in both the distribution and total abundance of benthic vegetation.

Salinity is a state variable of the circulation and transport model, and its distribution is obtained from the hydrodynamics component of this integrated model.

Density-Dependent Growth Rate

For *Thalassia*, Williams (1988) found maximum growth rates up to 27 g dry wt m⁻² day⁻¹ in pristine areas of the Virgin Islands, and Fourqurean and Zieman (1991) found maximum biomass to be 470 g dry wt m⁻² in Florida Bay. Powell *et al.* (1989) found that *Halodule* in Florida Bay can grow as fast as 16 g dry wt m⁻² day⁻¹, and a maximum biomass of 150 g dry wt m⁻². For *Syringodium*, Short *et al.* (1985) reported a maximum growth rate

of $6.3 \text{ g dry wt m}^{-2} \text{ day}^{-1}$, in the Bahamas, and a maximum biomass of $190 \text{ g dry wt m}^{-2}$. Thus, the hierarchy for growth rates is *Thalassia* > *Halodule* > *Syringodium* and for maximum biomass is *Thalassia* > *Halodule* \approx *Syringodium*, resulting in a density-dependent growth curve that favors *Thalassia* throughout the range of densities (Figure 5.5). These growth rates correspond to "optimal" environmental conditions, therefore, each maximum growth rate is further modified by light, temperature, salinity, and sediment nutrient concentration, resulting in a possible alteration in the growth-rate hierarchy.

Density-dependent Growth Rate

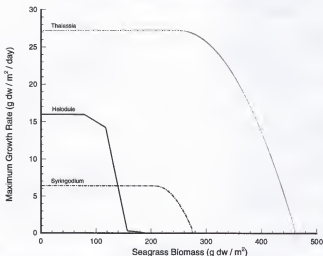


Figure 5.5 - Seagrass density-dependent maximum growth rate: *Thalassia* (dotted line), *Halodule* (solid line), and *Syringodium* (dash-dotted line).

Growth Rate Dependence on Light

Most studies on seagrass distribution and growth reveal that light is an important factor controlling seagrass distribution (e.g. Williams, 1987; Dawes and Tomasko, 1988; Dunton, 1990). Fourqurean and Zieman (1991) established the relationship between light and photosynthesis for *Thalassia*, specifying P_{\max} of $200 \mu\text{g O}_2 \cdot \text{g}^{-1} \cdot \text{min}^{-1}$. In this model, we assumed saturation occurring at $425 \mu\text{E m}^{-2} \text{s}^{-1}$, and no photoinhibition at high light levels; the compensation point is approximately $15.1 - 15.7 \mu\text{E m}^{-2} \text{s}^{-1}$. Williams (1987) found that light saturation levels for *Halodule* and *Syringodium* were similar. Fong and Harwell (1994) assumed that *Halodule* may require less light than the other species for maximum productivity, so in the model the saturation point for *Halodule* is $300 \mu\text{E m}^{-2} \text{s}^{-1}$. In other words, Fong and Harwell (1994) postulates that growth of *Thalassia* and *Syringodium* is reduced when available light is less than $425 \mu\text{E m}^{-2} \text{s}^{-1}$, while growth remains maximum for *Halodule* until light is below $300 \mu\text{E m}^{-2} \text{s}^{-1}$.

The mathematical formulation of the growth rate dependence on light is given by (Fig. 5.6):

$$\begin{aligned} T_{\text{light}} &= 1 - e^{-0.013 \cdot avll} \\ H_{\text{light}} &= 1 - e^{-0.008 \cdot avll} \\ S_{\text{light}} &= 1 - e^{-0.040 \cdot avll} \end{aligned} \quad (5.2)$$

where *avll* represents the available light at the seagrass bed.

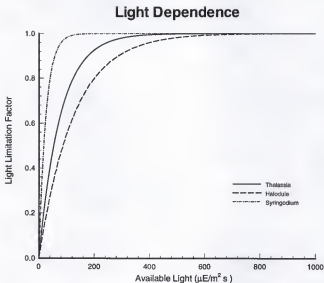


Figure 5.6 - Seagrass growth rate dependence on light: *Thalassia* (dotted line), *Halodule* (solid line), and *Syringodium* (dash-dotted line).

Growth Rate Dependence on Salinity

There are few studies that directly test the effect of altered salinity on seagrasses. We performed a laboratory experiment to study the response of three species of tropical seagrasses to salinity fluctuations (Yassuda *et al.*, 1996 - *manuscr. in preparation*), and preliminary results demonstrate that tolerance is species-specific, with *Halodule* being the most tolerant to salinity variations, and *Syringodium* being the least tolerant. This results agree with literature and the hypothesis of the original model (Fong and Harwell, 1994).

The seagrass growth-salinity relationship specific for each species shows that *Halodule* has the widest salinity optimum, with growth being reduced for salinity below 30 and above 45 ppt.

The mathematical formulation of the growth rate dependence on salinity is given by (Figure 5.7):

For *Thalassia*

$$\begin{aligned}
 & \text{salinity} < 31.67 \\
 & T_{sal} = 0.00035 \cdot e^{0.25 \cdot sal} \\
 & 31.67 < sal < 35.0 \\
 & T_{sal} = 0.009 \cdot sal + 0.685 \\
 & 35.0 < sal < 41.67 \\
 & T_{sal} = 1.0 \\
 & 41.67 < sal < 45.0 \\
 & T_{sal} = -0.003 \cdot sal + 1.125
 \end{aligned} \tag{5.3}$$

For *Halodule*

$$\text{salinity} < 18.0$$

$$H_{\text{sal}} = 0.006 \cdot \text{sal} - 0.0751$$

$$18.0 < \text{sal} < 28.0$$

$$H_{\text{sal}} = -0.0109 \cdot \text{sal}^2 + 0.5963 \cdot \text{sal} - 7.2$$

$$28.0 < \text{sal} < 32.0$$

$$H_{\text{sal}} = 0.0165 \cdot \text{sal} + 0.4785$$

$$32.0 < \text{sal} < 35.0$$

$$H_{\text{sal}} = 1.0$$

$$35.0 < \text{sal} < 38.0$$

$$H_{\text{sal}} = -0.3003 \cdot \text{sal} + 11.5105$$

$$\text{sal} > 38.0$$

$$H_{\text{sal}} = 0.0$$

(5.4)

For *Syringodium*

$$\text{salinity} < 18.0$$

$$S_{\text{sal}} = 0.0$$

$$18.0 < \text{sal} < 32.0$$

$$S_{\text{sal}} = 0.0065 \cdot \text{sal}^2 - 0.2551 \cdot \text{sal} + 2.5037$$

$$32.0 < \text{sal} < 38.0$$

$$S_{\text{sal}} = -0.0056 \cdot \text{sal}^2 + 0.3885 \cdot \text{sal} - 5.74$$

$$38.0 < \text{sal} < 52.0$$

$$S_{\text{sal}} = 0.0065 \cdot \text{sal}^2 - 0.6533 \cdot \text{sal} + 3.35$$

$$\text{sal} > 52.0$$

$$S_{\text{sal}} = 0.0$$

(5.5)

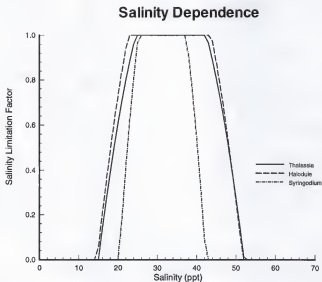


Figure 5.7 - Seagrass growth rate dependence on salinity: *Thalassia* (dotted line), *Halodule* (solid line), and *Syringodium* (dash-dotted line).

Growth Rate Dependence on Temperature

Tomasko and Dawes (1990) reported some seasonal trends in the growth rate of Sarasota Bay seagrasses. To be consistent with the hypothesis that *Halodule* is an opportunistic species that often dominates in transition areas, the model specifies a broader range of optimum temperature for *Halodule*, followed by *Thalassia*, and assigns to *Syringodium* the least temperature variation tolerance. Optimum growth for all three species of seagrass occurs at 26 °C, and growth rate decreases at higher or lower temperatures.

The mathematical formulation of the growth rate dependence on temperature is given by (Figure 5.8):

For *Thalassia*

$$T_{temp} = -0.0059 \cdot temp^2 + 0.329 \cdot temp - 3.5862 \quad (5.4)$$

For *Halodule*:

$$\begin{aligned} &temp < 23.0 \\ &H_{temp} = -0.0123 \cdot temp^2 + 0.6029 \cdot temp - 6.3436 \\ 23.0 &< temp < 26.0 \\ &H_{temp} = 1.0 \\ 26.0 &< temp < 52.0 \\ &H_{temp} = -0.0123 \cdot temp^2 + 0.6029 \cdot temp - 6.3436 \\ &temp > 52.0 \\ &H_{temp} = 0.0 \end{aligned} \quad (5.3)$$

For *Syringodium*

$$\begin{aligned}
 &temp < 18.0 \\
 &S_{temp} = 0.0 \\
 &18.0 < temp < 32.0 \\
 &S_{temp} = -0.0203 \cdot temp^2 + 1.021 \cdot temp - 11.83 \\
 &temp > 32.0 \\
 &S_{temp} = 0.0
 \end{aligned}
 \tag{5.3}$$

Temperature Dependence

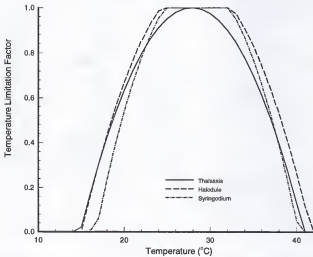


Figure 5.8 - Seagrass growth rate dependence on temperature: *Thalassia* (dotted line), *Halodule* (solid line), and *Syringodium* (dash-dotted line).

Growth Rate Dependence on Sediment Nutrients

According to the characterization presented in Chapter 2, Tampa Bay sediments are rich in phosphorus. If sediment nutrients limit seagrass production, it is most likely nitrogen. Seagrass takes up most of its nitrogen requirements as ammonium from the sediment via its root-rhizome system (Short and McRoy, 1984; Erftemeijer and Middelburg, 1995). In this study, the nitrogen uptake is proportional to a fixed internal concentration that is assumed to be 2% of the seagrass dry weight (Zimmerman *et al.*, 1987; Pellikaan and Nienhuis, 1988). Using a formulation similar to the one describing phytoplankton nutrient uptake, sediment nitrogen levels below 0.95% of the seagrass internal content is assumed to inhibit growth (Short, 1987; Pregall *et al.*, 1987; Zimmerman *et al.*, 1987).

Theoretically, specific sediment nutrient relationships should be formulated to describe species differentiation. Like for the physical parameters, *Halodule* would be favored in more extreme conditions of a eutrophic organic-rich sediment (Tomasko *et al.*, 1996). *Syringodium* would prevail in low suspended sediment concentration, since its distribution is restricted to more oceanic environments. *Thalassia* would present a wide range of sediment nutrient concentration tolerance, but could not survive in anaerobic conditions that commonly occur in nutrient-rich sediments (Tomasko *et al.*, 1996). The lack of literature data on tropical seagrasses and nitrogen uptake prevented a further refinement of the model formulation, and reveals the need for more experimental research in this area.

CHAPTER 6

APPLICATION OF THE CIRCULATION AND TRANSPORT MODEL

Design of Tampa Bay Grid

Previous hydrodynamic studies (Goodwin, 1987; Galperin *et al.* 1991; Hess, 1994; Sheng and Yassuda, 1995) demonstrated that complex geometrical and bathymetrical features in the Tampa Bay Estuarine System (Figure 2.1) have a profound influence on the circulation and transport within the Bay. Thus, to successfully apply an integrated model to Tampa Bay, it is essential to design a numerical grid which preserves the dominant geometrical/bathymetrical features. Using a boundary-fitted curvilinear grid, it is possible to design grid lines which coincide with shoreline, causeways, bridges, and the navigation channels. Sheng and Peene (1992), Peene (1995), and Sheng *et al.* (1995) used a relatively coarse boundary-fitted grid for Tampa Bay (15 x 51 horizontal cells and 4 vertical layers) in their studies of the entire Sarasota and Tampa Bay Systems (189 x 51 horizontal cells and 4 vertical layers). Preliminary studies of the navigation channel influence on the hydrodynamics (Yassuda *et al.*, 1992) demonstrate the importance of accurate representation of navigation channel in simulating the circulation pattern in Tampa Bay. Sheng and Yassuda (1995) refined the grid to 39 x 62 horizontal cells and 4 vertical layers in order to simulate residual flow and salinity field under four different forcing conditions. Their results suggest that simulation results could be improved by refining the horizontal grid along the East side of the Bay, where most of the freshwater inflow occurs. Model tests with 4, 8, and 15 vertical

layers were performed and the optimal balance between computational cost and accuracy was obtained with 8 layers. Furthermore, the grid was extended offshore so that the ocean boundary coincided with the NOAA C-1 station, where tidal data was obtained for the period of August 1990 to September 1991. Figure 6.1 shows the location of the NOAA's "Tampa Bay Oceanographic Project" stations, where "C" stands for current meters, "M" for meteorological, "T" for tidal gages, and "S" for salinity.

The computational grid used for the integrated model of the Tampa Bay Estuarine System is shown in Figure 6.2. It contains 45 by 85 horizontal cells and 8 vertical layers, with a total of 30600 grid cells. Grid spacing varies from 100 to 1500 meters. This grid was generated using a grid generation program originally developed by Thompson (1985), and digitized Florida coastline data.

The depth information was based on the raw data obtained from NOAA's National Geophysical Data Center. Inasmuch as these data sets were obtained from surveys done during the 1960's and 1970's, they lack a good representation of the navigation channel. Hess(1994), during the calibration process of the NOAA/Princeton model of Tampa Bay, reported that the best result was obtained by multiplying the original cell depth by spatially varying constants. In an attempt to improve model results, the raw bathymetric data was modified by "dredging" the navigation channel up to the depth recorded by NOAA's instruments in 1991 (NOAA, 1994), and then smoothing the bathymetry along the cross-section. The bathymetric contours used in this study are plotted in Figure 6.3.

Causeways, small spoil islands, and any other sub-grid scale features are represented as bars in the computational grid. Flow and transport are not allowed to go through the bars.

For the purpose of studying advective fluxes throughout the Bay, Sheng and Yassuda (1995) further divided the computational grid of Figure 6.2 into 14 Bay segments,

approximately corresponding to the WASP segments of AScl (1996) study. This segmentation, shown in Figure 6.4, will be used in this study to evaluate the flushing characteristics of each Bay segment.

NOAA's Tampa Bay Oceanographic Project Stations

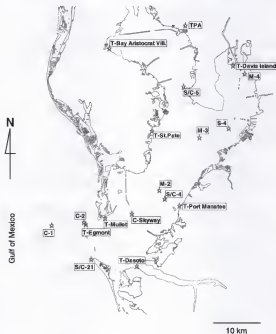


Figure 6.1 - NOAA's TOP station locations in Tampa Bay.

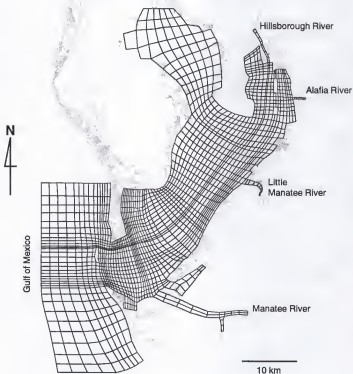
TAMPA BAY**Computational Grid - 45 x 85 cells**

Figure 6.2 - A boundary-fitted grid for the Tampa Bay Estuarine System.

TAMPA BAY

Bathymetry

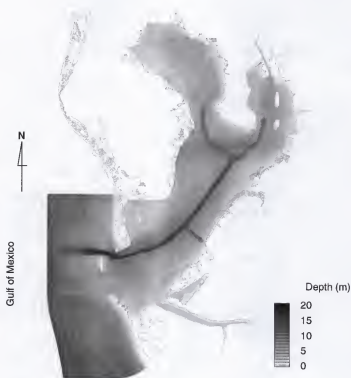


Figure 6.3 - Tampa Bay bathymetric contours.

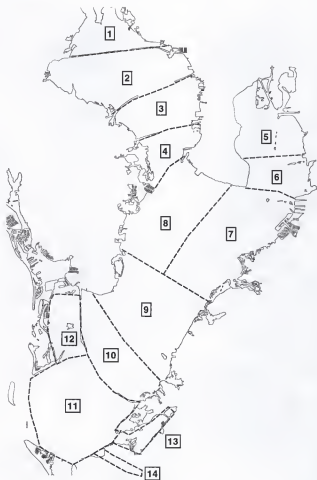


Figure 6.4 - Bay segments (Sheng and Yassuda, 1995).

Forcing Mechanisms and Boundary Conditions

The tidal forcing along the Gulf of Mexico boundary was prescribed by real data obtained at the NOAA C-1 station (Figure 6.5 and 6.6). The time series were obtained from a pressure transducer fixed to a bottom-mounted ADCP (Acoustic Doppler Current Profiler) unit positioned approximately 8 km west of the mouth of the Bay. The tidal spectrum clearly shows the diurnal and semidiurnal frequency dominance. From these figures, it is possible to classify the incident tide as mixed, mainly semidiurnal, which is in accordance with the results obtained by NOAA (1993) using the Defant (1961) criteria .

The baroclinic simulation requires a realistic initial salinity field in order to minimize effects of the initial conditions on the solution, and to avoid longer "spin-up" time. Seasonal-averages of the salinity distribution in Tampa Bay (Boler, 1992) were used to determine an initial salinity at each grid cell. Since the data portrayed vertically averaged conditions, a 1 ppt difference was assumed between the bottom and the top layer in Lower and Middle Tampa Bay. For Hillsborough Bay and Old Tampa Bay, a 2 ppt vertical stratification was assumed. Figure 6.7 shows the initial salinity field (surface layer) used in the 1990 simulation, and Figure 6.8 shows the initial salinity field (surface layer) used in the 1991 simulation.

The offshore salinity boundary condition was determined from a 1-D advection for the ebb flow, and a prescribed value during the inflow. Based on NOAA's data (NOAA, 1993), the salinity in the Gulf of Mexico next to Tampa Bay is approximately constant, around 36 ppt. Hence, salinity value of 36 ppt was assigned as the prescribed boundary condition.

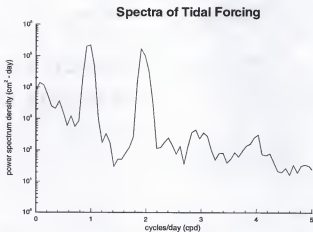
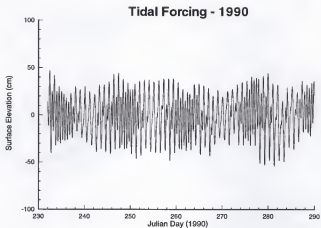


Figure 6.5 - Tidal forcing for the 1990 simulation.

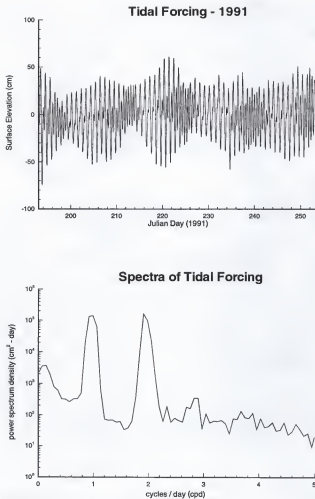


Figure 6.6 - Tidal forcing for the 1991 simulation.

Initial Salinity Distribution - Sep/1990

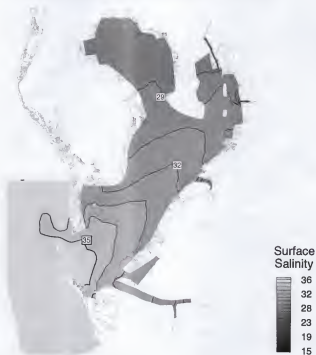


Figure 6.7 - Initial salinity distribution (surface) for the 1990 simulation.

Initial Salinity Distribution - Jul/1991

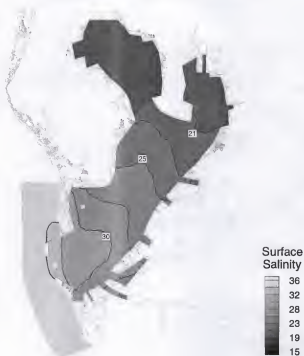


Figure 6.8 - Initial salinity distribution (surface) for the 1991 simulation.

River discharge and rainfall are the two principal sources of freshwater into the system. Hourly rainfall data were obtained from NOAA's National Climate Data Center (NCDC) at three stations (Tampa Bay Intl. Airport, St. Petersburg, and Parrish) (NOAA, 1991). Figure 6.9 shows the rainfall data for September to November of 1990 (dry-period), and July to August of 1991 (wet-period). The rainfall data were interpolated into the computational grid, with the weighting function inversely proportional to the distance to each of the three stations.

Daily river discharge for the Hillsborough River, Alafia River, Little Manatee River, Rocky Creek, and Sweetwater Creek were obtained from USGS (1991, 1992). Since these publications only report discharges upstream the Manatee River dam, and there was no record for Lake Tarpon Canal, historical values were used for these two rivers (Figure 6.10). At each river boundary, salinity was prescribed as constant based on seasonal values (Wolfe and Drew, 1990; Boler, 1992).

During the simulations, wind stress is applied at all surface cells. For the 1990 simulation, the wind field (velocity and direction) from two stations (Tampa Bay Intl. Airport and NOAA's station M-2) was obtained with a three-hour interval. For the 1991 simulation, data from four stations (Tampa Bay Intl. Airport and NOAA's stations M-2, M-3, and M-4) were used. Wind speed is transformed to wind stress using Garrat's formula (Garrat, 1977), and interpolated into the computational grid according to the same procedure used for rainfall. Figure 6.11 and 6.12 show stick diagrams of the wind velocities for September to November 1990, and July to August 1991, respectively.

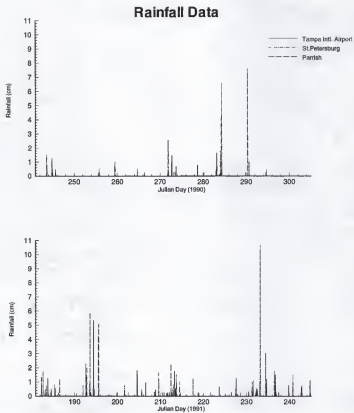
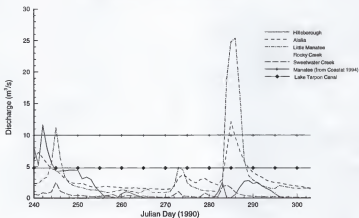


Figure 6.9 - Rainfall data for the 1990 and 1991 simulations.

1990 Simulation - River Discharges



1991 Simulation - River Discharges

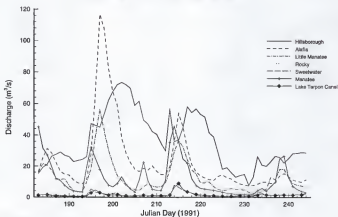


Figure 6.10 - River discharges for the 1990 and 1991 simulations.

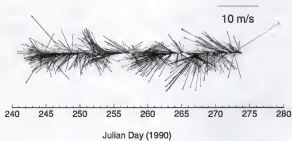
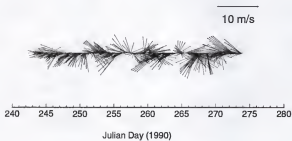
Station M-2**Tampa Intl. Airport**

Figure 6.11 - Wind velocity for the 1990 simulation.

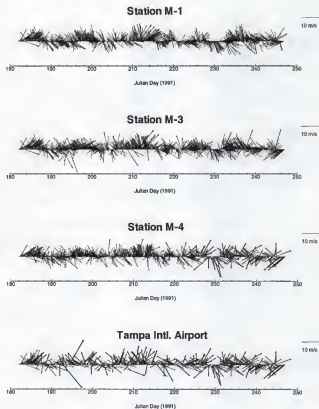


Figure 6.12 - Wind velocity for the 1991 simulation.

Modeling Strategy

During the calibration process, the model was adjusted to simulate a particular condition where enough data enabled tuning of model coefficients and inputs. For this purpose, September 1990 was selected because the "Tampa Bay Oceanographic Project" (NOAA, 1993) provided data for tidal stage, currents, and salinity at several locations throughout the Bay. As to validation, model coefficients were held fixed at the calibration values, and the hydrodynamic component of the model was tested using July and August 1991 data. The model's ability to reproduce episodic events was assessed by means of the simulation of the tropical storm "Marco" in October 1990.

Results of the Barotropic Simulation

Several simulations were performed in order to test the grid configuration, bottom roughness, horizontal diffusion constant, and bathymetry. The results evidenced that the model is particularly sensitive to water depth. Unfortunately, the "Tampa Bay Oceanographic Project" conducted by NOAA did not make any attempt to improve the bathymetric data of the Bay, which correspond to surveys done prior to major dredging.

Initial results showed that tidal amplitude and phase in the upper reaches of the Bay could be calibrated through bottom friction, although the corresponding bottom roughness height (0.01 cm) was an order of magnitude smaller than usual values reported in the literature (0.1 to 1.0 cm). Furthermore, a comparison between data and model results at the Sunshine Skyway Bridge revealed an offset in the vertical profile of the longitudinal residual

currents. This difference suggests that on an intertidal basis, more water should be entering the Bay. By dredging the navigation channel up to the depth reported by the instruments deployed in 1990 by NOAA, a better agreement was obtained between data and model results.

Figure 6.13 shows the comparison between measured and simulated surface elevation for Egmont Key, close to the mouth of the Bay, and St. Petersburg, in Middle Tampa Bay. Figure 6.14 shows data and model results for Davis Island in the upper reaches of Hillsborough Bay, and Bay Aristocrat Village in the upper reaches of Old Tampa Bay. In order to avoid offsets due to original leveling of the gages, the measured data sets were demeaned prior to comparison with model results. The plots show a good agreement between data and model results, both in amplitude and phase. From these figures, it can be seen that tidal range increases about 31% from the mouth to the upper reaches of the Bay. Also, the tidal wave takes about four to five hours to reach the head of Old Tampa Bay, and about three to four hours to reach the head of Hillsborough Bay.

Overall, the model is able to simulate surface elevation within 10%. This indicates that the propagation of the tidal wave can be accurately simulated with the barotropic model, and bathymetry, horizontal diffusion, and bottom roughness constant are reasonably calibrated.

Summing up, grid resolution and bathymetry are the most sensitive inputs to the model, with increased resolution improving model accuracy. Changes in bathymetry are usually directly related to changes in tidal amplitude. Bottom friction is inversely proportional to tidal amplitude, especially in the upper reaches of the Bay. Increasing bottom friction also reduces amplitude of currents, and increase the time lag of the tidal wave.

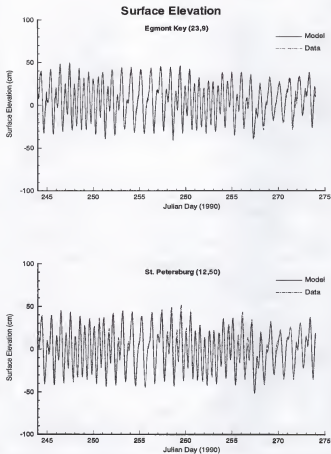


Figure 6.13 - Surface elevation at Egmont Key and St.Petersburg (September 1990).

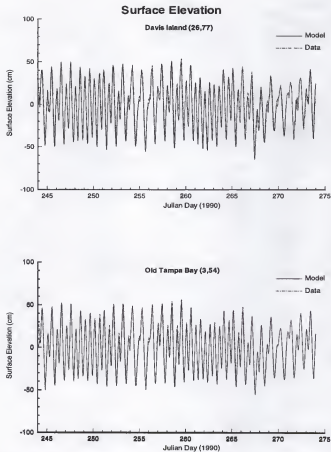


Figure 6.14 - Surface elevation at Davis Island and Old Tampa Bay (September 1990).

Results of the Baroclinic Simulation

Following the barotropic simulation with tidal forcing only, the model calibration proceeded with baroclinic and wind-driven circulation as well. The baroclinic simulation starts with a "spin-up" run which is summarized below:

- A initial salinity field (Figure 6.6), typical of dry-season conditions was generated based on available data collected by EPC throughout the Bay (Boler, 1992). As described in the "Forcing Mechanisms and Boundary Conditions" section, data from different stations were interpolated into the computational grid, using a weighting function inversely proportional to the distance from the three closest stations.

- Starting with a zero velocity field, and without any barotropic forcing mechanisms (tides, river discharges, and wind), a steady-state condition, representing the balance between the initial salinity distribution (that remained unchanged), the velocity field, and surface elevation was achieved in 5 days. The results showed that the horizontal salinity gradient between the Gulf of Mexico and the upper reaches of Bay is balanced by a setup of 4 cm towards the head of the Bay. This superelevation, as defined by Mehta (1990), is in agreement with the results of the conceptual model developed by Weisberg and Williams (1991) in a study of the role of buoyancy in driving a non-tidal circulation in Tampa Bay.

- After this period, tides (represented by the four major tidal constituents - M_2 , S_2 , O_1 , and K_1), and river discharges (averaged values for September 1990) were turned on

and the simulation continued for 90 days. This 90-day spin-up time was sufficient to allow the salinity field to reach a dynamic steady-state throughout the computational grid.

Using the results of the spin-up run (surface elevation, velocity, and salinity) as the initial condition, Tampa Bay circulation during September 1990 was simulated with real data of tidal forcing, river discharges, rainfall, and wind field.

To quantify the model's performance, time series statistics are presented in terms of the root-mean-square error (E_{rms}) and the normalized rms error, defined as the ratio between the rms error to the observed range. The normalized rms error gives a more meaningful indication on model's ability to reproduce the tidal signal at each station.

The rms error is calculated according to:

$$E_{rms} = \left[\frac{1}{N} \sum_1^N (\eta_{model} - \eta_{data})^2 \right]^{1/2} \quad (6.1)$$

where N is the total number of signal pairs, η_{model} is the model result, and η_{data} is the tidal data at each NOAA station.

Since tidal constituents do not vary significantly over the year inside Tampa Bay (NOAA, 1993), it is worthwhile to evaluate the model's ability to simulate measured tidal characteristics by using the method of harmonic analysis i.e., comparing simulated and measured tidal constituents at a few selected stations.

First, a Fourier analysis was performed to determine the spectral density of both measured and simulated data. Inasmuch as the area under the spectral density curve (variance) is proportional to the total energy of the signal, the breakdown of the spectral density in specific frequency-bands defines the relative energies within each band.

Subsequently, a least-squares harmonic analysis was performed. Simulated and measured data were compared in terms of the amplitude and phase of the four major tidal components (M_2 , S_2 , O_1 , and K_1).

The spectral analysis was performed using specific subroutines (power spectrum density - *psd*) of the data analysis program MATLAB. In calculating the spectral density, MATLAB utilizes Welch's method which performs an FFT transformation over a series of overlapping or non-overlapping data sets. Due to normalization done internally in the program, the energies calculated by MATLAB were utilized in a relative sense to determine the distribution of spectral densities, and to perform comparative analysis.

Tides

Table 6.1 presents the maximum measured tidal range, the rms error, and the normalized rms error percentile for Egmont Key, close to the mouth of the Bay, St. Petersburg, in Middle Tampa Bay, Davis Island in the upper reaches of Hillsborough Bay, and Bay Aristocrat Village in the upper reaches of Old Tampa Bay.

Table 6.1 -The rms error (Erms) between measured and simulated water surface elevation - September/90.

Station	Measured Tidal Range (cm)	Erms (cm)	Normalized Erms (%)
Egmont Key	86.57	4.02	4.6
Mullet Key	82.16	3.77	4.5
Desoto Point	86.71	4.63	5.3
St.Petersburg	87.79	6.59	7.5
Davis Island	106.28	7.95	7.5
Old Tampa Bay	99.15	5.90	5.9

The normalized errors are low, demonstrating the model's ability to accurately reproduce surface elevation in Tampa Bay. The highest errors presented in St. Petersburg and Davis Island can be attributed to the horizontal grid configuration, since the computational grid does not have a high resolution close to the area where the gages were located.

Figure 6.15 shows the spectra of water surface elevation (data and model results) for the same stations. These spectral curves reveal major energy bands centered around three frequencies: the subtidal band (up to 0.5 cycles per day); the diurnal band (between 0.8 to 1.2 cycles per day); and the semi-diurnal band (1.8 to 2.2 cycles per day). The three bands combined, represent the tides propagating from the Gulf of Mexico into the Bay. Secondary energy bands, representing non-linear interactions between diurnal and semi-diurnal tides with complex geometries and bathymetric features inside the Bay, are represented by the relatively small third and fourth diurnal peaks. As indicated by NOAA (1993), these overtides are not significant in the overall circulation pattern of the Bay. Model results agree quite well with data in terms of total spectral energies as well as in the representation of the major frequency bands. The diurnal band is particularly well represented by the model, from the entrance of the Bay up to the head of Hillsborough Bay and Old Tampa Bay. In St. Petersburg, model results show a broader spectrum in the semi-diurnal band than the one from measured data. Particularities of the location of the tidal gage, not resolved in the model could be causing that.

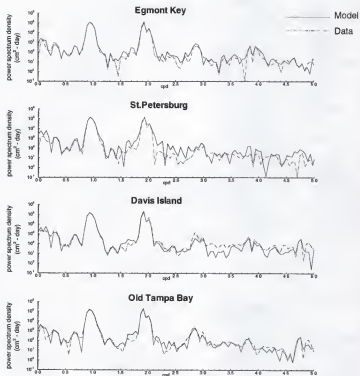


Figure 6.15 - Spectra of water surface elevation for the 1990 simulation.

Table 6.2 presents the distribution of energies for water surface elevation in terms of the total energy (area under the spectral density curve), the percent energies within each frequency bands, and the total energy represented by these four bands. It should be pointed out that energies associated with each frequency band include not only tidal components but also those related to the wind field. As an example, the diurnal pattern of the seabreeze is incorporated into the diurnal band, and meteorological fronts can be associated to subtidal fluctuations (Peene, 1995).

Table 6.2 - The distribution of tidal energy for water surface elevation - September 1990.

Station		Total Energy (cm ² - day)	Sub Tidal (%)	Diurnal (%)	Semi Diurnal (%)	Overtide (%)	Percent Total
Egmont Key	Data	4.7E5	1.7	59.2	37.4	0.8	99.2
	Model	5.2E5	1.0	55.7	42.1	0.6	99.4
St.Petersburg	Data	5.9E5	3.5	55.4	39.5	0.4	98.8
	Model	5.7E5	1.2	55.2	42.9	0.2	99.5
Davis Island	Data	6.5E5	2.7	53.2	42.4	0.5	99.0
	Model	7.4E5	1.7	47.4	49.1	1.0	99.2
Old Tampa Bay	Data	7.4E5	1.6	52.9	43.9	0.9	99.2
	Model	6.9E5	1.2	52.7	44.2	1.3	99.3

In terms of total energy, the model overpredicts surface elevation in Egmont Key and Davis Island, while underpredicting it in St. Petersburg and Old Tampa Bay, with no clear pattern of inconsistency. The simulated and measured subtidal band are in the same order of magnitude, with the model constantly underpredicting subtidal energy. The greatest difference occurs in St. Petersburg. As part of the conclusions of the NOAA's "Tampa Bay Oceanographic Project" (NOAA, 1993), it was found that water level fluctuations at

Clearwater Beach were coherent with longshore winds over the continental shelf, and also that subtidal fluctuations in Clearwater and St. Petersburg were highly coherent. This phenomenon suggested that transport perpendicular to the coast would affect water levels in Clearwater, penetrate Tampa Bay through Boca Ciega Bay and Egmont Channel, and cause subtidal fluctuations in St. Petersburg. Peene (1995) also found that the measured residual currents in Anna Maria Sound could only be reproduced in the model if a longitudinal setup was imposed in the oceanic boundary condition. In his conclusions, he attributed this mechanisms to Ekman transport generated by alongshore winds in the Gulf of Mexico. In the computational grid of the integrated model of the Tampa Bay Estuarine System only a small portion of the Gulf of Mexico is represented, therefore large scale circulation features cannot be resolved, and some of them will appear as subtidal fluctuations.

The simulated and measured energy within the diurnal band were very similar. However, the agreement in the semi-diurnal band is not as good, and the model consistently overpredicts water level fluctuations. The major discrepancy occurs in Hillsborough Bay, where the data shows a clear diurnal dominance, while the energies in the model are equally split, with a small dominance of the semi-diurnal band. In the secondary energy band, the model is able to capture the general trend, presenting not only the same order of magnitude of overtides energy, but also the same distribution inside this band (Figure 6.15).

Unlike Sarasota Bay, where inlets and restrictions act as low pass filters (Peene, 1995), Tampa Bay does not exhibit any damping in the higher frequencies as the tidal wave propagates from the mouth (Egmont Key) to the head (Hillsborough Bay and Old Tampa Bay). The total energy at the upper reaches of Old Tampa Bay and Hillsborough Bay is

almost 60% and 40% greater than the total energy at Egmont Key, respectively. This amplification suggests that the tidal wave gradually changes from a progressive wave entering from the Gulf of Mexico to a partially standing wave at the upper reaches of the Bay. Numerical experiments using a 5 by 10 horizontal grid were able to reproduce this amplification, when the longitudinal dimension of the basin became closer to a quarter of the tidal wave length. Considering the idealized simulation of a closed-end frictionless tidal basin, the ratio between the surface displacement at the head of the basin to the incident tide tends to infinity when the longitudinal length approaches a quarter of the tidal wave length (Ippen, 1966).

The results of the harmonic analysis revealed that the major tidal constituents are: the lunar (M_2 , N_2) and solar (S_2) semi-diurnal constituents; and the lunar (O_1) and solar (K_1) diurnal constituents. Table 6.3 presents comparisons between measured and simulated tidal harmonic constituents (amplitudes and phases) for the water surface elevation at Egmont Key (entrance of the Bay), St. Petersburg (Middle Tampa Bay), Davis Island (head of Hillsborough Bay), and Bay Aristocrat Village (head of Old Tampa Bay). The forcing tide at the offshore boundary is also presented. The phases are relative to the first observation (Julian Day 250 at 01:00), and phase differences are presented in hours in order to allow comparison between constituents of different period.

Throughout the Bay, the model simulates the data with a satisfactory degree of accuracy. Like in the barotropic simulation, the errors were greater in St. Petersburg and Davis Island. The model consistently over-predicts amplitude and the simulated tidal wave is always ahead in phase, which would indicate that bottom friction is not satisfactorily

damping the tidal wave as it propagates through the estuarine system. But, as it will be seen from the analysis of currents, simulated velocity profiles at the Sunshine Skyway Bridge present lower magnitudes, indicating a need for decreasing friction. A plausible explanation would be that bathymetry is not well represented, and the mean water depth should be greater up to Middle Tampa Bay, and shallower thereafter.

Overall, the model is able to better simulate the diurnal components than semi-diurnal. The greatest difference in Davis Island suggests that the lateral boundaries of the Bay (e.g. bayous, mangroves, and wetlands) not represented in the model could help damping the semidiurnal tidal wave that in the model is amplified due to the approximately quarter wave length dimension of the Bay.

Table 6.3 - Major tidal constituents in Tampa Bay - September/1990.

Station	Constituent	Amplitude Data (cm)	Amplitude Model (cm)	Error (cm)	Phase Data (degrees)	Phase Model (degrees)	Error (hours)
Offshore Tide	M2	18.0	18.0	-	221.7	221.7	-
	S2	11.0	11.0	-	317.8	317.8	-
	N2	4.0	4.0	-	97.3	97.3	-
	O1	16.0	16.0	-	90.1	90.1	-
	K1	10.0	10.0	-	39.5	39.5	-
Egmont Key	M2	17.0	18.0	-1.0	248.0	229.6	0.63
	S2	9.0	11.0	-2.0	347.8	326.0	0.72
	N2	3.0	4.0	-1.0	120.7	104.9	0.55
	O1	16.0	16.0	0.0	103.0	92.4	0.76
	K1	10.0	10.0	0.0	50.0	41.7	0.55

Table 6.3 - continued.

Station	Constituent	Amplitude Data (cm)	Amplitude Model (cm)	Error (cm)	Phase Data (degrees)	Phase Model (degrees)	Error (hours)
St. Petersburg	M2	20.0	20.0	0.0	316.8	286.0	1.06
	S2	9.0	11.0	-2.0	61.7	25.9	1.19
	N2	4.0	4.0	0.0	196.5	166.7	1.04
	O1	17.0	16.0	1.0	127.6	117.1	0.75
	K1	11.0	11.0	0.0	77.8	67.0	0.71
Davis Island	M2	21.0	24.0	-3.0	321.1	292.6	0.98
	S2	11.0	13.0	-2.0	63.9	34.6	0.97
	N2	4.0	5.0	-1.0	201.3	174.9	0.92
	O1	17.0	17.0	0.0	130.4	119.4	0.78
	K1	11.0	11.0	0.0	80.6	69.5	0.73
Old Tampa Bay	M2	23.0	22.0	1.0	354.5	333.6	0.72
	S2	11.0	12.0	-1.0	98.9	78.2	0.69
	N2	4.0	4.0	0.0	246.1	220.0	0.91
	O1	18.0	18.0	0.0	144.1	139.2	0.35
	K1	13.0	12.0	1.0	91.3	88.6	0.17

Currents

For the purpose of assessing the model's ability to reproduce the velocity field in the Tampa Bay Estuarine System, time series of bottom and surface currents are compared in terms of rms error, spectrum, and harmonic analysis.

In the deeper parts of the Bay, NOAA collected water velocity data using an ADCP. The instruments were deployed on the bottom looking upward, with the velocity profile obtained from measurements every meter from the bottom up to the surface.

Figure 6.16 shows the simulated and measured bottom velocity components at NOAA' station C-2 in the Egmont Channel (entrance of the Bay). The model underpredicts the magnitude of bottom currents throughout the simulation period, which would indicate an overestimation of bottom stress. However, as discussed in the surface elevation analysis, forcing bottom stress to be smaller through adjustment of coefficients would make the tidal ranges in the upper reaches of the Bay unrealistically bigger than measured data. A plausible reason for the discrepancy between simulated and measured data could be attributed to particularities in bottom topography not resolved by the computational grid, as well as the precise location of the sensor not coinciding with model output. Nevertheless, the model appears to simulate the general characteristics of the flow, both in the East-West and North-South directions.

Figure 6.17 shows the simulated and measured surface velocity components at NOAA' station C-2 in the Egmont Channel (entrance of the Bay). The magnitude of the surface currents are well simulated, both in East-West and North-South directions. This indicates that the model is able to capture the details of the local circulation, marked by a complex pattern of unidirectional (along channel axis) flow.

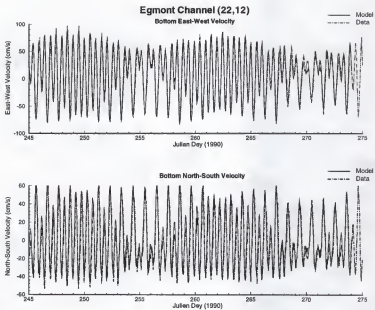


Figure 6.16 - Simulated and measured bottom velocity at Egmont Channel - September 1990.

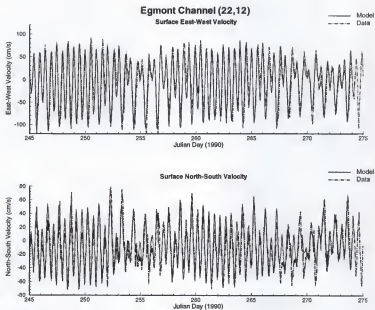


Figure 6.17 - Simulated and measured surface velocity at Egmont Channel - September 1990.

Figure 6.18 shows the simulated and measured bottom velocity components at the Sunshine Skyway Bridge. This station, located inside the navigation channel at about Middle Tampa Bay, presents high velocities in the along-channel direction, and a low across-channel component. Since the navigation channel axis lies between 60 °T and 70 °T, the East-West component is much greater than the North-South counterpart. The model appears to accurately simulate the ebb flow, while systematically underpredicting flood flow. Moreover, the along-channel currents are better represented than the across-channel ones.

Figure 6.19 shows the simulated and measured mid-depth velocity components at the Sunshine Skyway Bridge. Likewise bottom currents, the model is able to reproduce the overall circulation at mid-depth, corresponding to the ADCP signal at about 7 meters from the bottom.

Figure 6.20 shows the simulated and measured surface velocity components at the Sunshine Skyway Bridge. The comparison is made through the model results at the second layer (from the surface) and the ADCP signal at about 13 meters from the bottom. Similar to the bottom and mid-depth results, the model seems to accurately simulate the tidal flow characteristics, despite of underpredicting currents during flood tide.

Comparing Figures 6.17 and 6.20 it is reasonable to argue that during flood tide, the currents are well represented up to Egmont Channel, and somehow the model is misrepresenting the flood flow thereafter. Due to small scale morphological features (e.g. Cabbage Key, Mullet Key, and the Pinellas Bayway connecting them) and the shallowness of the region, the computational grid developed in this study does not resolve the connection

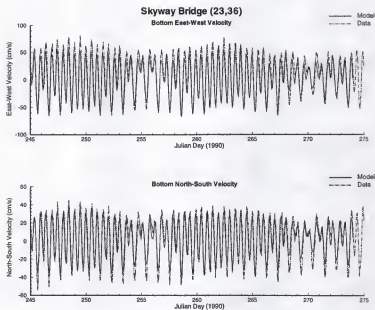


Figure 6.18 - Simulated and measured bottom velocity at Skyway Bridge - September 1990.

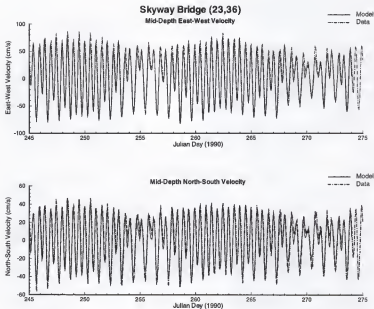


Figure 6.19 - Simulated and measured mid-depth velocity at Skyway Bridge - September 1990.

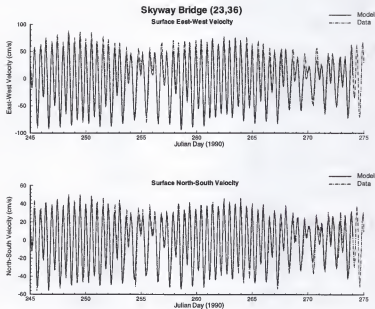


Figure 6.20 - Simulated and measured surface velocity at Skyway Bridge - September 1990.

between Boca Ciega Bay and the Gulf of Mexico. Hence, it is possible that the solid boundary imposed in this region is causing this problem.

Figure 6.21 shows the simulated and measured bottom velocity components, and Figure 6.22 shows the simulated and measured surface velocity components at NOAA's station C-4 in the Port of Manatee Channel. Among all the stations analyzed, C-4 shows the poorest agreement between measured data and model results. Bottom currents are underpredicted by the model, both during ebb and flood, although the phase appears to be well represented. As to the surface flow, the model seems to better represent flood than ebb flows, with the model not capturing a localized event that occurred around Julian Day 261 to 265. During this period, ebb flow velocities were much higher than usual values, with no apparent correlation with other stations or with the wind field.

The Port Manatee Channel, dredged in the early 80's to a nominal depth of 10 meters and width of about 150 m, is surrounded by underwater spoil areas and bathymetrical features that may originate localized currents that are highly variable in space and time. Therefore, it would be expected that any inaccuracy on matching the exact sensor location would produce such results. So long as the model can reproduce the general characteristics of the East-West and North-South surface and bottom velocities around the region, it will be termed satisfactorily calibrated.

Figure 6.23 shows the simulated and measured bottom velocity components at NOAA's station C-5 in the Port of Tampa Channel. Located next to the "Cut K Channel" (which runs along 15 °T), this station presents a much stronger North-South velocity component than the East-West velocity. The model appears to slightly underpredict the

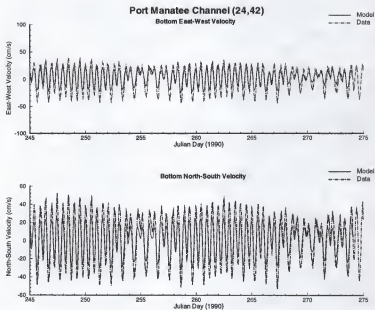


Figure 6.21 - Simulated and measured bottom velocity at Port of Manatee Channel - September/1990.

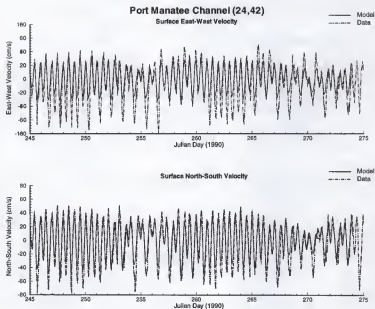


Figure 6.22 - Simulated and measured surface velocity at Port of Manatee Channel - September 1990.

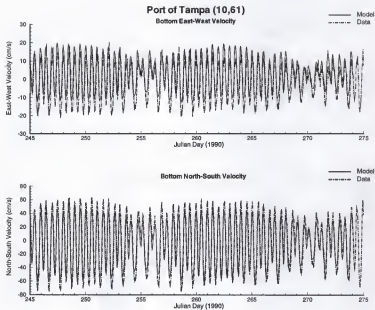


Figure 6.23 - Simulated and measured bottom velocity at Port of Tampa Channel - September 1990.

North-South component (along-channel). The East-West component is not only under predict, but there is also a phase shift between measured and simulated results. Bottom topography and lack of horizontal resolution in defining the navigation channel can be attributed as the primary causes for inaccuracies.

Figure 6.24 shows the simulated and measured surface velocity components at NOAA's station C-5 in the Port of Tampa Channel. The model seems to accurately simulate the North-South currents (along-channel), while presenting an offset towards East in the across-channel currents (East-West). In the southwest corner of the Interbay Peninsula there is a small spoil area running parallel to the channel in a "spit" like formation that is not represented in the computational grid, and possibly causing a small change in the flow direction.

Table 6.4 shows the rms errors for the surface and bottom velocity vector components along with measured data range and the normalized percent error (as defined for the surface elevation comparisons).

Velocities inside the Egmont Channel present the highest ranges in Tampa Bay, and the model appears to simulate both East-West and North-South component within 10% accuracy. The across-channel surface velocity present the highest error, which would indicate a small deviation in the orientation of the channel axis.

The errors for the Skyway Bridge station were also around 10%, with the greatest magnitude presented in the surface along-channel direction. As shown in Figure 6.20, the model appears to have a problem in simulating the flood flow at this station.

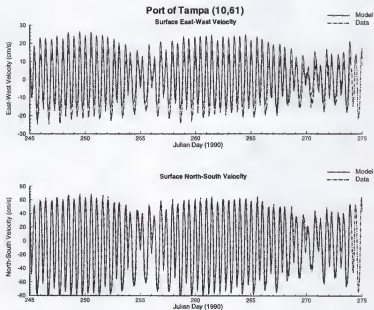


Figure 6.24 - Simulated and measured surface velocity at Port of Tampa Channel - September 1990.

Table 6.4 - The rms error between measured and simulated bottom (b) and surface (s) currents - September/1990.

Station	Component	Velocity Range (cm)	Erms (cm)	Normalized Erms (%)
Egmont Channel (C-2)	(E-W)b	174.15	14.25	8.2
	(N-S)b	123.66	11.53	9.3
	(E-W)s	226.18	20.32	9.0
	(N-S)s	147.79	15.18	10.3
Skyway Bridge	(E-W)b	146.08	11.74	8.0
	(N-S)b	98.44	7.55	7.7
	(E-W)s	173.41	17.46	10.1
	(N-S)s	105.00	5.99	5.7
Port Manatee Channel (C-4)	(E-W)b	81.16	8.99	11.1
	(N-S)b	102.34	10.4	11.5
	(E-W)s	124.33	13.9	11.6
	(N-S)s	126.05	12.47	11.1
Port of Tampa (C-5)	(E-W)b	41.65	6.56	15.7
	(N-S)b	139.15	14.03	10.1
	(E-W)s	43.92	7.26	16.5
	(N-S)s	152.22	16.1	10.6

The normalized rms errors for the Port Manatee Channel were uniformly distributed around 11%. Although differences in magnitude appears to be significant (Figures 6.21 and 6.22), the good agreement in phases helped keeping the errors in an acceptable range.

On the other hand, graphical comparisons between model results and measured data for the Port of Tampa station (Figures 6.23 and 6.24) showed a good agreement in magnitude, but a shift in phase. Since the model currents peak ahead of the measured data, this shift produces error in the rms calculations even though the magnitudes are well represented. The highest percent error is presented in the across-channel direction, once again revealing that the channel orientation and the grid resolution can be improved if the details of the circulation and transport in that area need to be resolved.

Figure 6.25 shows the energy density spectra for simulated and measured bottom velocities and Figure 6.26 shows the energy density spectra for simulated and measured surface velocities at the Sunshine Skyway Bridge. These figures demonstrate the dominance of the tidal oscillation, with the semi-diurnal signal being the strongest one. Like the spectral density curve for surface elevation, the area under the spectrum is proportional to the total energy (square of the amplitude) of the signal. Therefore, performing a spectral analysis of the currents at specific stations throughout the Bay, it is possible to make comparisons between modeled and measured energy distribution of the velocity components.

Table 6.5 presents comparisons between the simulated and measured current spectral energy within the sub-tidal, diurnal, and semi-diurnal frequency bands (as defined for surface elevation) for the September 1990 simulation. The table shows the total energy over the entire frequency range, and the percent of the total energy located within each primary sub-band.

Energy Density Spectra of Currents at Skyway Bridge

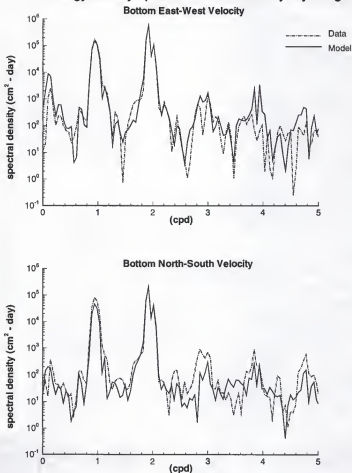


Figure 6.25 - Energy density spectra of bottom currents at Skyway Bridge - September 1990.

Energy Density Spectra of Currents at Skyway Bridge

Surface East-West Velocity

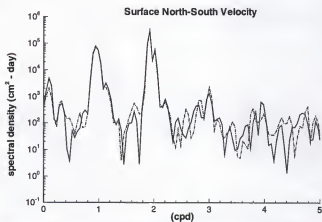
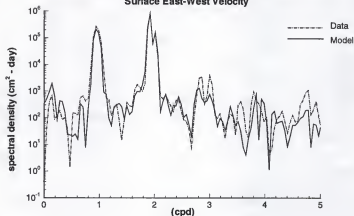


Figure 6.26 - Energy density spectra of surface currents at Skyway Bridge - September 1990.

Table 6.5 - The distribution of tidal energy for bottom (b) and surface (s) currents - September 1990.

Station Component	Source	Total energy (cm/s-day) ²	Sub-tidal (%)	Diurnal (%)	Semi-diurnal (%)
Egmont Channel (C-2)	(E-W)b data	1.8E6	0.2	34.1	63.6
	model	1.6E6	0.7	26.7	71.4
	(N-S)b data	9.1E5	0.1	37.2	59.5
	model	8.9E5	0.8	30.3	67.2
	(E-W)s data	2.7E6	2.9	39.8	53.9
	model	2.5E6	0.3	26.4	72.1
	(N-S)s data	9.3E5	5.1	33.0	52.0
	model	8.3E5	1.3	23.0	72.3
Skyway Bridge	(E-W)b data	1.4E6	0.4	31.3	67.2
	model	1.4E6	1.5	27.3	69.5
	(N-S)b data	5.5E5	0.1	36.6	60.6
	model	4.5E5	0.1	23.9	75.1
	(E-W)s data	2.0E6	0.01	33.9	64.3
	model	1.9E6	0.3	26.4	72.5
	(N-S)s data	6.9E5	0.9	30.2	66.2
	model	7.2E5	1.5	27.0	69.6
Port Manatee Channel (C-4)	(E-W)b data	4.4E5	0.6	36.1	61.3
	model	2.2E5	2.7	22.0	73.6
	(N-S)b data	6.8E5	0.3	33.2	64.7
	model	3.2E5	0.2	24.0	74.6
	(E-W)s data	7.9E5	4.9	34.1	56.2
	model	4.2E5	1.1	24.3	72.7
	(N-S)s data	9.3E5	1.5	34.4	58.9
	model	5.1E5	1.6	22.0	74.8

Table 6.5 - continued.

Station Component	Source	Total energy (cm/s-day) ²	Sub-tidal (%)	Diurnal (%)	Semi-diurnal (%)	
Port of Tampa (C-5)	(E-W)b	data	1.0E5	0.6	24.7	70.3
		model	1.1E5	0.4	15.7	79.0
	(N-S)b	data	1.6E6	0.1	27.4	69.6
		model	1.3E6	0.1	17.1	78.8
	(E-W)s	data	1.3E5	0.3	25.2	70.6
		model	1.7E5	2.1	12.4	80.0
	(N-S)s	data	1.8E6	0.1	27.3	69.7
		model	2.2E6	0.3	17.6	78.5

From the simulated and measured "Total Energy" information (which is actually proportional to the total energy), it can be concluded that the model captures the characteristics of the circulation throughout the Bay. The highest discrepancy is found in the Port of Manatee Channel (C-4), because of grid resolution and localized bathymetrical features not represented in the model. Nonetheless, the model was able to simulate the diurnal and semi-diurnal distribution, reproducing the semi-diurnal dominance of the currents. The total energy represented by these four sub-bands accounted for more than 90% of the signal at all stations.

Results of the harmonic analysis help determine the character of the tidal currents. Where they are rectilinear, the tidal ellipses present a much smaller minor axis, relative to the magnitude of the major axis. Furthermore, the ellipses for different components are nearly aligned. Where the tidal currents are rotary, the ellipses are not necessarily aligned, and there

is a more even distribution between the minor and major axis. Figure 6.27 shows the simulated and measured tidal ellipses for the semi-diurnal components, and Figure 6.28 shows the simulated and measured tidal ellipses for the diurnal components of the surface velocity for the Skyway Bridge station. From these figures, it can be seen that, first the semi-diurnal components are much greater. Second, the orientation of the navigation channel is well represented in the model, and the simulated results slightly underpredicts the measured components.

Salinity

Salinity and temperature present significant annual variations in the Tampa Bay Estuarine System. Figure 6.29, from NOAA (1994), shows near-bottom salinity and temperature for the station S-4 at the entrance of Hillsborough Bay. Since the simulations in this study focus on specific periods (Julian Days 244 to 274 in 1990) when temperature is uniform (around 30 °C), temperature fluctuations are not taken into consideration.

In order to isolate the sub-tidal salinity fluctuations from the signal, a low pass filter was designed. Using the data analysis program MATLAB, a chebychev-II filter with a 24-hour cutoff period was designed to remove all tidal components while minimizing the noise within the cutoff frequency band, and producing the steepest possible response curve.

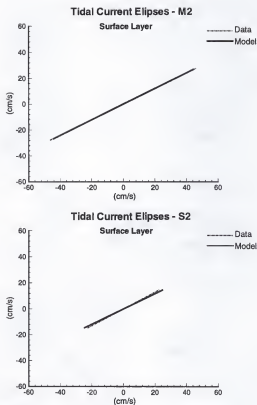


Figure 6.27 - Tidal current ellipses for the semi-diurnal components - September 1990.

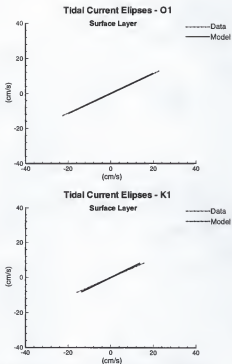


Figure 6.28 - Tidal current ellipses for the diurnal components - September 1990.

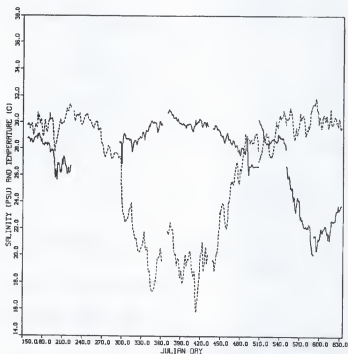


Figure 6.29 - Near-bottom salinity (solid line) and temperature (dashed line) at NOAA station S-4 starting at Julian Day 150 in 1990 (from Hess, 1994).

Figure 6.30 compares simulated and measured mid-depth salinity at station C-21 in the entrance of the Bay. The model appears to represent the general characteristics of the salinity distribution, with the difference between filtered simulated and measured salinities not exceeding 1 ppt. During ebb tide, the model overpredicts the drop in salinity. This error is probably caused by the geographical position of the station, and an artificial boundary imposed in the computational grid. This station is located next to Anna Maria Sound, in the south part of the Bay's entrance. Since the model does not resolve the connection between Tampa and Sarasota Bay, all the discharge of the Manatee River is forced outside Tampa Bay. Sheng *et al.* (1995) suggested that a southerly residual current in Anna Maria Sound is caused among other factors by the discharge of the Manatee River.

Figure 6.31 shows the near-bottom simulated and measured salinity at NOAA station C-23. Similar to station C-21, the difference between filtered simulated and measured salinities did not exceed 1 ppt. In this station, the model appears to better simulate ebb than flood tide. During ebb tide, simulated and measured salinities agree well, but during flood the model overpredicts the rise in salinity. The most likely cause of the discrepancy is Boca Ciega Bay not being resolved in the computational grid. In the case of salinity, it becomes clear that the source of error comes from the transport during flood, because it is only in this upwind condition that the model is lacking accuracy.

Figure 6.32 shows the near-bottom simulated and measured salinity at NOAA station C-4, in the Port Manatee Channel. Once again the model is able to capture the general dynamics of the salinity distribution. Since salinity is highly influenced by hydrodynamic transport, discrepancies in the velocity field will be translated to differences between simulated and measured salinities.

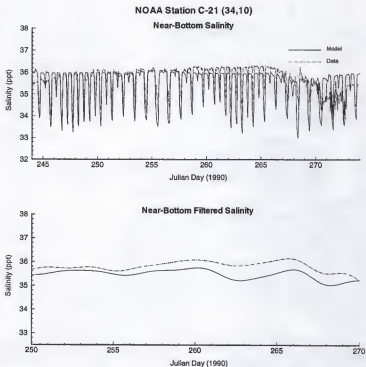


Figure 6.30 - Simulated and measured near-bottom salinity at NOAA station C-21 - September/1990.

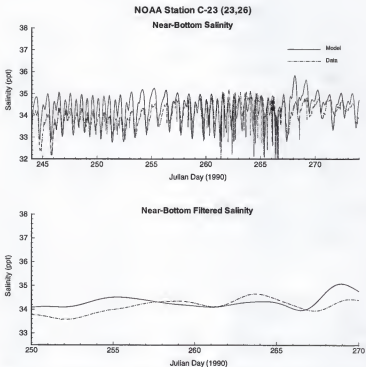


Figure 6.31 - Simulated and measured near-bottom salinity at C-23 - September 1990.

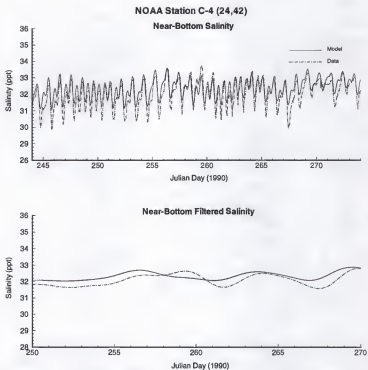


Figure 6.32 - Simulated and measured near-bottom salinity at C-4 - September 1990.

Table 6.6 shows the rms errors for the near-bottom salinity along with measured data range and the normalized percent error (as defined for the surface elevation comparisons).

Table 6.6 - The rms error between measured and simulated salinity - September 1990.

Station	Measured Salinity Range(ppt)	Erms (ppt)	Normalized Erms (%)
NOAA C-21	2.41	0.53	22.1
NOAA C-23	3.28	0.53	16.1
NOAA C-4	3.82	0.39	10.3

The results show the model's ability to simulate salinity within 25% accuracy. So, even though comparisons between filtered salinity indicate that differences are below 1 ppt most of the time, the range of salinity fluctuations are also quite small.

Validation of the Model

Based on the results presented, the model was considered calibrated, and two additional simulations were performed to validate the model. First, a short-term simulation was performed around Julian Day 284 (October 11, 1990), when the tropical storm "Marco" passed just West of the Bay. Additionally, the wet-season conditions of July 1991, when river discharges and rainfall were above historical averages, were simulated.

Figure 6.33 shows the simulated and measured surface elevation for the tropical storm "Marco" simulation, and Figure 6.34 shows the simulated and measured surface elevation for the July 1991 simulation at St. Petersburg and Davis Island. These two stations presented the greatest normalized rms errors during calibration. The model constantly overpredicts surface elevation at these stations. A probable source of error could be the bathymetry, indicating that the computational grid is deeper than reality. Once again, it has

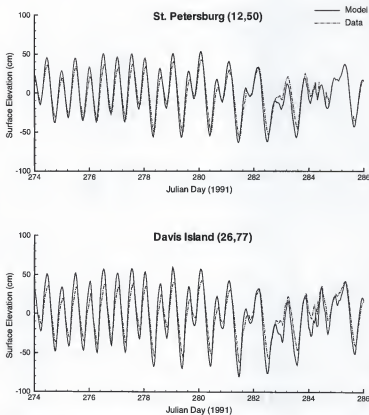


Figure 6.33 - Surface elevation at St.Petersburg and Davis Island - "Marco" Storm (October 1990).

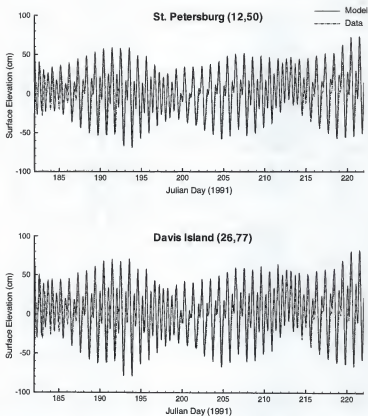


Figure 6.34 - Surface elevation at St.Petersburg and Davis Island - July 1991.

been demonstrated the sensitivity of the model to bathymetry, and the necessity of accurate bathymetric data to avoid uncertainties. Figure 6.33 demonstrates the model's ability to simulate episodic events. In both stations, model results for Julian Day 284 show the change in surface elevation, going from a predominantly tidally-driven pattern towards a more wind-driven one, with the storm surge well represented. In Davis Island, the data shows that the water level remained higher than model results during the ebb flows of the storm. It is possible that the runoff in Hillsborough Bay, which is not represented in the model, became strong enough to be responsible for that.

Table 6.7 presents the maximum measured tidal range, the rms error, and the normalized rms error percentile for St. Petersburg, in Middle Tampa Bay, and Davis Island in the upper reaches of Hillsborough Bay.

Table 6.7 - The rms error between measured and simulated water surface elevation October/1990 and July/91.

Station	Simulation Period	Tidal Range (cm)	Erms (cm)	Normalized Erms (%)
St.Petersburg	Oct/90	101.79	18.73	18.5
	Jul/91	112.22	12.56	11.2
Davis Island	Oct/90	105.46	12.84	12.2
	Jul/91	128.63	15.41	11.9

The normalized errors are comparable to those of the calibration simulation (Table 6.1). Only in St. Petersburg the error seems to be excessively higher; however, as it is shown in Figure 6.33, the source of error is more related to a phase difference, with the amplitude being well represented.

Figure 6.35 shows the simulated and measured bottom velocity components and Figure 6.36 shows the simulated and measured surface velocity components at the Sunshine Skyway Bridge, during the tropical storm "Marco" simulation. The model seems to accurately simulate the tidal flow characteristics, despite of underpredicting currents during flood tide.

Table 6.8 shows the rms errors for the surface and bottom velocity vector components along with measured data range and the normalized percent error.

Table 6.8 - The rms error between measured and simulated bottom (b) and surface (s) currents - "Marco" Storm.

Station	Component	Velocity Range (cm)	Erms (cm)	Normalized Erms (%)
Skyway Bridge	(E-W)b	151.94	14.65	9.6
	(N-S)b	92.89	8.71	9.4
	(E-W)s	164.55	18.62	11.3
	(N-S)s	106.48	6.74	6.3

The model is able to simulate both East-West and North-South component within 15% accuracy. Likewise the calibration simulation, the model appears simulates the ebb better than the flood flow, and the reasons have been discussed along with Figure 6.18 through Figure 6.20.

Figures 6.37 and 6.38 show the near-bottom and near-surface simulated and measured salinity at NOAA station S-4, near the entrance of Hillsborough Bay, during July of 1991. Similar to the calibration simulation, the difference between filtered simulated and measured salinities did not exceed 1 ppt. The model is able to capture the general dynamics of the salinity distribution. Hess (1993) reports likely errors in the data, since the top sensor

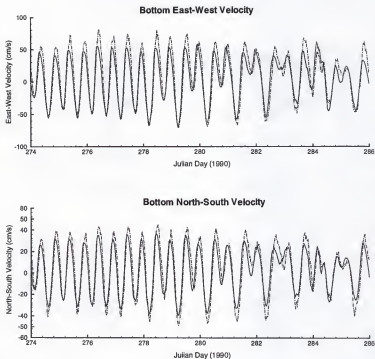


Figure 6.35 - Simulated and measured bottom current at Skyway Bridge - "Marco" Storm (October/1990).

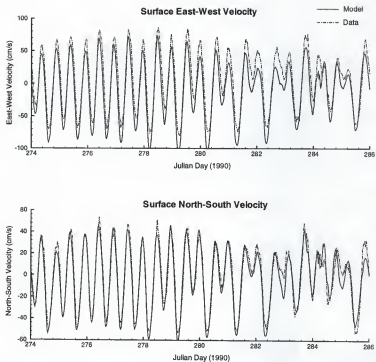


Figure 6.36 - Simulated and measured surface current at Skyway Bridge - "Marco" Storm (October/1990).

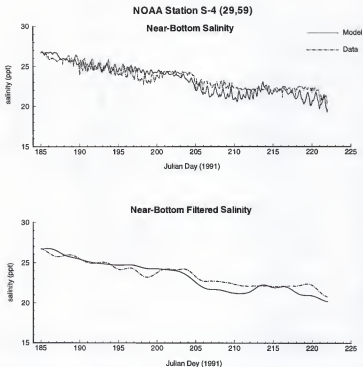


Figure 6.37 - Simulated and measured near-bottom salinity at station S-4 - (July/1991).

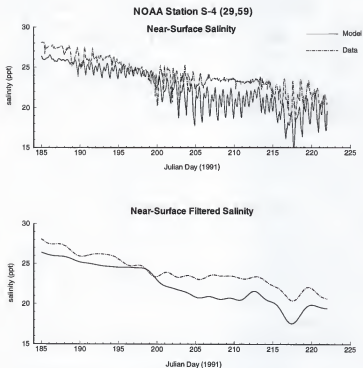


Figure 6.38 - Simulated and measured near-surface salinity at station S-4 - (July/1991).

constantly presents higher salinity than the bottom sensor. Since model results show no apparent reason for this vertical instability, the agreement between the model and measured data is better for the bottom layer.

Table 6.9 shows the rms errors for the near-bottom and surface salinity along with measured data range and the normalized percent error (as defined for the surface elevation comparisons).

Table 6.9 - The rms error between measured and simulated salinity - July/1991.

Station	Layer	Salinity Range(ppt)	Erms (ppt)	Normalized Erms (%)
S-4	Bottom	6.62	0.84	12.7
	Surface	10.40	1.43	13.3

Likewise the calibration simulation, the results show the model's ability to simulate salinity within 15%.

Flushing Characteristics of Bay Segments

An important management issues to be addressed by an integrated model, intended to support ecosystem management, deals with the relative flushing characteristics of the various segments defined in the Bay (Sheng and Yassuda, 1995).

In order to calculate the flushing rates for each specific segment in the Bay, the model simulates the transport of a conservative species (i.e., without considering any biogeochemical transformation). Initially, one segment is filled with a uniform concentration, while remaining zero everywhere else in the Bay. After a certain amount of time, the conservative species is transported by advection and dispersion due to the flow

field. The flushing rate is then determined by the fraction of mass flushed out of the segment over that period of time. The relative flushing rates for various segments of the Bay were calculated by independently repeating this procedure over a 10-day period simulation. Figure 6.39 shows the time-varying relative flushing for segments 2 (upper reaches of Old Tampa Bay), segment 4 (entrance of Old Tampa Bay), segment 5 (upper reaches of Hillsborough Bay), segment 6 (entrance of Hillsborough Bay), segment 9 (Middle Tampa Bay), and segment 11 (entrance of Tampa Bay). As expected, the results show the lowest flushing rate for the upper reaches of Old Tampa Bay, where 40% of the conservative species mass was flushed out of the segment. In the upper reaches of Hillsborough Bay, about 55% of the initial mass was flushed out. The difference between Old Tampa Bay and Hillsborough Bay flushing rates can be attributed to higher freshwater discharges in the latter. The segment located at the entrance of Old Tampa Bay presented a high flushing rate due to the strong velocities field that develops along the Port of Tampa navigation channel. Approximately 75% of the initial mass was flushed out of the segment 4 in the 10-day period simulation. Segment 6, at the entrance of Hillsborough Bay was able to flush about 70% of the initial mass. The segments in Middle Tampa Bay and Lower Tampa Bay presented similar flushing characteristics, flushing out between 80 to 90% of the initial mass.

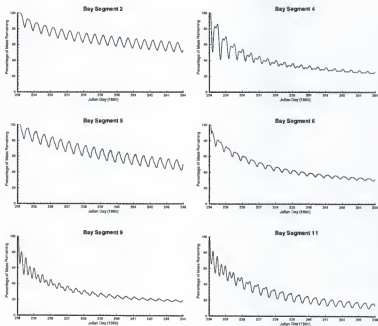


Figure 6.39 - Relative flushing for several bay segments - September/1990.

Residual Circulation

In order to be an effective tool to support ecosystem management, the integrated model of the Tampa Bay Estuarine System needs to be able to address issues with time scales greater than a few tidal cycles. The concept of residual circulation and transport has been referred to filtering or averaging out the intratidal fluctuations. Two methodologies can be applied in determining these residuals. The Eulerian residual circulation and transport is obtained by simply averaging variables over several tidal cycles (e.g., usually a period of the order of a month). While, the Lagrangian residual circulation and transport are related to the Lagrangian mean velocities, which are defined as the net displacement of a specific particle over a tidal cycle, divided by the displacement time (Cheng and Casulli, 1982). The first-order Lagrangian residual circulation and transport is the sum of the Eulerian residual and the Stoke's drift.

The analysis of surface elevation and currents showed that it is reasonable to assume the Tampa Bay Estuarine System as a relatively weak non-linear system; therefore, only the Eulerian residual circulation and transport will be assessed.

Figure 6.40 shows the residual circulation and salinity distribution for September 1990. The residual circulation generated a two-layer velocity field, with a seaward surface flow, and a landward bottom layer flow. During this period (characterized as dry-season), the saltier waters of the Gulf of Mexico penetrate the Bay along the bottom-layer of the navigation channel, up to the head of Hillsborough Bay. Model results show that along the shallow sides of the Bay the residual flow is seaward over the entire water column, which

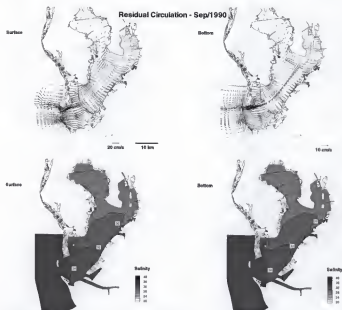


Figure 6.40 - Residual circulation after 30 days - September/1990.

agrees with the findings of Weisberg and Williams (1991). Galperin *et al.* (1992) presented a residual circulation suggesting a much strong stratification, with the entire bottom layer flowing landward, and a seaward flow in the surface layer. Their results may be explained by historical-averages river discharge used as well as a zero salinity used for the river boundaries. In their study, they also refuted the "residual gyres" described by the barotropic two-dimensional models of Ross (1973) and Goodwin (1987), by concluding that the barotropic residual circulation is overwhelmed by the baroclinic counterpart. Figure 6.40 shows that the complex shoreline and bathymetrical features of the Bay are also important components in generating residual circulation and transport. Numerous gyres were formed next to the causeways, specially in the bottom layer. The greater depths in the upper reaches of Middle Tampa Bay induce a large scale counter-clock gyre that forces the flow from Hillsborough Bay to the west side of Middle Tampa Bay, towards St. Petersburg. This feature may help to explain the lower salinities presented in the west side, compared to the east side, where most of the freshwater inflow occurs, and where one would expect to find the lower salinity levels.

In an intertidal basis, the flow is spatially uniform, as shown in Figure 6.41 for the ebb flow, and Figure 6.42 for the flood flow. These figures show that the greatest velocities are found in the Egmont Channel and in the entrance of Old Tampa Bay, which is in agreement with the findings of the NOAA's "Tampa Bay Oceanographic Project" (NOAA, 1993).

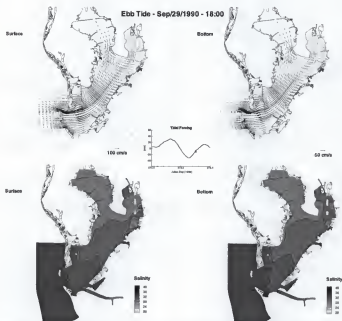


Figure 6.41 - Simulated velocity field representing maximum ebb currents - September/29/1990 - 18:00.

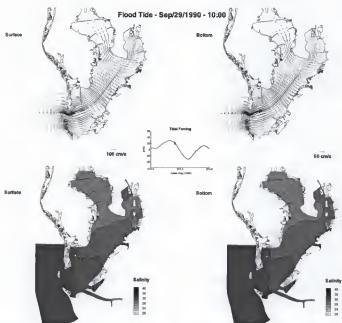


Figure 6.42 - Simulated velocity field representing maximum flood currents - September/29/1990 - 10:00.

Figure 6.43 shows the velocity cross-section simulated along the Sunshine Skyway Bridge. The ebb flow of September, 29 1990 (14:00) presents a typical estuarine circulation, with stronger ebb velocities concentrated in the center of the surface layer. The magnitude of the flood velocities are smaller, and dispersed throughout the cross-section. This ebb-flood pattern can be explained by the fact that the period of ebb flow is shorter than the flood period. The residual cross-section shows a landward flow restricted to the bottom layer of the navigation channel and the shallow sides of the Bay, and a seaward flow in the surface layer.

Figure 6.44 shows the salinity cross-section simulated along the Sunshine Skyway Bridge. As a consequence of the circulation pattern, higher salinities are confined to the deeper parts of the navigation channel, with lower salinities along the shallow sides of the Bay.

Figure 6.45 shows the longitudinal salinity distribution along the navigation channel, from the Gulf of Mexico to Hillsborough River. There is a mild vertical stratification, with surface to bottom salinities differences never exceeding 2 ppt. However, it is interesting to notice the roughness in the 32 ppt contour line during ebb flow. Apparently, the lower-salinity water mass flowing seaward is trying to overcome a higher-salinity water mass flowing landward, generating a small front like feature in Lower Tampa Bay.

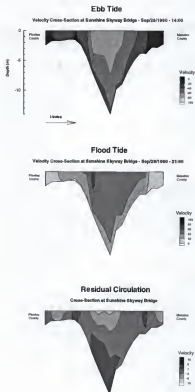


Figure 6.43 - Velocity cross-section at Skyway Bridge looking up the Bay. Vertical scale in meters, and horizontal scale in computational grid j-index.

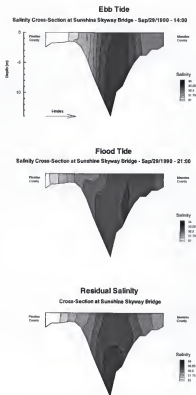


Figure 6.44 - Salinity cross-section at Skyway Bridge looking up the Bay. Vertical scale in meters, and horizontal scale in computational grid j-index.

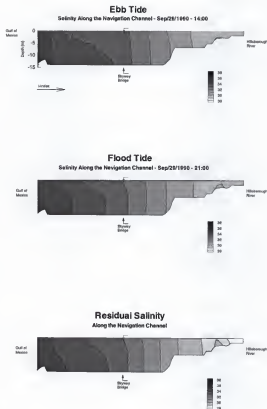


Figure 6.45 - Longitudinal distribution of salinity along the navigation channel. Vertical scale in meters, and horizontal scale in computational grid i-index.

Summing up, currents inside Tampa Bay are distinctly tidal oscillations, with the mixed tide signal presenting a strong dominance of the semi-diurnal component. Throughout the Bay, the tidal ellipses reflect an uni-directional flow aligned with the navigation channel. Filtering the tidally driven flow, a baroclinic circulation is revealed, with a two-layer pattern flowing landward in the bottom layers, and seaward along the surface. The salinity distribution closely follows the circulation pattern. The model reveals a low-salinity distribution along the western side of the Bay, originated from the freshwater discharge in Hillsborough Bay, and transported there through "topographical" residual currents.

Results of the Suspended Sediment Simulation

The role of suspended sediments in the integrated model of an estuarine system can be demonstrated by the importance of its concentration in determining light availability, supply of water column nutrients, and fate of sorbed pollutants.

Erosion rates, critical shear stress, settling velocities and other model parameters were determined by previous studies in Tampa Bay (Ross, 1988; Sheng *et al.*, 1992 and 1993; and Schoellhammer, 1993). The bottom shear stress due to the combined action of waves and currents was calculated in the hydrodynamics component of this integrated model, and then used to determine the erosion and deposition rates.

Schoellhammer (1993) showed that net sediment resuspension in Old Tampa Bay is primarily driven by strong and sustained winds associated with episodic events. In order to test the sediment component of this integrated model, results of a 10 days simulation and data are compared. The simulation comprises the period when the tropical storm "Marco"

moved northward along the Gulf coast on October 11, 1990, and suspended sediment concentration data were collected at the USGS platform (Schoellhammer, 1993). Figure 6.46 shows the location of the USGS platform in Old Tampa Bay. During the storm, the wind shifted from easterly (at about 5 m/s) in the afternoon of October 10 to southerly (at about 15 m/s) during the morning of October 11 (Figure 6.47). The wind magnitude returned to normal in the afternoon of October 11. Suspended sediment concentration was measured at two vertical levels (24 cm and 183 cm above the bed), although near-bottom data stopped at 1200 hours on October 11. Figure 6.48 shows the simulated significant wave height and period, suggesting a transition from deep water wave condition (40 cm wave height, 2 seconds period in a 4.5 m water depth) to a shallow water wave condition during the passage of the storm (Shore Protection Manual, 1984). Figure 6.49 shows the simulated wave-induced bottom shear stress and the suspended sediment concentration at the USGS station for October 10 and 11, 1990. Prior to the storm, the bottom shear stress fluctuates around the Shields critical stress, calculated to be around 1.6 dyne/cm^2 . During the storm, the significant wave height basically doubled, hence, the bottom shear stress, which is proportional to the square of the wave height (Kajiura, 1968), increased to about four times the original value. Both measured data (Figure 6.47) and simulated results (Figure 6.49) show that the near-bottom suspended sediment concentration increased to about 200–300 mg/L during the peak of the storm. It is interesting to notice the prompt response of the Bay to the wind action. The maximum concentration correspond to the maximum southerly wind, and it decreased as wind velocities decreases during the afternoon. Figure 6.50 shows a contour plot of the suspended sediment distribution at 6:00 am of October 11. The lack of suspended sediment data throughout the Bay during the event prevents further comparisons.

Although wind-generated waves are represented by the simple SMB model (which consist of a single wave amplitude and wave period), whereas episodic events are characterized by many wave amplitudes and frequencies, the model appears to reproduce the general trend of the event, which is probably due to an accurate representation of the bottom shear stress.

The suspended sediment simulations were carried out using the settling velocity proposed by Ross (1973) (Equation B-4) for the mud region, and constant settling velocity for the sandy bottom, with the values obtained from Schoellhammer (1993). The resuspension rates were calculated using the Power Law (Equation B-5) with $T_d = 1$ and $p = 1$. The critical shear stress utilized in this simulation was $\tau_{cr} = 1.6 \text{ dyne/cm}^2$ for the sandy region and $\tau_{cr} = 1.2 \text{ dyne/cm}^2$ for the mud region. The deposition velocity was assumed to be equal to the settling velocity at the bottom layer, which corresponds to a Krone's probability of deposition $p = 1$.

The suspended sediment dynamics in Tampa Bay are primarily driven by episodic events, when short period waves are responsible for resuspension, while strong currents are responsible for the vertical mixing. Model results showed that current-induced bottom stress have negligible effects on the resuspension flux of sediments, however, the combined action of waves and currents can be responsible for high levels of suspended sediments during episodic events.

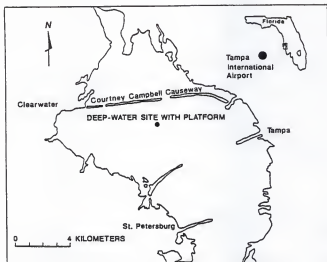


Figure 6.46 - Location of the USGS station in Old Tampa Bay (Schoellhammer, 1993).

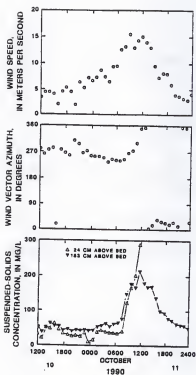


Figure 6.47 - Wind speed and direction, and suspended sediment concentration at USGS station during tropical storm "Marco" (Schoellhammer, 1993).

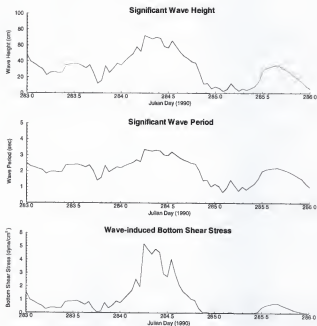


Figure 6.48 - Simulated significant wave height and period during tropical storm "Marco" (October/1990).

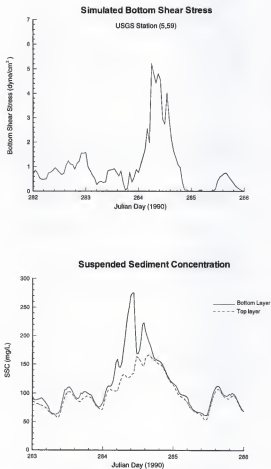


Figure 6.49 - Simulated wave-induced bottom shear stress and suspended sediment concentration at the USGS station for October 10 and 11, 1990.

**Near-Bottom Suspended Sediment Concentration
October/11/1990 - 06:00am**

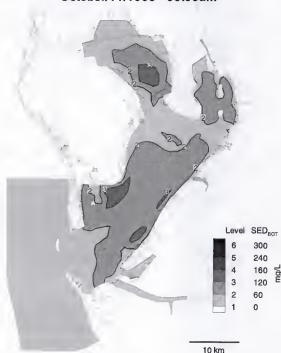


Figure 6.50 - Simulated suspended sediment concentration at 6:00am - October 11, 1990.

CHAPTER 7

CALIBRATION OF THE WATER QUALITY MODEL

The primary goal of this integrated modeling effort is to develop a water quality model that is fully coupled with the three-dimensional hydrodynamics model for Tampa Bay. In other words, a water quality model that runs simultaneously with the same time step and computational grid, hence eliminating the need for ad-hoc tuning of advective fluxes and dispersion coefficients.

The model which includes the processes described in Chapters 3, 4, and 5 can be used to study Tampa Bay as an integrated system, and provide a detailed characterization of the hydrodynamics and water quality dynamics within the system. At this stage of development, the model can assist ecosystem managers in determining which water quality data need to be obtained, and the processes to be further investigated in order to solve for the uncertainty of model coefficients. A preliminary nutrient budget, accounting for external loading, benthic fluxes, and exchange with the Gulf of Mexico can be obtained. Model results can also be used to maximize management efforts by determining the best location of sampling stations in order to be representative of each of the Bay sub-divisions. A subsequent refinement of the model can be used to address such ecosystem management issues as controlling estuarine eutrophication and determining allowable external nutrient loading levels to restore seagrass to a target level throughout the Bay.

This chapter describes the calibration of the water quality model for the Tampa Bay Estuarine System. The major objective of model calibration is to synthesize some available Tampa Bay water quality data with the water quality model described in Chapter 4. Of particular interest is the summer of 1991 data which showed a decline in water quality, especially in the upper reaches of Hillsborough Bay, as measured by the Hillsborough County Environmental Protection Commission (EPC) water quality index. An attempt will be made to simulate the summer 1991 condition by determining the proper combination of model coefficients. In this regard, model calibration can help to identify specific processes for which basic research is needed, and the type and amount of additional data required.

Due to the vast spatial and temporal variability in hydrodynamics and water quality dynamics, it is impossible to rely only on field and laboratory experiments to develop a system-wide understanding of the Bay. To understand the water quality dynamics in Tampa Bay, model must be used to synthesize field and laboratory data. As noted in previous studies (e.g., Fanning and Bell, 1985; Spaulding *et al.*, 1989), the lack of a well coordinated and long-term water quality data collection efforts for determining process rates and boundary/initial conditions impose a major challenge towards the development of a predictive water quality model for the Tampa Bay Estuarine System. Water quality data were collected in various parts of Tampa Bay at different times. Therefore, a major task of the present water quality modeling effort of the Tampa Bay Estuarine System is the synthesis and integration of available data, and the calibration of the model, prior to any attempt of model prediction. Using the process-based modeling system described in previous chapters, it is possible to synthesize the data collected from various parts of the Bay at different times, so long as one

takes into consideration the uncertainty of model coefficients. Typical laboratory studies on rate constant and model coefficients determine the constant/coefficient at one or two ambient conditions only, and hence do not adequately describe the natural variability of the processes. As a result, model can be used to bridge the gap of data. For example, model sensitivity studies can be conducted to investigate the relative importance of various processes and coefficients. Chen and Sheng (1994) used a process-based hydrodynamics-water quality model to investigate the phosphorus transport and to demonstrate the effects of DO and pH on desorption of dissolved inorganic phosphorus in Lake Okeechobee.

An exception to the available Tampa Bay data is the water quality data provided by the EPC since 1972 (Boler, 1992). With monthly sampling at 52 Bay stations and 40 tributary stations, the EPC water quality data enabled a preliminary evaluation of the present water quality model. Data during the month of June 1991 were selected to determine the initial condition of water quality model for two reasons: they reflect the water quality characteristics of the Bay prior to the wet season, and because the EPC water quality index (Boler, 1992) for Hillsborough Bay in June 1991 was relatively higher compared to the July and August values. From July to September, several water quality parameters like chlorophyll-a, color, and total Kjeldahl nitrogen showed a marked increase. The EPC water quality index for October recovered to a value comparable to the June level, hence showing the effects of rainfall and increased freshwater discharge during the wet season. One of the goals of this study is to simulate this dynamic response of the Bay to increased freshwater discharge and loading during June to September 1991.

Initial and Boundary Conditions of the Water Quality Model

For the model simulation of Summer 1991, initial and boundary conditions must be developed from available data. As described earlier, this is not an easy task. Available synoptic data were not collected simultaneously and data are inadequate, particularly in the sediment column. The following discussions are given in terms of the water column data first, and then sediment column data.

Water Column

The water column initial concentrations of several water quality parameters were determined from the EPC data of June 1991. Figure 7.1 shows the locations of the EPC water quality monitoring stations in Tampa Bay. The water quality data at the sampling stations were interpolated to each curvilinear grid cell by using the data at the closest three EPC stations, with a weighting function inversely proportional to the distance to each of the three stations. Since the water quality data were collected at only mid-depth, it is reasonable to assume a vertically uniform nutrient distribution as the initial condition for water quality simulation. Dissolved oxygen concentrations were measured at three vertical levels, hence the near-bottom concentration was assigned to the first two sigma-grid levels near the bottom, the mid-depth concentration to the intermediate three sigma levels, and the near-surface concentration to the top three sigma levels. Figures 7.2 to 7.9 show the resulting initial concentration fields for dissolved oxygen at the bottom sigma level, dissolved oxygen at the top sigma level, organic nitrogen, ammonium, nitrate+nitrite, chlorophyll-a, color, and

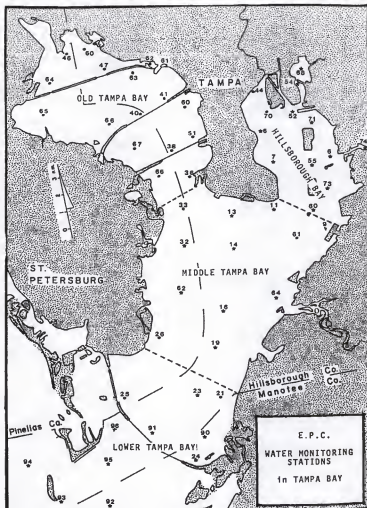


Figure 7.1 - Water quality monitoring stations of the Hillsborough County Environmental Protection Commission (EPC) (Boler, 1992).

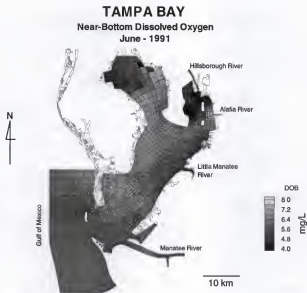


Figure 7.2 - Measured near-bottom dissolved oxygen concentration (mg/L) in Tampa Bay (June 1991).

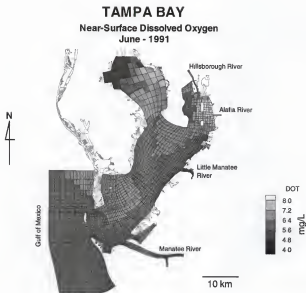


Figure 7.3 - Measured near-surface dissolved oxygen concentration (mg/L) in Tampa Bay (June 1991).

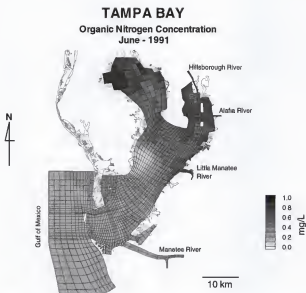


Figure 7.4 - Measured organic nitrogen concentration (mg/L) in Tampa Bay (June 1991).

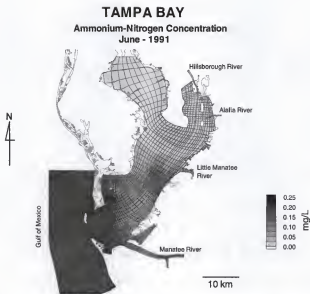


Figure 7.5 - Measured dissolved ammonium-nitrogen concentration (mg/L) in Tampa Bay (June 1991).

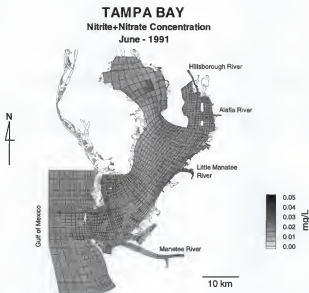


Figure 7.6 - Measured nitrite+nitrate concentration (mg/L) in Tampa Bay (June 1991).

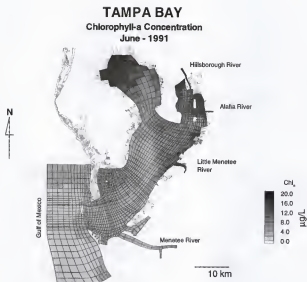


Figure 7.7 - Measured chlorophyll-a concentration ($\mu\text{g/L}$) in Tampa Bay (June 1991).

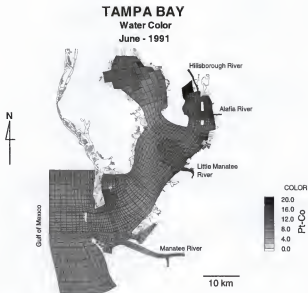


Figure 7.8 - Measured color (Pt-Co) in Tampa Bay (June 1991).

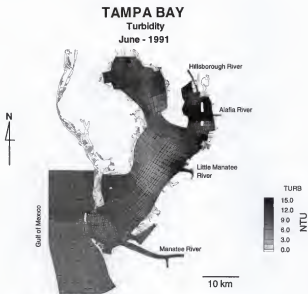


Figure 7.9 - Measured turbidity (NTU) in Tampa Bay (June 1991).

turbidity. These figures do not represent exact snapshots of the Bay conditions, since the data were not collected simultaneously at all 52 stations, but were collected from June 4 to 19, between 9:00am and 3:00pm. The organic nitrogen data exhibit the overall trend of higher concentrations in Hillsborough Bay and the upper reaches of Old Tampa Bay, and a rapid decrease in concentration towards the mouth of the Bay. An isolated low organic nitrogen concentration was noticed around St. Petersburg area. In Middle and Lower Tampa Bay, the nitrite+nitrate and dissolved ammonium data show uniformly low level (around 0.01 mg/L) throughout the Bay. Since the EPC data for tributaries show discharges into the Bay of an order of magnitude higher (0.1 to 0.3 mg/L) than the Bay values, it is reasonable to assume that dissolved inorganic nitrogen was readily uptaken by phytoplankton, which is consistent with the hypothesis that phytoplankton growth in Tampa Bay is limited by nitrogen. Another possibility for lower dissolved ammonium and nitrite+nitrate may be the loss of nitrogen through high nitrification and denitrification rates, as found by Nixon (1981) in Narragansett Bay, Rhode Island.

Riverine boundary conditions required for the model simulations were determined from the nutrient loading study of Coastal, Inc. (1994), which provided estimated monthly nitrogen loading in terms of total nitrogen (TN). In order to divide it among the nitrogen species considered in this study, some assumptions had to be made. The data at the EPC tributary stations were analyzed for total nitrogen partitioning. Based on the averaged ratios, the total nitrogen (TN) provided by Coastal, Inc. (1994) was divided into organic nitrogen (corresponding to 60% of TN), nitrate+nitrite (consisting of 28% of TN), and ammonium

nitrogen (consisting of 12% of TN). This same partitioning procedure was adopted by AScl (1996) to determine the external loading input for their box model of Tampa Bay.

In model simulations, water quality parameters along the oceanic boundary are computed similarly to the salinity simulation. During the outflow, open boundary concentrations are computed from a 1-D advection equation. During the inflow, the open boundary concentrations take on the value of the previous time step, which corresponds to assume the estuarine system as an exporter of nutrients. Although this assumption is generally correct, it may be questionable for some nitrogen species like nitrate, which can be actually imported to the estuary during tidal inflow (Vargo, 1996, pers. comm.). However, since nitrate values in the Gulf of Mexico region adjacent to Tampa Bay during summer 1991 were not available, the exporting assumption will be used in the water quality simulations.

For the present water quality modeling, most model coefficients were initially set to values used by AScl (1996) in their Tampa Bay modeling study, and literature values of coefficients were used for those processes not included in the AScl study, e.g., zooplankton, benthic processes, volatilization. Based on the EPC water quality data shown in Figures 7.2 to 7.9, and the surface sediment composition in Figures 2.5 and 2.6, Tampa Bay was divided into four different zones with distinct sediment types. Zone 1 corresponds to the fine silt and clay sediments of Hillsborough Bay and the upper reaches of Old Tampa Bay. Zone 2 corresponds to the fine sand of the upper reaches of Middle Tampa Bay. Zone 4 corresponds to the coarser sediments of Lower Tampa Bay and adjacent Gulf of Mexico, and Zone 3 corresponds to a transition zone between zones 2 and 4. Figure 7.10 shows the water quality zonation in the curvilinear grid used in this study. For each of the four zones, model

coefficients were then selected and calibrated according to its distinct biogeochemical characteristics.

For the mud zone in Hillsborough Bay, the partition coefficients and desorption constant rates in the water column were determined from the resuspension study of Sheng *et al.* (1993). For the sandy regions, the water column partition coefficients were estimated based on data. Total suspended solids, dissolved and particulate Kjeldahl nitrogen, dissolved ammonium, and nitrate data from Rines (1991), and the EPC water quality data were used

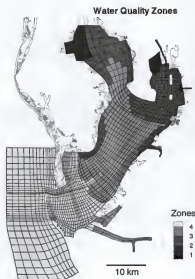


Figure 7.10 - Water quality zones in Tampa Bay used in the model simulations of the summer of 1991 conditions.

to determine the fraction of dissolved and particulate forms of organic and inorganic nitrogen in the water column. Table 7.1 shows the estimated total suspended solids concentration, and the calculated water column partition coefficients for particulate organic nitrogen and particulate inorganic nitrogen (adsorbed ammonium) used in the simulations.

Table 7.1 - Estimated total suspended solids concentration (TSS), and calculated water column partition coefficients for particulate organic nitrogen (pcon) and adsorbed ammonium (pcan).

Zone	TSS (mg/L)	pcon (L/mg)	pcan (L/mg)
1	22.0	1.0E-5	5.0E-7
2	15.0	7.5E-6	7.5E-8
3	12.5	5.E-6	5.0E-8
4	10.0	1.0E-6	1.0E-8

Sediment Column

Studies on sediment nitrogen (dissolved and particulate species) in the top 2 cm of Tampa Bay sediment were performed in 1963 (Taylor and Saloman, 1969), 1985-1986 (COT, 1986; FDER, 1988, Brooks and Doyle, 1992), and 1991-1992 (NOAA, 1994). A literature review showed that studies by Taylor and Saloman (1963), COT (1986), and Brooks and Doyle (1992) used the same sampling methodology (grab samplers), and the results were presented on the same dry-weight basis.

In 1991 and 1992, as part of the National Status and Trends Program for Marine Environmental Quality, NOAA (1994) performed a survey of the sediment toxicity in Tampa Bay, with total sediment nitrogen being part of the sediment chemistry analysis. Sediment samples were collected aboard a research vessel with a van Veen grab sampler, and all chemical analyses were performed by the Skidway Institute of Oceanography, Savannah, Georgia.

No core samples were taken in all the data mentioned above. The data did not include complete fractionation of all nitrogen and phosphorus species, particularly the refractory and non-labile fractions of nitrogen and phosphorus. Nevertheless, useful insight can be developed from these data, and reasonable sediment nutrient distributions can be constructed by making use of all available data from the sediment and water columns.

Assuming the sediment composition presented in these studies is relative to the same dry-weight basis, the following nitrogen enrichment hypothesis may be postulated. Using the sedimentary nitrogen concentration of the 60's as the background sediment composition (Figure 7.11), one can state that the upper reaches of the Bay were heavily stressed during the 70's and early 80's (Figure 7.12). External loadings of organic and inorganic nitrogen exceeded limits that could be naturally recycled or flushed, and led to accumulation in the sediment layer. Brooks and Doyle (1992) reported that this nutrient enrichment occurred mainly in Hillsborough Bay, with the rest of the Bay showing a negligible change in sediment nutrient composition between 1963 and the mid-80's. The primary source of contaminants in Hillsborough Bay during this period was the discharge of the Hooker's Point Wastewater Treatment Plant, which achieved advanced waste treatment (AWT) standards only after 1979 (Boler, 1992). Starting in the 80's, a steady improvement in the water quality of Hillsborough Bay, due primarily to a reduction in phosphorus and nitrogen loading (Boler, 1992),

apparently reversed the process of sediment nutrient enrichment. The 1991 study by NOAA (1994) showed that levels of nitrogen species in the surface sediments are returning to levels comparable to the early 60's. As shown in Figure 7.11, the total organic nitrogen in 1963 was between 0.05 to 0.1% of the sediment, Figure 7.12 shows a partial map of the total Kjeldahl nitrogen in Tampa Bay sediments during 1982-1986 with values between 0.1 and 0.2%, and Figure 7.13 shows the sediment nitrogen in 1986, with values as high as 0.3% throughout Hillsborough Bay.

Figure 7.14 shows the location of the NOAA's sediment sampling stations in 1991 (phase 1) and 1992 (phase 2). Figure 7.15 shows the total nitrogen concentration in the sediment layer obtained from the surveys, and interpolated into the curvilinear grid using the same procedure used for the water column data. The contour values of TN in Figure 7.15 appear to have returned to the 1963's values shown in Figure 7.11.

The initial condition of sediment nitrogen concentrations for the simulations performed in this study is based on the total nitrogen data provided by NOAA (1994). In order to fractionate the total nitrogen into the organic and inorganic forms required by the model, the following assumptions were made. First, the nitrogen dry weight percentage in the surface sediments (NOAA, 1994) was converted to concentration using the sediment dry density. For the mud zone in Hillsborough Bay, the dry density was determined by Sheng *et al.* (1993), with a vertical profile showing a density which increases with depth (Figure 7.16). For the sand region, literature values relating sediment size and porosity were used to determine the dry density (Lambe and Whitman, 1969). Table 7.2 shows the dry density for each of the three sandy zones, along with the mean sediment size.

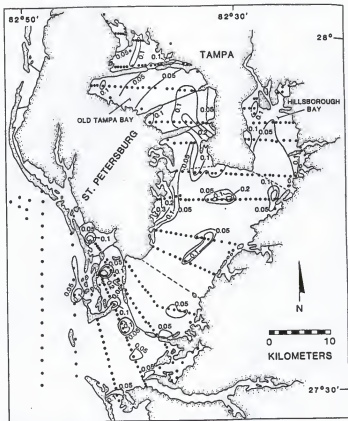


Figure 7.11 - Total organic nitrogen (dry weight %) in the surface sediments of Tampa Bay during 1963 (Taylor and Saloman, 1969).

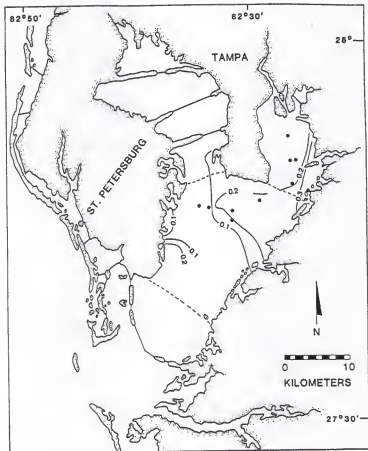


Figure 7.12 - Total Kjeldahl nitrogen (dry weight %) in Tampa Bay sediments, 1982-86 (Brooks and Doyle, 1992).

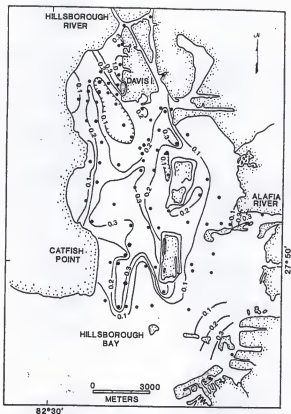


Figure 7.13 - Sedimentary nitrogen (dry weight %) in Hillsborough Bay in 1986 (COT, 1988).

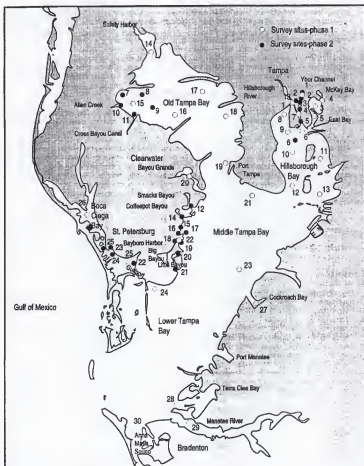


Figure 7.14 - Location of the NOAA sediment sampling stations in 1991 (phase 1) and 1992 (phase 2) (NOAA, 1994).

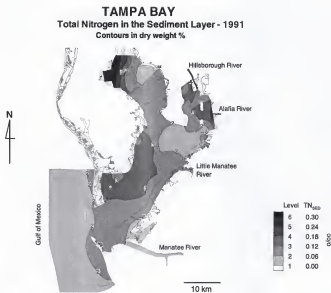


Figure 7.15 - Total sediment nitrogen (dry weight %) obtained from NOAA (1994) data.

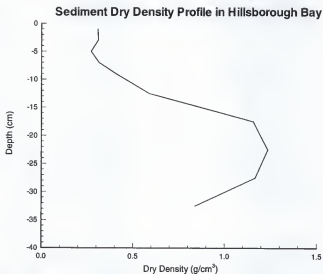


Figure 7.16 - Dry density profile for water quality zone 1 in Tampa Bay (Sheng *et al.*, 1993).

Table 7.2 - Estimated dry density for the sandy zones of Tampa Bay.

Zone	d_{30} (mm)	Dry density (g/cm^3)
2	0.090	1.40
3	0.125	1.44
4	0.210	1.48

The various particulate and dissolved nitrogen species in the sediment column were calculated using the sediment dry density and the same composition obtained by Simon (1989) for the Potomac Estuary. The results show that the total sedimentary nitrogen is divided into organic (90% of total nitrogen) and inorganic (10% of total nitrogen) forms. The same procedure for fractionating the particulate and dissolved nitrogen forms in the water column was applied to the sediment column. In agreement with Simon (1989) results, the adsorbed ammonium averaged approximately 8% of the total sedimentary nitrogen.

The vertical profiles of nitrogen sediment are expected to contain spatial and temporal variations, due to changes in redox potential and aerobic and anaerobic conditions. In the absence of information on vertical profiles of 1991 sediment nutrient data, initially uniform vertical profiles were assumed for the anaerobic and aerobic sediment layers. For modeling purposes, the thickness of the aerobic layer was set to 1 cm (Fanning, 1996, pers. comm.). The initial nutrient concentrations in the aerobic and anaerobic sediment layers are presented in Table 7.3.

Table 7.4 summarizes the final selection of model coefficients for the biogeochemical processes in four lateral water quality regions and three different vertical layers (water column, aerobic, and anaerobic sediment layers).

Table 7.3 - Initial nitrogen concentration in the sediment (Ae) aerobic layer, and (An) anaerobic layer for each water quality zone. (SON) soluble organic nitrogen, (NH4) dissolved ammonium nitrogen, (NO3) nitrite+nitrate.

		Zone 1 (mg/L)	Zone 2 (mg/L)	Zone 3 (mg/L)	Zone 4 (mg/L)
SON	Ae	40.0	30.0	20.0	10.0
	An	80.0	60.0	40.0	20.0
NH4	Ae	4.5	4.2	2.8	1.5
	An	8.5	6.0	3.0	1.5
NO3	Ae	0.6	0.5	0.4	0.4
	An	0.01	0.01	0.01	0.01

Table 7.4 - Model coefficients in the (W) water column, (Ae) aerobic layer, and (An) anaerobic layer for each water quality zone.

	Zone 1			Zone 2			Zone 3			Zone 4		
	W	Ae	An	W	Ae	An	W	Ae	An	W	Ae	An
d_{an}	36	4	4	36	4	4	36	4	4	36	4	4
d_{on}	36	4	4	36	4	4	36	4	4	36	4	4
$d_{m o l}$	1E-5	1E-5	1E-5	1E-5	1E-5	1E-5	1E-5	1E-5	1E-5	1E-5	1E-5	1E-5
K_D	0.25	0.03	0.01	0.20	0.02	0.01	0.15	0.01	0.01	0.05	0.01	0.01
$K_{D N}$	0.05	0.10	1.50	0.05	0.10	1.20	0.04	0.10	1.00	0.04	0.08	1.00
$K_{N N}$	0.06	0.10	0.00	0.05	0.10	0.00	0.06	0.10	0.00	0.06	0.10	0.00
$K_{O N M}$	0.08	0.02	0.01	0.10	0.05	0.01	0.10	0.05	0.01	0.10	0.10	0.05

Modeling Strategy

The model simulations to be presented consist of (1) a model sensitivity analysis which was designed to test the sensitivity of model results in an idealized Tampa Bay to such parameters as molecular diffusion coefficients for the sediment layer, thickness of aerobic layer, desorption rates and partition coefficients, mineralization rates, nitrification, denitrification, algae growth, death, and excretion rates; (2) model simulations of the summer 1991 condition in Tampa Bay using the nutrient loading provided by Coastal, Inc. (1994), which defines the present condition of the Bay; and (3) two loading reduction cases (100% and 40% loading reduction) to study the response of the Bay to improvements in point-source discharges into the system.

Sensitivity Analysis

The sensitivity analysis refers to a study of the sensitivity of model results (measured as the percent variation in model results vs. the baseline simulation results) given a range of possible variation for each of several model parameters. A thorough sensitivity analysis for all model coefficients and input parameters is prohibitively time-consuming. Therefore, a set of sensitivity tests were performed to identify the most important model coefficients and input parameters. Through this sensitivity analysis, it is also possible to identify the type and amount of additional data required. In this study, the sensitivity analysis was conducted for such model coefficients and input parameters as molecular diffusion coefficient, thickness of

sediment aerobic layer, partition coefficients between dissolved and particulate nitrogen species, nitrification rate, denitrification rate, mineralization rate for organic nitrogen, maximum algal growth, half saturation constant for algal uptake, algal nitrogen to carbon ratio, deoxygenation rate, CBOD settling velocity, sediment composition, erosion rates, and linear oxygen balance.

In order to test the model response to variation of these specific parameters, the sensitivity tests were conducted in an idealized rectangular basin, with dimensions similar to Tampa Bay. Like Tampa Bay, the test basin was divided in four water quality zones, and initial condition for water quality parameters were set to average values of the same zones in Tampa Bay. During 30-day simulations, no external forcing (e.g., tide, wind, and river discharge) were applied, so that variations in nutrient composition could be directly related to biogeochemical processes. The tests were performed by varying each parameter within "reasonable" ranges. Table 7.5 shows the parameters considered in the sensitivity analysis, the baseline value used in the simulations, and the range of variation tested. Table 7.6 describes each sensitivity test, and specifies a test identification code that will be used during analysis of results. The baseline simulation corresponds to the configuration of model parameters and coefficients used in the Tampa Bay simulations.

Table 7.5 - Parameters, baseline values, and range used in the sensitivity analysis.

Parameter	Literature Range	Tampa Bay	Test Range
Molecular Diffusion Coefficient (cm^2/s)	1.E-2 ~ 1.E-6	1.E-5	1.E-4 ~ 1.E-6
Thickness of Sediment Aerobic Layer (cm)	0.0 ~ 5.0	1.0	0.5 ~ 2.0
Partition Coefficient (L/mg)	5.E-7 ~ 1.E-5	5.E-7 ~ 1.E-5	5.E-8 ~ 1.E-4
Nitrification Constant Rate (day^{-1})	0.001 ~ 0.6	0.2	0.02 ~ 2.0
Denitrification Constant Rate (day^{-1})	0.02 ~ 1.0	0.9	0.09 ~ 1.5
Mineralization Constant Rate (day^{-1})	0.01 ~ 0.4	0.1	0.01 ~ 0.4
Maximum Algal Growth (mg/L/day)	0.2 ~ 8.0	1.4	0.7 ~ 2.8
Half Saturation Constant for Uptake (mg/L)	0.0015 ~ 0.4	0.05	0.01 ~ 0.1
Algal Nitrogen to Carbon Ratio	0.05 ~ 0.43	0.15	0.07 ~ 0.25
Deoxygenation Constant Rate (day^{-1})	0.02 ~ 0.6	0.2	0.02 ~ 2.0
Fraction of dissolved CBOD (%)	0 ~ 100	50 ~ 85	1 ~ 99
Particulate CBOD Settling Velocity (m/day)	-	ws/2.	ws/10. ~ ws
Sediment Composition	-	Bulk Density (ρ_b)	0.5 ρ_B ~ 1.5 ρ_B

Table 7.6 - Sensitivity tests description.

Description	Range	Test #
Baseline	-	T1
Molecular Diffusion Coefficient	Baseline * 10.	T2.1
	Baseline * 0.1	T2.2
Thickness of Sediment Aerobic Layer	0.5 cm	T3.1
	2 cm	T3.2
Partition Coefficient	Baseline * 10.	T4.1
	Baseline * 0.1	T4.2
Nitrification Constant Rate	Baseline * 10.	T5.1
	Baseline * 0.1	T5.2
Denitrification Constant Rate	Baseline * 10.	T6.1
	Baseline * 0.1	T6.2
Mineralization Constant Rate	Baseline * 4.0	T7.1
	Baseline * 0.1	T7.2
Maximum Algal Growth	Baseline * 2.0	T8.1
	Baseline * 0.5	T8.2
Half Saturation Constant for Uptake	Baseline * 2.0	T9.1
	Baseline * 0.5	T9.2
Algal Nitrogen to Carbon Ratio	Baseline * 2.0	T10.1
	Baseline * 0.5	T10.2
Non-linear Oxygen Balance	-	T11.1
Deoxygenation Constant Rate	Baseline * 10.	T12.1
	Baseline * 0.1	T12.2
Fraction of Dissolved CBOD	Baseline * 10.	T13.1
	Baseline * 0.1	T13.2

Table 7.6 - continued

Description	Range	Test #
CBOD Settling Velocity	Baseline * 10.	T14.1
	Baseline * 0.1	T14.2
Sediment Composition	Bulk density*1.2	T15.1
	Bulk density*0.7	T15.2

The tests were conducted by varying each coefficient between the extreme values within literature range. Table 7.7 shows the partition between water column soluble organic nitrogen, ammonium, nitrite+nitrate, and phytoplankton concentration for the baseline run, the total percent of the water column nitrogen accounted in these three species, and the dissolved oxygen concentration at the bottom layer. The results of the sensitivity tests for the nitrogen species are presented in terms of percent variation from the baseline run. Positive values corresponding to an increase percent in concentration, relative to the baseline run, and negative values corresponding to a decrease. The non-linear oxygen balance test (T11.1) was conducted to evaluate the amount of "spin-up" time required by a fully non-linear equation, and the sensitivity of model results to linear and fully non-linear options.

The results of the tests showed mineralization constant rate as the most sensitive parameter in the water quality model. Increasing mineralization (T7.1) is more influential on phytoplankton than decreasing it (T7.2). Results of test T7.1 show that soluble organic nitrogen (SON) is rapidly mineralized to ammonium nitrogen (NH₄). Nitrite+nitrate (NO₃)

Table 7.7 - Sensitivity analysis results.

Test	SON (%)	NH4 (%)	NO3 (%)	ALGN (%)	TN (%)	DOB (mg/L)
T1	57.5	6.2	0.5	35.0	99.2	6.4
T2.1	<0.01	<0.01	<0.01	<0.01	99.2	6.4
T2.2	<0.01	<0.01	<0.01	<0.01	99.2	6.4
T3.1	0.6	-0.5	-0.1	-1.04	99.2	6.4
T3.2	-0.6	0.5	0.1	1.1	99.2	6.4
T4.1	-5.0	-0.2	1.5	4.2	97.8	6.3
T4.2	0.7	0.2	0.5	-0.6	99.4	6.4
T5.1	-0.2	-44.3	543.6	0.2	99.3	5.8
T5.2	-0.1	7.6	-89.5	0.04	99.2	6.4
T6.1	1.1	1.2	-41.4	-1.4	99.2	6.4
T6.2	<0.01	<0.01	<0.01	<0.01	96.4	6.5
T7.1	-55.5	81.0	109.5	74.2	98.8	6.3
T7.2	55.1	-62.6	-22.8	-77.9	99.6	6.1
T8.1	3.9	-51.3	-73.7	4.3	99.3	6.6
T8.2	-11.5	152.0	540.3	-17.5	98.8	6.2
T9.1	-5.3	68.0	189.3	-6.9	99.0	6.3
T9.2	3.0	-39.6	-62.0	3.4	99.3	6.5
T10.1	1.6	-21.8	-40.5	2.3	99.3	6.4
T10.2	-4.1	52.3	153.7	-6.0	98.8	6.2
T11.1	0.01	0.09	-0.5	-0.01	96.4	4.1
T12.1	<0.01	<0.01	<0.01	<0.01	96.4	5.8
T12.2	<0.01	<0.01	<0.01	<0.01	96.4	7.5
T13.1	<0.01	<0.01	<0.01	<0.01	99.2	1.9
T13.2	<0.01	<0.01	<0.01	<0.01	99.2	6.5
T14.1	-0.6	-0.5	0.1	1.1	99.2	6.9
T14.2	-0.6	-0.5	0.1	1.1	99.2	3.1

Table 7.7 - continued

Test	SON (%)	NH ₄ (%)	NO ₃ (%)	ALGN (%)	TN (%)	DOB (mg/L)
T15.1	-1.1	-1.1	-2.8	2.1	99.2	6.4
T15.2	0.1	0.4	5.2	0.3	99.2	6.4

levels also increased due to nitrification. Since more inorganic nutrients were available, an expected increase in uptake resulted in a noticeable increase in phytoplankton nitrogen (ALGN). On the other hand, decreasing mineralization promoted an increase in SON, and decrease in NH₄, NO₃, and ALGN.

The second most important parameter revealed by the sensitivity tests is maximum algal growth (T8.1 and T8.2), followed by the half saturation constant for uptake (T9.1 and T9.2). These two parameters are related and their major impact should be detected in the phytoplankton biomass. However, the ALGN seems to be more sensitive to mineralization than maximum growth or half saturation, which reveals the extension of nitrogen limitation to phytoplankton growth. Moreover, the effect of reducing maximum growth rate (T8.2) is more pronounced in ALGN than increasing it (T8.1). Inorganic nitrogen, both NH₄ and NO₃, are more sensitive to variations of these parameters. Test T8.2 showed that maximum growth rate is the most sensitive parameter for ammonium nitrogen. As to NO₃, the maximum growth rate is the second most sensitive coefficient, right after nitrification rate constant. Inorganic nitrogen species are more sensitive to a decrease in maximum growth rate (T8.2) and increase in half saturation constant (T9.1), than to the opposite (T8.1 and T9.2), which reinforces the evidence of nitrogen limitation.

The partition coefficients are not the most sensitive parameters in this water quality model. Tests T4.1 and T4.2 demonstrated that increasing the partition coefficient (T4.1) has more effect than decreasing it (T4.2). The variation of partition coefficients regulate not only the relative composition between species, but also the availability of inorganic nutrients for algal uptake. An increase in the partition coefficient corresponds to a decrease in available inorganic nutrients, hence limiting phytoplankton uptake.

The thickness of the aerobic layer (T3) did not show a major impact in the distribution of nitrogen species. Water column soluble organic nitrogen, ammonium, nitrate+nitrite, and algal nitrogen do not seem to be sensitive to this parameter.

Results of the non-linear oxygen balance test (T11.1) showed that it does not affect the relative composition of the nitrogen species in the water column. However, since a longer "spin-up" time is required by the fully non-linear option, the near-bottom dissolved oxygen value after 30 days was different from the baseline run. The other tests (T12 to T14) that were designed to evaluate the oxygen balance equations, revealed that fraction of dissolved CBOD is the most sensitive parameter, followed by particulate CBOD settling velocity and deoxygenation coefficient. Actually, these three parameters are closely correlated. It is the nature of the organic matter present in the water column and the ability of the micro-organisms to utilize it that will dictate the fraction of dissolved CBOD, the CBOD settling velocity, and the rate of biochemical oxidation (Sawyer and McCarty, 1978). In order to improve the model, not only DO and BOD have to be measured, but also the nature of the organic matter has to be known, so that laboratory experiments can be performed to determine f_{CBOD} , ws_{CBOD} , and K_D (Equation 4.23).

The sediment composition tests (T15) showed that, in a 30-day simulation, variations in the bulk density have a minimal effect on the water column nutrient distribution.

In order to show the effects of the sensitivity tests in Tampa Bay, two simulations using the lower and upper limits of the mineralization coefficients were performed. Figure 7.17 shows the soluble organic nitrogen, chlorophyll-a, ammonium nitrogen, and nitrite+nitrate contours after 30 days of simulation using the lower limit of the mineralization constant rate. As it would be expected, there is an accumulation of soluble organic nitrogen throughout the Bay. Consequently, ammonium nitrogen is not readily formed, thus limiting phytoplankton growth and nitrification. Figure 7.18 shows the soluble organic nitrogen, chlorophyll-a, ammonium nitrogen, and nitrite+nitrate contours after a 30-day simulation using the upper limit of the mineralization constant rate. In contrast with the previous case, the results of the higher mineralization constant rate showed low concentration of organic nitrogen throughout the Bay, and an increase in phytoplankton concentration. Due to an increase in respiration, decomposition, and nitrification, dissolved oxygen levels decreased mainly in Hillsborough Bay as shown in Figure 7.19.

The information obtained from the sensitivity tests enabled a fine tuning of the model coefficients, using the EPC monthly data. The final values for mineralization constant rate, phytoplankton maximum growth rate, and half saturation constant were determined from phytoplankton, dissolved oxygen, and soluble organic nitrogen measured concentrations.

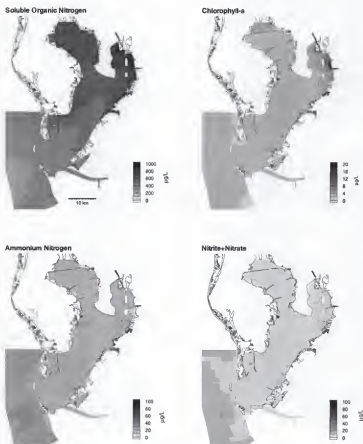


Figure 7.17 - Water quality parameters after 30 days for a simulation using the lower limit of the mineralization constant rate.

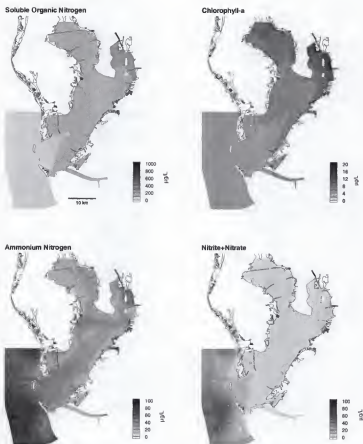


Figure 7.18 - Water quality parameters after 30 days for a simulation using the higher limit of the mineralization constant rate.

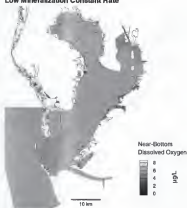
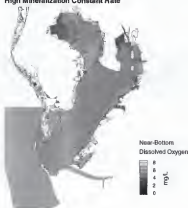
Low Mineralization Constant Rate**High Mineralization Constant Rate**

Figure 7.19 - Near-bottom dissolved oxygen levels after 30 days for the mineralization constant rate tests.

Simulation of the Summer 1991 Condition

The integrated model of the Tampa Bay Estuarine System was used to perform a four-month simulation of the hydrodynamics and water quality dynamics during the summer of 1991. Using the salinity distribution of the hydrodynamics simulation described in Chapter 6 as initial condition, the water quality dynamics in Tampa Bay was simulated with real data of tidal forcing, river discharges, rainfall, and wind field. The initial conditions for the water quality parameters were described in the "Initial and Boundary Conditions of the Water Quality Model" section.

The calibration of model coefficients and water quality zonation were performed using the monthly water column data provided by the EPC. The assumption implicit in this methodology is that the EPC stations inside each of the four major sub-basins (Hillsborough Bay, Old Tampa Bay, Middle Tampa Bay, and Lower Tampa Bay) are representative of the whole area. In the following, model results will be presented for dissolved oxygen, phytoplankton, and nitrogen species in terms of time series at specific grid cells that coincide with EPC stations, contour plots that give a snapshot of the Bay in each month (June to September of 1991), the simulated fluxes across the mouth of the Bay (upstream Egmont Key), entrance to Hillsborough Bay, and the benthic fluxes for organic and inorganic nitrogen species.

Dissolved Oxygen

The dissolved oxygen balance is the most important process in any aquatic environment, because living organisms depend on oxygen in one form or another to maintain their metabolic processes. In the model, dissolved oxygen is a function of photosynthesis and respiration by planktonic organisms, reaeration, nitrification and denitrification, decomposition of organic matter, tidal and wind mixing, and loading. In this sense, the model's accuracy to simulate the dynamics of DO can be linked to the overall ability of the model to synthesize the water quality dynamics within the system.

Figures 7.20 to 7.23 show the evolution of DO concentration through the summer months. Figure 7.20 shows a snapshot of the near-bottom DO distribution in Tampa Bay for June 26, after 30 days of simulation. Figure 7.21 shows the snapshot for July 26, after 60 days of simulation, Figure 7.22 shows the snapshot for August 25, after 90 days of simulation, and Figure 7.23 shows the snapshot for September 24, after 120 days of simulation.

Due to its shallowness, wind, and tidal mixing, Tampa Bay generally exhibits a vertically well-mixed distribution of DO. In Hillsborough Bay, which usually presents the lowest levels of DO, some stratification may occur due to high consumption near the bottom and super-saturation near the surface. High oscillations in DO concentration that are commonly seen in Hillsborough Bay are characteristic of an eutrophic water body. The upper reaches of Old Tampa Bay also exhibited some low levels of DO (between 5 and 6 mg/L), but Figures 7.20 to 7.23 show that it does not seem to evolve throughout the summer. Model results showed that DO variations in Middle and Lower Tampa Bay are mild, without a distinct trend from June to September of 1991.

Near-Bottom Dissolved Oxygen

After 30 days (June 26, 1991)



Figure 7.20 - Near-bottom dissolved oxygen concentration in Tampa Bay for June 26, after 30 days of simulation.

Near-Bottom Dissolved Oxygen

After 60 days (July 26, 1991)

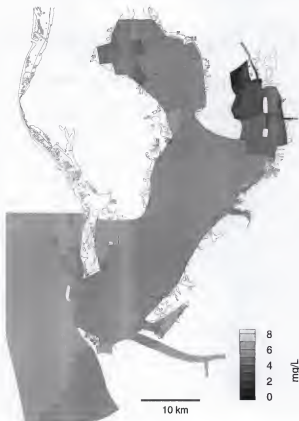


Figure 7.21 - Near-bottom dissolved oxygen concentration in Tampa Bay for July 26, after 60 days of simulation.

Near-Bottom Dissolved Oxygen

After 90 days (August 25, 1991)

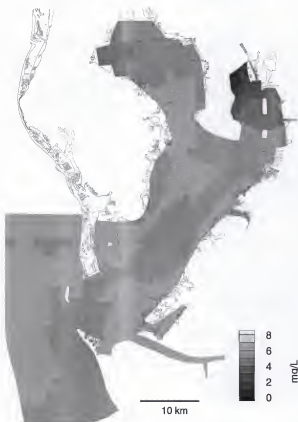


Figure 7.22 - Near-bottom dissolved oxygen concentration in Tampa Bay for August 25, after 90 days of simulation.

Near-Bottom Dissolved Oxygen

After 120 days (September 24, 1991)

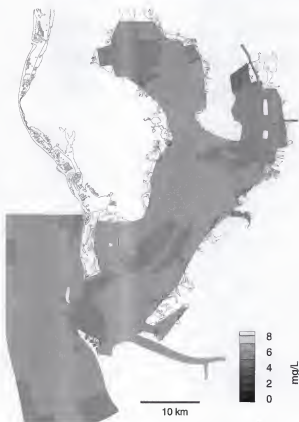


Figure 7.23 - Near-bottom dissolved oxygen concentration in Tampa Bay for September 24, after 120 days of simulation.

Assuming that the EPC data are representative of the Bay conditions, model results were plotted along with the measured data for comparison. Figures 7.24 shows the time series of model results for the segment-averaged DO (near-bottom) and the EPC data inside Hillsborough Bay. The model results for the segment-averaged DO appears to reproduce the EPC averages, as well as the maximum and minimum peaks. Figure 7.25 shows the model results for the segment-averaged DO (near-bottom) and the EPC data inside Old Tampa Bay. Like in Hillsborough Bay, the model seems to accurately reproduce the overall trend in DO, expressed in terms of the EPC averages and the model results for segment-averaged DO. The maximum and minimum values obtained from model simulations are within the range of the measured data. Comparing Figures 7.24 and 7.25, it is possible to visualize the differences between these two water bodies. Both Bays exhibit minimum DO concentrations that are comparable to hypoxic or even anoxic conditions. It appears that organic matter decomposition and nitrification/denitrification processes are the major sinks for DO in the bottom layers of these Bays. As to the maximum peaks, Old Tampa Bay presents an almost flat curve, close to saturation levels of DO. On the other hand, Hillsborough Bay exhibits a very dynamic maximum fluctuation, with the above saturation levels suggesting high phytoplankton activity, typical of eutrophic conditions.

A more direct assessment of model's accuracy was performed by comparing model results at specific grid cells, corresponding to the location of the EPC stations. Figures 7.26 and 7.27 show the model results and measured data for near-bottom dissolved oxygen at EPC stations 8, 70, 73, and 80, in Hillsborough Bay. These figures show that the model was able

Near-Bottom Dissolved Oxygen - Hillsborough Bay

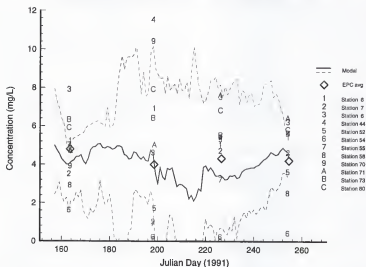


Figure 7.24 - Model results for segment-averaged near-bottom DO (solid line), segment maximum and minimum (dashed line), and the EPC data inside Hillsborough Bay.

Near-Bottom Dissolved Oxygen - Old Tampa Bay

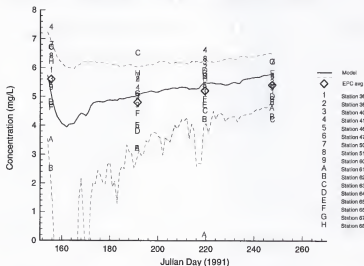


Figure 7.25 - Model results for segment-averaged near-bottom DO (solid line), segment maximum and minimum (dashed line), and the EPC data inside Old Tampa Bay.

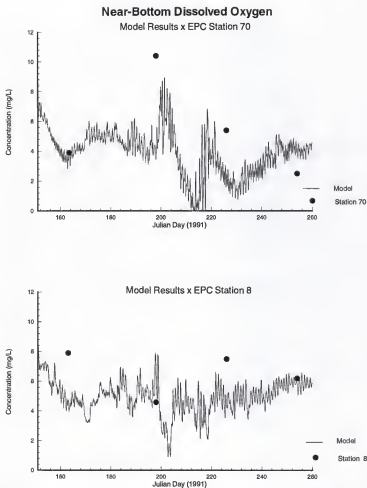


Figure 7.26 - Model results and measured data for near-bottom DO at EPC stations 70 and 8.

Near-Bottom Dissolved Oxygen

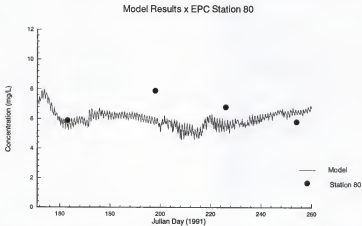
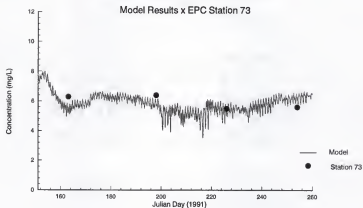


Figure 7.27 - Model results and measured data for near-bottom DO at EPC stations 73 and 80.

to capture the different dynamics of the dissolved oxygen balance occurring on specific areas in Hillsborough Bay. The near-bottom dissolved oxygen balance in the upper reaches of Hillsborough Bay (Figure 7.26) shows a very dynamic environment, with concentrations varying from super-saturation values to hypoxic conditions. On the other hand, Figure 7.27 shows that, close to the mouth of Hillsborough Bay, the near-bottom dissolved oxygen exhibits a more stable balance, similar to the average conditions found in the other parts of Tampa Bay. Moreover, these figures show the importance of using a three-dimensional fine-resolution model to fully understand the water quality dynamics in Hillsborough Bay.

Figure 7.28 and 7.29 show the model results for the segment-averaged DO (near-bottom) and the EPC data inside Middle and Lower Tampa Bay, respectively. Simulated DO for Middle and Lower Tampa Bay was not able to accurately reproduce the EPC data, although the segment-averaged DO was within the data range. Both Middle and Lower Tampa Bay EPC-average showed a sharp decrease in DO during August that was not captured by the model. Possible reasons for this discrepancy are two-fold: the phytoplankton dynamics, and the offshore boundary conditions. In the first one, the phytoplankton simulations could not be reflecting the dynamics of the system, with an unbalanced relationship between photosynthesis and respiration in late summer causing the drop in the DO levels. Tests with different phytoplankton/zooplankton relationships were able to shift the segment-averaged DO curve up and down, but were not capable of reproducing the dynamics shown in the EPC data. The second reason could be the offshore boundary condition. The EPC data at the most offshore station (station 94) present one of the lowest

Near-Bottom Dissolved Oxygen - Middle Tampa Bay

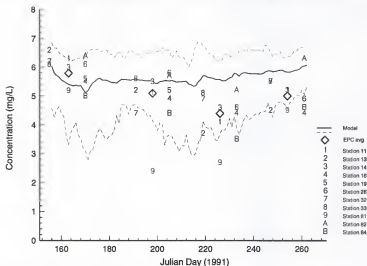


Figure 7.28 - Model results for segment-averaged near-bottom DO (solid line), segment maximum and minimum (dashed line), and the EPC data inside Middle Tampa Bay.

Near-Bottom Dissolved Oxygen - Lower Tampa Bay

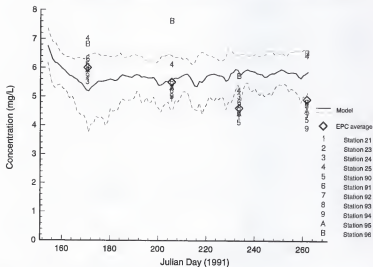


Figure 7.29 - Model results for segment-averaged near-bottom DO (solid line), segment maximum and minimum (dashed line), and the EPC data inside Lower Tampa Bay.

levels of DO (Figure 7.29), and it seems to be driving the trend of low DO during July and August. If that is the case, the boundary condition used by the model, which does not account for disturbances originated in the Gulf of Mexico, may be compromising the results.

Phytoplankton

The phytoplankton dynamics is also one of the most important processes simulated in this study. It is closely related to the nutrient recycling through uptake during growth, and excretion/decay during respiration and senescence. The diurnal variations exhibited by the dissolved oxygen cycle is a result of photosynthetic oxygen production during daylight combined with consumption during the night. As one of the dominant components of the primary producers in Tampa Bay (Pomeroy, 1960), phytoplankton forms the basis of the food chain, affecting the dynamics of all successive trophic levels (Steidinger and Gardiner, 1985). Phytoplankton also presents an important feedback to the circulation and water quality models through its contribution to total suspended solids and light attenuation simulations.

In this integrated model of the Tampa Bay Estuarine System, the phytoplankton community is aggregated into a single constituent, and simulated in a mass per volume basis. In order to make comparisons with the data obtained by EPC, the conversion of model results to chlorophyll-a had to be made. Although a rigorous stoichiometric conversion considers the variability due to species composition, cell size, physiological conditions, and environmental parameters (external nutrient concentration, light, and temperature), most water quality models (e.g., Di Toro *et al.*, 1971; Najarian, 1984; Ambrose *et al.*, 1991; Chen

and Sheng, 1994) consider a fixed carbon to chlorophyll-a ratio in the absence of specific data.

Figures 7.30 to 7.33 show the evolution of chlorophyll-a concentration through the summer months. Figure 7.30 shows a snapshot of the near-surface chlorophyll-a distribution in Tampa Bay for June 26, after 30 days of simulation. Figure 7.31 shows the snapshot for July 26, after 60 days of simulation, Figure 7.32 shows the snapshot for August 25, after 90 days of simulation, and Figure 7.33 shows the snapshot for September 24, after 120 days of simulation. From the initial condition (Figure 7.7) to the end of June snap-shot (Figure 7.30) it is possible to conceive of the development of high planktonic activity as summer progresses. Only a few spots in upper Hillsborough Bay exhibit chlorophyll-a concentrations above 20 $\mu\text{g/L}$, and they seem to originate from Hillsborough River and Alafia River discharges. Old Tampa Bay, which started with chlorophyll-a levels comparable to Hillsborough Bay, does not seem to develop high concentrations towards the summer months. Middle and Lower Tampa Bay showed uniformly low concentrations, with a small increase towards the shallow areas, on both sides of the Bay.

After 60 days (Figure 7.31), the model results showed that Hillsborough Bay maintains the highest concentrations of chlorophyll-a, with most of the upper reaches of the Bay exhibiting chlorophyll-a concentrations of 20 $\mu\text{g/L}$ or higher. The highest concentrations of chlorophyll-a found in the upper Hillsborough Bay can be attributed to high nutrient concentration and poor flushing, an ideal combination for the development of algae blooms. Algal blooms are always related to high turbidity, odors, depletion of dissolved oxygen, and sometimes associated with extensive fish kills. According to the EPC report (Boler, 1992), the tributaries of the upper Hillsborough Bay have been the source of many complaints from residents concerned with algal blooms and fish kills.

Chlorophyll-a Concentration

After 30 days (June 26, 1991)

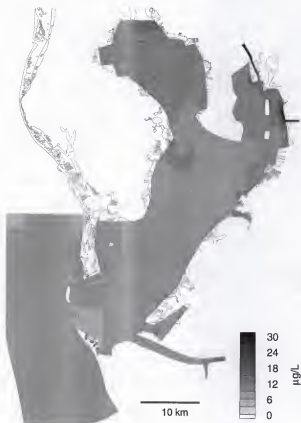


Figure 7.30 - Near-surface chlorophyll-a concentration in Tampa Bay for June 26, after 30 days of simulation.

Chlorophyll-a Concentration

After 60 days (July 26, 1991)

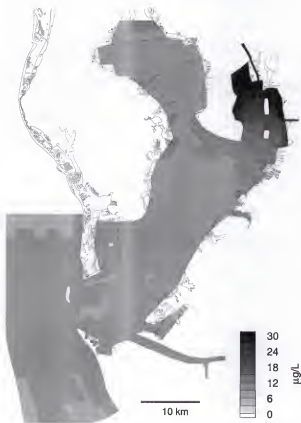


Figure 7.31 - Near-surface chlorophyll-a concentration in Tampa Bay for July 26, after 60 days of simulation.

Chlorophyll-a Concentration

After 90 days (August 25, 1991)

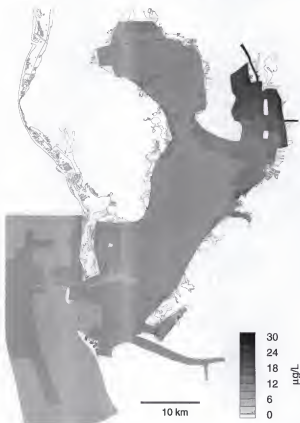


Figure 7.32 - Near-surface chlorophyll-a concentration in Tampa Bay for August 25, after 90 days of simulation.

Chlorophyll-a Concentration

After 120 days (September 24, 1991)

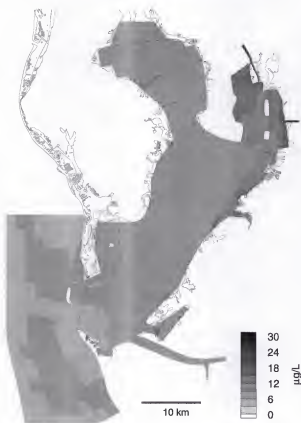


Figure 7.33 - Near-surface chlorophyll-a concentration in Tampa Bay for September 24, after 120 days of simulation.

Figure 7.34 shows the time series of model results for the segment-averaged chlorophyll-a and the EPC data in Hillsborough Bay. After the first 30 days, model results and data were within the same range (Julian Day 163). Model results show a steady curve for phytoplankton dynamics up to the beginning of July (Julian Day 182), when chlorophyll-a levels start to increase. The maximum peak of 27 $\mu\text{g/L}$ occurs around Julian Day 204, after which the chlorophyll-a levels decrease. A closer look to the rainfall (Figure 6.9) and river discharge (Figure 6.10) data suggests that the high rainfall between Julian Days 192 and 196, leading to an abnormal river discharge into Hillsborough Bay, especially from Alafia River, may have triggered this event.

Figure 7.35 shows the time series of model results for the segment-averaged chlorophyll-a and the EPC data in Old Tampa Bay. The model was able to capture the general trend described by the EPC averages, although the small increase of the August EPC-average (Julian Day 219) was not shown in the model results. It is clear that the outlier represented by the EPC station 62 (represented by the symbol "B" in Figure 7.35) is pulling the average upward. EPC station 62 is located at the mouth of Sweetwater Creek, whose discharge does not show any particular increase during this period. In the model, the concentration for each water quality parameter is fixed, and linked to the total loading through the river discharge. Therefore, the difference between the EPC data and model results could be attributed to a localized change in environmental conditions, that was not captured by the fixed riverine boundary condition of the model.

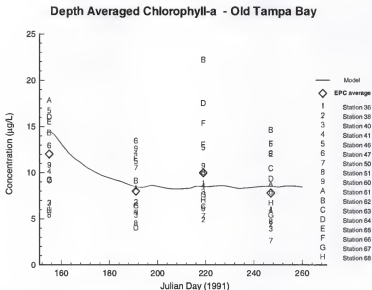


Figure 7.35 - Model results for segment-averaged near-surface chlorophyll-a (solid line) and the EPC data inside Old Tampa Bay.

Figure 7.36 shows the time series of model results for the segment-averaged chlorophyll-a and the EPC data in Middle Tampa Bay. For this particular subdivision of Tampa Bay, the data is so scattered, with both spatial and temporal variations, that it is difficult to draw any conclusion. After the first 30 days, the model is over predicting the EPC average, with only a few stations showing chlorophyll-a levels higher than the model segment-average. For the August data (between Julian Days 219 and 233), an excessive high concentration in EPC station 32 (represented by the symbol "7" in Figure 7.36) shifts the EPC averages upward, and causes an under prediction by the model results.

Figure 7.37 shows the time series of model results for the segment-averaged chlorophyll-a and the EPC data in Lower Tampa Bay. As discussed for dissolved oxygen, model results for segment-averaged chlorophyll-a are within the data range, although they did not reflect the dynamics of the phytoplankton in Lower Tampa Bay. For the first 30 and 60 days, the model over predicts chlorophyll-a in Lower Tampa Bay, and it appears that the low average levels are driven by the most offshore stations (EPC stations 93 and 94). In August (Julian Day 236), all the EPC stations showed an increase in chlorophyll-a concentration, with the EPC station 94 presenting the highest relative increase.

The analysis of the dissolved oxygen and chlorophyll-a concentrations in Lower Tampa Bay suggests the necessity of specific data for the oceanic boundary condition. During flood flow, the model should use a prescribed value obtained from temporal interpolation of measured data. During ebb flow, the water quality parameters would be computed internally. Therefore, disturbances originated in the Gulf of Mexico could be captured by model simulations. Thomman *et al.* (1994) reported the use of an ocean boundary sub-model to specifically study the effects of the coastal zone as part of the Integrated Chesapeake Bay Models.

Segment Averaged Chlorophyll-a - Middle Tampa Bay

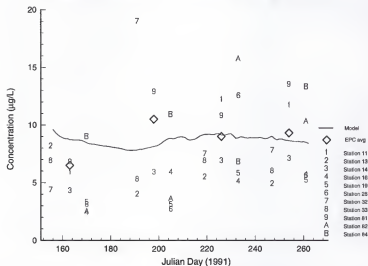


Figure 7.36 - Model results for segment-averaged near-surface chlorophyll-a (solid line) and the EPC data inside Middle Tampa Bay.

Depth Averaged Chlorophyll-a - Lower Tampa Bay

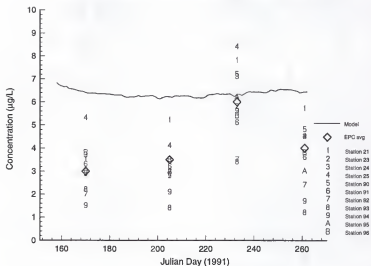


Figure 7.37 - Model results for segment-averaged near-surface chlorophyll-a (solid line) and the EPC data inside Lower Tampa Bay.

Nitrogen Species

In order to compare the nitrogen cycle simulations with the nitrogen species data presented by EPC, simulated soluble organic nitrogen, dissolved ammonium and ammonia nitrogen concentrations were combined and compared with the EPC total Kjeldahl nitrogen. Since most organic compounds containing nitrogen are derivatives of ammonia, the Kjeldahl method employs sulfuric acid to oxidize the organic portion of the molecules and release the nitrogen as ammonia, which is then measured by standard laboratory procedures. The EPC total Kjeldahl nitrogen included nitrogen from ammonia, amino acids, polypeptides and proteins, mostly of biological origin (Boler, 1992). It can be anticipated that model results are going to under predict the Kjeldahl nitrogen data due to the fact that the methodology applied by the EPC makes use of unfiltered samples, therefore, including some particulate species (Boler, 1996 - pers. comm.).

Figures 7.38 to 7.41 show the evolution of near-bottom Kjeldahl nitrogen concentration through the summer months. Figure 7.38 shows a snapshot of the near-bottom Kjeldahl nitrogen distribution in Tampa Bay for June 26, after 30 days of simulation. Figure 7.39 shows the snapshot for July 26, after 60 days of simulation, Figure 7.40 shows the snapshot for August 25, after 90 days of simulation, and Figure 7.41 shows the snapshot for September 24, after 120 days of simulation. Following the same pattern of the phytoplankton distribution, the Kjeldahl nitrogen exhibits higher concentrations in Hillsborough Bay, with a sharp decrease towards the mouth of Tampa Bay. This same spatial gradient was kept throughout the summer months. According to model results, Lower and Middle Tampa Bay

Kjeldahl Nitrogen

After 30 days (June 26, 1991)

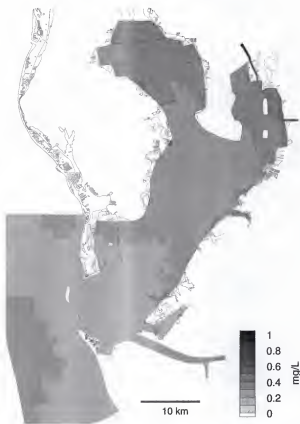


Figure 7.38 - Near-surface Kjeldahl nitrogen concentration in Tampa Bay for June 26, after 30 days of simulation.

Kjeldahl Nitrogen

After 60 days (July 26, 1991)

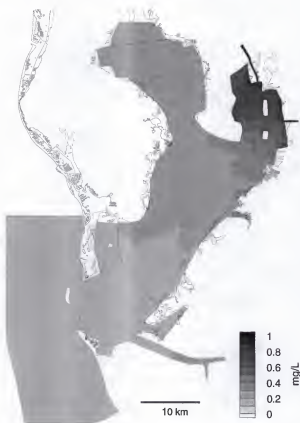


Figure 7.39 - Near-surface Kjeldahl nitrogen concentration in Tampa Bay for July 26, after 60 days of simulation.

Kjeldahl Nitrogen

After 90 days (August 25, 1991)

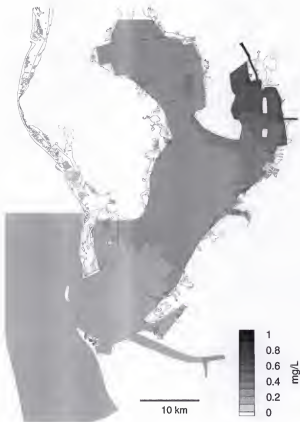


Figure 7.40 - Near-surface Kjeldahl nitrogen concentration in Tampa Bay for August 25, after 90 days of simulation.

Kjeldahl Nitrogen

After 120 days (September 24, 1991)

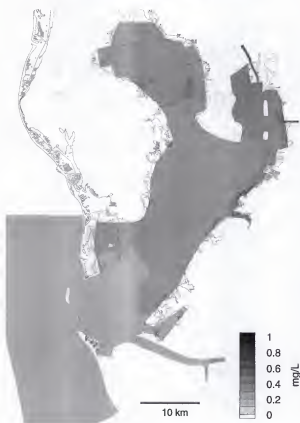


Figure 7.41 - Near-surface Kjeldahl nitrogen concentration in Tampa Bay for September 24, after 120 days of simulation.

were not significantly affected by summer conditions, maintaining low concentration on the order of 0.10 to 0.2 mg/L. Figure 7.39 shows that in late summer, Kjeldahl nitrogen concentrations can rise up to 0.70 mg/L in upper Hillsborough Bay. The source of these high concentrations can be attributed to high phytoplankton activity and loading, but the fate of this nutrient enriched waters needs further investigation. As discussed in Chapter 6, the ebb currents flowing out of the Hillsborough Bay may take the direction parallel to the Interbay Peninsula shoreline towards Old Tampa Bay, causing an advective flux of nutrient enriched waters from Hillsborough Bay to the entrance of Old Tampa Bay. To answer specific management questions regarding the effects of Hillsborough Bay nutrients in Old Tampa Bay, a more intensive numerical study could be performed using particle trajectory simulations.

Figure 7.42 shows the time series of model results for the segment-averaged Kjeldahl nitrogen and the EPC data in Hillsborough Bay. Model results seems to capture the overall trend of the EPC data. The July (around Julian Day 200) peak in concentration was captured by model results, which follows a similar pattern to the chlorophyll-a distribution (Figure 7.34). Figure 7.43 shows the time series of model results for the segment-averaged Kjeldahl nitrogen and the EPC data in Old Tampa Bay. Model results under predict Kjeldahl nitrogen throughout the summer months. As explained for the chlorophyll-a distribution, it seems that the outlier of station 62 (represented by the symbol "B" in Figure 7.43) is forcing the average upward. Both data and model results showed that Kjeldahl nitrogen in Old Tampa Bay does not seem to show any particular dynamics during the summer months of 1991. Figure 7.44 shows the time series of model results for the segment-averaged Kjeldahl nitrogen and the

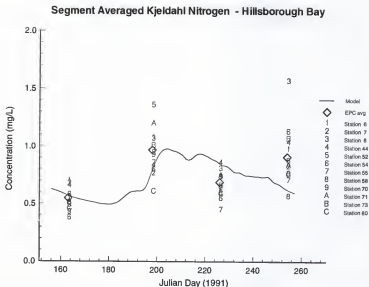


Figure 7.42 - Model results for near-bottom segment-averaged Kjeldahl nitrogen (solid line) and the EPC data inside Hillsborough Bay.

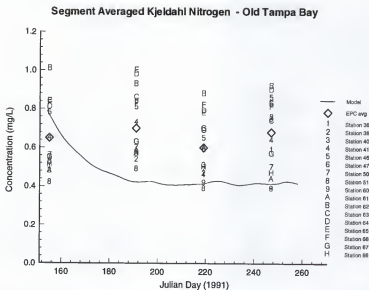


Figure 7.43 - Model results for near-bottom segment-averaged Kjeldahl nitrogen (solid line) and the EPC data inside Old Tampa Bay.

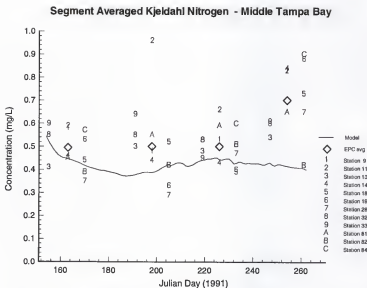


Figure 7.44 - Model results for near-bottom segment-averaged Kjeldahl nitrogen (solid line) and the EPC data inside Middle Tampa Bay.

EPC data in Middle Tampa Bay. Once more, model results under predict Kjeldahl nitrogen throughout the summer months, with both model and data showing no particular event during the summer months of 1991. Figure 7.45 shows the time series of model results for the segment-averaged Kjeldahl nitrogen and the EPC data in Lower Tampa Bay. Although model results under predict the Kjeldahl nitrogen throughout the simulation, the difference between model and data appears to be smaller for Lower Tampa Bay. Unlike model results for chlorophyll-a, the simulated Kjeldahl nitrogen does not seem to be affected by the oceanic boundary condition. Actually, all the measured data exhibit a narrow range of variation, suggesting a uniform distribution of Kjeldahl nitrogen in Lower Tampa Bay, that is maintained throughout the summer of 1991.

From the modeling point of view, it is difficult to compare the EPC unfiltered samples with model results. The fraction of particulate organic nitrogen, particulate inorganic nitrogen and even phytoplankton cells accounted in the samples is not well defined and prevent a more rigorous comparison. Nevertheless, the constant pattern of model under predicting Kjeldahl nitrogen was maintained for all the sub-divisions of Tampa Bay (Figures 7.42 to 7.45). Numerically, the difference could be improved by changing the algal nitrogen to carbon ratio (a_{nc}). Like the carbon to chlorophyll-a ratio, a_{nc} can vary with species composition, cell size, and physiological conditions. The sensitivity test T10 showed that decreasing a_{nc} would cause an increase in inorganic nitrogen, with a proportional decrease in algal nitrogen. Since the model results for phytoplankton are in good agreement with the EPC data in the upper reaches of the Bay, a spatially variant coefficient would be required.

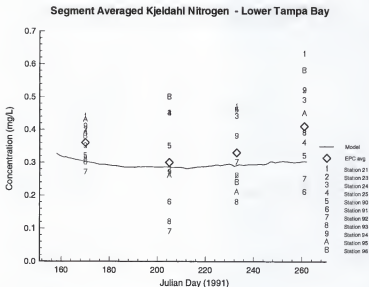


Figure 7.45 - Model results for near-bottom segment-averaged Kjeldahl nitrogen (solid line) and the EPC data inside Lower Tampa Bay.

Without specific data on the composition of the phytoplankton community, arbitrary tuning of model coefficients can be dangerous, and compromise the model's credibility.

Model results for nitrate+nitrite and ammonium nitrogen are presented in Appendix E in terms of contour plots that give a snapshot of the Bay in each of the summer months (June to September of 1991). Also presented in Appendix E are time series for dissolved oxygen, chlorophyll-a, and TKN at specific grid cells that coincide with EPC stations.

Tidal Exchange

During August 25-30, 1991, NOAA used a remote acoustic Doppler sensor (RADS) mounted in a downward-looking mode to measure current profiles along three transects in Tampa Bay. Volumetric flow rates were calculated from the RADS data in four steps: (1) computing the eastward and northward components of flow rate per unit width at each RADS station; (2) multiplying the normal component by the horizontal distance between stations to get flow rate per segment; (3) summing all segment flow rates to get a total for the pass; and (4) estimating the flow rate in the parts of the cross-section that were not measured. The detailed description of the methodology for volumetric flow calculation is presented in Hess (1991). Rines (1991) presented the results of a nutrient sampling survey, which coincides with the NOAA transect across the mouth of Hillsborough Bay and the entrance to Tampa Bay. Along the transect, three stations were sampled, at two to four depths, every three hours over a 24-hour cycle, for a total of eight sampling events. Figure 7.46 shows the measured and simulated transport across the mouth of Hillsborough Bay, along with the Kjeldahl nitrogen concentration (mean and standard deviation) presented by Rines (1991).

In the top figure, model results and the flow rate calculated from RADS data showed reasonable agreement, both in magnitude and phase. It is noteworthy that model results were obtained after 94 days of simulation. Also, the top figure shows the simulated Kjeldahl nitrogen flux across the mouth of Hillsborough Bay. It appears that the inflow and outflow of Kjeldahl nitrogen are in balance, for this particular period. The Kjeldahl nitrogen concentration was calculated from the simulated tidal flow and Kjeldahl nitrogen flux. Figure 7.46 (bottom) shows the simulated Kjeldahl nitrogen concentration along with the calculated averages and standard deviations presented by Rines (1991). According to the analysis presented by Rines (1991), a variety of parameters may influence the analysis of the results. The sampling station location, depth, and tidal cycle accounted for a significant variability in the calculation of the mean and standard deviation presented.

Figure 7.47 shows the measured and simulated transport across the mouth of Tampa Bay (upstream Egmont Key), along with the Kjeldahl nitrogen concentration (mean and standard deviation) presented by Rines (1991). In the top figure, the flow rate calculated from RADS data and the model results are in reasonable agreement, both in magnitude and phase. Again, model results were obtained after 90 days of simulation. The simulated Kjeldahl nitrogen flux across the mouth of Tampa Bay is also presented in the top figure. It appears that the inflow and outflow of Kjeldahl nitrogen are in balance, for this particular period. The Kjeldahl nitrogen concentration was also obtained from the simulated tidal flow and Kjeldahl nitrogen flux. Figure 7.47 (bottom) shows the simulated Kjeldahl nitrogen concentration along with the calculated averages and standard deviations presented by Rines (1991).

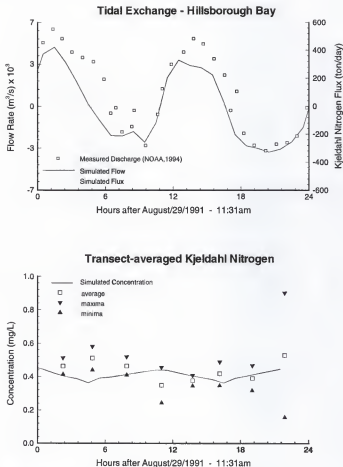


Figure 7.46 - Measured and simulated transport across the mouth of Hillsborough Bay, along with the Kjeldahl nitrogen concentration (mean and standard deviation) presented by Rines (1991).

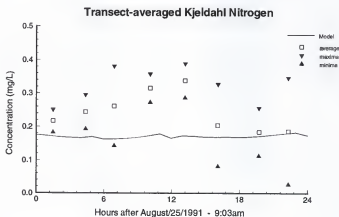
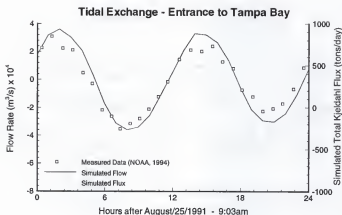


Figure 7.47 - Measured and simulated transport across the entrance of Tampa Bay, along with the Kjeldahl nitrogen concentration (mean and standard deviation) presented by Rines (1991).

Nutrient Budget

Another application of this integrated model of the Tampa Bay Estuarine System that can support ecosystem management is the determination of a nutrient budget for the Bay. Model results were used to compute the net amount of soluble organic nitrogen, ammonium nitrogen, and nitrite+nitrate entering the Bay through point-source loading, benthic fluxes, and exchange with the Gulf of Mexico. The total point-source loading is an input parameter of the model, and it is calculated through a constant concentration multiplied by real data of river discharges.

The subject of benthic fluxes have been discussed by Berner (1971), and applied in a variety of water bodies (e.g., Fanning, 1992; Sheng, 1993). The simplified solution of the diffusion equation gives:

$$J_i = -d_{mol} \cdot \phi \cdot \left(\frac{C_{zI} - C_{z0}}{Z} \right) \quad (7.1)$$

where, J_i is the flux of species i in mass per unit area of sediment and time, d_{mol} is the molecular diffusion coefficient, ϕ is the porosity, C_{zI} is the concentration of i at a depth zI in the sediment layer, C_{z0} is the concentration of i at a depth $z0$ in the sediment or water column layer, and Z is the shallow depth within the linear gradient (taken as the mid-point between $z0$ and zI). In the model, the molecular diffusion coefficient is a constant set to $1.0 \times 10^{-5} \text{ cm}^2 \text{ s}^{-1}$. The resuspension flux, as defined by Sheng (1993), can be used to calculate the amount of nutrients released by sediments in the case of sediment resuspension events. The analysis of the sediment net resuspension (erosion - deposition) throughout

Tampa Bay showed that no major resuspension event occurred during the summer of 1991, resulting in a net depositional flux. The net resuspension and depositional fluxes of particulate nitrogen species were calculated in the model according to:

$$\begin{aligned} \text{Net Flux}(PON, PIN) = & D \cdot (PON, PIN)_{\text{bottom layer of water column}} \\ & - E \cdot (PON, PIN)_{\text{top layer of sediment column}} \end{aligned} \quad (7.2)$$

where D is the deposition rate, and E is the erosion rate.

The tidal exchange with the Gulf of Mexico was computed similarly to the transect calculations at the entrance to Tampa Bay (Figure 7.47). At each vertical grid cell, the velocity normal to the direction of the mouth of the Bay was multiplied by the vertical cross-sectional area of the grid cell and the nutrient concentration. The values were accumulated during a 24-hour period, giving the net exchange per day. Since the tidal period contains diurnal and semi-diurnal information, model results were averaged over a two-month period in order to provide a better estimation of the nutrient exchange with the Gulf of Mexico. Table 7.8 summarizes the nutrient budget between July 1 and August 31, 1991. The total nitrogen represents the sum of soluble organic nitrogen, ammonium nitrogen, ammonia, nitrite+nitrate, algal and zooplankton nitrogen, particulate organic and inorganic nitrogen, obtained from the summer of 1991 simulation.

Table 7.8 - Nitrogen budget between July 1 and August 31, 1991.

	Total Nitrogen (kg)
Initial Mass (July 1, 1991)	1.351×10^6
Loading	1.640×10^6
Exported to the Gulf of Mexico	2.313×10^6
Benthic Flux (into the water column)	0.733×10^6
Final Mass (August 31, 1991)	1.411×10^6

Results of the simulation of the summer of 1991 conditions suggested a conceptual model for the water quality dynamics in the Tampa Bay Estuarine System that is summarized in Figure 7.48. Just for illustrative purposes, the nitrogen cycle was divided in three separate steps, corresponding to (a) loading, (b) water-column-related biogeochemical processes, and (c) sediment-column-related biogeochemical processes. For the loading step, Figure 7.48(a) shows organic and inorganic nitrogen species and phytoplankton been released into the Bay through point sources, non-point sources, and atmospheric deposition (collectively combined into point discharges during model simulations). The net results of the water-column-related biogeochemical processes shown in Figure 7.48(b) demonstrated the central role played by soluble organic nitrogen. The rate at which it is mineralized dictates both the formation of nitrite+nitrate, through nitrification, and the availability of dissolved inorganic nitrogen to phytoplankton uptake. The high levels of soluble organic nitrogen and phytoplankton inside the Bay produce a net export of these water quality parameters to the Gulf of Mexico. On the other hand, the nitrogen limiting condition of the Bay causes a depletion of dissolved inorganic nitrogen species, and the net transport generated is from the Gulf of Mexico into

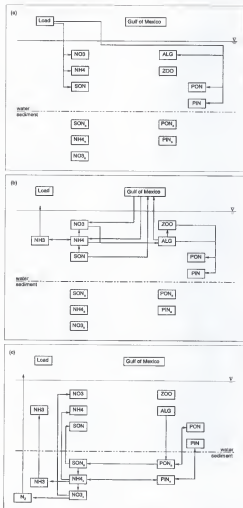


Figure 7.48 - Simulated nitrogen cycle for the summer of 1991 conditions: (a) Loading, (b) biogeochemical processes in the water column, (c) biogeochemical processes in the sediment column.

the Bay. Figure 7.48(c) shows that particulate organic and inorganic nitrogen have a net depositional flux. Two sources were considered in the simulations: the settling and deposition of particulate species, following the suspended sediment dynamics, and the burial of algal cells from the first vertical layer next to the bottom. Particulate inorganic nitrogen (adsorbed ammonium nitrogen) and interstitial ammonium interchange according to the sorption/desorption reaction. Particulate organic nitrogen is converted to soluble organic nitrogen at a constant hydrolysis rate. Since both organic and inorganic dissolved species exhibit higher concentrations in the sediment layer than in the water column, the net diffusive flux is from the sediment into the water column.

Load Reduction Simulations

One of the primary objectives of this integrated model of the Tampa Bay Estuarine System is to provide a tool to study management options and the corresponding response of the system. At this point of development, the model has been tested using monthly water quality data provided by the Hillsborough County Environmental Protection Commission (EPC), and a more comprehensive data set is needed to fully validate the water quality model. Nevertheless, a preliminary analysis of the potential impact of reduced nutrient loadings to the system was carried out by model simulations using 100% and 40% nutrient load reduction.

The 100% load reduction simulation was performed with all the nitrogen species, chlorophyll-a, and CBOD concentrations set to 0 mg/L at the river boundaries. Dissolved oxygen concentration at river boundaries were set to saturation values. In the 40% load

reduction simulation, water quality parameters were set to 40% of the summer of 1991 condition. Figure 7.49 shows the predicted response of the near-bottom dissolved oxygen, after 60 days of the load reduction simulations. As expected, the upper reaches of Hillsborough Bay, which receives most of the freshwater inflow, is the most sensitive segment of the Bay to load reduction. With 40% load reduction, no hypoxic events were found during the simulations, and with 100% load reduction the dissolved oxygen distribution exhibit minimal vertical stratification, with concentration values fluctuating around saturation. In upper Old Tampa Bay (between Courtney Campbell Parkway and W. Howard Frankland Bridge), some localized low levels of near-bottom dissolved oxygen were maintained even during the 100% load reduction scenario. Since there is only one EPC monitoring station (station 65) in the area, model results can be used to recommend a refinement of the monitoring network in order to provide a better representation of the entire Old Tampa Bay. In Middle and Lower Tampa Bay, the effects of the 60-day load reduction simulation seems to be restricted to the vicinity of the mouth of rivers (Little Manatee and Manatee).

Figure 7.50 shows the predicted response of the near-surface chlorophyll-a, after 60 days of the load reduction simulations. The 100% load reduction simulation demonstrated the importance of loading to the system. With no external source of inorganic nitrogen and phytoplankton, the initial phytoplankton distribution was flushed out of Hillsborough Bay, and after 60 days of simulation, the chlorophyll-a concentration was around 5µg/L throughout Hillsborough Bay. In agreement with the analysis of Figures 7.30 to 7.33 and the segment-averaged time series (Figures 7.34 to 7.37), the other sub-divisions of the Bay (Old Tampa Bay, Middle Tampa Bay, and Lower Tampa Bay) did not exhibit major dynamic events during

the summer months of 1991. Therefore, the effects of load reduction in a 60-day simulation were not significant for these Bay sub-divisions.

Comparison with ASCL (1996) study

The box model utilized by the ASCL (1996) study solves a mass balance equation for 8 state variables (ammonia, nitrate, dissolved inorganic phosphorus, phytoplankton biomass, CBOD, dissolved oxygen, organic nitrogen, and organic phosphorus). The biogeochemical processes simulated include four interacting systems: phytoplankton kinetics, the phosphorus cycle, the nitrogen cycle, and the dissolved oxygen balance. Apparently, the strongest advantage of the ASCL box model is related to its ability to perform long term simulations, however, the monthly time scale utilized was exceedingly large. Water quality issues related to eutrophication processes and hypoxia events cannot be addressed at this level of resolution. Furthermore, the main limitation of the model was the descriptive hydrodynamics approach, in which circulation and transport were represented by prescribed values for advective and diffusive fluxes. First, the dynamic circulation generated by tides, wind, and baroclinic forcing were all averaged and combined into an advective flux. Next, the simulated salinity was adjusted to segment- and monthly-averaged salinity data through tuning of the so-called dispersive flux. Results of the summer of 1991 simulation presented in this study demonstrated that the water quality dynamics within each segment of the Bay is highly variable (e.g., Figures 7.26 and 7.27) both in time and space, and could not be fully

Near-Bottom Dissolved Oxygen
After 60 days (July 26, 1991)

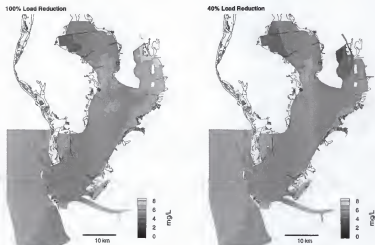


Figure 7.49 - Near-bottom dissolved oxygen concentration in Tampa Bay, after 60 days of the load reduction simulation.

Near-Surface Chlorophyll-a
After 60 days (July 26, 1991)

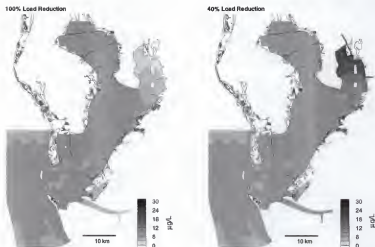


Figure 7.50 - Near-surface chlorophyll-a concentration in Tampa Bay, after 60 days of the load reduction simulation.

captured by a box model using monthly-averaged exchange between segments. Therefore, the segmentation scheme used by ASCI (1996) (only 13 segments, with one vertical layer) could not solve for the horizontal and vertical gradients, characteristics of this estuarine system.

The WASP box modeling framework has proven to be an excellent water quality model for riverine systems, where the steady state assumption is applicable. In addition, this simple box model can be successfully used to perform numerical experiments like the sensitivity tests described in this chapter, or "what if" simulations using segment-averaged output from more robust models. However, in marine environments, it should not be used without the proper linkage with three-dimensional hydrodynamics and sediment models, because tide, wind and baroclinic forcing interact in an unsteady balance.

Comparison with Coastal Inc. (1995) study

The Coastal, Inc. (1995) study was based on regression models developed to investigate the relationships among loadings, water quality, and light levels at the seagrass bed. The complex process of validation of such stochastic models was performed using the extensive data set available from the EPC monitoring network. The available data were considered sufficient to define external nutrient loading levels that were consistent with the light requirements of existing seagrass meadows in Tampa Bay. The Tampa Bay National Estuary Program (TBNEP) has established a range of target light requirements between 20%

and 25% of incident light. This range corresponds to the average light conditions historically observed along the deep edge of the seagrass beds (around 2 meters) in Lower Tampa Bay.

The relationship between nitrogen loading and light attenuation was obtained through a two-step modeling approach. First, the response of chlorophyll-a to nitrogen loading was assumed to be linear, and the relationship was obtained by fitting a regression equation to the chlorophyll-a concentration response to total nitrogen loads. Second, the response of diffuse light attenuation to chlorophyll-a and turbidity was assumed to be linear, and the relationship was obtained by fitting a regression equation to the light attenuation coefficient response to the additive effects of chlorophyll-a concentration and turbidity.

The determination of nutrient load management targets based on the results obtained by Coastal, Inc. (1995) must take into account that the dynamic response of the Bay to different loading scenarios was not considered. The simple linear approach could not explain the relationships between nitrogen loading and ambient nitrogen concentrations, which strongly suggest that internal sources of nitrogen (e.g., phytoplankton kinetics, and exchange with the sediment layer) and the exchange with the Gulf of Mexico play a major role in the water quality dynamics of the Tampa Bay Estuarine System.

Advantages and Limitations of this Integrated Modeling Approach

Due to the vast spatial and temporal variability in hydrodynamics and water quality dynamics, a system-wide understanding of the Tampa Bay Estuarine System cannot be achieved if studies rely only on field monitoring and laboratory experiments. Using the

process-based modeling system developed in this study, it is possible to synthesize the data collected from various parts of Tampa Bay at different times, taking into account the uncertainty of model coefficients. Presently, basic research is needed to reduce the range of model coefficients to specific conditions of Tampa Bay, especially the parameters related to the sediment layer, the water-sediment interface, and the oceanic boundary condition.

Research to improve this integrated modeling approach would certainly enhance our understanding of the relationships between nutrient loading, water quality conditions, and the response of seagrass. Moreover, this modeling approach would benefit management resources agencies that want to develop a management tool, built on process-based understanding rather than regression coefficients. Subsequent refinement of this integrated model can be used to address ecosystem management issues such as controlling estuarine eutrophication and determining allowable external nutrient loading levels to restore seagrass throughout the Bay.

CHAPTER 8

CALIBRATION OF THE SEAGRASS MODEL

Several studies focusing on Florida seagrass beds and associated communities (e.g., Lewis *et al.*, 1985; Zieman and Zieman, 1989; Haddad, 1989; Lewis *et al.*, 1991; Tomasko *et al.*, 1996) have demonstrated the ecological and economical value of seagrass to estuarine systems. In Tampa Bay, the reduction of seagrass meadows can be directly correlated to the extended period of increasingly poor water quality and destruction of habitats experienced throughout the Bay until the early 80's (Coastal Inc., 1995). Taylor and Saloman (1969) estimated that the dredging operations in Boca Ciega Bay resulted in an annual monetary loss of 1.4 million dollars in fishery activities due to the destruction of the seagrass habitat. In a review of the seagrass meadows of Tampa Bay, Lewis *et al.* (1985) found that areal coverage of seagrass beds has been reduced in about 80% from its historical coverage (Figure 8.1). These past studies arrived at a common conclusion that the loss of seagrass habitats is related more to anthropogenic effects than to natural causes. Moreover, these studies suggested that the consequences of this destruction would bounce back, decreasing landings of fishery products, promoting more erosion along the shoreline, and reducing the aesthetic value of the Bay. Fortunately, water quality within the Tampa Bay Estuarine System has been improving since the late 80's (Boler, 1992). As a result, seagrass meadows are expanding in Tampa Bay (Coastal Inc., 1995).

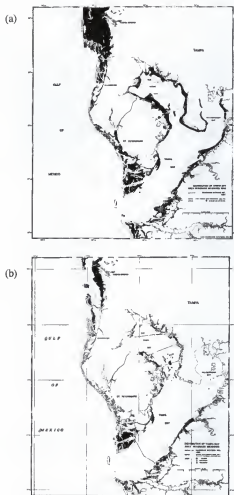


Figure 8.1 - Extent of seagrass meadows in Tampa Bay. (a) corresponding to 1943, and (b) to 1983 (Lewis *et al.*, 1985).

Tomasko *et al.* (1996) studied the effects of anthropogenic nutrient enrichment on *Thalassia testudinum* in Sarasota Bay (Florida). The authors concluded that traditional water quality monitoring programs, based on sparse sampling stations, may fail to detect differences between locations where high gradients of anthropogenic nutrient enrichment exist. They suggested that well-coordinated water quality monitoring programs, in areas with extensive seagrass beds, should incorporate the status of seagrass habitats (e.g., biomass, productivity, species diversity, etc).

This integrated model utilizes seagrass as a bioindicator of the environmental quality of the Tampa Bay Estuarine System. In other words, the basic hypothesis of this integrated modeling study is that the Tampa Bay seagrass community can be used as a bioindicator capable of synthesizing all the dynamic functions (hydrodynamics, water quality, primary production, etc.) of the system. This chapter describes the calibration of the seagrass model. The major objectives of model calibration are: (1) to test the sensitivity of the seagrass model described in Chapter 5 to such model assumptions as density-dependent growth rate, growth rate dependence on temperature, salinity, light, and sediment nutrient concentration; and (2) to simulate the response of the Bay to the dynamics of the summer of 1991 conditions.

The above-ground biomass of three tropical seagrass species (*Thalassia*, *Halodule*, *Syringodium*) was simulated based on their specific relationships with physical and biogeochemical parameters. The seagrass component of this integrated model can run simultaneously with the hydrodynamics and water quality components, or it can use average conditions to run long term simulations (order of years).

Initial Conditions

The initial distribution of seagrass in Tampa Bay was determined based on literature data presented in Lewis *et al.* (1985), Zieman and Zieman (1989), Haddad (1989), Lewis *et al.* (1991). Lewis and Phillips (1980) reported the results of 226 samples collected seasonally throughout the Bay, and determined a percent species occurrence in which *Thalassia* comprises 42.5%, *Halodule* 40.7%, and *Syringodium* 19.0% of the sampling distribution. Figure 8.2 shows the initial seagrass distribution used in the simulations, along with the location of grid cells that will be used for time series analysis. In addition to the information obtained from Figure 8.1, the occurrence of seagrass meadows in the computational grid was restricted to a maximum depth of 2.0 meters. This depth limit correspond to 20% of incident light penetration, historically observed in Lower Tampa Bay (Coastal Inc., 1995). In the beginning of the simulation, the same initial biomass (100 grams of dry weight per square meter - gdw/m^2) was given to all three species of seagrass studied (*Thalassia*, *Halodule*, and *Syringodium*). Based on different responses to environmental conditions, each species of seagrass should prevail in regions where they are able to thrive close to their specific optimum growth.

Initial Seagrass Distribution

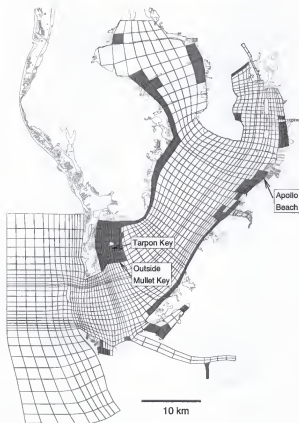


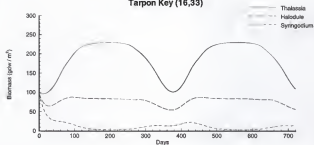
Figure 8.2 - Initial seagrass distribution in the computational grid. Dark areas indicate seagrass meadows (100 gdw/m^2).

Sensitivity Analysis

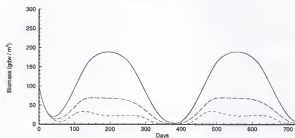
In order to test the seagrass relationships described in Chapter 5, the sensitivity analysis was conducted for such model formulations as density-dependent growth rate, growth rate dependence on temperature, salinity, light, and sediment nutrient concentration. The baseline consisted of a two-year simulation using the relationships described in Chapter 5, average conditions for the water quality parameters (nutrient concentrations, color, turbidity), and a seasonal variation for water temperature, salinity, and incident light. The lack of specific data on epiphytic algae prevent the use of this component on the simulations. Temperature is not dynamically simulated in this integrated model, and its seasonal variation is described by Equation (5.1). In order to give a more realistic representation of the temperature distribution with depth, a linear decrease of two degrees Celsius between the surface and 3-meter depth was assumed.

Figure 8.3 shows the time series of seagrass biomass for the baseline simulation, at three grid cells located in the shallow area close to Sunshine Skyway Bridge (top), in the deep edge of the seagrass bed, outside Mullet Key (middle), and in a shallow area located in the upper reaches of Middle Tampa Bay, close to Apollo Beach (bottom). In 30 days, the species-specific response to environmental conditions was already determining the seagrass distribution. Hence, demonstrating that the initial condition (same initial biomass for all three species) had a minor effect on the results of the simulation. In all three places, *Thalassia*

Seagrass Biomass Tarpon Key (16,33)



Mullet Key (19,34)



Apollo Beach (33,55)

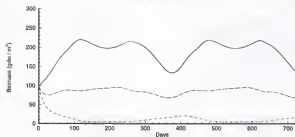
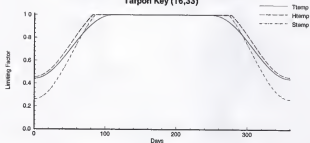


Figure 8.3 - Simulated seagrass biomass in Tampa Bay.

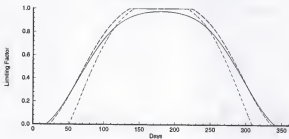
is the dominant species, with the shallow areas exhibiting a maximum biomass of 230 gdw/m² during the summer months. The seasonal fluctuation in biomass for the two cells located in Lower Tampa Bay (Figure 8.3 - top and middle) seems to be driven only by temperature variations and the density-dependent growth rate. During summer, when temperature is close to its optimal conditions, *Thalassia* dominates the distribution. *Syringodium*, which has been hypothesized as sensitive to both low and high temperatures, exhibits the lowest biomass throughout the year. The deep edge of the seagrass bed also showed a clear dominance of *Thalassia*, although the maximum biomass during mid-summer was smaller than the one occurring in the shallow area. Since *Thalassia* and *Halodule* have similar growth dependence on temperature and salinity, the density-dependent growth rate that favors *Thalassia* is the probable cause for its dominance. In the upper reaches of the Bay, a mid-summer decrease in biomass can be attributed to salinity levels below optimum conditions.

Figures 8.4 to 8.7 show the relationships controlling the seagrass dynamics in the baseline simulation. Figure 8.4 (top and bottom) shows the growth rate dependence on temperature for grid cells (16, 33) and (33,55), located in shallow areas. The negative effect of low temperatures on the Tampa Bay seagrass is revealed by the sharp decrease during the winter months. On the other hand, *Thalassia*, *Halodule*, and *Syringodium* seem to tolerate the water temperature commonly found during the summer. Figure 8.4 (middle) shows the growth rate dependence on temperature for the grid cell (19,34), located in the deep edge of the seagrass bed outside Mullet Key. According to model assumptions, temperature is the environmental parameter limiting seagrass growth during winter, with the reduction factor

Growth Rate Dependence on Temperature
Tarpon Key (16,33)



Outside Mullet Key (19,34)



Apollo Beach (33,55)

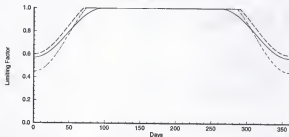
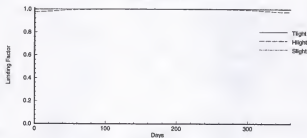
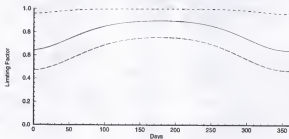


Figure 8.4 - Growth rate dependence on temperature (baseline simulation).

Growth Rate Dependence on Light
Tarpon Key (16,33)



Outside Mullet Key (19,34)



Apollo Beach (33,55)

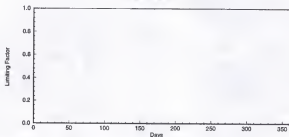
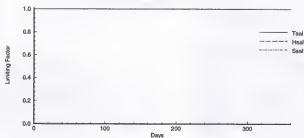
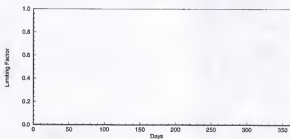


Figure 8.5 - Growth rate dependence on light (baseline simulation).

Growth Rate Dependence on Salinity
Tarpon Key (16,33)



Outside Mullet Key (19,34)



Apollo Beach (33,55)

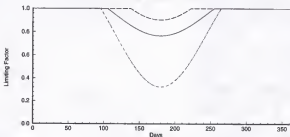
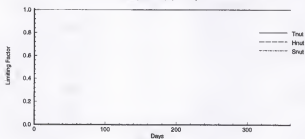
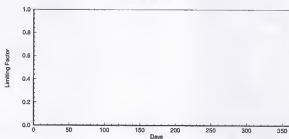


Figure 8.6 - Growth rate dependence on salinity (baseline simulation).

Growth Rate Dependence on Substrate
Tarpon Key (16,33)



Outside Mullet Key (19,34)



Apollo Beach (33,55)

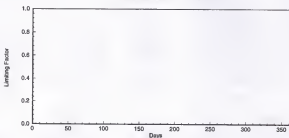


Figure 8.7 - Growth rate dependence on sediment nutrient concentration (baseline simulation).

reaching zero value for all three species during the coldest period of the year (mid-December to mid-February). Lewis *et al.* (1985) presented a comprehensive review of the seagrass meadows of Tampa Bay, and postulated that the seagrass distribution is largely controlled by water temperature. Figure 8.5 (top and bottom) shows the growth rate dependence on light for grid cells (16, 33) and (33,55), located in shallow areas. As expected, the shallow areas do not exhibit any light limitation throughout the year. Along the deep edge of the seagrass bed (Figure 8.5 - middle), the available light seems to limit seagrass growth. According to the model assumptions, the light limiting effects are more sensitive in *Halodule* and *Thalassia*. Figure 8.6 shows the growth rate dependence on salinity. As expected, the seasonal fluctuation of salinity in Lower Tampa Bay is within the optimum range for all three species simulated, therefore, the seagrass beds of Lower Tampa Bay are not limited by salinity. In the upper reaches of the Bay, where salinity levels decrease to less than 20 ppt during the summer months, the seagrass growth is noticeably influenced by salinity, especially *Syringodium*. Figure 8.7 shows the growth rate dependence on sediment nutrient concentration. In all three sites, shallow and deep areas of Tampa Bay, sediment nutrient concentration values are within the optimum range for all three species, and it does not limit seagrass growth throughout the year.

Also for the baseline simulation, Figure 8.8 shows the contour plots of *Thalassia* for mid-summer and winter conditions. During the summer months, the biomass of *Thalassia* reach as much as 300 gdw/m² in the border with Boca Ciega Bay, Anna Maria Sound, and Terra Ceia Bay. During the winter, the biomass decreases, reaching its minimum level in mid-January as shown in Figures 8.3 and 8.8.

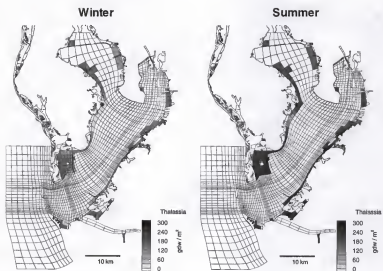


Figure 8.8 - Simulated seasonal distribution of *Thalassia*.

During the sensitivity tests, one-year simulations were performed with no external forcing (e.g. tide, wind, and river discharge). Therefore, variations in seagrass distribution could be directly related to the assumptions of the seagrass model. Table 8.1 describes each sensitivity test, and specifies a test identification code that will be used during analysis of results.

Table 8.1 - Sensitivity tests description.

Description	Range	Test #
Density-dependent growth rate	Constant maximum growth rate	S1.1
	Constant growth rate	S1.2
Growth rate dependence on temperature	Broadest range for all three species	S2.1
	Narrowest range for all three species	S2.2
	No temperature dependence	S2.3
Growth rate dependence on salinity	Broadest range for all three species	S3.1
	Narrowest range for all three species	S3.2
	No salinity dependence	S3.3
Growth rate dependence on light	Broadest range for all three species	S4.1
	Narrowest range for all three species	S4.2
Growth rate dependence on sediment nutrient concentration	10% of seagrass biomass	S5.1
	0.1% of seagrass biomass	S5.2

Tests S1.1 and S1.2 were designed to assess the sensitivity of the model to the density-dependent maximum growth rate. For test S1.1, the maximum growth rate was set to values obtained from the literature (Pomeroy, 1960 and Heffernan and Gibson, 1985), and maintaining the effects of environmental variability in light, temperature, salinity, and sediment nutrient concentration as described in Chapter 5. Test S1.2 used the growth rates of test S1.1 as a constant growth rate, without considering the effects of light, temperature, salinity, and sediment nutrient concentration. Tests S2.1, S2.2, and S2.3 were designed to assess the sensitivity of the model to the formulation of the species-specific growth rate dependence on temperature. Test S2.1 used the growth rate dependence on temperature, formulated for *Thalassia*, in all three species, while test S2.2 used the growth rate dependence on temperature formulated for *Syringodium*. In test S2.3, it was assumed that temperature does not affect seagrass growth rate, hence the values for the temperature limiting factors were set to unity. Tests S3.1, S3.2, and S3.3 were designed to assess the sensitivity of the model to the formulation of the species-specific growth rate dependence on salinity. Test S3.1 used the growth rate dependence on salinity, formulated for *Halodule*, in all three species, while test S3.2 used the growth rate dependence on salinity formulated for *Syringodium*. In test S3.3, it was assumed that salinity does not affect seagrass growth rate, hence the values for the salinity limiting factors were set to unity. Tests S4.1, and S4.2 were designed to assess the sensitivity of the model to the formulation of the species-specific growth rate dependence on light. Test S4.1 used the growth rate dependence on light, formulated for *Syringodium*, in all three species, while test S4.2 used the growth rate dependence on light formulated for *Halodule*. Tests S5.1, and S5.2 were designed to assess the sensitivity of the model to the

formulation of the species-specific growth rate dependence on sediment nutrient concentration. For test S5.1, it was assumed that the nitrogen uptake was proportional to 10% of the seagrass biomass, while test S4.2 assumed that the nitrogen uptake was proportional to 0.1% of the seagrass biomass. The results of the simulated biomass for tests S1.1 to S5.2 are presented in Appendix F.

The sensitivity analysis revealed the density-dependent maximum growth rate as the most important parameter in the seagrass model, determining not only the maximum seagrass biomass, but also the *Thalassia* dominance when the environmental conditions are within the optimum range for all three species. Previously reported from field studies (e.g., Lewis *et al.*, 1985), the seagrass distribution in this subtropical estuarine system is largely controlled by water temperature, and the growth rate dependence on temperature is also an important parameter of the model. Changing from the broadest to the narrowest range did not show as much effect as setting the temperature limiting factor to unity. In this latest case (test S2.3), the seagrass biomass was almost constant throughout the year, with minor fluctuations due to light and salinity variations. These two parameters, density-dependent growth rate and temperature limiting factor have their influence extended over the entire Bay, and they dictate the overall distribution and composition of the seagrass beds in Tampa Bay. In addition, salinity and available light were responsible for two distinct limiting conditions also found in the Bay. Along the bathymetric gradient, the deep edge of the seagrass bed is determined by the available light. From the mouth of the Bay to its upper reaches, salinity level (or its lower limit) dictates the seagrass distribution and composition, although seagrass species tolerant to low salinity levels (e.g., *Ruppia maritima*) were not simulated.

Simulation of the Summer 1991 Condition

The integrated model of the Tampa Bay Estuarine System was used to study the seagrass dynamics of the summer of 1991 conditions. The primary objective was to further the understanding of the relationships between circulation and transport, nutrient loading, biogeochemical transformations and the response of the of the seagrass community in Tampa Bay. A four-month simulation was performed using the results of the baseline simulation as initial condition for seagrass, and the initial conditions described in Chapter 6 and 7 for the hydrodynamics and water quality parameters.

Model results showed that during the four-month simulation the seagrass distribution did not vary significantly, with its biomass close to the maximum values obtained from the baseline simulation. Table 8.2 shows the simulated biomass along with some available literature data for the Tampa Bay region (Lewis *et al.*, 1985).

Table 8.2 - Simulated and reported seagrass biomass in the Tampa Bay area.

Location	Biomass (gdw/m ²)		Reference
	Above-ground	Below-ground	
<i>Thalassia testudinum</i>			
Simulated (summer 1991)	190 - 230	-	
Boca Ciega Bay	32.4	48.6	Pomeroy (1960)
Tampa Bay	0.41 - 52.7	-	Heffernan and Gibson (1982)
Tampa Bay	25 - 180	600 - 900	Lewis and Phillips (1980)

Table 8.2 - continued.

Location	Biomass (gdw/m ²)		Reference
	Above-ground	Below-ground	
<i>Halodule wrightii</i>			
Simulated (summer 1991)	60 - 80	-	
Tampa Bay	4 - 27	-	Heffernan and Gibson (1982)
Tampa Bay	38 - 50	60 - 140	Lewis and Phillips (1980)
<i>Syringodium filiforme</i>			
Simulated (summer 1991)	5 - 25	-	
Tampa Bay	5 - 11	-	Heffernan and Gibson (1982)
Tampa Bay	50 - 170	160 - 400	Lewis and Phillips (1980)

Model results seem to be in accordance with field investigations, determining *Thalassia* as the dominant species in Tampa Bay. Considering the summer months as the maximum biomass period, the spatial distribution of seagrass in Tampa Bay is dictated by two environmental parameters: available light and salinity. Described in the sensitivity tests, light attenuation determines the maximum depth seagrass can grow, and the species composition at low light levels. The head to mouth salinity gradient, highly accentuated during summer, is also responsible for the species zonation and maximum biomass, specially in the upper reaches of the Bay. Historically, human developments in the Tampa Bay Estuarine System have caused great impact and disturbance on these two environmental parameters. Changes in freshwater discharges, flushing rates, and anthropogenic nutrient enrichment have been directly related to the reduction of the seagrass meadows in the system.

Figures 8.9 to 8.11 show the contour plots for *Thalassia*, *Halodule*, and *Syringodium* biomass in July 26, after 60 days of simulation. Figure 8.12 shows the available light at the first sigma level, near the bottom. Model results seem to describe the general characteristics of the spatial and temporal seagrass composition and distribution in Tampa Bay. *Thalassia* exhibits its annual-maximum biomass throughout the seagrass beds (Figure 8.9), except along the deep edges, which allows *Syringodium* to achieve its maximum biomass (Figure 8.11). *Halodule* is also seen throughout the seagrass beds (Figure 8.10), mixed with *Thalassia* and *Syringodium*. A much finer grid resolution would be required to show that close to the shore, *Halodule* would be the prevailing species.

Since reducing nutrient loading is expected to have a greater impact on the light levels reaching the bottom of the Bay, comparisons with subsequent load reduction simulations were made in terms of improvement in available light at the seagrass beds.

Load Reduction Simulations

The results of the water quality simulations suggested that nutrient load reduction is expected to lower the concentration of dissolved inorganic nitrogen, and phytoplankton in the water column. These changes are expected to increase the available light for seagrass and hence, increase the maximum depth of seagrass bed.

Figure 8.13 shows the comparison between the Present Condition and the 100% Load Reduction simulations. The response of available light was not noticed in the first 60 days

Thalassia Biomass

After 60 Days (July 26, 1991)

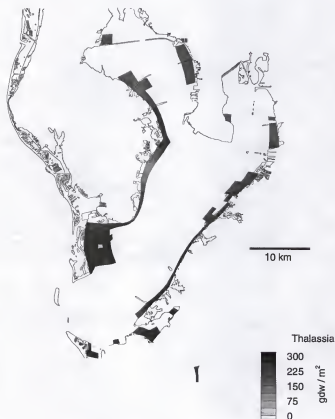


Figure 8.9 - Simulated *Thalassia* biomass in Tampa Bay for July 26, after 60 days of simulation.

Halodule Biomass

After 60 Days (July 26, 1991)

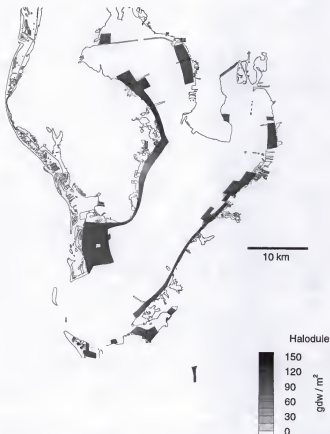


Figure 8.10 - Simulated *Halodule* biomass in Tampa Bay for July 26, after 60 days of simulation.

Syringodium Biomass

After 60 Days (July 26, 1991)

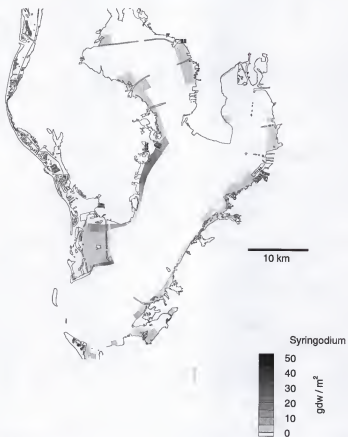


Figure 8.11 - Simulated *Syringodium* biomass in Tampa Bay for July 26, after 60 days of simulation.

Available Light
After 60 Days (July 26, 1991)

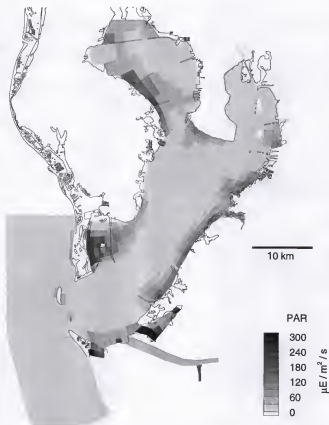


Figure 8.12 - Near-bottom light levels in Tampa Bay for July 26, after 60 days of simulation.

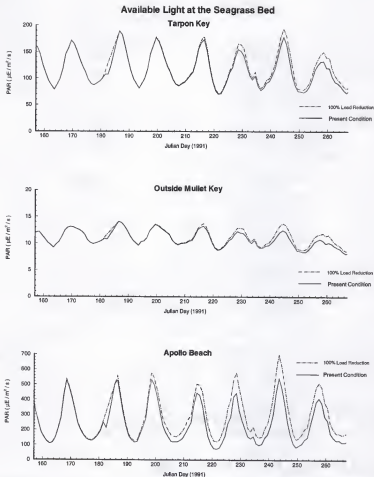


Figure 8.13 - Comparison between simulated light levels for the Present Condition simulation (solid line) and the 100% Load Reduction (dashed line).

of simulation, and the four-month simulation was not long enough to produce any improvement in the seagrass biomass. Figure 8.13 (bottom) shows that the upper reaches of the Bay are more sensitive to load reduction, due to its proximity to the freshwater discharges. However, as discussed in the sensitivity analysis, light limitation is more likely to influence the deep edge of the seagrass bed, determining the depth at which seagrass can grow.

Summing up, the sensitivity analysis revealed the seagrass model inputs and parameters that are most sensitive to variations. These include: density-dependent growth rate, growth rate dependence on temperature, light, salinity, and a detailed mapping of species distribution. Field and mesocosms experiments designed to determine these model inputs for Tampa Bay would provide this integrated model with the realism required for predictive simulations. Existing monitoring programs (e.g., EPC monthly monitoring) could be redesigned to include stations in areas covered by seagrass, where ongoing management agencies (e.g., Department of Environmental Protection) or university (e.g., University of South Florida) projects could measure seagrass parameters (e.g., biomass, productivity, leaf length and color, species diversity, etc). In the long term, this coordinated programs would not only enhance our understanding of the ecological relationships between environmental conditions and the seagrass community, but would also provide important inputs for a model that can be used to evaluate management alternatives for seagrass restoration.

CHAPTER 9

CONCLUSION AND RECOMMENDATIONS

An integrated model, combining the enhanced versions of a 3-D hydrodynamics model (Sheng, 1989), a 3-D water quality model (Chen and Sheng, 1994), and a seagrass model (Fong and Harwell, 1994), has been developed for the Tampa Bay Estuarine System. Major conclusions of the study are summarized in the following:

- 1) A fine-resolution and smooth numerical grid which accurately represents the complex geometrical and bathymetrical features in Tampa Bay was generated. Circulation patterns produced by the hydrodynamic model revealed flow features which agree well with existing information on Tampa Bay circulation, available from past modeling and field studies. Flow and salinity features, which were not reported previously, were identified. The normalized rms error analysis demonstrated the model's ability to simulate surface elevation, currents, and salinity within 7.5%, 20%, and 25% accuracy, respectively.

The residual advective fluxes and salinity distributions present a distinctive annual variability. Wet season results indicate much stronger horizontal and vertical salinity gradients than the dry season results. Rainfall has a significant effect on the salinity distribution, but not on the velocity field.

A two-layer flow structure was found in the residual flows for all the hydrodynamics simulations. This suggests the importance of considering vertical structure in any modeling study of hydrodynamics and water quality dynamics of the Bay.

2) Because it incorporated increased understanding of the complex relationships among hydrodynamics, sediment dynamics, nutrients, phytoplankton, light, and seagrass, the integrated modeling allowed a direct coupling between all the components. The same time step and spatial grid were used, and the effects of hydrodynamics were incorporated into the water quality model without any ad-hoc tuning of advective fluxes and dispersion coefficients.

Simple water quality models such as regression model and WASP5 model are important first steps towards the development of a comprehensive "broad-based" model of the entire Tampa Bay Estuarine System. They can be used in preliminary steps to help the determination of relevant processes, and test causal relationships between state variables. They are a powerful tool for calibration of water quality model coefficients in the absence of process-specific data (e.g., nitrification, denitrification, etc). However, in marine environments, where tide, wind and baroclinic forcing interact in an unsteady balance, their predictive capability is limited.

The summer of 1991 simulation demonstrated the central role that organic nitrogen and mineralization of organic matter have on the water quality dynamics of the Tampa Bay Estuarine System. Simulation results showed that high levels of water column soluble organic nitrogen and phytoplankton inside the Bay produce a net export of these water quality parameters to the Gulf of Mexico. On the other hand, the nitrogen limiting condition of the Bay cause a depletion of dissolved inorganic nitrogen species, and the net transport generated is from the Gulf of Mexico into the Bay. Model results also showed that during the summer of 1991, particulate organic and inorganic nitrogen have a net depositional flux. Since both organic and inorganic dissolved species exhibited higher concentrations in the

sediment layer than in the water column, the net diffusive flux was from the sediment into the water column.

Hillsborough Bay has the poorest water quality in the Bay. Although the EPC water quality index has consistently increased since 1987 (Boler, 1992), eutrophic conditions and hypoxia events still occur in the upper reaches of the Bay. Model results demonstrated that external loading, nutrient-enriched sediments, and limited flushing capacity are the primary causes of these characteristics.

Load reduction simulations demonstrated that loading has a direct effect on nutrient concentration, phytoplankton production, and light attenuation. Model results showed that water quality can respond quickly (within 2 months) to changes in load reduction. This time scale is in agreement with Coastal's (1995) estimation of 3-month response time, but much less than Johansson's (1991) estimate of 3-year response time.

3) The seagrass model has been used to investigate the ecological relationships between nutrient loading, water quality dynamics, and the response of seagrass. Model results showed that the seagrass distribution in Tampa Bay is largely controlled by seasonal water temperature. Simulated growth rate is completely inhibited for all three species during the coldest period of the year (mid-December to mid-February).

The second most important environmental parameters in the seagrass model are light attenuation and salinity. Light attenuation determines the maximum depth seagrass can grow, and the species composition at low light levels. The head to mouth salinity gradient, highly accentuated during summer, is also responsible for the species zonation and maximum biomass, specially in the upper reaches of the Bay.

Considering that light attenuation and salinity distribution have been highly altered due to anthropogenic effects, restoration of seagrass beds can be linked to changes in freshwater-discharge regime, flushing rates in each specific segment of the Bay, total suspended solids concentration, and external nutrient loading.

The model presented in this study is still far from being a comprehensive model that would explain all the processes occurring in the Tampa Bay Estuarine System and be used as a predictive tool. Nevertheless, it is a model that integrates the major components (hydrodynamics, sediment dynamics, water quality, and seagrass) that drive the system, and it establishes a framework for future developments to answer specific management questions.

The dynamic response of the estuarine system to different load reduction levels cannot be directly observed in the Bay, and can only be predicted by a reliable model. Using the process-based and integrated modeling approach described in this study, it is possible to synthesize field and laboratory data collected from various parts of the Bay. Model simulation could then be performed to predict the Bay's response to various management practices. Once fully validated, this integrated model can be used to address such ecosystem management issues as controlling estuarine eutrophication and determining allowable external nutrient loading levels to restore seagrass in the Bay.

Future developments that are necessary to allow this integrated model to perform predictive simulations are described in the following:

- Basic research is needed to reduce the range of the water quality model coefficients to specific conditions of Tampa Bay, especially the parameters related to the sediment layer, the water-sediment interface, and the oceanic boundary condition.

- With the grid resolution used in this study, the model cannot solve for the dynamics of the shallow regions of the Bay (below 1m deep), where wave interactions become an important issue. More field data and modeling effort should be focused on the shallow regions.

- During episodic events, resuspension of sediments can release as much as three orders of magnitude more nutrients than diffusive fluxes (Sheng *et al.*, 1993). In this case, sediment model parameters (e.g., erosion and deposition rates) should be determined throughout the Bay. Again, field and modeling experiments are needed to further quantify the resuspension and deposition fluxes.

- The seagrass model can be improved by field and mesocosms experiments designed to determine the relationships between environmental parameters and seagrass for Tampa Bay.

- Long-term (1-5 years) field data need to be collected to allow long-term calibration and validation of the integrated model. This exercise will also allow us to quantitatively compare the performance of the integrated model vs. simpler models in making long-term predictions.

Data collection programs in Florida estuarine systems in the past have generally focused only on a limited number of parameters. In view of the complex relationships among the various components of the ecosystem and the site-specific nature of the estuarine environment, it is prudent to design monitoring programs which will collect all essential parameters at the same locations over long periods to augment the typical monthly or quarterly synoptic surveys. It is also recommended that such monitoring programs be designed with participation of modelers, to ensure that the data could be directly used for trend analysis and model development.

APPENDIX A NUMERICAL SOLUTION OF THE INTEGRATED MODEL

Governing Equations in the σ -grid Coordinate System

The transformation from the Cartesian grid (x, y, z, t) to the vertically-stretched grid (x', y', σ, t') was defined in Chapter 3 as

$$\begin{aligned}x' &= x \\y' &= y \\ \sigma(x, y, z, t) &= \frac{z - \zeta(x, y, t)}{h(x, y) + \zeta(x, y, t)} \\t' &= t\end{aligned}\tag{A.1}$$

where h is the water depth relative to the mean sea level, and ζ is the free surface elevation. σ is the transformed vertical coordinate such that $\sigma = 0$ at the free surface and $\sigma = -1$ at the bottom.

Using the chain rule, the first-order differential operators in the (x, y, z, t) are related to those in the (x', y', σ, t') coordinate system through:

$$\begin{aligned}
\frac{\partial}{\partial t} &= \frac{\partial t'}{\partial t} \cdot \frac{\partial}{\partial t} + \frac{\partial \sigma}{\partial t} \cdot \frac{\partial}{\partial \sigma} \\
\frac{\partial}{\partial z} &= \frac{\partial \sigma}{\partial z} \cdot \frac{\partial}{\partial \sigma} = \frac{1}{H} \cdot \frac{\partial}{\partial \sigma} \\
\frac{\partial}{\partial x} &= \frac{\partial x'}{\partial x} \cdot \frac{\partial}{\partial x'} + \frac{\partial y'}{\partial x} \cdot \frac{\partial}{\partial y'} + \frac{\partial \sigma}{\partial x} \cdot \frac{\partial}{\partial \sigma} \\
\frac{\partial \sigma}{\partial x} &= \frac{\partial}{\partial x} \left(\frac{z - \zeta}{H} \right) = -\frac{z}{H^2} \cdot \frac{\partial H}{\partial x} - \frac{1}{H} \cdot \frac{\partial \zeta}{\partial x} + \frac{\zeta}{H^2} \cdot \frac{\partial H}{\partial x} \\
&= -\frac{z - \zeta}{H^2} \cdot \frac{\partial H}{\partial x} - \frac{1}{H} \cdot \frac{\partial \zeta}{\partial x} = -\frac{\sigma}{H} \cdot \frac{\partial H}{\partial x} - \frac{1}{H} \cdot \frac{\partial \zeta}{\partial x} \\
\frac{\partial}{\partial x} &= \frac{\partial}{\partial x'} - \frac{1}{H} \cdot \frac{\partial \zeta}{\partial x} \cdot \frac{\partial}{\partial \sigma} - \frac{\sigma}{H} \cdot \frac{\partial H}{\partial x} \cdot \frac{\partial}{\partial \sigma}
\end{aligned} \tag{A.2}$$

Similarly,

$$\frac{\partial}{\partial y} = \frac{\partial}{\partial y'} - \frac{1}{H} \cdot \frac{\partial \zeta}{\partial y} \cdot \frac{\partial}{\partial \sigma} - \frac{\sigma}{H} \cdot \frac{\partial H}{\partial y} \cdot \frac{\partial}{\partial \sigma}$$

In the σ -grid, the hydrostatic relation is transformed to:

$$\partial p = -\rho g \partial z = -\rho g \partial \sigma \tag{A.3}$$

which, integrated from some depth σ to the surface ($\sigma = 0$) gives,

$$p(\sigma) = p_a - g \int_{\sigma}^0 \rho H d\sigma \tag{A.4}$$

where p_a is the atmospheric pressure.

The x-derivative in the transformed coordinate system is given by:

$$\frac{\partial p}{\partial x} = \frac{\partial p_a}{\partial x'} - g \int_{\sigma}^0 H \frac{\partial \rho}{\partial x'} d\sigma + g \frac{\partial H}{\partial x'} \sigma \rho + g \frac{\partial \zeta}{\partial x'} \tag{A.5}$$

Using the flux conservative for the non-linear advective terms, and neglecting the atmospheric pressure gradient term, the Equations (3.1), (3.2), (3.3), and (3.5) can be re-written, dropping the primes.

Continuity Equation

$$\frac{\partial \zeta}{\partial t} + \frac{\partial Hu}{\partial x} + \frac{\partial Hv}{\partial y} + H \frac{\partial \omega}{\partial \sigma} = 0 \quad (\text{A.6})$$

X-Component of Momentum Equation

$$\begin{aligned} \frac{1}{H} \left(\frac{\partial Hu}{\partial t} + \frac{\partial Huu}{\partial x} + \frac{\partial Huv}{\partial y} \right) + \frac{\partial u \omega}{\partial \sigma} = f v - g \frac{\partial \zeta}{\partial x} \\ + \frac{g}{\rho_o} \left[H \int_{\sigma}^0 \frac{\partial \rho}{\partial x} d\sigma + \frac{\partial H}{\partial x} \left(\int_{\sigma}^0 \rho d\sigma + \sigma \rho \right) \right] \\ + \frac{\partial}{\partial x} \left(A_H \frac{\partial u}{\partial x} \right) + \frac{\partial}{\partial y} \left(A_H \frac{\partial u}{\partial y} \right) \\ + \frac{1}{H^2} \frac{\partial}{\partial \sigma} \left(A_v \frac{\partial u}{\partial \sigma} \right) + (H.O.T)_x \end{aligned} \quad (\text{A.7})$$

Y-Component of Momentum Equation

$$\begin{aligned} \frac{1}{H} \left(\frac{\partial Hv}{\partial t} + \frac{\partial Hv}{\partial x} + \frac{\partial Hv v}{\partial y} \right) + \frac{\partial v \omega}{\partial \sigma} = -f u - g \frac{\partial \zeta}{\partial y} \\ + \frac{g}{\rho_o} \left[H \int_{\sigma}^0 \frac{\partial \rho}{\partial y} d\sigma + \frac{\partial H}{\partial y} \left(\int_{\sigma}^0 \rho d\sigma + \sigma \rho \right) \right] \\ + \frac{\partial}{\partial x} \left(A_H \frac{\partial v}{\partial x} \right) + \frac{\partial}{\partial y} \left(A_H \frac{\partial v}{\partial y} \right) \\ + \frac{1}{H^2} \frac{\partial}{\partial \sigma} \left(A_v \frac{\partial v}{\partial \sigma} \right) + (H.O.T)_y \end{aligned} \quad (\text{A.8})$$

where the vertical velocity, ω , is given by:

$$\omega = \frac{d\sigma}{dt} = \frac{w}{H} - \frac{1}{H}(1 + \sigma) \frac{\partial \zeta}{\partial t} - \gamma_x u - \gamma_y v \quad (\text{A.9})$$

The transformation of the diffusion terms produces some higher order terms which are considered to be negligible when compared to the first order terms, and therefore ignored in the computational solution. The higher order terms $(H.O.T.)_x$, and $(H.O.T.)_y$ are:

$$\begin{aligned} (H.O.T.)_x = & -\frac{1}{H} \left(\frac{\partial \zeta}{\partial x} + \sigma \frac{\partial H}{\partial x} \right) \left[\frac{\partial}{\partial \sigma} \left(A_H \frac{\partial u}{\partial x} \right) + \frac{\partial}{\partial x} \left(A_H \frac{\partial u}{\partial x} \right) \right] \\ & - A_H \frac{\partial u}{\partial \sigma} \left[\frac{1}{H} \left(\frac{\partial^2 \zeta}{\partial x^2} + \sigma \frac{\partial^2 H}{\partial x^2} \right) - \frac{1}{H^2} \left(\frac{\partial \zeta}{\partial x} + \sigma \frac{\partial H}{\partial x} \right) \frac{\partial H}{\partial x} \right] \\ & + \frac{1}{H^2} \left(\frac{\partial \zeta}{\partial x} + \sigma \frac{\partial H}{\partial x} \right)^2 \frac{\partial}{\partial \sigma} \left(A_H \frac{\partial u}{\partial \sigma} \right) \end{aligned} \quad (\text{A.10})$$

$$\begin{aligned} (H.O.T.)_y = & -\frac{1}{H} \left(\frac{\partial \zeta}{\partial y} + \sigma \frac{\partial H}{\partial y} \right) \left[\frac{\partial}{\partial \sigma} \left(A_H \frac{\partial v}{\partial y} \right) + \frac{\partial}{\partial y} \left(A_H \frac{\partial v}{\partial y} \right) \right] \\ & - A_H \frac{\partial v}{\partial \sigma} \left[\frac{1}{H} \left(\frac{\partial^2 \zeta}{\partial y^2} + \sigma \frac{\partial^2 H}{\partial y^2} \right) - \frac{1}{H^2} \left(\frac{\partial \zeta}{\partial y} + \sigma \frac{\partial H}{\partial y} \right) \frac{\partial H}{\partial y} \right] \\ & + \frac{1}{H^2} \left(\frac{\partial \zeta}{\partial y} + \sigma \frac{\partial H}{\partial y} \right)^2 \frac{\partial}{\partial \sigma} \left(A_H \frac{\partial v}{\partial \sigma} \right) \end{aligned} \quad (\text{A.11})$$

The Transport Equation

The transformation of the transport equation in the (x', y', σ, t') system can be shown in terms of the salinity equation:

$$\begin{aligned}
& \frac{\partial S}{\partial t'} - \frac{(\sigma + 1)}{H} \frac{\partial \zeta}{\partial t} \frac{\partial S}{\partial \sigma} + \frac{\partial(uS)}{\partial x'} - \frac{1}{H} \frac{\partial \zeta}{\partial x} \frac{\partial(uS)}{\partial \sigma} - \frac{\sigma}{H} \frac{\partial H}{\partial x} \frac{\partial(uS)}{\partial \sigma} \\
& + \frac{\partial(vS)}{\partial y'} - \frac{1}{H} \frac{\partial \zeta}{\partial y} \frac{\partial(vS)}{\partial \sigma} - \frac{\sigma}{H} \frac{\partial H}{\partial y} \frac{\partial(vS)}{\partial \sigma} \\
& + \frac{1}{H} \frac{\partial}{\partial \sigma} \left[H \omega S + \sigma \left(u S \frac{\partial h}{\partial x} + v S \frac{\partial h}{\partial y} + S \frac{\partial \zeta}{\partial t} + u S \frac{\partial \zeta}{\partial x} + v S \frac{\partial \zeta}{\partial y} \right) \right. \\
& \left. + S \frac{\partial \zeta}{\partial t} + u S \frac{\partial \zeta}{\partial x} + v S \frac{\partial \zeta}{\partial y} \right] = \text{Diffusion Terms}
\end{aligned} \tag{A.12}$$

Re-arranging and canceling the proper terms,

$$\frac{\partial S}{\partial t'} + \frac{\partial(uS)}{\partial x'} + \frac{\partial(vS)}{\partial y'} + \frac{1}{H} \frac{\partial(H \omega S)}{\partial \sigma} = \text{Diffusion Terms} \tag{A.13}$$

Using the continuity equation times $S \rightarrow S \frac{\partial H}{\partial t'} + S \frac{\partial H u}{\partial x'} + S \frac{\partial H v}{\partial y'} + S \frac{\partial H \omega}{\partial \sigma}$,

the salinity equation can be written in a conservative form as:

$$\frac{1}{H} \left[\frac{\partial H S}{\partial t'} + \frac{\partial H u S}{\partial x'} + \frac{\partial H v S}{\partial y'} + \frac{\partial H \omega S}{\partial \sigma} \right] = \text{Diffusion Terms} \tag{A.14}$$

The diffusion terms are obtained through the second-order derivatives, expressed as:

$$\begin{aligned}
 & \left[\frac{\partial}{\partial x'} - \frac{1}{H} \frac{\partial \zeta}{\partial x} \frac{\partial}{\partial \sigma} - \frac{\sigma}{H} \frac{\partial H}{\partial x} \frac{\partial}{\partial \sigma} \right] \cdot \left[D_H \left(\frac{\partial S}{\partial x'} - \frac{1}{H} \frac{\partial \zeta}{\partial x} \frac{\partial S}{\partial \sigma} - \frac{\sigma}{H} \frac{\partial H}{\partial x} \frac{\partial S}{\partial \sigma} \right) \right] = \quad (\text{A.15}) \\
 & \frac{\partial}{\partial x'} \left(D_H \frac{\partial S}{\partial x'} \right) - \frac{\partial}{\partial x'} \left(\frac{D_H}{H} \frac{\partial \zeta}{\partial x} \frac{\partial S}{\partial \sigma} \right) - \frac{\partial}{\partial x'} \left(\frac{D_H \sigma}{H} \frac{\partial H}{\partial x} \frac{\partial S}{\partial \sigma} \right) \\
 & - \frac{1}{H} \frac{\partial \zeta}{\partial x} \frac{\partial}{\partial \sigma} \left(D_H \frac{\partial S}{\partial x'} \right) + \frac{1}{H} \frac{\partial \zeta}{\partial x} \frac{\partial}{\partial \sigma} \left(\frac{D_H}{H} \frac{\partial \zeta}{\partial x} \frac{\partial S}{\partial \sigma} \right) + \frac{1}{H} \frac{\partial \zeta}{\partial x} \frac{\partial}{\partial \sigma} \left(\frac{D_H \sigma}{H} \frac{\partial H}{\partial x} \frac{\partial S}{\partial \sigma} \right) \\
 & - \frac{\sigma}{H} \frac{\partial H}{\partial x} \frac{\partial}{\partial \sigma} \left(D_H \frac{\partial S}{\partial x'} \right) + \frac{\sigma}{H} \frac{\partial H}{\partial x} \frac{\partial}{\partial \sigma} \left(\frac{D_H}{H} \frac{\partial \zeta}{\partial x} \frac{\partial S}{\partial \sigma} \right) + \frac{\sigma}{H} \frac{\partial H}{\partial x} \frac{\partial}{\partial \sigma} \left(\frac{D_H \sigma}{H} \frac{\partial H}{\partial x} \frac{\partial S}{\partial \sigma} \right)
 \end{aligned}$$

for the horizontal diffusion, x -direction (with similar development for the y -direction). The vertical diffusion term is given by:

$$\frac{1}{H} \frac{\partial}{\partial \sigma} \left(D_v \frac{1}{H} \frac{\partial S}{\partial \sigma} \right) = \frac{1}{H^2} \frac{\partial}{\partial \sigma} \left(D_v \frac{\partial S}{\partial \sigma} \right) \quad (\text{A.16})$$

The salinity equation in the sigma grid system can be written as (dropping the primes):

$$\begin{aligned}
 & \frac{1}{H} \left[\frac{\partial HS}{\partial t} + \frac{\partial HuS}{\partial x} + \frac{\partial HvS}{\partial y} + \frac{\partial H\omega S}{\partial \sigma} \right] = \frac{1}{H} \left[\frac{\partial}{\partial x} \left(D_H \frac{\partial HS}{\partial x} \right) \right. \\
 & \quad \left. + \frac{\partial}{\partial y} \left(D_H \frac{\partial HS}{\partial y} \right) \right] + \frac{1}{H^2} \frac{\partial}{\partial \sigma} \left(D_v \frac{\partial S}{\partial \sigma} \right) + (H.O.T)_s \quad (\text{A.17})
 \end{aligned}$$

where $(H.O.T)_s$ is given by:

$$\begin{aligned}
(H.O.T)_s = & \frac{1}{H} \left[+ \frac{\partial}{\partial x} \left(\frac{D_H}{H} \frac{\partial \zeta}{\partial x} \frac{\partial HS}{\partial \sigma} \right) - \frac{\partial}{\partial x} \left(\frac{D_H \sigma}{H} \frac{\partial H}{\partial x} \frac{\partial HS}{\partial \sigma} \right) \right. \\
& - \frac{1}{H} \frac{\partial \zeta}{\partial x} \frac{\partial}{\partial \sigma} \left(D_H \frac{\partial HS}{\partial x} \right) \\
& + \frac{1}{H} \frac{\partial \zeta}{\partial x} \frac{\partial}{\partial \sigma} \left(\frac{D_H}{H} \frac{\partial \zeta}{\partial x} \frac{\partial HS}{\partial \sigma} \right) + \frac{1}{H} \frac{\partial \zeta}{\partial x} \frac{\partial}{\partial \sigma} \left(\frac{\sigma}{H} \frac{\partial H}{\partial x} \frac{\partial HS}{\partial \sigma} \right) \\
& - \frac{\sigma}{H} \frac{\partial H}{\partial x} \frac{\partial}{\partial \sigma} \left(D_H \frac{\partial HS}{\partial x} \right) + \frac{\sigma}{H} \frac{\partial H}{\partial x} \frac{\partial}{\partial \sigma} \left(\frac{D_H}{H} \frac{\partial \zeta}{\partial x} \frac{\partial HS}{\partial \sigma} \right) \\
& + \frac{\sigma}{H} \frac{\partial H}{\partial x} \frac{\partial}{\partial \sigma} \left(\frac{\sigma}{H} \frac{\partial H}{\partial x} \frac{\partial HS}{\partial \sigma} \right) \quad (A.18) \\
& + \frac{\partial}{\partial y} \left(\frac{D_H}{H} \frac{\partial \zeta}{\partial y} \frac{\partial HS}{\partial \sigma} \right) - \frac{\partial}{\partial y} \left(\frac{D_H \sigma}{H} \frac{\partial H}{\partial y} \frac{\partial HS}{\partial \sigma} \right) \\
& - \frac{1}{H} \frac{\partial \zeta}{\partial y} \frac{\partial}{\partial \sigma} \left(D_H \frac{\partial HS}{\partial y} \right) + \frac{1}{H} \frac{\partial \zeta}{\partial y} \frac{\partial}{\partial \sigma} \left(\frac{D_H}{H} \frac{\partial \zeta}{\partial y} \frac{\partial HS}{\partial \sigma} \right) \\
& + \frac{1}{H} \frac{\partial \zeta}{\partial y} \frac{\partial}{\partial \sigma} \left(\frac{\sigma}{H} \frac{\partial H}{\partial y} \frac{\partial HS}{\partial \sigma} \right) - \frac{\sigma}{H} \frac{\partial H}{\partial y} \frac{\partial}{\partial \sigma} \left(D_H \frac{\partial HS}{\partial y} \right) \\
& + \frac{\sigma}{H} \frac{\partial H}{\partial y} \frac{\partial}{\partial \sigma} \left(\frac{D_H}{H} \frac{\partial \zeta}{\partial y} \frac{\partial HS}{\partial \sigma} \right) + \frac{\sigma}{H} \frac{\partial H}{\partial y} \frac{\partial}{\partial \sigma} \left(\frac{\sigma}{H} \frac{\partial H}{\partial y} \frac{\partial HS}{\partial \sigma} \right) \left. \right]
\end{aligned}$$

Time Scales and Dimensionless Equations

In order to reveal the relative importance of each term in the governing equations, Sheng (1983) examined the characteristic time scales associated with various physical processes in lakes and estuaries (Table A.1), and presented the above system of equations in a dimensionless form.

Table A.1 - Characteristic time scales of physical processes in estuaries (Sheng, 1983).

Physical Process	Time Scale	Order of Magnitude
Periodic Function	t_f	$1 / \omega$
Advection	t_c	X_r / U_r
Inertia Oscillation	t_i	$1 / f$
Vertical Turbulent Diffusion	t_{vdm}, t_{vds}	$Z_r^2 / A_{vr}, Z_r^2 / D_{vr}$
Horizontal Turbulent Diffusion	t_{hdm}, t_{hds}	$X_r^2 / A_{hr}, X_r^2 / D_{hr}$
Gravity Wave	t_{ge}	$X_r / \sqrt{g Z_r}$
Internal Gravity Wave	t_{gi}	$X_r / \sqrt{g Z_r \Delta \rho / \rho_0}$

First, the following reference scales are introduced: X_r and Z_r as the reference lengths in the vertical and horizontal directions, U_r as the reference velocity, ρ_r and $\Delta \rho$ as the reference density and density gradient in a stratified flow, $(A_H)_r$, $(A_v)_r$, $(D_H)_r$, and $(D_v)_r$ as the reference eddy coefficients. Therefore, each term in the dimensionless equations is composed of two parts: the dimensionless variable of the order unity, and the part containing the dimensionless number, indicating the order of magnitude of the term.

Dimensionless Variables

$$\begin{aligned}
 (x^*, y^*, z^*) &= (u, v, w X_r / Z_r) / U_r \\
 (u^*, v^*, w^*) &= (x, y, z X_r / Z_r) / X_r \\
 \omega^* &= \omega X_r / U_r \\
 t^* &= t f
 \end{aligned}
 \tag{A.19}$$

$$\begin{aligned}
(\tau_x^*, \tau_y^*) &= (\tau_x^w, \tau_y^w) / (\rho_o f Z_r U_r) = (\tau_x^w, \tau_y^w) / \tau_r \\
\zeta^* &= g \zeta / (f U_r X_r) = \zeta / S_r \\
\rho^* &= (\rho - \rho_o) / (\rho_r - \rho_o) \\
A_H^* &= A_H / A_{Hr} \\
A_v^* &= A_v / A_{vr} \\
D_H^* &= D_H / D_{Hr} \\
D_v^* &= D_v / D_{vr}
\end{aligned} \tag{A.20}$$

Dimensionless Parameters

$$\begin{aligned}
\text{Rossby Number:} \quad R_o &= \frac{U_r}{(f X_r)} = t_i / t_c \\
\text{Froude Number:} \quad F_r &= \frac{U_r}{\sqrt{g Z_r}} = t_i / t_c \\
\text{Densimetric Froude Number:} \quad F_{rD} &= \frac{F_r}{\sqrt{\epsilon}} = t_{ri} / t_c \\
\text{Vertical Ekman Number:} \quad E_v &= \frac{A_{vr}}{(f Z_r^2)} = t_i / t_{vdm} \\
\text{Horizontal Ekman Number:} \quad E_H &= \frac{A_{Hr}}{(f X_r^2)} = t_i / t_{hdm} \\
\text{Vertical Schmidt Number:} \quad S_{cv} &= \frac{A_{vr}}{D_{vr}} = t_{vdr} / t_{vdm} \\
\text{Horizontal Schmidt Number:} \quad S_{cH} &= \frac{A_{Hr}}{D_{Hr}} = t_{hdr} / t_{hdm} \\
\epsilon &= \frac{(\rho_r - \rho_o)}{\rho_o} \\
\beta &= \frac{g Z_r}{f^2 X_r^2} = (R_o / F_r)^2 = (t_i / t_{ge})^2
\end{aligned}$$

Dimensionless Equations

Utilizing the dimensionless variables and parameters defined above, the governing equations become:

$$\frac{\partial \zeta}{\partial t} + \beta \frac{\partial Hu}{\partial x} + \beta \frac{\partial Hv}{\partial y} + \beta H \frac{\partial \omega}{\partial \sigma} = 0 \quad (\text{A.22})$$

$$\begin{aligned} \frac{1}{H} \frac{\partial Hu}{\partial t} = & -\frac{\partial \zeta}{\partial x} + \frac{E_v}{H^2} \frac{\partial}{\partial \sigma} \left(A_v \frac{\partial u}{\partial \sigma} \right) + v \\ & - \frac{R_o}{H} \left(\frac{\partial Huu}{\partial x} + \frac{\partial Hv u}{\partial y} + \frac{\partial H \omega u}{\partial \sigma} \right) \\ & - E_H \left[\frac{\partial}{\partial x} \left(A_H \frac{\partial u}{\partial x} \right) + \frac{\partial}{\partial y} \left(A_H \frac{\partial}{\partial y} \right) \right] \\ & - \frac{R_o}{F_{\sigma D}^2} \left[H \int_{\sigma}^0 \frac{\partial \rho}{\partial x} d\sigma + \frac{\partial H}{\partial x} \left(\int_{\sigma}^0 \rho d\sigma + \sigma \rho \right) \right] \end{aligned} \quad (\text{A.23})$$

$$\begin{aligned} \frac{1}{H} \frac{\partial Hv}{\partial t} = & -\frac{\partial \zeta}{\partial y} + \frac{E_v}{H^2} \frac{\partial}{\partial \sigma} \left(A_v \frac{\partial v}{\partial \sigma} \right) - u \\ & - \frac{R_o}{H} \left(\frac{\partial Huv}{\partial x} + \frac{\partial Hv v}{\partial y} + \frac{\partial H \omega v}{\partial \sigma} \right) \\ & + E_H \left[\frac{\partial}{\partial x} \left(A_H \frac{\partial v}{\partial x} \right) + \frac{\partial}{\partial y} \left(A_H \frac{\partial}{\partial y} \right) \right] \\ & - \frac{R_o}{F_{\sigma D}^2} \left[H \int_{\sigma}^0 \frac{\partial \rho}{\partial y} d\sigma + \frac{\partial H}{\partial y} \left(\int_{\sigma}^0 \rho d\sigma + \sigma \rho \right) \right] \end{aligned} \quad (\text{A.24})$$

$$\begin{aligned} \frac{1}{H} \frac{\partial HS}{\partial t} + \frac{R_o}{H} \left(\frac{\partial HuS}{\partial x} + \frac{\partial HvS}{\partial y} + \frac{\partial H\omega S}{\partial \sigma} \right) &= \frac{E_v}{Sc_v H^2} \frac{\partial}{\partial \sigma} \left(D_v \frac{\partial S}{\partial \sigma} \right) \\ &+ \frac{E_H}{Sc_H} \left[\frac{\partial}{\partial x} \left(D_H \frac{\partial v}{\partial x} \right) + \frac{\partial}{\partial y} \left(D_H \frac{\partial u}{\partial y} \right) \right] \end{aligned} \quad (\text{A.25})$$

$$\rho = \rho(T, S) \quad (\text{A.26})$$

Dimensionless Equations in Boundary-Fitted Coordinates

For most estuarine systems, not only the bathymetry but the geometry is also quite complex and irregular. In order to accurately represent the hydrodynamic and water quality processes, a curvilinear non-orthogonal boundary-fitted grid that conforms to complex shorelines is necessary.

In CH3D, the independent variables (x, y) are transformed into a dimensionless system (ξ, η) , and the velocities are expressed in terms of contravariant fluxes derived from tensor analysis (Sheng, 1986). The contravariant and physical velocity components are locally orthogonal to the grid line, whereas the covariant components generally are not. The three components are identical in a Cartesian coordinate system. In a curvilinear non-orthogonal boundary-fitted grid system, the relationship between the physical velocity and the contravariant velocity is given by (Sheng, 1986):

$$u^i = \frac{u(i)}{\sqrt{g_{ii}}} \quad (\text{A.27})$$

with no summation on i .

The metric relationships required to transform the contravariant velocity components

to the same dimension of the physical velocity are defined as:

$$\begin{aligned}
 \sqrt{g_{\xi\xi}} &= \sqrt{\left(\frac{\partial x}{\partial \xi}\right)^2 + \left(\frac{\partial y}{\partial \xi}\right)^2} \\
 \sqrt{g_{\eta\eta}} &= \sqrt{\left(\frac{\partial x}{\partial \eta}\right)^2 + \left(\frac{\partial y}{\partial \eta}\right)^2}
 \end{aligned}
 \left. \vphantom{\begin{aligned} \sqrt{g_{\xi\xi}} \\ \sqrt{g_{\eta\eta}} \end{aligned}} \right\} \text{Horizontal measures of lengths}$$

$$g_{\xi\eta} = g_{\eta\xi} = \frac{\partial x}{\partial \xi} \frac{\partial x}{\partial \eta} + \frac{\partial y}{\partial \xi} \frac{\partial y}{\partial \eta} \quad (\text{A.28})$$

$$\sqrt{g_o} = \sqrt{\left(\frac{\partial x}{\partial \xi} \frac{\partial y}{\partial \eta} - \frac{\partial x}{\partial \eta} \frac{\partial y}{\partial \xi}\right)^2} \left. \vphantom{\sqrt{g_o}} \right\} \text{Jacobian of horizontal transformation}$$

The Jacobian of horizontal transformation is used to obtain the surface area within a grid cell, and to scale the contravariant velocity to a physical flow (per unit depth) according to (Sheng, 1986):

$$\begin{aligned}
 \text{Area} &= \sqrt{g_o} \cdot d\xi \cdot d\eta \\
 Q_\xi &= \sqrt{g_{\xi\xi}} u^\xi \\
 Q_\eta &= \sqrt{g_{\eta\eta}} v^\eta
 \end{aligned} \quad (\text{A.29})$$

In the boundary-fitted curvilinear grid system shown in Figure 6.1, the three-dimensional equations of motion written in terms of contravariant velocity components in the transformed coordinates (ξ, η, σ) are (Sheng, 1987, 1989):

$$\frac{\partial \zeta}{\partial t} + \frac{\beta}{\sqrt{g_o}} \left[\frac{\partial}{\partial \xi} (\sqrt{g_o} H u) + \frac{\partial}{\partial \eta} (\sqrt{g_o} H v) \right] + \beta \frac{\partial H \omega}{\partial \sigma} = 0 \quad (\text{A.30})$$

$$\begin{aligned}
\frac{1}{H} \frac{\partial Hu}{\partial t} = & - \left(g^{11} \frac{\partial \zeta}{\partial \xi} + g^{12} \frac{\partial \zeta}{\partial \eta} \right) + \frac{g^{12}}{\sqrt{g_o}} u + \frac{g^{22}}{\sqrt{g_o}} v \\
& + \frac{R_o}{g_o H} \left\{ x_\eta \left[\frac{\partial}{\partial \xi} (y_\xi \sqrt{g_o} Huu + y_\eta \sqrt{g_o} Huv) \right. \right. \\
& \left. \left. + \frac{\partial}{\partial \eta} (y_\xi \sqrt{g_o} Huv + y_\eta \sqrt{g_o} Hvv) \right] \right. \\
& \left. - y_\eta \left[\frac{\partial}{\partial \xi} (x_\xi \sqrt{g_o} Huu + x_\eta \sqrt{g_o} Huv) \right. \right. \\
& \left. \left. + \frac{\partial}{\partial \eta} (x_\xi \sqrt{g_o} Huv + x_\eta \sqrt{g_o} Hvv) \right] \right. \\
& \left. - g_o \frac{\partial Hu\omega}{\partial \sigma} \right\} \\
& + \frac{E_v}{H^2} \frac{\partial}{\partial \sigma} \left(A_v \frac{\partial u}{\partial \sigma} \right) \\
& + \frac{R_o}{F^2} \left[H \int_\sigma^0 \left(g^{11} \frac{\partial \rho}{\partial \xi} + g^{12} \frac{\partial \rho}{\partial \eta} \right) d\sigma \right. \\
& \left. + \left(g^{11} \frac{\partial H}{\partial \xi} + g^{12} \frac{\partial H}{\partial \eta} \right) \left(\int_\sigma^0 \rho d\sigma + \sigma \rho \right) \right] \\
& + E_H A_H \text{ (Horizontal Diffusion)}
\end{aligned} \tag{A.31}$$

An equation similar to (A.31) can be derived for v . The following equation is for ϕ , which can be either salinity S or water quality species (if a reaction term is added):

$$\begin{aligned}
\frac{1}{H} \frac{\partial H\phi}{\partial t} = & \frac{1}{H^2} \frac{\partial}{\partial \sigma} \left(D_v \frac{\partial \phi}{\partial \sigma} \right) \\
& - \frac{1}{H\sqrt{g_o}} \left[\frac{\partial}{\partial \xi} (\sqrt{g_o} Hu\phi) + \frac{\partial}{\partial \eta} (\sqrt{g_o} Hv\phi) \right] - \frac{1}{H} \frac{\partial H\omega\phi}{\partial \sigma} \\
& + D_H \left[g^{11} \frac{\partial^2 \phi}{\partial \xi^2} + 2g^{12} \frac{\partial^2 \phi}{\partial \xi \partial \eta} + g^{22} \frac{\partial^2 \phi}{\partial \eta^2} \right]
\end{aligned} \tag{A.32}$$

Turbulence Parameterization

One of the most important features in numerical circulation and transport models is the parameterization of turbulence. Since the spatial scale of horizontal motion in an estuarine system is typically 2-3 orders of magnitude larger than that of the vertical motion, it is common to treat the vertical and horizontal turbulence separately (Sheng, 1983). Vertical turbulent mixing is a very important process which can significantly affect the circulation and transport in an estuarine system (Sheng *et al.*, 1995). Since turbulence is a property of the flow rather than the fluid, it is essential to make use of a robust turbulence model to parameterize the vertical turbulent mixing. In this study, the vertical turbulent eddy coefficients are obtained from a simplified second-order closure model of Sheng (1982) and Sheng (1989).

A Simplified Second-Order Closure Model - Equilibrium Closure

Second-order closure models resolve the dynamics of turbulence by including the differential transport equations for the turbulence variables, i.e., the second-order correlations (e.g., $-\overline{u_i' u_j'}$, $-\overline{u_i' S'}$, and $\overline{\rho' \rho'}$). The equilibrium closure model solves for the following algebraic equations, in addition to the mean flow equations:

$$\begin{aligned}
0 = & -\overline{u'_i u'_k} \frac{\partial u_j}{\partial x_k} - \overline{u'_j u'_k} \frac{\partial u_i}{\partial x_k} - g_i \frac{\overline{u'_j \rho'}}{\rho_o} - g_j \frac{\overline{u'_i \rho'}}{\rho_o} \\
& - 2\epsilon_{ijk} \Omega_k \overline{u'_i u'_j} - \epsilon_{ijk} \Omega_i \overline{u'_j u'_k} \\
& - \frac{q}{\Lambda} \left(\overline{u'_i u'_j} - \delta_{ij} \frac{q^2}{3} \right) - \delta_{ij} \frac{q^3}{12\Lambda}
\end{aligned} \tag{A.33}$$

$$\begin{aligned}
0 = & -\overline{u'_i u'_j} \frac{\partial \rho}{\partial x_j} - \overline{u'_j \rho'} \frac{\partial u_i}{\partial x_j} - g_i \frac{\overline{\rho' \rho'}}{\rho_o} \\
& - 2\epsilon_{ijk} \Omega_j \overline{u'_k \rho'} - 0.75 q \frac{\overline{u'_i \rho'}}{\Lambda}
\end{aligned} \tag{A.34}$$

$$0 = 2 \overline{u'_j \rho'} \frac{\partial \rho}{\partial x_j} + 0.45 q \frac{\overline{\rho' \rho'}}{\Lambda} \tag{A.35}$$

where the subscripts i, j, k can take on the values of 1, 2, or 3. x_i are the coordinate axis, (u_i, u_j, u_k) are the mean velocity components, (u'_i, u'_j, u'_k) are the fluctuating velocity components, ρ_o , and ρ' are the mean and fluctuating water density, ϵ_{ijk} is the alternating tensor, Ω is the earth rotation, and δ_{ij} is the Kronecker delta. Λ is the turbulence macroscale, and $q = \left(\overline{u'_i u'_i} \right)^{1/2}$ is the total rms fluctuating velocity. The above equations contains a total of five model coefficients. These coefficients were determined from laboratory experiments, and remain "invariants" in applications of the equilibrium closure model.

As shown in Sheng *et al.* (1989), q^2 can be determined from the following dimensional equations when the mean flow variables are known:

$$3A^2b^2sQ^4 + A[(bs + 3b + 7b^2s)Ri - Abs(1 - 2b)]Q^2 + b(s + 3 + 4bs)Ri^2 + (bs - A)(1 - 2b)Ri = 0 \quad (\text{A.36})$$

where A , b , and s are model constants, Ri is the Richardson number, and

$$q = Q\Lambda\sqrt{\left(\frac{\partial u}{\partial z}\right)^2 + \left(\frac{\partial v}{\partial z}\right)^2} \quad (\text{A.37})$$

Once q^2 is computed, the vertical eddy coefficients can be computed from

$$A_v = \frac{A + w\overline{w'w'}}{A - wq^2}\Lambda q \quad (\text{A.38})$$

$$D_v = \frac{bs}{(bs - w)A} \frac{\overline{w'w'}}{q^2}\Lambda q \quad (\text{A.39})$$

where

$$\begin{aligned} w &= Ri/(AQ^2) \\ \overline{w} &= w/(1 - w/b) \\ \overline{w'w'} &= \frac{1 - 2b}{3(1 - 2\overline{w})}q^2 \end{aligned} \quad (\text{A.40})$$

In a complete Reynolds stress model, a differential transport equation for the turbulent macroscale Λ is usually derived. However, the Λ equation contains four model coefficients that must be calibrated with experimental data. For ease of application, the turbulent macroscale Λ is often assumed to satisfy a number of integral constraints. First of all, Λ is

assumed to be a linear function of the vertical distance immediately above the bottom or below the free surface. In addition, the turbulent macroscale Λ must satisfy the following relationships:

$$\left| \frac{d\Lambda}{dz} \right| \leq 0.65 \quad (\text{A.41})$$

$$\Lambda \leq C_1 \cdot H \quad (\text{A.42})$$

$$\Lambda \leq C_1 \cdot H_p \quad (\text{A.43})$$

$$\Lambda \leq C_2 \cdot \delta_q^2 \quad (\text{A.44})$$

$$\Lambda \leq \frac{q}{N} \quad (\text{A.45})$$

where C_1 is a number usually within the range of 0.1 to 0.25, H is the total depth, H_p is the depth of the pycnocline, C_2 , ranging from 0.1 and 0.25, is the fractional cut-off limitation of turbulent macroscale based on δ_q^2 , the spread of the turbulence determined from the turbulent kinetic energy (q^2) profile, and N is the Brunt-Väisälä frequency, defined as:

$$N = \left(-\frac{g}{\rho} \frac{\partial \rho}{\partial z} \right)^{1/2} \quad (\text{A.46})$$

Although the simplified second-order closure model is strictly valid when the turbulent time scale (Mq) is much smaller than the mean flow time scale and when turbulence does not change rapidly over Λ , it has been found to be quite successful in simulating vertical flow

structures in estuarine and coastal waters (Sheng *et al.*, 1989a; Sheng *et al.*, 1989b; Sheng *et al.*, 1993; Sheng *et al.*, 1995).

Solution Technique for the Water Quality Model

In the finite difference solution of the water quality model, the advection and horizontal diffusion terms are treated explicitly, whereas the vertical diffusion and biogeochemical transformations are treated implicitly. Following Chen (1994), a fractional step method, which guarantees numerical stability and prevents negative concentrations is applied in the numerical solution. First, the horizontal advection and diffusion, and the vertical advection terms are calculated. Second, the numerical solution proceeds with the calculation of the vertical diffusion and the transformation reactions that do not involve sorption/desorption. Finally, the species that are coupled through dissolved and particulated forms are solved simultaneously. Equations (A.46) shows a schematic of the numerical solution algorithm method used in this study.

$$\begin{aligned}
 \frac{N^{*1} - N^n}{\Delta t} &= [\text{Horiz. Advection} + \text{Horiz. Diffusion} + \text{Vertical Advection}]^n \\
 \frac{N^{*2} - N^{*1}}{\Delta t} &= [\text{Vertical Diffusion}]^{*2} + [Q]^{*2} \\
 \frac{N^{n+1} - N^{*2}}{\Delta t} &= [\text{Sorption}]^{n+1} + [\text{Desorption}]^{n+1}
 \end{aligned}
 \tag{A.47}$$

The coupling between the suspended sediment and water quality models takes place during the solution of the sorption/desorption reactions. Assuming that any particulate species (P) can be given in terms of mass per unit mass of sediment (p):

$$P = p \cdot c \quad (\text{A.48})$$

where c represents the suspended sediment concentration. The solution of the second step of the fractional method (*2) (Equation A.46) gives:

$$\frac{\partial pc}{\partial t} = \frac{\partial}{\partial z} \left(w_s pc + D_v \frac{\partial pc}{\partial z} \right) + Q \quad (\text{A.49})$$

which can be expanded into:

$$p \frac{\partial c}{\partial t} + c \frac{\partial p}{\partial t} = \frac{\partial}{\partial z} \left[p \left(w_s c + D_v \frac{\partial c}{\partial z} \right) \right] + \frac{\partial}{\partial z} \left(D_v \frac{\partial p}{\partial z} \right) + Q \quad (\text{A.50})$$

Using the vertical one-dimensional suspended sediment equation:

$$\frac{\partial c}{\partial t} = \frac{\partial}{\partial z} \left(w_s c + D_v \frac{\partial c}{\partial z} \right) \quad (\text{A.51})$$

Equation (A.49) becomes:

$$c \frac{\partial p}{\partial t} = \frac{\partial p}{\partial z} \left(w_s c + D_v \frac{\partial c}{\partial z} \right) + \frac{\partial}{\partial z} \left(D_v c \frac{\partial p}{\partial z} \right) + Q \quad (\text{A.52})$$

At the sediment water interface, Equation (A.51) uses the balance between erosion and deposition, and calculates the net flux of the particulate species coming out of the sorption/desorption processes:

$$c \frac{\partial p}{\partial t} = \frac{\partial p}{\partial z} (D - E) + \frac{\partial}{\partial z} \left(D_v c \frac{\partial p}{\partial z} \right) + Q \quad (\text{A.53})$$

APPENDIX B MODELING SEDIMENT DYNAMICS

Equation (3.10) in Chapter 3 represents the governing equation for modeling sediment dynamics in Estuarine Systems. The lateral boundary conditions along open and river boundaries are applied similarly to the salinity equation. The vertical boundary condition impose a zero flux at the free-surface, and a net flux determined by the balance between erosion and deposition at the bottom (Figure B.1). Therefore, three important processes need to be evaluated in the sediment model: settling, erosion, and deposition.

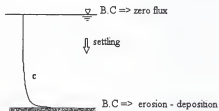


Figure B.1 - Vertical boundary conditions.

Settling Velocity

Due to its higher density, sediment particles tend to sink to the bottom, through a process called settling. In this study, four options were used to determine the settling velocity, depending on sediment characteristics.

Constant Settling

A constant settling velocity, determined from laboratory or field experiments can be used in the sediment model:

$$w_s = \text{constant} \quad (\text{B.1})$$

Schoellhammer and Sheng (1993) studying resuspension events of non-cohesive sediments in Old Tampa Bay used a constant settling velocity of 0.021 cm/s. In their study, the mean particle diameter, $d_{50} = 127 \mu\text{m}$, and the density of bottom sediment, $\rho_s = 2.68 \text{ g/cm}^3$.

Stokes' Formula

For individual grain of fixed density (ρ_s), diameter (d), and fluid kinematic viscosity (ν), the terminal settling velocity is given by:

$$w_s = \frac{1}{18} \frac{(\rho_s - \rho_w) g d^2}{\nu} \quad (\text{B.2})$$

Hwang & Mehta

Based on a laboratory experiment, Hwang and Mehta (1989) parameterize the effects of flocculation and hindered settling on the settling velocity using:

$$w_s = \frac{a c^n}{(c^2 + b^2)^m} \quad (\text{B.3})$$

where a , b , m , and n are empirical constants to be determined from laboratory experiments. The shape of w_s as function of c is shown in Figure B.2 for sediments from a site in Lake Okeechobee, Florida (Hwang and Mehta, 1989). At low concentration ($c < 100$ mg/L), w_s is constant and can be described by Stoke's law. At higher concentration ($100 < c < 1000$ mg/L), flocculation occurs as the result of increased collision among particles, resulting in a higher settling velocity. As c exceeds 3000 mg/L, w_s starts to decrease due to hindered settling, i.e., interference on settling due to the presence of other particles.

Ross' Formula

Settling velocity variation with concentration for the cohesive mud of Hillsborough Bay was determined in a laboratory experiment by Ross (1988), according to a power law (Figure B.3). For lower concentrations, more likely to occur in the field ($c < 1000$ mg/L), the settling velocity is given by:

$$w_s = 0.11 c^{1.6} \quad (\text{B.4})$$

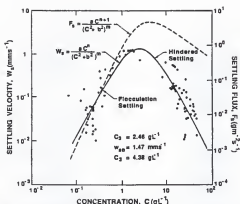


Figure B.2 - Settling velocity as a function of concentration (Hwang & Mehta, 1989).

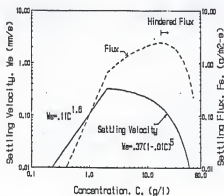


Figure B.3 - Settling velocity as a function of concentration (Ross, 1988).

Erosion

Erosion, defined as the process by which sediment is resuspended to the water column due to bottom shear stress, is one of the primary links between the hydrodynamics and sediment components of this integrated model. The erosion and ensuing resuspension of bottom sediments depends on the bed structure and the characteristics of the flow just above the bed. For non-cohesive sediments, erosion starts when the lift force acting on a grain is larger than the downward force. For cohesive sediments, fluidization of the cohesive bed and entrainment of fluid mud due to hydrodynamic forcing are considered erosional processes, and thus, need to be assessed (Mehta, 1989).

Currently, three options for calculating erosion rates based on critical shear stress are available in the model.

Power Law

$$E = \frac{E_o'}{T_d^2} \left\{ \frac{1}{2} \left[\left(\frac{\tau_b}{\tau_{ce}} - 1 \right) + \left| \frac{\tau_b}{\tau_{ce}} - 1 \right| \right] \right\}^p \quad (\text{B.5})$$

where E_o' is the erosion rate constant per unit stress (i.e., it has the same units as E divided by stress), τ_b is the bottom shear stress, τ_{ce} is the critical shear stress for erosion, p is an empirical constant, and T_d is a dimensionless erosion time constant. Non-dimensionalization of the erosion time constant is obtained through $T_d = T_d' / T_{do}$, where T_d' is the dimensional time constant for erosion, and T_{do} is the amount of time the sediment bed has been lying

undisturbed. Typically, T_{do} is about one day, so the units of T_{do} and T_d' are days. E_o , T_d , τ_{ce} , and p are empirical constants which must be determined from laboratory or field experiments (Sheng and Chen, 1992).

In Schoellhammer and Sheng (1993) study, a general erosion equation was applied by setting the erosion rate equal to a power of the bottom shear stress:

$$E = \alpha |\tau_b|^\eta \quad (\text{B.6})$$

where the coefficients $\alpha = 4.08 \times 10^{-6} \text{ g/cm}^2\text{s}$, and $\eta = 1.6$ were determined during the calibration process.

Exponential Law

Parchure and Mehta (1985) pointed out that the "Power Law" is pertinent to a dense bed in which properties are vertically uniform. For a partially consolidated bed, both the density and the bed strength increase with depth, and the erosion rate is better represented by an exponential equation:

$$E = \frac{E_o}{T_d} e^{\alpha \left\{ \frac{1}{2} \left[\left(\frac{\tau_b}{\tau_{ce}} - 1 \right) + \left| \frac{\tau_b}{\tau_{ce}} - 1 \right| \right] \right\}^{\frac{1}{2}}} \quad (\text{B.7})$$

Bottom Shear Stress

Sediments from the bottom are resuspended into the water column by the combine action of waves and currents. The sediment component of this integrated model utilizes the Sverdrup-Munk-Bretschneider (SMB) model (U.S. Army Coastal Engineering Research

Center, 1984) to determine the characteristics of the wave field which induces bottom shear stress. The wave-induced bottom shear stress is then calculated using the relationship develop by Kajiura (1964, 1968). The primary assumption of the SMB model is that the wind has been blowing long enough in one direction so that the wave field had time to come into an equilibrium with the wind. Consequently, the wind input to the SMB model is averaged over one-hour intervals. Details of the SMB model can be found in the Shore Protection Manual (U.S.Army Corps of Engineers, 1984), Ahn (1989), and Sheng and Chen (1992).

Deposition

Deposition and consolidation (in the case of cohesive sediments) are the processes responsible for removal of sediment particles from the water column. The deposition velocity can be defined in terms of the rate at which particles are removed from the water column. The deposition in estuarine systems can be determined by the settling velocity, shear strength, and concentration of depositing aggregates (Sheng, 1986; Chen, 1994), or it can be assumed as the same as the settling velocity closed to the sediment bed (Schoellhammer and Sheng, 1993). Krone (1993) defining deposition as a stochastic process, introduced a probability function for deposition:

$$p = \frac{1}{2} \left(1 - \frac{\tau_b}{\tau_{cd}} + \left| 1 - \frac{\tau_b}{\tau_{cd}} \right| \right) \quad (\text{B.8})$$

where p is the probability of deposition, τ_b is the bottom shear stress, and τ_{cd} is the critical shear stress for deposition. Equation (B.8) shows that when $\tau_b = 0$, the probability of

deposition is 1, and when $\tau_b \geq \tau_{cd}$, there is no deposition. The probability of deposition of sediment particles inversely proportional to the bottom shear stress.

Sheng's Model

Sheng (1986) and Chen (1994) considered the flow over a surface covered with several layers with the possible presence of vegetation, by expressing the deposition velocity as:

$$-\frac{\overline{(w'c')}}{c_1} = v_d = \frac{\rho}{(v_{dh})^{-1} + (v_{ds})^{-1} + (v_{dc})^{-1}} \quad (\text{B.9})$$

where $-\overline{(w'c')}$ represents the depositional flux at the bed, c_1 is the suspended sediment concentration at the first grid point above the bottom. v_{dh} , v_{ds} , and v_{dc} , representing the deposition velocity within the hydrodynamic logarithmic layer, the viscous sublayer, and the canopy layer, respectively, are given by:

$$v_{dh} = \frac{\kappa u_*}{.75 \ln(z_1/z_o)} \quad (\text{B.10})$$

$$v_{ds} = \left(\frac{4}{3}\right)^{0.3} \left(\frac{D_B}{\nu}\right)^{0.7} \frac{u_*^2}{u_t} + 0.1 \frac{u_*^2}{u_t} \frac{\tau_r u_*^2}{\nu} \left[1 - \exp(-0.08 q^2 \tau_r / \nu)\right] + \tau_r g \quad (\text{B.11})$$

$$v_{dc} = v_{ds} \frac{1 + LAI}{1 + D_p/D_f} \quad (\text{B.12})$$

where z_1 is the distance of the first grid point above the bottom, $D_B = 2.176 \times 10^{-9} / r_p$ is the Brownian diffusion coefficient, ν is fluid kinematic viscosity, $u_* = \sqrt{\tau_b / \rho_w}$ is the friction velocity, τ_b is the bottom shear stress, $u_i = (u_* / \kappa) \ln(z_0 / z_o)$ is the fluid velocity outside the laminar sublayer, $z_0 = 10 z / u_*$ is the height of the viscous sublayer. $\tau_r = w_s / g$ is the relaxation time of sediment particles, $q = (32)^{1/4} u_*$ is the total turbulent fluctuating velocity, LAI is the leaf area index (total wetted leaf area per unit bottom area). In the absence of a vegetation canopy, $v_{dc} = 0$.

The derivation of Sheng's deposition model is based on fundamental consideration of fluid dynamics principles and the fact that the inverse of v_d express the "resistance", which is additive through the various layers. The advantage of Sheng's model is that v_d can be explicitly computed if the turbulence and sediment parameters are known. The disadvantage, however, is that it is difficult to obtain the field data required to validate the model.

Solution Technique

Like the hydrodynamics component of the model, the sediment dynamics is discretized using a finite difference formulation. Details of the numerical solution algorithms used in this study are documented in Sheng and Chen (1992) and Sheng *et al.* (1993). For completeness, a brief description of the finite difference formulation for the vertical component is presented below.

$$\frac{C_k^{n+1} - C_k^n}{\Delta t} = \frac{1}{\Delta Z_k} \left[\left(W_{s_{k+1}} \cdot C_{k+1}^{n+1} + Dv_k \frac{C_{k+1}^{n+1} - C_k^{n+1}}{\Delta Z_{k+1}} \right) - \left(W_{s_k} \cdot C_k^{n+1} + Dv_{k-1} \frac{C_k^{n+1} - C_{k-1}^{n+1}}{\Delta Z_{k-1}} \right) \right] \quad (\text{B.13})$$

$$\text{for } k = 1 \rightarrow \frac{C_k^{n+1} - C_k^n}{\Delta t} = \frac{1}{\Delta Z_k} \left[\left(W_{s_{k+1}} \cdot C_{k+1}^{n+1} + Dv_k \frac{C_{k+1}^{n+1} - C_k^{n+1}}{\Delta Z_{k+1}} \right) - (D - E) \right]$$

$$\text{for } k = km \rightarrow \frac{C_k^{n+1} - C_k^n}{\Delta t} = \frac{1}{\Delta Z_k} \left[0 - \left(W_{s_k} \cdot C_k^{n+1} + Dv_{k-1} \frac{C_k^{n+1} - C_{k-1}^{n+1}}{\Delta Z_{k-1}} \right) \right]$$

where the superscript indicates time level, the subscript indicates vertical layer, C is the suspended sediment concentration, D is the deposition rate, E is the erosion rate, W_s is the settling velocity, Δt is the time step, Dv is the vertical diffusivity coefficient, and ΔZ_k , ΔZ_{kb} , and ΔZ_{kt} are the vertical grid spacing as shown in Figure B.4.

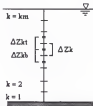


Figure B.4 - Vertical grid spacing.

APPENDIX C DISSOLVED OXYGEN SATURATION AND REAERATION EQUATIONS

Following APHA (1985), the concentration of dissolved oxygen in water (at different temperatures and salinity) at equilibrium with water saturated air can be calculated as:

$$\begin{aligned} \ln DO_s = & -139.34 + (1.5757 \times 10^5 / T) \\ & - (6.6423 \times 10^7 / T^2) + (1.2438 \times 10^{10} / T^3) \\ & - (8.6219 \times 10^{11} / T^4) - 0.5535 \cdot S \cdot [(3.1929 \times 10^{-2}) \\ & - (1.5428 \times 10 / T) + (3.8673 \times 10^3 / T^2)] \end{aligned} \quad (C.1)$$

where DO_s is the dissolved oxygen saturation, in mg/L; and T is the temperature, in degrees K.

The reaeration rate constant, K_{AE} is calculated in the model using the formula proposed by Thomann and Fitzpatrick (1982) for the Potomac Estuary. This method calculates reaeration as a function of velocity, depth, and wind speed as:

$$K_{AE} = \frac{13 U_{avg}^{0.5}}{H^{1.5}} + \frac{3.281}{H} (0.728 W^{0.5} - 0.371 W + 0.0372 W^2) \quad (C.2)$$

where U_{avg} is the depth average velocity, in fps; H is the local water ft, in meters; and W is the wind speed, in m/s.

APPENDIX D LIGHT MODEL EQUATIONS

Miller and McPherson (1995), developed a model that uses simple geometry to compute the significant loss of scalar irradiance at the air-sea interface and to compute the average angle of the light path just beneath the water surface.

During model simulations, the solar elevation angle is computed at each time step from the date and time for the average latitude and longitude of Tampa Bay area, according to:

$$\Psi = (d - 1) \cdot \frac{360}{365 \cdot 242} \quad (\text{D.1})$$

$$\begin{aligned} \delta = & 12.0 + 0.1236 \sin(\Psi) - 0.0043 \cos(\Psi) \\ & + 0.1538 \sin(2\Psi) + 0.0608 \cos(2\Psi) \end{aligned} \quad (\text{D.2})$$

$$\Upsilon = 15.0(\tau - \delta) - \lambda \quad (\text{D.3})$$

$$\begin{aligned} \sigma = & 279.9348 + \Psi + 1.9148 \sin(\Psi) - 0.0795 \cos(\Psi) \\ & + 0.0199 \sin(2\Psi) - 0.0016 \cos(2\Psi) \end{aligned} \quad (\text{D.4})$$

$$\kappa = \arcsin(0.39785077 \cdot \sin(\sigma)) \quad (\text{D.5})$$

$$\sin(\beta) = \sin(\gamma) \cdot \sin(\kappa) + \cos(\gamma) \cdot \cos(\kappa) \cdot \cos(\Upsilon) \quad (\text{D.6})$$

where Ψ is the angular fraction of the year, in degrees; d is the Julian date; δ is the true solar noon, in hours; Υ is the solar hour angle, in degrees; τ is the Greenwich Mean Time, in hours; λ is the local longitude, in degrees; σ is an estimate of the true longitude of the sun, in degrees; κ is the solar declination, in degrees; γ is the local latitude, in degrees; and β is the solar elevation angle, in degrees.

The average zenith angle (Θ) of the refracted direct solar beam in water is computed from the solar elevation angle by using Snell's law and the assumption that the effects of the wave action average to the refracted angle of a calm sea surface by:

$$\Theta = \arcsin[\sin(90^\circ - \beta)/1.33] \quad (\text{D.7})$$

PAR data obtained from Tampa Bay were used to develop a cubic polynomial that describes the upper limit of the averages as a function of the solar elevation angles on very clear days in the Bay:

$$E_o(\max) = 216.47456 + 125.22091 \cdot \beta - 1.8501726 \cdot \beta^2 + 0.0093917741 \cdot \beta^3 \quad (\text{D.8})$$

The weighted average cosine, μ_{wd} , for all refracted PAR is then calculated by:

$$\mu_{\text{wd}} = \frac{\mu_{\text{diff}} \{b_0 - b_1 [E_o(\max)]\} + \cos(\Theta) b_2 \sin(\beta) [E_o(I)/E_o(\max)]}{b_0 - b_1 [E_o(I)/E_o(\max)] + b_2 \sin(\beta) [E_o(I)/E_o(\max)]} \quad (\text{D.9})$$

where b_0 , b_1 , and b_2 are regression coefficients determined from Tampa Bay data, and $E_o(I)$ is the irradiance data from the in-air sensor.

APPENDIX E
CONTOUR PLOTS FOR THE SUMMER OF 1991 SIMULATION

Ammonium Nitrogen

After 30 days (June 26, 1991)

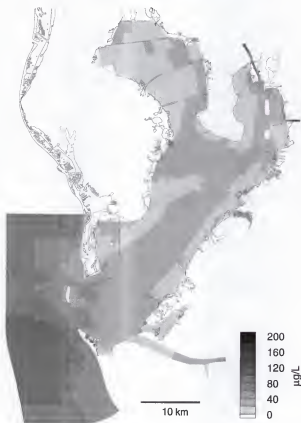


Figure E.1 - Near-bottom ammonium nitrogen distribution in Tampa Bay for June 26, after 30 days of simulation.

Ammonium Nitrogen

After 60 days (July 26, 1991)

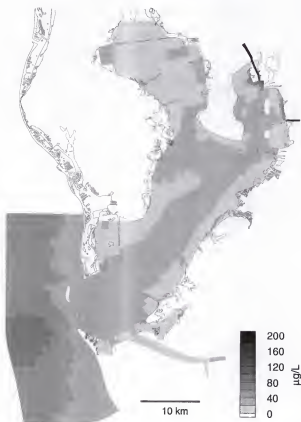


Figure E.2 - Near-bottom ammonium nitrogen distribution in Tampa Bay for July 26, after 60 days of simulation.

Ammonium Nitrogen

After 90 days (August 25, 1991)

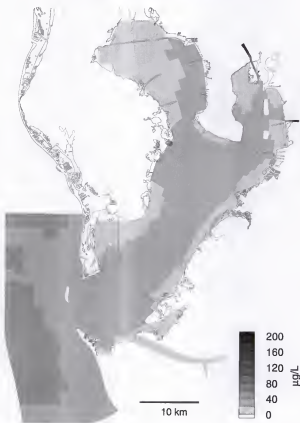


Figure E.3 - Near-bottom ammonium nitrogen distribution in Tampa Bay for August 25, after 90 days of simulation.

Ammonium Nitrogen

After 120 days (September 24, 1991)

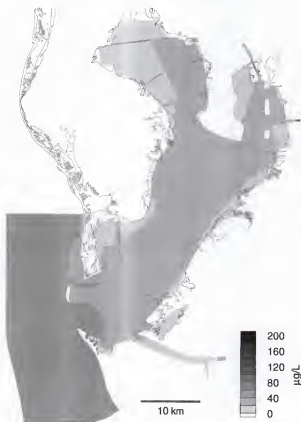


Figure E.4 - Near-bottom ammonium nitrogen distribution in Tampa Bay for September 24, after 120 days of simulation.

Nitrate+Nitrite

After 30 days (June 26, 1991)

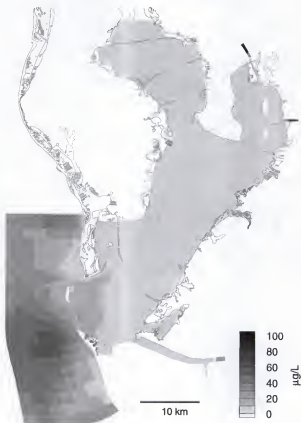


Figure E.5 - Near-bottom nitrate+nitrite distribution in Tampa Bay for June 26, after 30 days of simulation.

Nitrate+Nitrite

After 60 days (July 26, 1991)

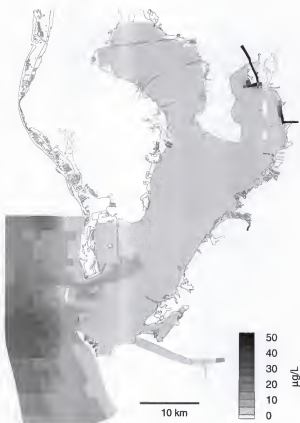


Figure E.6 - Near-bottom nitrate+nitrite distribution in Tampa Bay for July 26, after 60 days of simulation.

Nitrate+Nitrite

After 90 days (August 25, 1991)

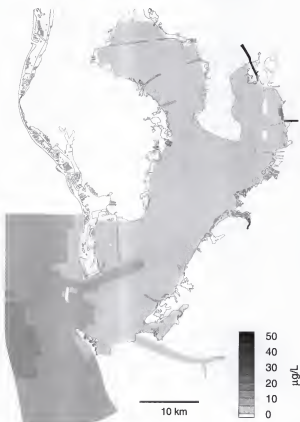


Figure E.7 - Near-bottom nitrate+nitrite distribution in Tampa Bay for August 25, after 90 days of simulation.

Nitrate+Nitrite

After 120 days (September 24, 1991)

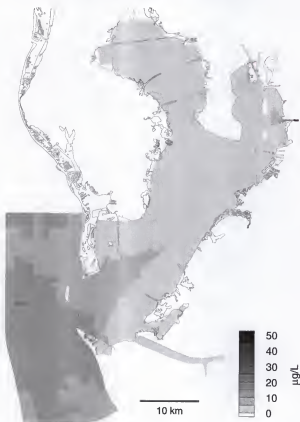


Figure E.8 - Near-bottom nitrate+nitrite distribution in Tampa Bay for September 24, after 120 days of simulation.

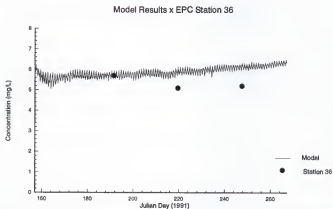
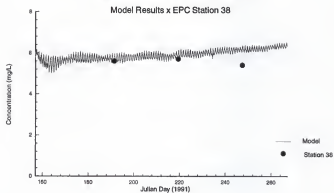
Near-Bottom Dissolved Oxygen

Figure E.9 - Model results and measured data for near-bottom dissolved oxygen at EPC stations 36 and 38.

Near-Bottom Dissolved Oxygen

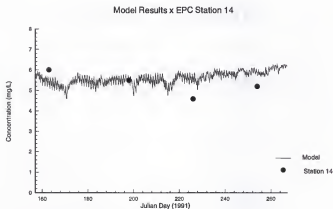
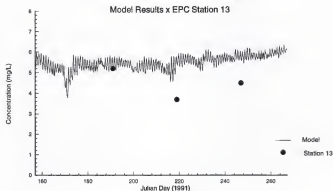


Figure E.10 - Model results and measured data for near-bottom dissolved oxygen at EPC stations 13 and 14.

Near-Bottom Dissolved Oxygen

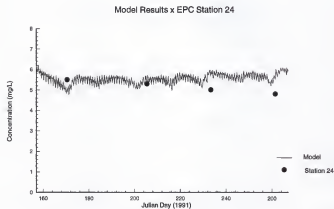
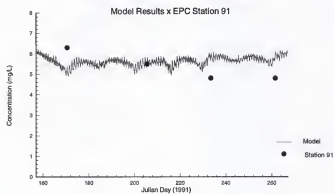


Figure E.11 - Model results and measured data for near-bottom dissolved oxygen at EPC stations 91 and 24.

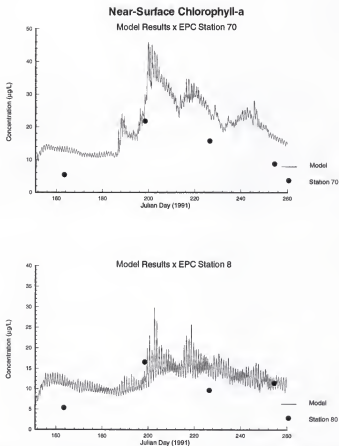


Figure E.12 - Model results and measured data for near-surface chlorophyll-a concentration at EPC station 70 and 8.

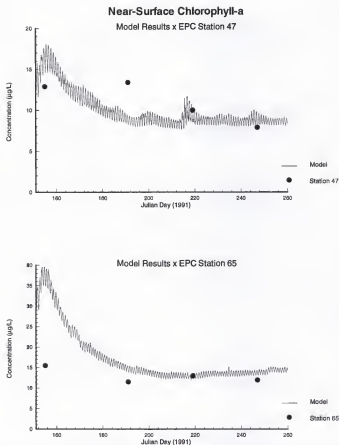


Figure E.13 - Model results and measured data for near-surface chlorophyll-a concentration at EPC station 47 and 65.

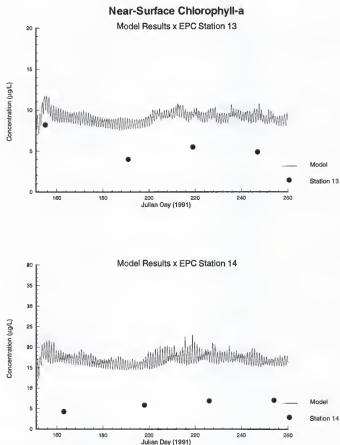


Figure E.14 - Model results and measured data for near-surface chlorophyll-a concentration at EPC station 13 and 14.

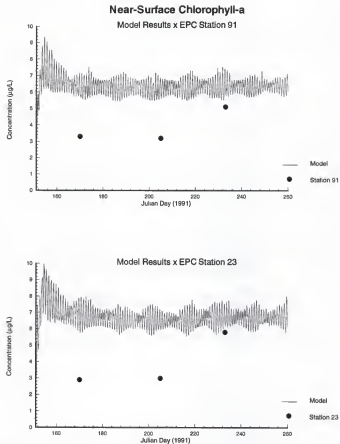


Figure E.15 - Model results and measured data for near-surface chlorophyll-a concentration at EPC station 91 and 23.

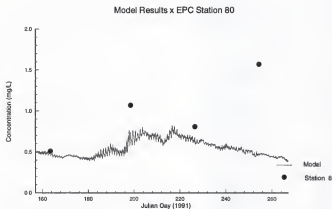
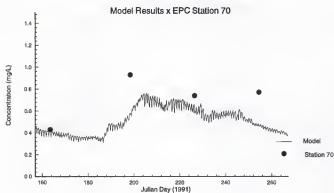
Near-Bottom Kjeldahl Nitrogen

Figure E.16 - Model results and measured data for near-bottom Kjeldahl nitrogen concentration at EPC station 70 and 8.

Near-Bottom Kjeldahl Nitrogen

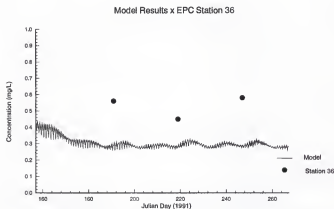
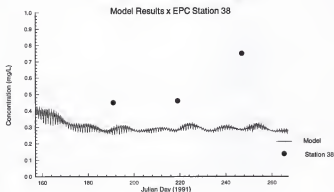


Figure E.17 - Model results and measured data for near-bottom Kjeldahl nitrogen concentration at EPC station 36 and 38.

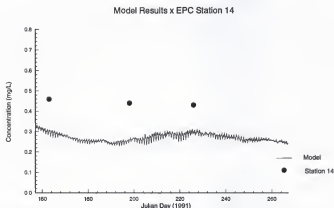
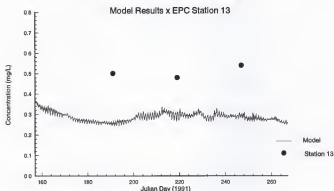
Near-Bottom Kjeldahl Nitrogen

Figure E.18 - Model results and measured data for near-bottom Kjeldahl nitrogen concentration at EPC station 13 and 14.

Near-Bottom Kjeldahl Nitrogen

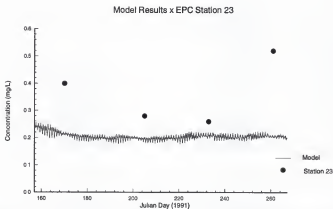
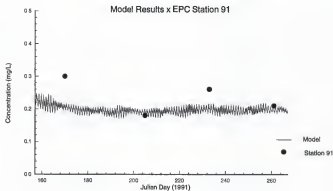
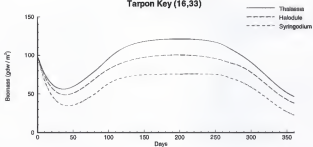


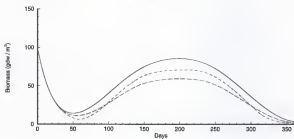
Figure E.19 - Model results and measured data for near-bottom Kjeldahl nitrogen concentration at EPC station 91 and 23.

APPENDIX F
SENSITIVITY TESTS OF THE SEAGRASS MODEL

Seagrass Biomass Tarpon Key (16,33)



Mullet Key (19,34)



Apollo Beach (33,55)

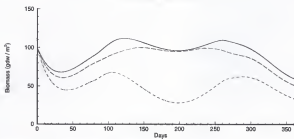
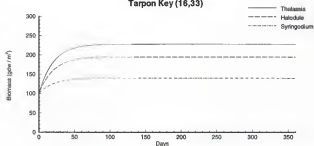
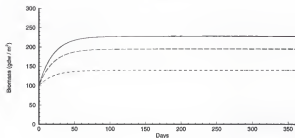
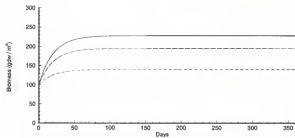


Figure F.1 - Simulated seagrass biomass for test S1.1.

**Seagrass Biomass
Tarpon Key (16,33)****Mullet Key (19,34)****Apollo Beach (33,55)****Figure F.2 - Simulated seagrass biomass for test S1.2.**

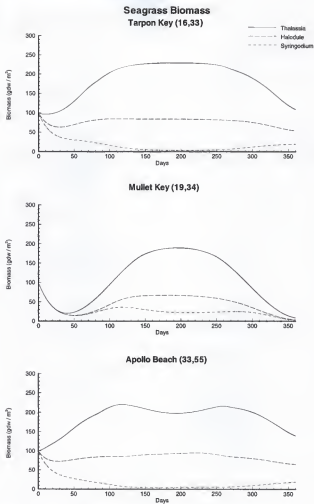
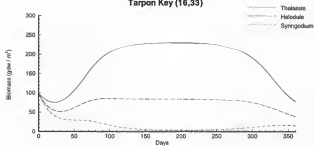
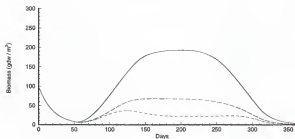


Figure F.3 - Simulated seagrass biomass for test S2.1.

Seagrass Biomass Tarpon Key (16,33)



Mullet Key (19,34)



Apollo Beach (33,55)

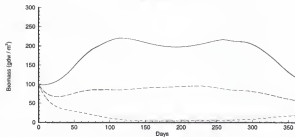
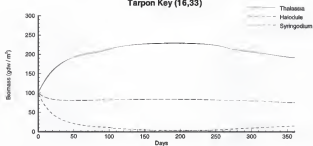
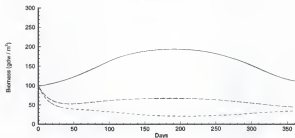


Figure F.4 - Simulated seagrass biomass for test S2.2.

Seagrass Biomass Tarpon Key (16,33)



Mullet Key (19,34)



Apollo Beach (33,55)

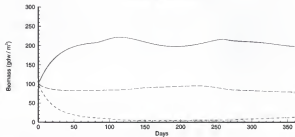
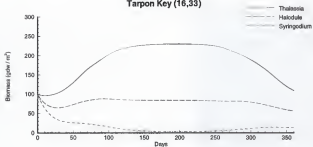
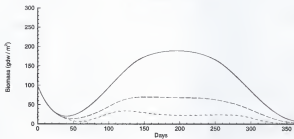


Figure F.5 - Simulated seagrass biomass for test S2.3.

Seagrass Biomass Tarpon Key (16,33)



Mullet Key (19,34)



Apollo Beach (33,55)

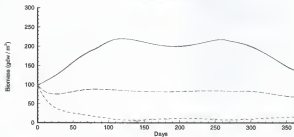
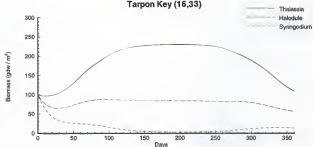
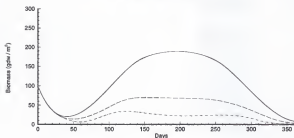


Figure F.6 - Simulated seagrass biomass for test S3.1.

Seagrass Biomass Tarpon Key (16,33)



Mullet Key (19,34)



Apollo Beach (33,55)

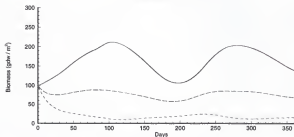
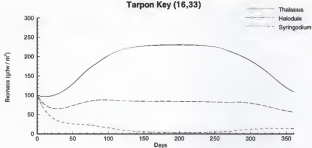
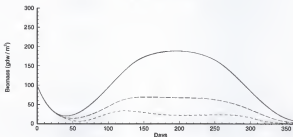


Figure F.7 - Simulated seagrass biomass for test S3.2.

Seagrass Biomass Tarpon Key (16,33)



Mullet Key (19,34)



Apollo Beach (33,55)

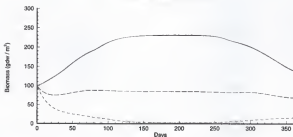
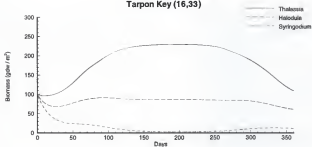
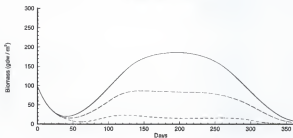


Figure F.8 - Simulated seagrass biomass for test S3.3.

Seagrass Biomass Tarpon Key (16,33)



Mullet Key (19,34)



Apollo Beach (33,55)

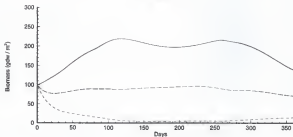
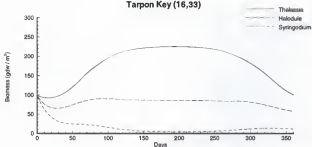
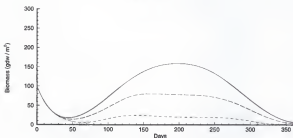


Figure F.9 - Simulated seagrass biomass for test S4.1.

Seagrass Biomass Tarpon Key (16,33)



Mullet Key (19,34)



Apollo Beach (33,55)

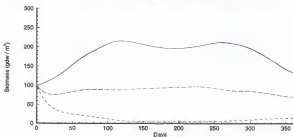
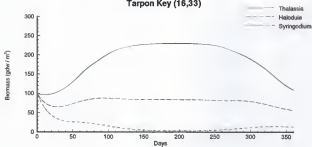
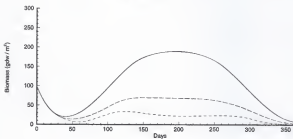


Figure F.10 - Simulated seagrass biomass for test S4.2.

Seagrass Biomass Tarpon Key (16,33)



Mullet Key (19,34)



Apollo Beach (33,55)

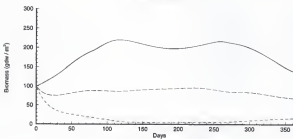
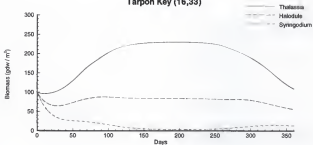
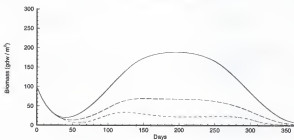


Figure F.11 - Simulated seagrass biomass for test S5.1.

Seagrass Biomass Tarpon Key (16,33)



Mullet Key (19,34)



Apollo Beach (33,55)

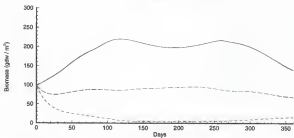


Figure F.12 - Simulated seagrass biomass for test S5.2.

REFERENCES

- Ahn, K., 1989: "Wind-wave hindcasting and estimation of bottom shear-stress in Lake Okeechobee." M.Sc. Thesis. University of Florida.
- Ambrose, R.B. Jr., T.A. Wool, J.L. Martin, J.P. Connolly, R.W. Schanz, 1994: "WASP5, A hydrodynamic and water quality model - model theory, user's manual, and programmer's guide." U.S.EPA Environmental Research Laboratory. Athens, Georgia
- American Public Health Association (APHA), 1985: "Standard methods for the examination of water and wastewater." APHA. Washington, D.C.
- ASCI, 1994: "Phase II: Tampa Bay water quality model." Draft final report prepared for the Southwest Florida Water Management District. Tampa, FL.
- Baca, R.G. and R.C. Amett, 1976: "A limnological model for eutrophic lakes and impoundments." Battelle, Inc., Pacific Northwest Laboratories. Richland, Washington.
- Bach, H.K., 1993: "A dynamic model describing the seasonal variations in growth and the distribution of eelgrass (*Zostera marina* L.) - I. Model theory." *Ecological Modelling*, 65: 31-50.
- Bartleson, R.D., 1988: "The relative influence of current reduction by seagrasses on sediment nutrients and seagrass growth in high and low nutrient waters : a simulation model and field observations." M.Sc. Thesis. University of Florida.
- Berkheiser, V.E., J.J. Street, P.S.C. Rao, and T.L. Yuan, 1980: "Partitioning of inorganic orthophosphate in soil-water systems." *CRC Critical Review in Environmental Control*.
- Berner, R.A., 1971: "Principles of chemical sedimentology." McGraw-Hill. New York, NY.

- Blumberg, A.F., and G.L. Mellor, 1987: "A description of a three-dimensional coastal ocean circulation model." In (Heaps, ed.) *Three-Dimensional Coastal Ocean Models of Marine and Estuaries Dynamics*. American Geophysical Union. Washington, DC. pp. 1-16.
- Boler, R.N. (ed.), 1992: "Surface water quality, Hillsborough County, Florida: 1990-1991." Hillsborough County Environmental Protection Commission. Tampa, FL.
- Boler, R.N. (ed.), 1990: "Surface water quality, Hillsborough County, Florida: 1988-1989." Hillsborough County Environmental Protection Commission. Tampa, FL.
- Boler, R.N., R.C. Malloy, and E.M. Lesnett, 1991: "Surface water quality monitoring by the Environmental Protection Commission of Hillsborough County." In (S.F. Treat and Clark P.A., eds.) *Proceedings of Tampa Bay Area Scientific Information Symposium 2*, 1991. Tampa, FL.
- Bowie, G.L., C.W. Chen, and D.H. Dykstra, 1980: "Lake Ontario ecological modeling, phase III." Tectra-Tech, Inc., Lafayette, CA.
- Brooks, G.R., and L.J. Doyle, 1992: "A characterization of Tampa Bay sediments, phase III." *Final Report to the Southwest Florida Water Management District*. University of South Florida. St. Petersburg, FL.
- Cambridge, M.L. and A.J. McComb, 1984: "The loss of seagrass in Cockburn Sound, Western Australia. I. The time course and magnitude of seagrass decline in relation to industrial development." *Aquat. Bot.* 20:229-243.
- Cameron, W.M. and D.W. Pritchard, 1963: "Estuaries." In (Hill, N.M., ed.) *The Seas*. Vol.2. John Wiley & Sons. New York.
- Chen, X., 1994: "Effects of hydrodynamics and sediment transport processes on nutrient dynamics in shallow lakes and estuaries." Ph.D. dissertation. University of Florida.
- Cheng, R.T., and V. Casulli, 1982: "On lagrangian residual currents with applications in South San Francisco Bay, California." *Water Resources Research*, 18(6):1652-1662.
- City of Tampa, Dept. of Public Works (COT), 1986: "Surface sediment composition and distribution in Hillsborough Bay, Florida." *Rept. to Fla. Dept. of Environ. Reg.* City of Tampa Dept. of Sanit. Sewers, Bay Study Group. Tampa, FL.

- Coastal Environmental, Inc., 1994: "Estimates of total nitrogen, total phosphorus, and total suspended solids loadings to Tampa Bay, Florida." *Report to the Tampa Bay National Estuary Program*. Tampa, FL.
- Coastal Environmental, Inc., 1995: "Estimating critical nitrogen loads for the Tampa Bay estuary: an empirically-based approach to setting management targets." *Final Report to the Tampa Bay National Estuary Program*. Tampa, FL.
- Covar, A.P., 1976: "Selecting the proper reaeration coefficient for use in water quality models." *Proceedings of the U.S.EPA Conference on Environmental Simulation and Modeling*. April 19-22. Cincinnati, OH.
- Culter, J., 1992: "Estuarine bottom habitat assessment", In (Roat, P., C. Ciccolella, H. Smith, D. Tomasko, eds.) *Sarasota Bay Framework for Action*. Sarasota Bay National Estuary Program. Sarasota, Fla.
- Dawes, C.J. and D.A. Tomasko, 1988: "Depth distribution of *Thalassia testudinum* in two meadows on the west coast of Florida: a difference in effect of light availability." *Mar. Ecol.* 9:123-130.
- Dawes, C.J., M.O. Hall, R.K. Riechert, 1985: "Seasonal biomass and energy content in seagrass communities on the west coast of Florida." *J. Coast. Res.* 1:255-262.
- Day Jr., J.W., C.A.S. Hall, W.M. Kemp, A.Y. Arancibia, 1989: *Estuarine Ecology*. John Wiley & Sons. New York.
- Defant, A., 1961: *Physical Oceanography*. Vol. 2. Pergamon-Press. New York.
- DeGrove, B.D., 1984: "Manatee River survey documentation." *Fla. Dep. Environ. Reg. Water Qual. Tech. Serv.* 1(84). Tallahassee.
- den Hartog, C., 1970: *The Seagrasses of the World*. North Polland Publ. Co. Amsterdam.
- Dennison, W.C., 1987: "Effects of light on seagrass photosynthesis, growth and depth distribution." *Aquat. Bot.* 27:15-26.
- Dennison, W.C., R.J. Orth, K.A. Moore, J.C. Stevenson, V. Carter, S. Kollar, P.W. Bergstrom, and R.A. Batiuk, 1993: "Assessing water quality with submerged aquatic vegetation." *BioScience* 43(2):86-94.

- Di Toro, D.M., 1980: "Applicability of cellular equilibrium and Monod theory to phytoplankton growth kinetics." *Ecological Modeling*, 8:201-218.
- Di Toro, D.M., J.F. Connolly, 1980: "Mathematical models of water quality in large lakes, part II: Lake Erie." *U.S.EPA Ecological Research Series*. EPA-600/3-80-065. Athens, GA.
- Di Toro, D.M., D.J. O'Connor, and R.V. Thomann, 1971: "A dynamic model of the phytoplankton population in the Sacramento San Joaquin Delta." *Adv. Chem. Ser.* 106.
- Dooris P.M., G.M. Dooris, 1985: "Surface flows to Tampa Bay: quantity and quality aspects." In (S.F. Treat, J.L. Simon, R.R. Lewis III, and R.L. Whitman Jr., eds.) *Proceedings of Tampa Bay Area Scientific Information Symposium*, May 1982. University of South Florida, Tampa.
- Doyle, L.J., G.R. Brooks, K.A. Fanning, E.S. Van Fleet, R.H. Byrne, and N.J. Blake, 1989: "A characterization of Tampa Bay sediments - Phase I - Literature review." *Report to Southwest Florida Water Management District*. Tampa, FL.
- Dunton, K. H., 1990: "Production ecology of *Rupia maritima* L. s.l. and *Halodule wrightii* Aschers. in two subtropical estuaries." *J. Exp. Mar. Biol. Ecol.* 143:147-164.
- Echternacht, K.L., 1975: "A study of the precipitation regimes of the Kissimmee River-Lake Okeechobee watershed." *Florida Department of Environmental Regulation Technical Service (3)1*. Tallahassee, FL.
- Eckart, C., 1958: "Properties of water. Part II: The equations of state of water and seawater at low temperatures and pressures." *Amer. J. Sci.*, 256:225-240.
- Edmond, J.M., A. Spivack, B.C. Grant, H. Ming-Hui, and C. Zexia, 1985: "Chemical dynamics of the estuary of the Chiang-jiang." *Continental Shelf Research*, 4:17-36.
- Erfteemeijer, P.L.A., and J.J. Middelburg, 1995: "Mass balance constraints on nutrient cycling in tropical seagrass beds." *Aquatic Botany* 50: 21-36.
- Fanning, K.A., 1992: "Sediment nutrient release study." In (Brooks, G.R., and L.J. Doyle) *A characterization of Tampa Bay sediments, phase III - Final Report to the Southwest Florida Water Management District*. University of South Florida. St. Petersburg, FL.

- Fanning, K.A., and L.M. Bell, 1985: "Nutrients in Tampa Bay." In (S.F. Treat, J.L. Simon, R.R. Lewis III, and R.L. Whitman Jr., eds.) *Proceedings of Tampa Bay Area Scientific Information Symposium*, May 1982. University of South Florida, Tampa.
- Fears, S., 1993: "The role of salinity fluctuation in determining seagrass distribution and species composition." M.Sc. Thesis. University of Florida.
- Fillery, I.R.P., S.K. DeDatta, 1986: "Ammonia volatilization from nitrogen sources applied to rice fields: I. Methodology, ammonia fluxes, and nitrogen-15 loss." *Soil Science* 50:80-86.
- Flannery, M.S. 1989: "Tampa and Sarasota Bays: watershed and tributaries." In (Estevez, E.D. ed.) *NOAA Estuary-of-the-Month*, 11, 18-48. Washington D.C.
- Florida Department of Environmental Regulation (FDER), 1988: "Contaminant concentrations in sediments from the Tampa Bay area." *Draft Report, Fla. Dept. Environ. Reg.* Tallahassee, FL.
- Fong, P. and M.A. Harwell, 1994: "Modeling seagrass communities in tropical and subtropical bays and estuaries: a mathematical model synthesis of current hypotheses." *Bull. Mar. Sci.* 54(3):757-781.
- Fonseca, M.S., J.S. Fisher, J.C. Zieman, and G.W. Thayer, 1982: "Influence of the seagrass *Zostera marina* L., on current flow." *Estuarine and Shelf Science* 15:351-364.
- Fourqurean, J.W. and J.C. Zieman, 1991: "Photosynthesis, respiration and whole plant carbon budget of the seagrass *Thalassia testudinum*." *Mar. Ecol. Prog. Ser.* 69:161-170.
- Freney, J.R., J.R. Simpson, O.T. Denmead, 1981: "Ammonia volatilization." *Ecological Bulletin* 33:291-302.
- Freclich, P.N., 1988: "Kinetic control of dissolved phosphate in natural rivers and estuaries: a primer on the phosphate buffer mechanism." *Limnology and Oceanography* 33:649-668.
- Federal Water Pollution Control Administration (FWPCA), 1969: "Problems and Management of Water Quality in Hillsborough Bay, Florida." Hillsborough Bay Technical Assistance Project, Technical Programs, Southeast Region.

- Galperin, B., A.F. Blumberg, R.H. Weisberg, 1991: "A Time-Dependent Three-Dimensional Model of Circulation in Tampa Bay." In: (S.F. Treat, P.A. Clark, eds.) *Proceedings of the Tampa Bay Area Scientific Information Symposium 2*, pp. 67-75. Tampa, FL.
- Garrat, J.R., 1977: "Review of drag coefficients over oceans and continents." *Monthly Weather Review* **105**: 915-929.
- Giovanelli, R.F., 1981: "Relation between freshwater flow and salinity distribution in the Alafia River, Bullfrog Creek, and Hillsborough Bay, Florida." *U.S. Geol. Surv. Wat. Res. Invest.* 80-102.
- Goetz, C.L., and C.R. Goodwin, 1980: "Water quality of Tampa Bay, Florida, June 1972-May 1976." *U.S. Geol. Surv. Wat.-Res. Inv.* 80-12. Tampa, FL.
- Goodell, H.G., and D.S. Gorsline, 1961: "A sedimentologic study of Tampa Bay, Florida." *Fla. State Univ. Oceanogr. Inst. Contrib.* 167. Tallahassee.
- Goodwin, C.R., 1987: "Tidal-flow, circulation, and flushing changes caused by dredge and fill in Tampa Bay, Florida." *U.S. Geological Survey Water-Supply Paper* 2282. Tampa, FL.
- Haddad, K., 1989: "Habitat trends and fisheries in Tampa and Sarasota Bays." In (Estevez, E.D. ed.) *NOAA Estuary-of-the-Month*, **11**, 113-128. Washington D.C.
- Haney, R.L., 1990: "Notes and Correspondence: On the pressure gradient force over steep topography in sigma coordinate ocean models." *J. of Physical Oceanography*, **21**:610-619.
- Hansen, D.V. and M. Rattray Jr., 1965: "Gravitational circulation in straits and estuaries. *J. Mar. Res.* **23**(1):102-122.
- Harleman, D.R.F., 1971: "One-dimensional models." In (Ward Jr., G.H. and W.H. Espey Jr.) *Estuarine Modelling: An Assessment*. EPA Technical Report. Washington, D.C.
- Harleman, D.R.F., 1992: Section 14.2. In: "Technical guidance manual for performing waste load allocations. Book III: Estuaries - Part 4, Critical review of coastal embayment and estuarine waste load allocation modeling." *U.S. EPA Technical Report EPA-823-R-92-005*. Washington, D.C.

- Heath, R.C., and C.S. Conner, 1981: "Hydrologic almanac of Florida." *U.S. Geol. Surv. Open-file Rep. 81-1107*.
- Heffernan, J.J., and R.A. Gibson, 1985: "Seagrass productivity in Tampa Bay: a comparison with other subtropical communities." In (S.F. Treat, J.L. Simon, R.R. Lewis III, and R.L. Whitman Jr., eds.) *Proceedings of Tampa Bay Area Scientific Information Symposium*, May 1982. University of South Florida, Tampa.
- Hess, K.W., 1994: "Tampa Bay oceanographic project: development and application of the numerical circulation model." *NOAA Technical Report NOS OES 005*. Silver Spring, MD.
- Hess, K.W., 1991: "Analysis of SWIM towed RADS transect data." *NOAA Technical Report for the Southwest Florida Water Management District*. Silver Spring, MD.
- Hess, K.W. and K. Bosley, 1992: "Methodology for validation of a Tampa Bay circulation model." In: (M.L. Spaulding, ed.) *Proceedings of the 2nd Estuarine and Coastal Modeling Conference*. ASCE, Tampa, FL, pp. 83-94.
- Heyl, M.G., 1982: "Manatee River ecological study: a technical basis for best management practices." *Final Report, OCM contract n. CM-51*. Florida Department of Environmental Regulation. Bradenton, FL.
- Howarth, R.W., R. Marino, and J. Lane, 1988: "Nitrogen fixation in freshwater, estuarine, and marine ecosystems. I. Rates and importance." *Limnol. Oceanogr.* **33**(4):669-687.
- Hwang, K.N. and A.J. Mehta, 1989: "Fine sediment erodibility in Lake Okeechobee, Florida." *Coastal and Oceanographic Eng. Dept. Tech. Report COEL-89/019*. University of Florida.
- Johansson, J.O.R., 1991: "Long-term trends of nitrogen loading: water quality and biological indicators in Hillsborough Bay, Florida." In: (S.F. Treat, P.A. Clark, eds.) *Proceedings of the Tampa Bay Area Scientific Information Symposium 2*. pp. 157-176. Tampa, FL.
- Johansson, J.O.R., and A.P. Squires, 1989: "Surface sediments and their relationship to water quality in Hillsborough Bay, a highly impacted subdivision of Tampa Bay, Florida." In (Estevez, E.D. ed.) *NOAA Estuary-of-the-Month*, **11**:18-48. Washington D.C.

- Jørgensen, S.E., 1976: "A eutrophication model for a lake." *Ecological Modelling* 2:147-165.
- Jørgensen, S.E., 1983: "Modeling the ecological processes." In: (G.T. Orlob, ed.) *Mathematical Modeling of Water Quality: Streams, Lakes, and Reservoirs*. John Wiley and Sons. New York. pp 116-149.
- Jørgensen, S.E., B.H. Sørensen, and S.N. Nielsen (editors), 1996: *Handbook of Environmental and Ecological Modeling*. CRC Press, Inc.
- Jørgensen, S.E., M.J. Gromiec (editors), 1989: "Mathematical sub-models in water quality systems." *Development in Environmental Modelling*, 14. Elsevier Science Publishers.
- Kajiura, K., 1968: A model of the bottom boundary layer in water waves." *Bull. Earthquake Res. Inst.* 46:75-123.
- Keefe, C.W., 1994: "The contribution of inorganic compounds to the particulate carbon, nitrogen, and phosphorus in suspended matter and surface sediments of Chesapeake Bay." *Estuaries* 17(1B):122-130.
- Kennish, M.J., 1990: *Ecology of Estuaries, Vol. 2: Biological Aspects*. CRC Press. New York.
- Klump, J.V. and C.S. Martens: "Biogeochemical cycling in an organic rich coastal marine basin - II. Nutrient sediment-water exchange processes." *Geo. Cosmoch. Acta*, 45:101-121.
- Knox, G.A., 1986: *Estuarine Ecosystems: A Systems Approach - Vol. II*. CRC Press. Boca Raton. Florida.
- Krom, M.D., and R.A. Berner, 1980: "The diffusion coefficients of sulfate, ammonium, and phosphate ions in anoxic marine sediments." *Limnol. and Oceanogr.* 25:37.
- Krone, R.B., 1993: "Sediment revisited." In: (A.J. Mehta, ed.) *Coastal and Estuarine Studies*, 42: *Nearshore and Estuarine Cohesive Sediment Transport*. American Geophysical Union. Washington, D.C. pp. 108-125.

- Lambe, T.W., and R.V. Whitman, 1969: *Soil Mechanics*. John Wiley & Sons. New York.
- Lewis, R.R. III, and E.D. Estevez, 1988: "The ecology of Tampa Bay, Florida: an estuarine profile." *U.S. Fish and Wildlife Services Biological Report: 85(7.18)*. 132 pp.
- Lewis, R.R. III, K.D. Haddad, and J.O.R. Johansson, 1991: "Recent areal expansion of seagrass meadows in Tampa Bay, Florida: real bay improvement or drought-induced?" In: (S.F. Treat, P.A. Clark, eds.) *Proceedings of the Tampa Bay Area Scientific Information Symposium 2*. pp. 189-192. Tampa, Fla.
- Lewis, R.R. III, M.J. Durako, M.D. Moffler, and R.C. Phillips, 1985: "Seagrass meadows of Tampa Bay - a review." In (S.F. Treat, J.L. Simon, R.R. Lewis III, and R.L. Whitman Jr., eds.) *Proceedings of Tampa Bay Area Scientific Information Symposium*. University of South Florida, Tampa.
- Lewis, R.R. III, R.C. Phillips, 1980: "Seagrass mapping project, Hillsborough County, Florida." Prepared for Tampa Port Authority. Tampa, FL.
- Lewis, R.R. III, and R.L. Whitman, 1985: "A new geographic description of the boundaries and subdivisions of Tampa Bay." In (S.F. Treat, J.L. Simon, R.R. Lewis III, and R.L. Whitman Jr., eds.) *Proceedings of Tampa Bay Area Scientific Information Symposium*, May 1982. University of South Florida, Tampa.
- Lorenzen, C.J., 1972: "Extinction of light in the ocean by phytoplankton." *Journal in Conseil* **34**:262-267.
- Loucks, D.P., 1981: "Water quality models for river systems." In: (A.K. Biswas, ed.) *Models for Water Quality Management*. McGraw-Hill Intl. Co. New York.
- Madden, C.J., and W.M. Kemp, 1996: "Ecosystem model of an estuarine submersed plant community: calibration and simulation of eutrophication responses." *Estuaries* **19**(2B):457-474.
- Martin, J.F., 1995: "Modelling of nitrogen in a wetland treatment system." M.Sc. Thesis. University of Florida.
- Martinova, M.V., 1993: "Nitrogen and phosphorus compounds in bottom sediments: mechanisms of accumulation, transformation and release." *Hydrobiologia* **252**:1-22.

- McClelland, S., 1984: "Tampa Bay water quality impact study." *Fla. Dep. Environ. Reg. Water Qual. Tech. Serv.* 2(84). Tallahassee.
- McElroy, M.B., J.W. Elkins, S.C. Wofsy, C.E. Kolb, A.P. Duran, and W.A. Kaplan, 1978: "Production and release of N_2O from the Potomac Estuary." *Limnology and Oceanography* 23(6):1168-1182.
- McPherson, B.F. and R.L. Miller, 1994: "Causes of light attenuation in Tampa Bay and Charlotte Harbor, Southwest Florida." *Water Res. Bull.* 30(1):43-53.
- McRoy, C.P. and C. Helfferich, 1977: "Seagrass ecosystem, a scientific perspective." Marcel Mekker. New York. 314 pp.
- Mehta, A. J., 1989: "On estuarine cohesive sediment suspension behavior." *J. of Geophysical Research* 94(C10):14303-14314.
- Mehta, A. J., 1990: "Significance of bay superelevation in measurement of sea level change." *J. of Coastal Research* 6(4):801-813.
- Miller, R.L., and McPherson, B.F., 1995: "Modeling photosynthetically active radiation in water of Tampa Bay, Florida, with emphasis on the geometry of incidence irradiance." *Estuarine, Coastal and Shelf Science* 40.
- Mote Marine Laboratory, 1995: "Light attenuation with respect to seagrasses in Sarasota Bay, Florida." *Mote Marine Laboratory Technical Report 407*. Sarasota, FL.
- Najarian, T.O., P.J. Kaneta, J.L. Taft, M.L. Thatcher, 1984: "Application of nitrogen-cycle model to Manasquan Estuary." *J. of Environ. Eng.* 110(1):190-207. ASCE.
- National Oceanic and Atmospheric Administration (NOAA), 1994: "Magnitude and extent of sediment toxicity in Tampa Bay, Florida." *NOAA Technical Report NOS ORCA 78*. Silver Spring, MD.
- National Oceanic and Atmospheric Administration (NOAA), 1993: "Tampa Bay oceanographic project: physical oceanographic synthesis." *NOAA Technical Report NOS OES 002*. Silver Spring, MD.
- National Oceanic and Atmospheric Administration (NOAA), 1991: "Local climatological data: annual summary for Tampa, Florida." National Climatic Data Center. Asheville, NC.

- National Research Council. Geophysical Study Committee, 1977: "Overview and recommendations." In *Estuaries, Geophysics, and the Environment*. National Academy of Science. Washington, D.C. pp. 1-10.
- O'Connor, D.J. and R.V. Thomann, 1972: "Water quality models: chemical, physical and biological constituents." In: *Estuarine Modeling: an Assessment*. EPA Water Pollution Control Research Series 16070 DZV, Section 702/71.
- Odum, H.T., 1971: *Environment Power and Society*. John Wiley & Sons. New York.
- Odum, H.T., 1994: *Ecological and General Systems*. John Wiley & Sons. New York.
- Olson, F.C.W., and J.B. Morrill, 1955: "Literature survey of the Tampa Bay area." *Fla. State Univ. Oceanogr. Inst. Report*. Tallahassee.
- Orlob, G.T., 1983: "One-dimensional models for simulating water quality in lakes and reservoirs." In: (G.T. Orlob, ed.) *Mathematical Modeling of Water Quality: Streams, Lakes, and Reservoirs*. John Wiley and Sons. New York. pp. 227-273.
- Orth, R.J. and R. Moore, 1984: "Distribution and abundance of submerged aquatic vegetation in Chesapeake Bay: an historical perspective." *Estuaries* 7:531-540.
- Palmer, C.E., 1978: "Climate." In: *1978 Executive Summary*, Appendix C. Southwest Florida Water Management District. Brooksville. pp. c1-c44.
- Parchure, T.M. and A.J. Mehta, 1985: "Erosion of soft cohesive sediment deposits." *J. of Hydr. Eng.* 111:1308-1326.
- Peene, S.J., 1995 "Circulation and transport within a system of shallow, interconnected barrier island lagoons." Ph.D. dissertation, University of Florida.
- Pellikaan, G.C., and P.H. Nienhuis, 1988: "Nutrient uptake and release during growth and decomposition of eelgrass and its effects on the nutrient dynamics of Lake Grevelingen." *Aquatic Botany* 30:189-214.
- Phillips, N.G., 1957: "A coordinate system having some special advantages for numerical forecasting." *J. of Meteor.* 14:184-185.
- Phillips R.C. and E.G. Mefiez, 1987: "Seagrasses." *Smithsonian Contrib. Mar. Sci.* 34.

- Phillips, R.C. and C.P. McRoy, eds. 1980: *A Handbook of Seagrass Biology: an Ecosystem Perspective*. Garland. New York.
- Pocklington, R., 1977: "Chemical processes and interactions involving marine organic matter." *Mar. Chem.* **5**:479-496.
- Pomeroy, L.R., 1960: "Primary productivity of Boca Ciega Bay, Florida." *Bull. Mar. Sci. of the Gulf and Caribbean* **10**(1):1-10.
- Powell G.V.N., W.J. Kenworthy and J.W. Fourqurean, 1989: "Experimental evidence of nutrient limitation of seagrass growth in a tropical estuary with restricted circulation." *Bull. Mar. Sci.* **44**:324-340.
- Pregnall, A.M., R.D. Smith, R.S. Albertele, 1987: "Glutamine synthase activity and free amino acid pools of eelgrass (*Zostera marina* L.) roots." *J. Exp. Mar. Biol. Ecol.* **106**:211-228.
- Pritchard, D.W., 1956: "The dynamic structure of coastal plain estuaries." *J. Mar. Res.* **15**(1) 33-42.
- Rao P.S.C., R.E. Jessup, K.R. Reddy, 1984: "Simulation of nitrogen dynamics in flooded soils." *Soil Science* **138**:54-62.
- Reddy, K.R., P.S.C. Rao, R.E. Jessup, 1990: "Transformation and transport of ammonium nitrogen in a flooded organic soil." *Ecological Modelling* **51**:205-216.
- Reddy, K.R., R.E. Jessup, P.S.C. Rao, 1988: "Nitrogen dynamics in a eutrophic lake sediment." *Hydrobiologia* **159**:177-188.
- Reddy, K.R., and W.H. Patrick, 1984: "Nitrogen transformations and loss in flooded soil and sediments." *CRC Critical Reviews in Environmental Control* **13**(4):273-309.
- Reddy, K.R., W.H. Patrick, and R.E. Phillips, 1978: "The role of nitrate diffusion in determining the order and rate of denitrification in flooded soils. I. Experimental results." *Soil Sci. Soc. Am. J.* **42**(268).
- Reeves, M.R., 1975: "The ecological significance of the zooplankton in the shallow subtropical waters of south Florida." In: (L.E. Cronin, ed.) *Estuarine Research*, Vol. **1**. Academic Press.

- Rice, D.L. and R.B. Hanson, 1984: "A kinetic model for detritus nitrogen: role of the associated bacteria in nitrogen accumulation." *Bull. Mar. Sci.* 35:326- .
- Riley, M.J. and H.G. Stefan, 1988: "MINLAKE: A dynamic lake water quality model." *Ecological Modeling*, 43:155-182.
- Rines, H.M., 1991: "August tidal flux study and nutrient flux calculations for the Tampa Bay monitoring project." *Technical Report prepared for the Southwest Florida Water Management District*. Tampa, FL.
- Ross, B.E., M.A. Ross, and P.D. Jenkins, 1984: "Waste load allocation study. Volume I: hydraulic model, Volume II: transport model, Volume III: model validation, Volume IV: nutrient box model." Florida Department of Environmental Regulation. Tallahassee, FL.
- Ross, M.A., 1988: "Vertical structure of estuarine fine sediment suspension." Ph.D. dissertation, University of Florida.
- Sawyer, C.N., and P.L. McCarty, 1978: *Chemistry for Environmental Engineering*. 3rd edition. McGraw-Hill, Inc. New York. NY.
- Sharp, J.H., C.H. Culberson, and T.M. Church, 1982: "The chemistry of the Delaware Estuary. General considerations." *Limnology and Oceanography*, 27:1015-1028.
- Sheng, Y.P., 1982: "Hydraulic applications of a second-order closure model of turbulent transport." In: (P. Smith, ed.) *Applying Research to Hydraulic Practice*. ASCE. New York. pp. 106-119.
- Sheng, Y.P., 1983: "Mathematical modeling of three-dimensional coastal currents and sediment dispersion: model development and application." *Coastal Engineering Research Center Tech. Rep. CERC-TR-83-2*. U.S. Army Corps of Engineers.
- Sheng, Y.P., 1986: "Modeling bottom boundary layers and cohesive sediment dynamics." In: (A.J. Mehta, ed.) *Estuarine Cohesive Sediment Dynamics*. pp. 360-400. Springer-Verlag. Berlin.
- Sheng, Y.P., 1989: "Evolution of a 3-D curvilinear grid hydrodynamic model: CH3D." In: (M.L. Spaulding, ed.) *Proceedings of the Estuarine and Coastal Modeling Conference*. ASCE, Newport, R.I., pp. 40-49.

- Sheng, Y.P., 1993: "Hydrodynamics, sediment transport and their effects on phosphorus dynamics in Lake Okeechobee." In: (A.J. Mehta, ed.) *Nearshore and Estuarine Cohesive Sediment Transport*. Coastal Estuarine Studies, vol. 42. American Geophysical Union.
- Sheng, Y.P., 1994: "Modeling hydrodynamics and water quality dynamics in shallow waters." *Proceedings of the International Symposium on Ecology and Engineering*. Kuala Lumpur, Malaysia.
- Sheng, Y.P., D.E. Eliason, X.-J. Chen, and J.K. Choi, 1991: "Three-dimensional numerical model of hydrodynamics and sediment transport in lakes and estuaries" *USEPA Cooperative Agreement CR-814345*. University of Florida.
- Sheng, Y.P. and E.A. Yassuda, 1995: "Application of a three-dimensional circulation model to Tampa Bay to support water quality modeling." *Coastal and Oceanographic Eng. Dept. Tech. Report*. University of Florida.
- Sheng, Y.P., E.A. Yassuda, and C. Yang, 1995a: "Modeling the impact of nutrient load reduction on water quality and seagrass in Roberts Bay and Little Sarasota Bay, Florida." *Coastal and Oceanographic Eng. Dept. Tech. Report*. University of Florida.
- Sheng, Y.P., H.K. Lee and K.H. Wang, 1989a: "On numerical strategies of estuarine and coastal modeling." In: (M.L. Spaulding, ed.) *Proceedings of the Estuarine and Coastal Modeling Conference*. ASCE, Newport, R.I., pp. 291-301.
- Sheng, Y.P., J.K. Choi, A.Y. Kuo, 1989b: "Three-dimensional numerical modeling of tidal circulation and salinity transport." In: (M.L. Spaulding, ed.) *Proceedings of the Estuarine and Coastal Modeling Conference*. ASCE, Newport, R.I.
- Sheng, Y.P., S.J. Peene, E.A. Yassuda, J. Davis, and S. Schofield, 1995b: "A field and modeling study on circulation and transport in Sarasota Bay." *Coastal and Oceanographic Eng. Dept. Tech. Report*. University of Florida.
- Sheng, Y.P., W. Lick, R.T. Gedney, and F. Molls, 1978: "Numerical computation of three-dimensional circulation in Lake Erie: A comparison of a free-surface model and a rigid-lid model." *J. Phys. Oceanogr.* 8:713-727.
- Sheng, Y.P., X.-J. Chen, and Yassuda, E.A., 1994: "Wave-induced sediment resuspension and mixing in shallow waters." *Proceedings of the 24th International Conference on Coastal Engineering - ICCE/ASCE*. p. 3281-3294. Kobe, Japan.

- Sheng, Y.P., X.-J. Chen, E.A. Yassuda, K.R. Reddy, M.M. Fisher, 1993: "Quantifying sediment resuspension flux of nutrients and contaminants in estuaries due to episodic events." *Coastal & Oceanographic Eng.Dept. Tech.Rep.*, University of Florida.
- Sheng, Y.P., and X.-J. Chen, 1992: "A three-dimensional numerical model of hydrodynamics, sediment transport, and phosphorus dynamics in Lake Okeechobee: theory, model development and documentation." *Coastal & Oceanographic Eng.Dept. Tech.Rep.*, University of Florida.
- Schoellhammer, D.H., 1993: "Simulation and analysis of sediment resuspension observed in Old Tampa Bay, Florida." Ph.D. dissertation. University of Florida.
- Schomer, N.S, R.D. Drew, and P. Johnson, 1990: "Vegetation communities (habitats)." In (Wolfe, S.H., and R.D. Drew, eds.) *An Ecological Characterization of the Tampa Bay Watershed*. pp. 134-215. U.S. Fish Wildl. Serv. Biol. Rep. 90(20).
- Short, F.T., 1980: "A simulation model of the seagrass production system." In: (Phillips and McRoy, eds.) *A Handbook of Seagrass Biology: An Ecosystem Perspective*. Garland. New York.
- Short, F.T., 1987: "Effects of sediment nutrients on seagrass: literature review and mesocosm experiment." *Aquatic Botany* 27:41-57.
- Short, F.T., and C.P. McRoy, 1984: "Nitrogen uptake by leaves and roots of seagrass *Zostera marina* L. *Bot. Mar.* 17:547-555.
- Short, F.T., M.W. Davis, R.A. Gibson, C.F. Zimmerman, 1985: "Evidence for phosphorus limitation in carbonate sediments of the seagrass *Syringodium filiforme*." *Est. Coast. Shelf Sci.* 20:419-430.
- Simon, J.L., 1974: "Tampa Bay estuarine system - a synopsis." *Fla. Sci.* 37(4):217-245.
- Simon, N.S., 1988: "Nitrogen cycling between sediment and the shallow-water column in the transition zone of the Potomac River and Estuary. I. Nitrate and ammonium fluxes." *Estuarine, Coastal and Shelf Science* 26:483-497.
- Simon, N.S., 1989: "Nitrogen cycling between sediment and the shallow-water column in the transition zone of the Potomac River and Estuary. II. The role of wind-driven resuspension and adsorbed ammonium." *Estuarine, Coastal and Shelf Science* 28:531-547.

- Snoeyink, V.L., and D. Jenkins, 1980: *Water Chemistry*. John Wiley & Sons. New York.
- Solow, A.R., 1995: "Fitting population models to time series." In: (Powell T.M. and J.H. Steele, eds.) *Ecological Time Series*. Chapman & Hall. New York.
- Spaulding, M.L., D.P. French, and H. Rines, 1989: "A review of Tampa Bay water quality model system." Applied Science Associates, Inc., Narragansett, RI.
- Steele, J.M., 1965: "Notes on some theoretical problems in production ecology." In: (C.R. Goldman ed.) *Primary Production in Aquatic Environments*. Univ. of California Press. Berkeley.
- Steidinger K.A., and W.E. Gardiner, 1985: "Phytoplankton of Tampa Bay - a review." In (S.F. Treat, J.L. Simon, R.R. Lewis III, and R.L. Whitman Jr., eds.) *Proceedings of Tampa Bay Area Scientific Information Symposium*, May 1982. University of South Florida, Tampa, FL. pp. 147-183.
- Streeter, H.W. and E.B. Phelps, 1925: "A study of the pollution and natural purification of the Ohio River, III. Factors concerned in the phenomena of oxidation and reaeration." *U.S. Public Health Service Bulletin 146*. Washington, D.C.
- Taylor, J.L. and C.H. Saloman, 1969: "Sediments, oceanographic observation and floristic data from Tampa Bay, Florida and adjacent waters, 1961-1965." University of South Florida. St. Petersburg, FL.
- Thomann, R.V., 1992: Section 14.1. In "Technical guidance manual for performing waste load allocations. Book III: Estuaries - Part 4, Critical review of coastal embayment and estuarine waste load allocation modeling." *U.S. EPA Technical Report EPA-823-R-92-005*. Washington, D.C.
- Thomann, R.V., J.J. Fitzpatrick, 1982: "Calculation and verification of a mathematical model of the eutrophication of the Potomac Estuary." Prepared for the Department of Environmental Services, Government of the District of Columbia.
- Thomann, R.V., J.R. Collier, A. Butt, E. Casman, and L.C. Linker, 1994: "Technical analysis of response of Chesapeake Bay water quality model to loading scenarios." *A report of the Modeling Subcommittee Chesapeake Bay Program Office*. Annapolis, MD.
- Thompson, J.F., Z.U.A. Warsi, and C.W. Mastin, 1985: *Numerical Grid Generation: Foundations and Applications*. North-Holland. New York.


- Tiffany, W.J. III, and D.E. Wilkinson, 1989: "Ports and ports impacts." In (Estevez, E.D. ed.) *NOAA Estuary-of-the-Month*, 11:171-185. Washington D.C.
- Tomasko D.A. and C.J. Dawes, 1990: "Influences of season and water depth on the clonal biology of the seagrass *Thalassia testudinum*." *Mar. Biol.* 105:345-351.
- Tomasko D.A., C.J. Dawes, and M.O. Hall, 1996: "The effects of anthropogenic nutrient enrichment on turtle grass (*Thalassia testudinum*) in Sarasota Bay, Florida." *Estuaries* 19(2B):448-456.
- U.S. Army Coastal Engineering Research Center, 1984: *Shore Protection Manual: Vol. 1* Coastal Engineering Research Center, Department of the Army, Waterways Experiment Station. corps of Engineers, Vicksburg, MS.
- USGS, 1991: "Water resources data for Florida, 1990." Vol. 3A: Southwest Florida. *U.S. Geological Survey Rep. FL-90-3A*. Tampa, FL.
- USGS, 1992: "Water Resources Data for Florida, 1991." Vol. 3A: Southwest Florida. *U.S. Geological Survey Rep. FL-90-3A*. Tampa, FL.
- Wafar, M.V., P. Le Corre, and J.L. Birrien, 1989: "Transport of carbon, nitrogen, and phosphorus in a Brittany River, France." *Est., Coast. and Shelf Sci.* 29:489-500.
- Weisberg, R.H., and R.G. Williams, 1991: "Initial findings on the circulation of Tampa Bay." In: (S.F. Treat, P.A. Clark, eds.) *Proceedings of the Tampa Bay Area Scientific Information Symposium 2*. pp. 67-75. Tampa, FL.
- Williams, S.L., 1987: "Competition between the seagrasses *Thalassia testudinum* and *Syringodium filiforme* in a Caribbean lagoon." *Mar. Ecol. Prog. Ser.* 35:91-98.
- Williams, S.L., 1988: "*Thalassia testudinum* productivity and grazing by green turtles in a highly disturbed seagrass bed." *Mar. Biol.* 98:447-455.
- Williams, S.L., 1990: "Experimental studies of Caribbean seagrass bed development." *Ecol. Monogr.* 60:449-469.
- Wolfe, S.H., and R.D. Drew, eds., 1990: "An ecological characterization of the Tampa Bay Watershed." *U.S. Fish Wildl. Serv. Biol. Rep.* 90(20).

- Wooten, G.R., 1985: "Meteorology of Tampa Bay." In (S.F. Treat, J.L. Simon, R.R. Lewis III, and R.L. Whitman Jr., eds.) *Proceedings of Tampa Bay Area Scientific Information Symposium*, May 1982. University of South Florida, Tampa. pp19-26.
- Yassuda, E.A., and Y.P. Sheng, 1994: "Use of three-dimensional hydrodynamics model for tidal inlet studies." *Proceedings of the 24th International Conference on Coastal Engineering - ICCE/ASCE*. p. 3432-3446. Kobe, Japan.
- Yassuda, E.A., S.J. Peene, Y.P. Sheng, 1992: "Effect of grid on simulating flow in the navigation channel of Tampa Bay." Unpublished manuscript.
- Zieman, J.C. and R.T. Zieman, 1989: "The ecology of the seagrass meadows of the west coast of Florida: a community profile." *U.S. Fish and Wildlife Services Biological Report: 85(7.25)*. 155 pp.
- Zieman, J.C., 1982: "The ecology of the seagrass of south Florida: a community profile." *U.S. Fish and Wildlife Services Report: FWS/OBS-82/25*. 158 pp.
- Zimmerman, R.C., R.D. Smith, and R.S. Albertele, 1987: "Is growth of eelgrass nitrogen limited? A numerical simulation of the effects of light and nitrogen on the growth dynamics of *Zostera marina*." *Marine Ecology Progress Series* 41:167-176.

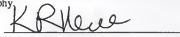
BIOGRAPHICAL SKETCH

Eduardo Ayres Yassuda was born in São Paulo, Brazil, on July 26, 1963. He received a Bachelor of Science degree in mechanical engineering at the Mackenzie University (São Paulo, Brazil) in 1986. After working for a couple of years, he started his graduate program at the Oceanographic Institute of the University of São Paulo, where he earned a Master of Science degree in physical oceanography in 1991. In order to integrate his engineering background with his passion for estuarine systems, he came to the U.S. to pursue a Ph.D. in coastal and oceanographic engineering with a minor in the Environmental Engineering and Science Department. Almost 5 years have gone by, and life has been very generous to him and his wife (Monica). They are going back to Brazil with not only their diplomas, but with Daniel, a three-year old wishful buddy, and another little one that up to this moment is growing up in mammy's belly.


I certify that I have read this study and that in my opinion it conforms to acceptable standards of scholarly presentation and is fully adequate, in scope and quality, as a dissertation for the degree of Doctor of Philosophy.


Y. Peter Sheng, Chairman
Professor of Coastal and
Oceanographic Engineering

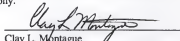
I certify that I have read this study and that in my opinion it conforms to acceptable standards of scholarly presentation and is fully adequate, in scope and quality, as a dissertation for the degree of Doctor of Philosophy.


K. R. Reddy
Graduate Research Professor of
Soil and Water Science

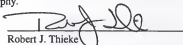
I certify that I have read this study and that in my opinion it conforms to acceptable standards of scholarly presentation and is fully adequate, in scope and quality, as a dissertation for the degree of Doctor of Philosophy.


Ashish J. Mehta
Professor of Coastal and
Oceanographic Engineering

I certify that I have read this study and that in my opinion it conforms to acceptable standards of scholarly presentation and is fully adequate, in scope and quality, as a dissertation for the degree of Doctor of Philosophy.



Clay L. Montague
Associate Professor of Environmental
Engineering and Sciences

I certify that I have read this study and that in my opinion it conforms to acceptable standards of scholarly presentation and is fully adequate, in scope and quality, as a dissertation for the degree of Doctor of Philosophy.


Robert J. Thieke
Assistant Professor of Coastal and
Oceanographic Engineering

This dissertation was submitted to the Graduate Faculty of the College of Engineering and to the Graduate School and was accepted as partial fulfillment of the requirements for the degree of Doctor of Philosophy.

December, 1996



Winfred M. Phillips
Dean, College of Engineering

Karen A. Holbrook
Dean, Graduate School

LD
1780
1996
.Y29

